IMPLEMENTATION OF SELF-TUNING CONTROL

FOR

TURBINE GENERATORS

by

Kankalil John Zachariah

Submitted to the University of Newcastle-upon-Tyne

for partial fulfilment of the degree of

Doctor of Philosophy

January 1994

Department of Electrical and Electronic Engineering

University of Newcastle-upon-Tyne

Newcastle-upon-Tyne, UK.

ABSTRACT

This thesis documents the work that has been done towards the development of a 'practical' self-tuning controller for turbine generator plant. It has been shown by simulation studies and practical investigations using a micro-alternator system that a significant enhancement in the overall performance in terms of control and stability can be achieved by improving the primary controls of a turbine generator using self-tuning control.

The self-tuning AVR is based on the Generalised Predictive Control strategy. The design of the controller has been done using standard off-the-shelf microprocessor hardware and structured software design techniques. The proposed design is thus flexible, cost-effective, and readily applicable to 'real' generating plant. Several practical issues have been tackled during the design of the self-tuning controller and techniques to improve the robustness of the measurement system, controller, and parameter estimator have been proposed and evaluated. A simple and robust measurement system for plant variables based on software techniques has been developed and its suitability for use in the self-tuning controller has been practically verified. The convergence, adaptability, and robustness aspects of the parameter estimator have been evaluated and shown to be suitable for long-term operation in 'real' self-tuning controllers.

The self-tuning AVR has been extensively evaluated under normal and fault conditions of the turbine generator. It has been shown that this new controller is superior in performance when compared with a conventional lag-lead type of fixed-parameter digital AVR. The use of electrical power as a supplementary feedback signal in the new AVR is shown to further improve the dynamic stability of the system.

The self-tuning AVR has been extended to a multivariable integrated self-tuning controller which combines the AVR and EHG functions. The flexibility of the new AVR to enable its expansion for more complex control applications has thus been demonstrated. Simple techniques to incorporate constraints on control inputs without upsetting the loop decoupling property of the multivariable controller have been proposed and evaluated. It is shown that a further improvement in control performance and stability can be achieved by the integrated controller.

ACKNOWLEDGEMENTS

This thesis presents work carried out under the supervision and guidance of Dr. J. W. Finch and Dr. M. Farsi. I wish to express my sincere thanks and appreciation to both of them for their invaluable assistance and the great interest they have taken throughout this project.

This work was sponsored by Parsons Turbine Generators Ltd as part of a research project. I wish to thank the Directors of PTGL for financial support to carry out this research programme and for sponsoring my study at the University.

A number of people at Parsons have helped me in various ways during the course of this work and I take this opportunity to thank them.

Special thanks are due to :

Mr. R. S. Hingston, for allowing sufficient time to progress the work and prepare this thesis;

Mr. P. A. L. Ham, for practical guidance and many helpful suggestions;

Mr. P. Lawson &
Mr. J. Fenwick, for assistance with the use of the micro-machine facility;

Mr. J. A. Denham &
Mr. N. A. Jackson, for showing great interest in the work.

Thanks to Dr. P. W. Rush, Aberdeen University, who initiated this research programme when he worked at Parsons.

Thanks to Dr. M. T. Tham, University of Newcastle-upon-Tyne for the useful discussions on multivariable self-tuning control.

My sincere thanks to all at Parsons who assisted me with the typing and tracing work during the preparation of this thesis. Miss. B. Atkinson deserves a special mention in this regard.

Finally, I wish to thank my wife Susan for her great understanding, patience and support during the course of this work.

Dedicated to

John and *Mary*

Let this be an inspiration to you both !

LIST OF SYMBOLS AND ABBREVIATIONS

β	-	forgetting factor of the parameter estimator
Δ	-	differencing operator $(1 - z^{-1})$
δ_b	-	rotor angle w.r.t the infinite busbar
δ_t	-	rotor angle w.r.t generator terminals
$\dot{\delta}$	-	rotor velocity
$\ddot{\delta}$	-	rotor acceleration
$\epsilon'(t)$	-	model error of the parameter estimator
$\epsilon(t)$	-	parameter estimation error
$\boldsymbol{\theta}$	-	vector of parameters of the ARMA plant model
$\hat{\boldsymbol{\theta}}$	-	vector of estimated parameters of the ARMA model
$\boldsymbol{\lambda}$	-	diagonal matrix of control weighting for MIMO plant
λ	-	control weighting factor
λ_{ii}	-	control weighting factor for loop i
ξ	-	damping factor
σ^2	-	expected noise variance of the plant
Φ	-	power factor angle
$\phi(t)$	-	auxiliary plant output
$\boldsymbol{\phi}(t)$	-	vector of $\phi(t)$ for MIMO plant
$\phi^*(t)$	-	prediction of $\phi(t)$
$\boldsymbol{\phi}^*(t)$	-	vector of $\phi^*(t)$ for MIMO plant
$\boldsymbol{\phi}_m^*$	-	column vector of ϕ^* for MIMO plant
ψ_d	-	flux in coil D of the dq-model of the generator
$\boldsymbol{\psi}_d$	-	flux matrix for the d-axis
$\dot{\boldsymbol{\psi}}_d$	-	d-axis flux derivative vector
ψ_f	-	flux in coil F of the dq-model of the generator
ψ_{kd}	-	flux in coil KD of the dq-model of the generator
ψ_{kq}	-	flux in coil KQ of the dq-model of the generator
ψ_q	-	flux in coil Q of the dq-model of the generator
$\boldsymbol{\psi}_q$	-	flux matrix for the q-axis
$\dot{\boldsymbol{\psi}}_q$	-	q-axis flux derivative vector
ω	-	rotor angular velocity (radians / sec)
ω'	-	speed deviation

ω_0	-	angular frequency of the power system (radians / sec)
ω_n	-	undamped natural frequency
$\boldsymbol{A}$	-	diagonal matrix of $A(z^{-1})$ polynomials for MIMO plant
$A(z^{-1})$	-	polynomial for output in the ARMA plant model
A_d	-	steam valve demand
A_p	-	steam valve position
$\boldsymbol{A}_{ps}$	-	state space system matrix of the power system
ARMA	-	Auto-Regressive Moving Average
AVR	-	Automatic Voltage Regulator
$\boldsymbol{B}$	-	diagonal matrix of $B(z^{-1})$ polynomials for MIMO plant
$B(z^{-1})$	-	polynomial for input in the ARMA plant model
B_d , B_q	-	susceptance matrices of d and q-axis coils
Boost	-	artificial gain boost value given to the plant
$\boldsymbol{B}_{ps}$	-	state space input matrix of the power system
$C(z^{-1})$	-	polynomial for noise in the ARMA plant model
CARIMA	-	Controlled Auto-Regressive Integrated Moving Average
CARMA	-	Controlled Auto-Regressive Moving Average
CMR	-	Continuous Maximum Rating
CPU	-	Central Processing Unit
D	-	damping of rotor
$\boldsymbol{d}(t)$	-	vector of past inputs and outputs of the plant
$\boldsymbol{D}(t)$	-	diagonal matrix which is a factor of $\boldsymbol{P}(t)$.
DFD	-	Data Flow Diagram
DGAVR	-	conventional lag / lead type digital AVR
DGAVR-F	-	'fast' conventional lag / lead digital AVR
DGAVR-S	-	'slow' conventional lag / lead digital AVR
DMA	-	Direct Memory Access
DSA	-	Dynamic Signal Analyser
$e(t)$	-	plant noise at time t
$\boldsymbol{e}(t)$	-	vector of random noise for MIMO plant
$(\Sigma e^2)_i$	-	sum of square of set point deviations for loop i
$E\{.\}$	-	expectation operator
EDR	-	Effective Damping Ratio
EHG	-	Electro-Hydraulic Governor

$\boldsymbol{E_j^f}$	-	diagonal matrix of $E(z^{-1})$ for MIMO plant
E_j^f	-	polynomial associated with future noise for output prediction
EnB	-	order of estimated $B(z^{-1})$ polynomial
FFT	-	Fast Fourier Transform
F_j^f	-	polynomial for filtered plant output to predict output
$\boldsymbol{F_j^f}$	-	diagonal matrix of $F(z^{-1})$ for MIMO plant
FPU	-	Floating Point Unit
FRA	-	Frequency Response Analyser
$\boldsymbol{g}$	-	N_y vector of weights for future set point deviations
$\tilde{\boldsymbol{g}}_i$	-	elements of the $\tilde{\boldsymbol{G}}$ matrix
$\tilde{\boldsymbol{G}}$	-	$(N_y \times N_u)$ matrix of unit step response sequence of plant
$\tilde{\boldsymbol{G}}_j$	-	diagonal matrix of $\tilde{G}_j$ for multivariable controller
G_e	-	exciter gain
G_g	-	governor gain
ΣG_{ij}	-	sum of first column of G_{ij} matrix
G_j^f	-	polynomial for filtered plant input to predict output
$\boldsymbol{G_j^f}$	-	diagonal matrix of $G_j^f(z^{-1})$ for MIMO plant
$\tilde{G}_j$	-	unit step response of plant j steps ahead
$\tilde{\boldsymbol{G}}_m$	-	matrix of $\tilde{\boldsymbol{G}}$ for multivariable GPC
G_p	-	weighting function for power in the GPC cost function J''
GPC	-	Generalised Predictive Control
G_s	-	weighting for speed deviation
h	-	numerical integration step length
I/O	-	input / output
$\boldsymbol{I}$	-	Identity matrix of the required size
i_a , i_b , i_c	-	currents in phase a, b, and c.
i_d	-	current in coil D of the dq-representation of the generator
$\boldsymbol{I}_d$	-	vector of currents in the coils on the d-axis
i_f	-	current in coil F of the dq-representation of the generator
i_{kd}	-	current in coil KD of the dq-representation of the generator
i_{kq}	-	current in coil KQ of the dq-representation of the generator
I_L	-	rms line current
I_{mt}	-	generator terminal current peak

i_q	-	current in coil Q of the dq-representation of the generator
$\boldsymbol{I}_q$	-	vector of currents in the coils on the q-axis
I_{td} , I_{tq}	-	d and q-axis components of I_{mt}
J	-	moment of inertia of rotor
J'	-	GPC cost function
J''	-	GPC cost function with real power
J_1	-	expectation of GPC cost function
$\frac{\partial J_1}{\partial \bar{u}}$	-	partial derivative w.r.t control increment vector
J_m	-	cost function of GPC for multivariable controller
$\boldsymbol{K}(t)$	-	gain vector for estimated parameters
K_{HP}	-	contribution of HP stage of the turbine
K_{LP}	-	contribution of IP/LP stages of the turbine
L	-	loss function of the parameter estimator
$M(z^{-1})$	-	model of the closed-loop system
MCB	-	Main Circuit Breaker
M_e	-	electrical torque
MIMO	-	Multi-Input Multi-Output
MMI	-	Man-Machine Interface
M_t	-	prime-mover torque
n_a	-	order of $A(z^{-1})$ polynomial of the ARMA model
n_b	-	order of $B(z^{-1})$ polynomial of the ARMA model
N_m	-	desired asymptotic memory length of the estimator
$\boldsymbol{N}_{ps}(x)$	-	vector of non-linearities of the power system
nT	-	order of disturbance tailoring polynomial $T(z^{-1})$
N_u	-	control horizon
N_y	-	output prediction horizon
OS_i	-	overshoot of control input of loop i
p'	-	instantaneous real power
p	-	scalar value to make $P(z^{-1})$ unity in steady state
$\boldsymbol{P}$	-	diagonal matrix of $P(z^{-1})$ for MIMO plant
P	-	real power
$P'(t)$	-	'washed-out' real power signal
$\boldsymbol{P}(t)$	-	covariance matrix of the parameter estimator

$P(z^{-1})$	-	transfer function to derive $\phi(t)$ from $y(t)$
$P_d(z^{-1})$	-	denominator polynomial of $P(z^{-1})$
$P_n(z^{-1})$	-	numerator polynomial of $P(z^{-1})$
P_{ref}	-	load set point
$\boldsymbol{P_s}$	-	vector containing cost of real power $P_s(t)$
$P_s(t)$	-	'cost' of real power in the GPC cost function J''
PSS	-	Power System Stabiliser
pu	-	per unit
q	-	instantaneous reactive power
Q	-	reactive volt-ampere
R_a	-	armature resistance
RAM	-	Random Access Memory
R_e	-	transmission line resistance
R_{ex}	-	external resistance
R_f	-	field resistance
$\boldsymbol{R_{gd}}$	-	resistance matrix for the d-axis components
$\boldsymbol{R_{gq}}$	-	resistance matrix for the q-axis components
R_{kd}	-	d-axis damper resistance
R_{kq}	-	q-axis damper resistance
$(RL)_i$	-	rate limit of control input for loop i
RLS	-	Recursive Least Squares
R_t	-	unit transformer resistance
$\boldsymbol{s}$	-	N_y vector of predicted auxiliary plant outputs
$\boldsymbol{s}_i$	-	prediction of ϕ for loop i
SISO	-	Single Input Single Output
$\boldsymbol{S}_m$	-	vector of future predictions $s(t+j)$ for MIMO plant
STAVR	-	Self-Tuning AVR
STAVR-F	-	'fast' self-tuning AVR
STAVR-S	-	'slow' self-tuning AVR
STAVR-SO	-	'slow and oscillatory' self-tuning AVR
STC	-	Self-Tuning Control
STEHG	-	Self-Tuning Electro-Hydraulic Governor
$\boldsymbol{T}$	-	diagonal matrix of $T(z^{-1})$ for MIMO plant
$T(z^{-1})$	-	disturbance tailoring polynomial

t_a , t_b	-	instants in time
TCR	-	Time Constant Regulator
T_{do}'	-	open circuit field time constant
T_e	-	exciter time constant
TG	-	Turbine Generator
T_{LP}	-	IP/LP turbine lag
TMR	-	Triplex Modular Redundant
T_{RH}	-	reheat time constant
T_s	-	turbine time constant
T_k	-	sampling period of the digital controller
T_v	-	steam valve time constant
T_w	-	wash-out time constant
$u(t)$	-	plant input at time t
$\boldsymbol{u}(t)$	-	vector of plant inputs for MIMO plant
$\bar{\boldsymbol{u}}$	-	N_u vector of control input increments
$\boldsymbol{U}(t)$	-	upper triangular matrix which is a factor of $\boldsymbol{P}(t)$.
U-D	-	Upper-Diagonal
$u\_act\ (t)$	-	control input actually applied to the plant
u_{11}	-	component of u_1 which regulates loop 1
u_{12}	-	component of u_1 which decouples loop 1 from loop 2
u_{21}	-	component of u_2 which decouples loop 2 from loop 1
u_{22}	-	component of u_2 which regulates loop 2
$\boldsymbol{u}^f$	-	vector of filtered past control inputs for MIMO plant
$u^f(t)$	-	filtered plant input
u_i^c	-	compensated control input for loop i
u_i^l	-	amplitude limited control input for loop i
u_i^r	-	raw control input for loop i
$\boldsymbol{u}_m$	-	vector of present and future control inputs for MIMO plant
UPF	-	Unity Power Factor
$\boldsymbol{u}_{ps}$	-	control input vector of the power system
v_a , v_b , v_c	-	voltages for phase a, b, and c.
VA	-	volt-ampere
VAr	-	reactive volt-ampere
v_{ba} etc.	-	line voltage between the specified phases

V_{bd} - d-axis component of infinite busbar peak voltage

V_{bq} - q-axis component of infinite busbar peak voltage

V_e - exciter input voltage

V_f - field voltage

V_L - rms line voltage

V_{mt} - Generator terminal voltage peak

V_t - generator terminal voltage (rms)

V_{td} - d-axis component of V_{mt}

V_{tq} - d-axis component of V_{mt}

$\boldsymbol{w}$ - N_y vector of future set point sequence

$w(t)$ - set point at time t

$\boldsymbol{w}_m$ - vector of future set points for MIMO plant

X_a - armature leakage reactance

X_e - transmission line leakage reactance

X_{ex} - external reactance

X_f - field leakage reactance

$\boldsymbol{X}_{gd}$ - reactance matrix for the d-axis

$\boldsymbol{X}_{gq}$ - reactance matrix for the q-axis

X_{kd} - d-axis damper leakage reactance

X_{kq} - q-axis damper leakage reactance

X_{md} - d-axis magnetising reactance

X_{mq} - q-axis magnetising reactance

$\boldsymbol{x}_{ps}$ - state vector of the power system

$\dot{\boldsymbol{x}}$ - $\frac{d\boldsymbol{x}}{dt}$

X_t - unit transformer leakage reactance

$\boldsymbol{y}(t)$ - vector of plant outputs for MIMO plant

$y(t)$ - plant output at time t

$\boldsymbol{y}^f$ - vector of filtered past outputs for MIMO plant

$y^f(t)$ - filtered plant output

CONTENTS

CHAPTER 1

INTRODUCTION

Synchronous generators and their turbines are essential components of an electric power system. The possible operating range of a generating plant which is synchronised to the power system can be extended by improving its control system [1]. Hence the control of turbine generators in modern power systems has received considerable attention in the past two to three decades. The design of modern generating units, the increasing complexity of power systems, their inherent nonlinearities, and the demands of economic and operational requirements all contribute to the need for more effective control.

With the advent of interconnection of electric power systems, many dynamic power system problems have emerged. The most significant of these is that of power system stability. The problem of stability has existed ever since the beginning of the parallel operation of generators and is a widely investigated topic. Whenever a sudden change occurs in the power system there are transients, and if the changes in the energy levels in the system during the transients are too large, the system becomes unstable. Stability can be maintained however if sufficient damping is provided by manipulating the power flows between inputs and outputs. Cost effectiveness is now achieved with larger unit sizes and higher per unit reactance generating and transmission equipment designs. These modern trends require more emphasis and reliance to be placed on controls to offset the resulting reduction in stability margins [2].

Recent developments in power systems, arising from advances in technology, changes in patterns of generation and load, and economic considerations, have exposed various problems and requirements [3]. However, with advances in computer technology and the developments of mathematical tools for modern control theory, the realisation of improved controllers for turbine generators to meet these demands has become possible. The use of these controllers can guarantee the extension of the stability margins and, more generally, the improvement of dynamic performance of generating units.

This chapter is organised as follows: Section 1.1 gives a brief introduction to the problem of stability that is encountered in power systems. The control systems which are used in the turbine generating plant for regulation and stability improvement are introduced in Section 1.2. The technological advances in the field of turbine generator control are briefly explained in Section 1.3, while Section 1.4 summarises the attempts to employ advanced control strategies for turbine generators. The use of self-tuning control for the generating plant is introduced in Section 1.5 which also includes an overview of the Generalised Predictive Control strategy and the Recursive Least Squares Parameter Estimator. Section 1.6 explains the structure of the thesis, its objectives, and original contributions.

1.1 Introduction to Power System Stability

Power system stability can be classified into three categories, viz. steady state, dynamic and transient stability. Steady-state stability of a generator is its ability to remain in synchronism under conditions of steady state operation. A machine operating close to its limits of steady state stability is less likely to cope with a moderate system disturbance. Dynamic stability is concerned with the damping of electro-mechanical oscillations in the machine and the power system. It refers to the machine's voltage and rotor angle recovery following small changes on the power system such as line switching and transformer tap changing. Transient stability is concerned with recovery following system faults. The ability of a generator to recover synchronism without a pole-slip after an electrical fault has been applied and then cleared, is a measure of its transient stability [4]. Recovery following a major power system disturbance depends largely on the nominal response of the excitation system which is a measure of the maximum rate of change of generator field voltage.

It has been recognised for a long time that the complexity of a large power system has an adverse effect on the system's dynamic and transient limits [5]. The complexity of the system can be attributed to several factors which include the use of long transmission lines, fast excitation systems and generators with large MVA ratings thus possessing high reactance and low inertias.

A generator connected to a power system is stable if both the synchronising and damping components of its accelerating torque are positive over the range of oscillation frequencies encountered [6]. Positive synchronising torque ensures the restoration of the rotor angle following a displacement, whereas positive damping torque helps to decay the rotor oscillations following such a displacement. A machine may loose its stability due to the lack of damping or inadequate synchronising torque [7].

1.2 Control Systems For Turbine Generators

A turbine generator conventionally has two independent regulating loops, one for the stator voltage and the other for shaft speed. These are classed as the primary controls of the system. A Power System Stabiliser also is usually employed for each machine in modern power systems to improve the dynamic stability margin of the system and is treated as a supplementary controller.

The inputs through which control can be applied to a turbine generator are the generator excitation system and the turbine inlet valves. The primary function of the excitation system is to provide the field current required by the generator to meet a specified range of power system operating conditions. The inlet valves supply the turbine with the required quantity of steam, water, or gas, as the case may be, in order that the necessary mechanical power is produced to meet the target load.

1.2.1 The Automatic Voltage Regulator

The excitation of the machine is controlled by the Automatic Voltage Regulator (AVR) which makes use of the stator terminal voltage as its feedback signal. For an isolated machine, the function of the AVR is solely to maintain a constant busbar voltage. When applied to a multi-generator power system, however, voltage regulation forms only a part of its function. The main effect is to maintain machine rotor angle and, therefore, to assist in maintaining steady state stability [1]. Several protection functions such as limiting of overvolts, overflux, leading power factor, and rotor current are also incorporated in the AVR.

Modern power systems are generally equipped with high gain, fast-acting voltage regulators to improve transient stability. Nowadays, the AVR forms an integral part of the design and operation of large generators since they have a high value of synchronous reactance and are therefore weak on inherent stability [1]. The AVR restores the machine 'stiffness', which is so necessary on a commercial power system. Excitation control systems thus play an important role in the transient and oscillatory stability of generating units and inter-connected systems [8].

1.2.2 The Electro-Hydraulic Governor

The Electro-Hydraulic Governor (EHG) controls the turbine by means of its inlet valves based on the shaft speed and load which are the main feedback signals. The shaft speed is regulated by the EHG on open-circuit and the load upon achieving synchronisation to the power system. The EHG incorporates several turbine protection functions such as overspeed limiting, acceleration detection, load demand limiting, condenser vacuum unloading etc. It also has several high-level control modes to co-ordinate the turbine with the boiler [9].

The EHG is generally set up as a slow-acting control system under normal conditions. It can however help in improving the transient stability of the system by reducing the unbalance between the input and output power of the turbine generator under severe disturbances. Another means of improving transient stability through the EHG is 'fast valving' whereby the intercept valves which control the inlet to the intermediate pressure cylinder of the turbine are rapidly closed and re-opened within a short time when a severe disturbance is detected [9].

1.2.3 The Power System Stabiliser

The Power System Stabiliser (PSS) is a supplementary controller which prevents the occurrences of dynamic instability in power systems due to poorly damped electromechanical oscillations [10,11]. It makes use of shaft speed, accelerating power, real power, or frequency as its input and generally acts through

the excitation system of the generator [2,10,12]. It thus interacts with the basic voltage regulation loop, modulating the excitation current to provide additional damping of the rotor oscillations following a disturbance. A similar stabilising signal can be fed into the EHG also, however, due to the larger delay in the turbine and the valve system, the speed loop has attracted less attention for this purpose. The use of a PSS prevents undesirable power transfer limitations and provides a secure operation of large interconnected power systems [13,14].

1.3 Technological Advances in Turbine Generator Control

Until late 1960's voltage regulators and speed governors for use in turbine generators were of the mechanical or electro-mechanical types. The governor consisted of a centrifugal flyball mechanism which operated the turbine valves through a hydraulic system. The excitation control system made use of magnetic amplifiers and amplidynes for power amplification and drove the generator field by means of a d.c exciter.

In the late 1960's electronic AVR's using analog integrated circuits were developed and installed. The 'availability' of the AVR was improved by having a 'standby' automatic control channel and 'manual' control channel in the system. The exciter also underwent a transition from d.c to a.c and started to employ rectifiers and thyristors. Various types of exciter systems such as rotating a.c exciters with static or rotating rectifiers, and static thyristor exciters began to emerge [15]. Dynamic instability in the form of low frequency oscillations in some large interconnected power systems became a serious problem during this time which led to the use of Power System Stabilisers [16].

Analog electronic governors were first fitted to machines in the UK in the early 1970's. The need for improved availability and fault tolerance in EHG systems began to be acknowledged and schemes such as the Triplex Modular Redundant architecture together with simple hardware majority-voting techniques were soon developed [9]. This led to improved EHG systems with enhanced availability and integrity.

The rapid developments in digital electronics and microprocessor technology in particular in the mid-1970's paved the way towards digital control for turbine generators. It was soon realised that turbine generators may greatly benefit from the flexibility of control, rapid access to performance data and fault diagnostic capability that these developments in electronic techniques can provide [9]. A microprocessor-based controller can offer significant advantages, for example, in the range of functions available, ease of altering control algorithms, improved operator interface, and reliability [18,19]. The design and development of microprocessor based EHG, AVR and PSS systems were therefore initiated in the late 1970's and soon became available for commercial use [9,13,18,19]. Several of these systems are in service today and their success in the field has prompted Utilities to specify digital control systems for turbine generators in the recent tenders [20].

1.4 Advanced Control For Turbine Generators

The need for improved control of power generation equipment has steadily been increasing over the past years due to several reasons [21]. A modern generator has a high per-unit value of reactance, but the plant has a comparatively lower inertia constant. Large power stations have been constructed in locations remote from load centres, thus requiring long transmission lines with high per-unit reactances. These factors coupled with the complexity of modern distribution systems have greatly reduced both transient and dynamic stability margins [22]. Modern generating sets thus tend to be less stable than their predecessors, and therefore require complex control systems for their successful operation [21].

Generators in power systems are subject to frequent small disturbances, substantial scheduled load changes, sudden changes in demand, effects of transformer tap changing and line switching on the transmission network, and occasional major disturbances due to lightning, short-circuits etc. Since the turbine generator is a non-linear system, its dynamic characteristics change with varying load and generation schedules as well as during disturbances. Conventional controllers based on classical control theory can therefore have difficulty in maintaining the same quality of performance under these varying operating

conditions [23]. The performance requirements in terms of unit control and stability have been given a significant emphasis with the recent privatisation of the UK power industry [24]. Thus improved control systems based on modern control theory have been favourably considered for use in turbine generators.

Advanced control systems generally require fast and powerful microcomputers for real-time operation due to the complexity of the algorithms employed. The rapid developments in semiconductor technology in recent years have led to the availability of such digital systems at reasonable cost. This has enabled even the computationally intense advanced control algorithms to be considered for use in turbine generators. Hence on-line advanced control for electric generating units has become feasible and realizable.

In recent years, a large number of papers have described novel controllers for turbine generators, based on modern control techniques. These can be broadly classified into three categories based on their objective, viz. to improve excitation control only, to improve excitation control as well as governing, and to improve supplementary control. A brief survey of these controllers is attempted here to illustrate the variety of techniques that have been proposed for turbine generator control.

Attempts to improve the AVR performance using modern control techniques have been on-going for the past 15 years or so. The work has been centred mostly around adaptive and self-tuning control [25,26,41]. Several self-tuning control strategies such as Minimum Variance [27], Generalised Minimum Variance [28], Pole Assignment [29], and Generalised Predictive Control [30], as well as variations of these basic types are available in this modern control field. It can be seen from the literature that most of these types have been proposed in one form or the other for excitation control. Minimum Variance self-tuning control has been evaluated using simulation [31] and laboratory model [23,32] turbine generators [22,33-35]. The Generalised Minimum Variance approach has also been tried out [36,37], and a detuned version of the same has been proposed [22,35]. The use of an optimal predictor which minimises the variance between the actual output and its desired track has been tried out for the AVR [21,38,39]. The Pole

Assignment self-tuning control has also been experimented [22,35]. The work on excitation control presented in this thesis is based on the Generalised Predictive Control strategy and has also been reported [20,23,40,43-49]. A significant enhancement in the performance of the AVR when using the self-tuning approach has been reported, and several techniques to improve the robustness of the controller have been proposed [21,24,39,47,50]. In most of the self-tuning AVR's proposed, the electric power or rotor speed has been used as an additional feedback signal to improve power system stability.

Integrated controllers combining the AVR and EHG functions based on modern control strategies have also been proposed during the past two decades. In the 1970's, the more popular approach was the use of Linear Optimal Control for the design of these multivariable controllers. Several methods to derive the optimal control law have been used. State Space methods based on a linearised turbine generator model have been proposed [32,51-53]. Linear plant models derived using offline parameter estimation schemes have been used for the design of the optimal controller [54-57]. Another approach has been the use of an optimal predictor [3], while the use of the Model Reference Adaptive Control method [25] has also been reported [58,59]. Multivariable as well as multi-loop self-tuning control based on an Auto-Regressive Moving Average plant model which is estimated on-line have also been proposed for turbine generator control [60,61]. Several self-tuning strategies have been employed in those designs, the Minimum Variance [61], detuned Minimum Variance [60,61] and Generalised Minimum Variance [62]. As with the self-tuning AVR, the integrated controller designs also make use of power and speed signals for power system stability improvement.

Modern control theory has been employed to improve the turbine generator supplementary control too. The advanced PSS's that have been evaluated can be divided into two types depending on where their outputs are applied. In the simple case, the PSS output acts only through the excitation system, while the more advanced versions act through the AVR and EHG systems. The simple type generally has a Single-Input Single-Output (SISO) structure and the advanced version is multivariable. For the SISO type, the improvement has been mostly achieved using the self-tuning strategy. Minimum Variance [63], Pole

Shifting [63-65], and Generalised Minimum Variance [5,67] approaches have been proposed in the literature which give encouraging results. More recently, the use of a rule based approach [68] and fuzzy logic control [69] have also been investigated to design a PSS. The more advanced multivariable supplementary controllers proposed in the literature are based on Linear Optimal control [70-72], or robust control such as H^{∞} [73], or self-tuning control such as the Generalised Minimum Variance [8].

It can be seen that a wide variety of techniques based on modern control theory has been proposed in the literature for turbine generator control. The techniques investigated are shown to provide improved performance over the existing control systems. It should however be noted that these improved controllers are evaluated mostly using simulation studies or experiments on a laboratory model turbine generator and have not been implemented in a commercial control system for a 'real' generating plant.

1.5 Self-tuning Control of Turbine Generators

It can be seen from the brief survey given in the previous section that a significant number of publications dealing with advanced control for turbine generating plant propose the use of self-tuning control. There are several reasons for choosing this approach. The primary reasons are the non-linear nature of the turbine generator and the wide range of disturbances that it is subjected to during its operation. A fixed-parameter linear controller whose design is strictly valid only at the chosen operating point is unable to respond in the best possible way over the whole range of the system operating conditions [22]. This can lead to unnecessary restrictions in the permissible operating region of the plant because of the possibility of reduced system stability margins at certain operating points. The adaptive self-tuning control technique has the ability to adjust in accordance with system variations and to perform consistently over a wide range of operating conditions.

The use of self-tuning control for turbine generators can give economic benefits also. The proposed settings of a fixed-parameter AVR are generally

required to be assessed for modern machines. The evaluation involves exhaustive simulation studies and on-site testing [74]. This is undesirable from both an economic and commissioning standpoint, and can sometimes result in expensive site modifications at a later date due to the subjective nature of the evaluation process. Operational experience with a 'real' generating plant has shown that a poorly tuned AVR can impose unnecessary restrictions on the maximum plant output under constrained operating conditions and that improving its tuning can result in enhanced plant availability thus leading to a significant economic benefit [75]. Considerable motivation thus exists for the implementation of control philosophies such as self-tuning which are not based on detailed pre-design information and have facility for successive or periodic redesign of the controller in response to changes in the generating plant dynamics [33].

The self-tuning approaches employed for excitation control are of the type which makes use of a low-order mathematical model of the generating plant which is identified on-line. Hence the self-tuning AVR has a recursive parameter estimator and a control design algorithm which makes use of information received from the estimator. The recursive parameter estimator generally uses a Controlled Auto-Regressive Moving Average (CARMA) model of the plant and estimates the parameters of that model recursively. Several techniques such as the Recursive Least Squares (RLS), Extended Recursive Least Squares (ERLS), Recursive Maximum Likelihood (RML), and Recursive Instrumental Variable (RIV) are available for parameter estimation [17,25,76,77]. A number of improvements to the basic estimation schemes have also been proposed which enhance the robustness and computational efficiency of the algorithms [78-81].

The control design algorithm of the self-tuning AVR can utilise one of several control laws with varying objectives, ie. optimal, sub-optimal, classical etc. The Minimum Variance (MV) control law is an optimal strategy which minimises the variance of the plant output [27,82]. It can however be highly sensitive to non-minimum phase plant behaviour and generally gives very lively control. The Generalised Minimum Variance (GMV) control law is a sub-optimal approach which aims to minimise a cost function made up of set-point deviations and control signals [28]. Although the GMV controller is a far more generalised and robust

approach, it is vulnerable to unknown / varying plant dead time due to its single-step prediction scheme. Moreover, the basic algorithm has difficulty in removing dc offsets in the plant output caused by load disturbances unless suitable steps are taken while formulating the cost function [83,84]. The Pole Assignment (PA) control law has its roots in classical control and aims to move the closed-loop poles of the system to pre-specified locations [29]. This strategy leads to 'smooth' controllers, but the numerical sensitivity of the algorithm when the plant model is over-parameterised is regarded as a significant drawback [30,83].

Many of the problems mentioned above can be tackled one way or another by ad-hoc techniques thus leading to a robust self-tuning controller. Some of those difficulties may not arise at all in the case of excitation control, and hence can be ignored. However, it is advantageous to employ a 'general-purpose' self-tuning algorithm suitable for the majority of 'real' processes for excitation control. This enables its use in other applications in the area of generating plant control with the minimum of modifications thus leading to a standardised approach which is an important consideration for use in industry. The Generalised Predictive Control (GPC) algorithm is considered to meet the above requirements [30,83].

GPC can effectively deal with a wide variety of systems characterised by non-minimum phase behaviour, open-loop unstable or badly damped poles, variable / unknown order and dead time, load disturbances etc. [30]. Its robustness is mainly due to the use of a multi-step predictor and a 'receding horizon' approach to derive the control signal. GPC has several 'tuning knobs' to make it flexible and can make use of a future set-point sequence when available [42]. This is a useful feature for turbine generator control during scheduled load / operating point changes, automatic excitation or shutdown, on-load valve testing etc. GPC has the framework with which simple controllers can be expanded to complex ones when the need arises. It is already being proposed for such demanding applications as boiler-turbine control [85] and boiler steam pressure control [86] for electricity generation. The main criticism against GPC however is the computational burden it imposes, but it has been shown that it is possible to achieve sampling frequencies of typically 50 to 100 Hz when a modern microprocessor with moderate power and speed is used for the implementation of the algorithm [26].

Since GPC was chosen as the most appropriate candidate for use in a self-tuning controller for the turbine generating plant, a brief overview of its theory is given in the following sub-section.

1.5.1 Generalised Predictive Control Theory: An Overview

GPC is a member of a family of algorithms called Model-Based Predictive Control (MBPC). These algorithms have the same basic strategy [87]: to perform long range prediction of future outputs based on a plant model and a set of suggested controls, to optimise a suitable cost function to get the 'best' control sequence, and to apply using receding horizon ideas the first of the set of control signals to the plant. Although GPC can be used for the control of SISO as well as multivariable plant, the review given here pertains to the SISO case only.

GPC employs a Controlled Auto-Regressive Integrated Moving Average (CARIMA) plant model which is given by:

$$A(z^{-1})\ y(t) = B(z^{-1})\ u(t-1) + C(z^{-1})\ \frac{e(t)}{\Delta} \qquad (1.1)$$

where $A(z^{-1})$, $B(z^{-1})$ and $C(z^{-1})$ are polynomials in z^{-1} and Δ is the differencing operator $(1 - z^{-1})$. $y(t)$ and $u(t)$ are the plant output and input at time t respectively and $e(t)$ is an uncorrelated random sequence of zero mean and finite variance. It can be observed from (1.1) that the disturbance is modelled as a non-stationary process with stationary increments which is considered to be a more accurate representation [30]. The use of the CARIMA model gives GPC an inherent integral action.

The objective of GPC is to minimise a cost function J' given by:

$$J' = \sum_{j=1}^{N_y} [\phi(t+j) - w(t+j)]^2 + \sum_{j=1}^{N_u} \lambda[\Delta u(t+j-1)]^2 \qquad (1.2)$$

where N_y is the prediction horizon, N_u is the control horizon, λ is a control weighting factor, and $w(t+j)$ is the future set-point sequence.

$\phi(t+j)$ is an auxiliary output derived from the actual plant output $y(t+j)$ as:

$$\phi(t+j) = P(z^{-1})\ y(t+j) \tag{1.3}$$

In its general form, $P(z^{-1})$ can be considered to be a transfer function of the form:

$$P(z^{-1}) = p\ \frac{P_n(z^{-1})}{P_d(z^{-1})} \tag{1.4}$$

where P_n and P_d are monic polynomials in z^{-1} and p is a scalar value such that $P(z^{-1}) = 1$ in steady state [23]. The transfer function $P(z^{-1})$ is related to the model of the closed-loop, $M(z^{-1})$ such that

$$M(z^{-1}) \simeq \frac{1}{P(z^{-1})} \tag{1.5}$$

Minimising the cost function J' with respect to Δu gives the control law as [30]:

$$\bar{u} = (\tilde{G}^T \tilde{G} + \lambda I)^{-1} \tilde{G}^T (w - s) \tag{1.6}$$

in which w and s are N_y vectors containing the future set-point sequence and the components of future auxiliary plant output ϕ which are known at the present sample interval t. $\tilde{G}$ is a $(N_y \times N_u)$ matrix and $\bar{u}$ is a N_u vector of present and future suggested control increments. The minimisation of the cost function to derive the control law given by (1.6) is described in Appendix A.

Since GPC is based on a receding horizon approach, only the first element of the control sequence, ie. $\Delta u(t)$ needs to be calculated. Thus the control law becomes:

$$u(t) = u(t-1) + g^T (w - s) \tag{1.7}$$

in which g is a N_y vector containing the first row of the $(N_u \times N_y)$ matrix, $(\tilde{G}^T \tilde{G} + \lambda I)^{-1} \tilde{G}^T$. It can be observed from (1.7) that GPC is an integral control law and is capable of minimising dc offsets when load disturbances occur in the plant.

In the self-tuning case, the matrix $\tilde{G}$ and the vector s have to be calculated at every sample interval to derive the control signal. This is done using the prediction of $\phi(t+j)$ at time t as:

$$\phi^*(t+j) = \tilde{G}_j \, \Delta u(t+j-1) + G_j^f \, \Delta u^f(t-1) + F_j^f \, \frac{y^f(t)}{P_d} \tag{1.8}$$

where $\phi^*(t+j)$ is the prediction of $\phi(t+j)$ at time t and $\tilde{G}_j$ is of order $(j-1)$. $\Delta u^f(t-1)$ and $y^f(t)$ are obtained by filtering with a disturbance tailoring polynomial $T(z^{-1})$ for high frequency noise rejection as:

$$\Delta u^f(t-1) = \frac{\Delta u(t-1)}{T(z^{-1})}$$
$$y^f(t) = \frac{y(t)}{T(z^{-1})} \tag{1.9}$$

$T(z^{-1})$ is chosen such that $1 / T(z^{-1})$ is a low pass filter to achieve detuned control activity for high frequency transient disturbances and to improve the robustness of the algorithm against unmodelled dynamics [88,89]. The derivation of (1.8) is given in Appendix B.

The polynomials $\tilde{G}_j$, G_j^f and F_j^f are derived from two Diophantine identities which are given by:

$$\frac{p \, P_n \, T}{A \, \Delta \, P_d} = E_j^f + \frac{z^{-j} \, F_j^f}{A \, \Delta \, P_d} \tag{1.10}$$

and

$$\frac{E_j^f \, B}{T} = \tilde{G}_j + z^{-j} \, \frac{G_j^f}{T} \tag{1.11}$$

Since (1.10) and (1.11) have to be solved for $j = 1$ to N_y at every sampling period, recursion techniques to improve the computational efficiency are used [30]. The recursive formulae for E_j^f and F_j^f are derived in Appendix C, while Appendix D gives the derivation for $\tilde{G}_j$ and G_j^f .

The elements of the vector s are derived from (1.8) by taking the known components at time t as:

$$s(t+j) = G_j^f \, \Delta u^f(t-1) + F_j^f \, \frac{y^f(t)}{P_d} \tag{1.12}$$

The $(N_y \times N_u)$ matrix $\tilde{G}$ is formed from the coefficients of the $\tilde{G}_j$ polynomial as:

$$\tilde{G} = \begin{bmatrix} \tilde{g}_0 & 0 & 0 & - & - & - & 0 \\ \tilde{g}_1 & \tilde{g}_0 & 0 & - & - & - & 0 \\ \tilde{g}_2 & \tilde{g}_1 & \tilde{g}_0 & - & - & - & 0 \\ | & | & & & & & \\ | & | & & & & & \\ \tilde{g}_{N_y-1} & \tilde{g}_{N_y-2} & - & - & - & - & \tilde{g}_{N_y-N_u} \end{bmatrix} \qquad (1.13)$$

The prediction and control horizons in GPC are very powerful features which enable robust control of a wide variety of systems [30]. Several extensions and interpretations to the basic algorithm have been proposed to further improve its performance [30,89-91]. Stability issues of the GPC algorithm are considered in [92,93] where it has been shown that the disturbance tailoring polynomial $T(z^{-1})$ plays an important role in reducing the controller's sensitivity to high frequency noise and unmodelled dynamics. It is also shown that the set-point response tailoring polynomial $P_n(z^{-1})$ affects robustness in exactly the same way as does the T polynomial, with the bonus that the liveliness of the controller can also be adjusted. It has been suggested that a combination of the two polynomials should always be used for $N_u > 1$ both to limit the control signal activity and to improve closed-loop robustness.

1.5.2 Review of Recursive Least Squares Parameter Estimator

Although several techniques for on-line parameter estimation are available, the Recursive Least Squares (RLS) method is considered for turbine generator self-tuning control because of its simplicity, robustness and relatively low computational requirement. RLS is one of the basic and more popular on-line parameter estimation schemes available and is based on minimising the sum of squares of the model equation errors.

Since the RLS estimator has to work in conjunction with the GPC algorithm for turbine generator control, the CARIMA plant model is used for its design. The estimated plant model can then be written as:

$$\Delta y(t) = \boldsymbol{d}^T(t)\ \hat{\boldsymbol{\theta}} + \epsilon'(t) \tag{1.14}$$

where $\boldsymbol{d}(t)$ is a vector of past values of input and output, $\hat{\boldsymbol{\theta}}$ is a vector containing the best possible estimate of the unknown parameters and $\epsilon'(t)$ is the model error.

The data vector $\boldsymbol{d}(t)$ and the estimated parameter vector $\hat{\boldsymbol{\theta}}$ can be defined as:

$$\begin{aligned} \boldsymbol{d}(t) &= [-\Delta y(t-1),\ -\Delta y(t-2),\ ---,\ -\Delta y(t-n_a),\\ &\qquad \Delta u(t-1),\ \Delta u(t-2),\ ---,\ \Delta u(t-1-n_b)]^T \\ \hat{\boldsymbol{\theta}} &= [\hat{a}_1,\ \hat{a}_2,\ ---,\ \hat{a}_{n_a},\ \hat{b}_0,\ \hat{b}_1,\ ---,\ \hat{b}_{n_b}]^T \end{aligned} \tag{1.15}$$

where n_a and n_b are the assumed order of $A(z^{-1})$ and $B(z^{-1})$ polynomials respectively.

A Least Squares (LS) estimator can be derived by minimising the loss function $L = \sum_{i=1}^{N} \epsilon^{/2}(t)$ with respect to $\hat{\boldsymbol{\theta}}$ for a large number of observations N.

The resulting equations are modified for the recursive estimator as [25,76]:

$$\hat{\boldsymbol{\theta}}(t) = \hat{\boldsymbol{\theta}}(t-1) + \boldsymbol{K}(t)\ \epsilon(t) \tag{1.16}$$

where the estimation error $\epsilon(t)$ is given by:

$$\epsilon(t) = \Delta y(t) - \boldsymbol{d}^T(t)\ \hat{\boldsymbol{\theta}}(t-1) \tag{1.17}$$

$\boldsymbol{K}(t)$ is a vector ('Kalman gain') containing the gain of correction which is calculated using a 'matrix inversion lemma' as [76]:

$$\begin{aligned} \boldsymbol{K}(t) &= \frac{\boldsymbol{P}(t-1)\ \boldsymbol{d}(t)}{[\beta + \boldsymbol{d}^T(t)\ \boldsymbol{P}(t-1)\ \boldsymbol{d}(t)]} \\ \boldsymbol{P}(t) &= \frac{1}{\beta}\ [\boldsymbol{I} - \boldsymbol{K}(t)\ \boldsymbol{d}^T(t)]\ \boldsymbol{P}(t-1) \end{aligned} \tag{1.18}$$

where $\boldsymbol{P}(t)$ is the covariance matrix and β is an exponential forgetting factor to slowly discard old data thereby staying 'in tune' with the plant all the time.

Improved numerical properties can be achieved by factorising the covariance matrix $P(t)$ into a product of matrices and updating them at every sampling instant [78,95]. This approach can guarantee the positive definitiveness of $P(t)$ at all times which is vital for retaining the convergence properties of the RLS algorithm [41]. A popular factorisation technique is the Upper-Diagonal (U-D) factorisation and is given as [78,95]:

$$P(t) = U(t)\ D(t)\ U^T(t) \tag{1.19}$$

where $D(t)$ is a diagonal matrix and $U(t)$ is an upper triangular matrix with all its diagonal elements equal to unity. The matrices $D(t)$ and $U(t)$ are recursively updated instead of $P(t)$ and the gain vector $K(t)$ is calculated from them. A comparative study of the performance of various factorisation algorithms has indicated that the U-D factored RLS estimator provides the best performance as well as computational efficiency[97]. The U-D factorisation algorithm is given in Appendix E.

The use of a fixed forgetting factor in (1.18) can cause a problem called 'estimator blow-up' during long periods of steady state operation of the plant. The phenomenon of 'blow-up' is due to forgetting of old data when little dynamic information is received from the plant. This causes the estimator to be extremely sensitive to even small disturbances and changes in the plant dynamics [41]. Hence a variable forgetting factor scheme which aims to keep the information content in the estimator constant has been used for turbine generator self-tuning control. The variable forgetting factor $\beta(t)$ is given by [81]:

$$\beta(t) = 1 - [1 - d^T(t)\ K(t)]\frac{\epsilon^2(t)}{N_m\ \sigma^2} \tag{1.20}$$

where N_m is the desired asymptotic memory length of the estimator and σ^2 is the expected noise variance of the plant. Since $\beta(t)$ is not available until the gain vector $K(t)$ has been calculated, a minor modification is done to (1.18) as [81]:

$$K(t) = \frac{P(t-1)\ d(t)}{[1 + d^T(t)\ P(t-1)\ d(t)]} \tag{1.21}$$

A computationally simpler equation for $\beta(t)$ can then be derived as [98]:

$$\beta(t) = 1 - \frac{\epsilon^2(t)}{[1+d^T(t)\ P(t-1)\ d(t)]\ N_m\ \sigma^2} \qquad (1.22)$$

1.6 Objectives, Original Contributions and Structure of the Thesis

The primary objective of this work is to develop a 'practical' self-tuning excitation controller for turbine generators. Since the work is aimed at evolving a design which can be readily tailored into a real product, several practical aspects have to be considered. The self-tuning control strategy chosen for excitation control should be flexible and expandable for use in other areas of turbine generating plant. The design of the self-tuning controller should be robust and suitable for long-term operation in the field with 'real' plant signals. The controller should use plant signals which are available from existing transducers. As far as possible, standard off-the-shelf microprocessor hardware which is used by the existing fixed-parameter digital AVR should be chosen for implementing the self-tuning controller. Practical considerations such as processing power and sampling period should be taken into account. A structured software design methodology leading to a modular approach is to be followed.

The self-tuning AVR should be extensively tested and evaluated on a physical small-scale model of a large turbine generator. An integrated self-tuning controller which incorporates the AVR and EHG functions should be designed by expanding the SISO system and a preliminary evaluation should be conducted.

The original contributions of this thesis are thought to be the following:

a. The design of a self-tuning excitation control system based on the Generalised Predictive Control strategy and its implementation using standard off-the-shelf microprocessor hardware.

b. Development of techniques for robustness improvement of the recursive parameter estimator of the self-tuning AVR.

c. Evaluation of the self-tuning AVR based on GPC using a software simulator of the turbine generator during transients.

d. Development of a simple and robust measurement system for plant variables based on software techniques suitable for the self-tuning control of turbine generators.

e. Performance evaluation of the self-tuning AVR based on GPC and the software measurement system under normal and fault conditions using a physical small-scale model of a large turbine generator, and comparison with a fixed parameter digital AVR.

f. Incorporation of the electrical power signal in the GPC AVR for improved power system stability and its evaluation using the laboratory model turbine generator.

g. Extension of the self-tuning AVR based on GPC to a multivariable integrated controller which combines the AVR and EHG functions.

h. Development of simple techniques to incorporate practical constraints in the multivariable integrated controller.

i. Evaluation of the self-tuning multivariable integrated controller based on GPC using the laboratory model turbine generator, and comparison with a multi-loop approach.

The remaining Chapters of the thesis are organised as follows: The tools used for the evaluation of the self-tuning controller, viz. a software TG simulator and a laboratory model turbine generator system, are described in Chapter 2. Chapter 3 presents the design of the self-tuning AVR using the GPC strategy and the software measurement system. This Chapter also explains the practical aspects considered during the design and the techniques adopted to improve the

robustness of the controller. A detailed evaluation of the performance of the self-tuning AVR under normal as well as fault conditions of the generating plant and a comparison with the fixed-parameter digital AVR are given in Chapter 4.

Chapter 5 explains the incorporation of the electrical power signal as a supplementary feedback to the self-tuning AVR and demonstrates the improvement in the dynamic stability thus obtained. The extension of the SISO self-tuning control algorithm for use as a multivariable TG controller is presented in Chapter 6 where simple techniques to incorporate practical constraints on control input are proposed and verified. The performance improvement that can be achieved by upgrading the self-tuning AVR to a self-tuning TG controller are also illustrated in this Chapter. Finally, the important conclusions that can be drawn from this work are summarised in Chapter 7 which also identifies areas of possible future work.

CHAPTER 2

MODELLING OF TG PLANT

A mathematical model of the system which is derived using analytical methods can serve two main purposes. Firstly, an analytical model of the plant is highly desirable or in some cases even essential for the design of its controller. Secondly, a reasonably accurate model of the plant can greatly enhance the performance evaluation of the proposed controller before it is actually tried out on the real plant.

The first application generally requires a simplified model of the plant. This means that although the plant considered exhibits some non-linearities, in many cases the model has to be linearised around the nominal operating point. Generally, the use of a high order plant model for some optimal controller designs such as LQG can lead to solutions which are too complex. Hence, some method of model order reduction is commonly employed. So, what is required for controller design is generally a linear low-order mathematical model of the plant.

The second use of the analytical plant model, for performance evaluation of the controller, however does not require simplifying assumptions such as linear behaviour, low order model etc. The model should represent the real plant as accurately as possible. This criterion often leads to rather complex models which take into account non-linearities, saturation effects etc. in the plant. The more accurate the plant model, the better is the confidence level achieved during off-line performance evaluation of the controller using that model.

Self-tuning control does not depend too heavily on an analytical model of the plant for controller design. This is mainly due to its ability to 'adapt' itself to the plant when the plant parameters are either unknown and / or varying with time. However, a certain knowledge of the plant is definitely required for a successful self-tuning control design. The aspects of the plant of interest in self-tuning control include the maximum and minimum dead time, the fastest and slowest dynamics

of the plant, the structure and order of the plant, the actuator positional and rate limits of the control input, etc.

The use of an analytical model of the plant for performance evaluation of the self-tuning controller during its development phase is of great advantage. In the case of the turbine generator, it is of considerable benefit to simulate abnormal ie. fault conditions of the plant and study the behaviour of the self-tuning controller under those circumstances. One of the most serious abnormalities that a turbine generator can be subjected to is a 3-phase short-circuit fault. In this work, a non-linear model of the turbine generator in state space form which represents a single machine connected to an infinite busbar has been used for initial fault simulation studies. The derivation of this power system model is explained in Section 2.1.

A laboratory model turbine generator system which is a scaled down replica of the real full size system is a popular means of testing and evaluating a controller designed for this application [32,56,23]. This model is complex; some parts closely resemble the real plant, for example the use of a 3-phase micro-alternator, and some other parts are simulated by hardware electronic circuits. The laboratory model power system has been extensively used during this work for evaluating the performance of the self-tuning controller under both normal and abnormal operating conditions of the system. The real advantage of such a set-up stems from the fact that the controller is connected to a physical plant and although it is a scaled down version, the model exhibits practical aspects of a real plant such as measurement noise and system features such as harmonics, unbalance in load, etc. The laboratory model power system set-up used for this work is described in Section 2.2.

2.1 Mathematical Model of the Power System

A non-linear software model of the power system is required for transient stability analysis. The usual representation for this purpose is a single machine connected by means of a transmission line to the rest of the power system which

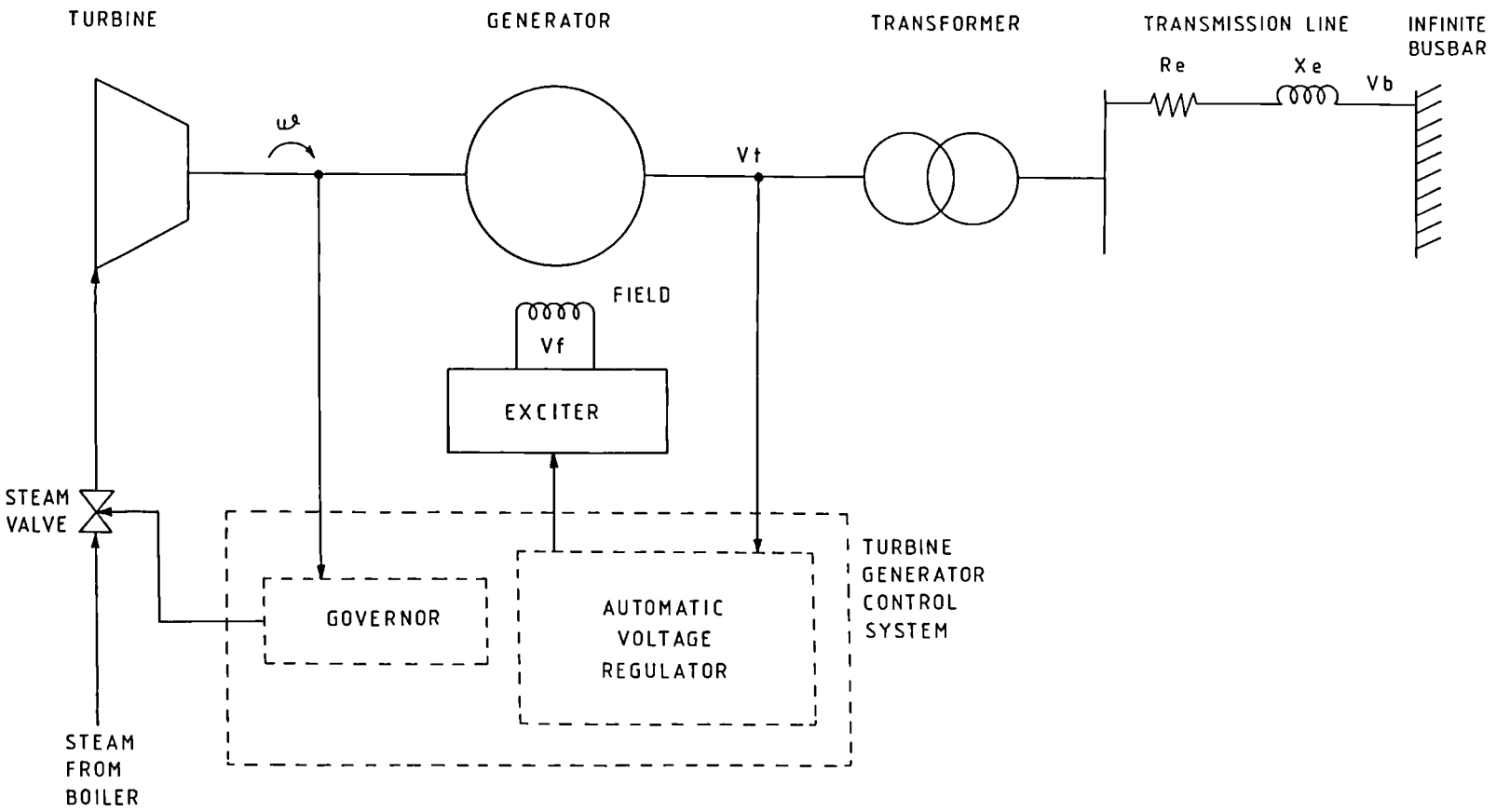

Fig. 2.1 Block diagram of a single machine infinite busbar power system.

is considered as an infinite busbar [31]. A block diagram representation of this system is given in Figure 2.1. An analytical model of each of the blocks shown is to be derived and combined into a single set of equations for deriving the power system simulator.

In deriving the state space model of the single machine infinite busbar power system for transient stability analysis, the following simplifying assumptions are made [99].

a) The machine reactances remain constant at their on-load pre-fault values and that the varying magnetic saturation during and following a fault can be ignored.

b) Space harmonics in the flux wave and capacitance in the generator windings and transmission system are neglected.

c) The system frequency at the infinite bus is taken to be constant at its nominal value of ω_o.

d) The turbine generator shaft is considered as a single-mass system with no flexible couplings.

e) The motoring sign convention and per-unit system used in [99] is employed here.

f) The impedance of the transformer and the transmission line are combined with that of the generator to form a 'modified' generator which has its terminals at the infinite busbar. Thus the rotor angle of the modified generator is defined as the angle relative to the infinite bus voltage. The formulation using a modified generator simplifies calculations.

2.1.1 Modelling of the Synchronous Generator

A state space model of the generator using flux linkages as state variables [99] was adopted. The electromagnetic dynamics of the generator are modelled by the standard 2-axis theory of electrical machines expressed in the rotor reference frame. This is based on Park's transformation [99] which replaces the three actual phase windings with two fictitious d and q-axis coils that would set up the same mmf wave. The synchronous machine together with its damper circuits are thus represented by three windings D, F and KD on the d-axis and two on the q-axis (Q and KQ).

The currents through the coils of the 2-axis generator representation are related to the fluxes by the following linear matrix equations (neglecting saturation):

$$\begin{aligned} \boldsymbol{I}_d &= \boldsymbol{X}_{gd}^{-1}\,[\omega_0 \boldsymbol{\psi}_d] \\ \boldsymbol{I}_q &= \boldsymbol{X}_{gq}^{-1}\,[\omega_0 \boldsymbol{\psi}_q] \end{aligned} \qquad (2.1)$$

where

$$\boldsymbol{I}_d = [i_d \;\; i_f \;\; i_{kd}]^T$$

$$\boldsymbol{I}_q = [i_q \;\; i_{kq}]^T$$

$$[\omega_0 \boldsymbol{\psi}_d] = [\omega_0 \psi_d \;\; \omega_0 \psi_f \;\; \omega_0 \psi_{kd}]^T$$

$$[\omega_0 \boldsymbol{\psi}_q] = [\omega_0 \psi_q \;\; \omega_0 \psi_{kq}]^T$$

The variables i_d, i_f, i_{kd}, i_q and i_{kq} are the currents in the coil D, F, KD, Q and KQ respectively. The fluxes in the coils are represented by Ψ with the appropriate subscript. The angular frequency of the power system is represented by ω_0.

The reactance matrices are given by:

$$\boldsymbol{X}_{gd} = \begin{bmatrix} (X_{md}+X_a+X_t+X_e) & X_{md} & X_{md} \\ X_{md} & (X_{md}+X_f) & X_{md} \\ X_{md} & X_{md} & (X_{md}+X_{kd}) \end{bmatrix}$$

$$\boldsymbol{X}_{gq} = \begin{bmatrix} (X_{mq}+X_a+X_t+X_e) & X_{mq} \\ X_{mq} & (X_{mq}+X_{kq}) \end{bmatrix}$$

where

X_{md}	=	d-axis magnetising reactance
X_{mq}	=	q-axis magnetising reactance
X_a	=	armature leakage reactance
X_t	=	unit transformer leakage reactance
X_e	=	transmission line leakage reactance
X_f	=	field leakage reactance
X_{kd}	=	d-axis damper leakage reactance
X_{kq}	=	q-axis damper leakage reactance

The machine equations relating the generator voltages to currents and fluxes are given by [99]:

$$\dot{\boldsymbol{\psi}}_d = \begin{bmatrix} (V_{bd}-\omega_0\psi_q+\psi_q\dot{\delta}) \\ V_f \\ 0 \end{bmatrix} - \boldsymbol{R}_{gd}\,\boldsymbol{I}_d \qquad (2.2)$$

$$\dot{\boldsymbol{\psi}}_q = \begin{bmatrix} (V_{bq}+\omega_0\psi_d-\psi_d\dot{\delta}) \\ 0 \end{bmatrix} - \boldsymbol{R}_{gq}\,\boldsymbol{I}_q$$

where

$$\boldsymbol{R}_{gd} = \begin{bmatrix} (R_a+R_t+R_e) & 0 & 0 \\ 0 & R_f & 0 \\ 0 & 0 & R_{kd} \end{bmatrix}$$

$$\boldsymbol{R}_{gq} = \begin{bmatrix} (R_a+R_t+R_e) & 0 \\ 0 & R_{kq} \end{bmatrix}$$

where

R_a	=	generator armature resistance
R_t	=	unit transformer resistance
R_e	=	transmission line resistance
R_f	=	generator field resistance
R_{kd}	=	d-axis damper winding resistance
R_{kq}	=	q-axis damper winding resistance

V_{bd} and V_{bq} are the d and q-axis components of the infinite busbar peak voltage. $\dot{\delta}$ is the rate of change of the rotor position and is equal to $(\omega_0 - \omega)$ where ω is the rotor angular velocity.

Combining (2.1) and (2.2) gives the state variable representation of the generator electromagnetics as:

$$[\omega_0\dot{\psi}_d] = -\omega_0 \boldsymbol{R}_{gd} \boldsymbol{X}_{gd}^{-1} [\omega_0\psi_d] + \omega_0 \begin{bmatrix} (V_{bd}-\omega_0\psi_q+\psi_q\dot{\delta}) \\ V_f \\ 0 \end{bmatrix} \qquad (2.3)$$

$$[\omega_0\dot{\psi}_q] = -\omega_0 \boldsymbol{R}_{gq} \boldsymbol{X}_{gq}^{-1} [\omega_0\psi_q] + \omega_0 \begin{bmatrix} (V_{bq}+\omega_0\psi_d-\psi_d\dot{\delta}) \\ 0 \end{bmatrix}$$

The electromagnetic torque M_e produced by the generator is given by [99]:

$$M_e = \frac{\omega_0}{2} (\psi_d i_q - \psi_q i_d) \tag{2.4}$$

where the currents i_q and i_d can be worked out from (2.1).

Assuming the shaft linking the turbine and generator to be rigid, the equation of motion for the rotor is:

$$J \ddot{\delta} + D \dot{\delta} + M_t = M_e \tag{2.5}$$

where J is the moment of inertia of the rotor and is given by $(2H / \omega_0)$ in which H is the inertia constant, D is the damping arising from the bearings and windage, δ is the rotor angle relative to the infinite bus, and M_t is the turbine shaft torque which is also known as the prime mover torque.

Equation (2.5) can be written in state variable form as:

$$\begin{bmatrix} \dot{\delta} \\ \ddot{\delta} \end{bmatrix} = \begin{bmatrix} 0 & 1 \\ 0 & -\frac{D}{J} \end{bmatrix} \begin{bmatrix} \delta \\ \dot{\delta} \end{bmatrix} + \begin{bmatrix} 0 \\ \frac{(M_e - M_t)}{J} \end{bmatrix} \tag{2.6}$$

Combining (2.3) and (2.6) yields a seven state non-linear model of the generator.

2.1.2 Modelling of the Transmission Line

The model developed in Section 2.1.1 is that of a modified generator which has its terminals at the infinite busbar. However, the voltage at the real stator terminals of the generator is required for feedback into the AVR. An uncompensated transmission line is assumed here as shown in Figure 2.1 and its resistance and reactance can be combined with those of the unit transformer to give:

$$\begin{aligned} R_{ex} &= R_t + R_e \\ X_{ex} &= X_t + X_e \end{aligned} \tag{2.7}$$

The terminal voltage of the generator can be derived from the infinite bus voltage by subtracting the resistive and reactive drops.

Let the maximum terminal voltage V_{mt} be given by:

$$V_{mt} = (V_{td}^2 + V_{tq}^2)^{\frac{1}{2}} \tag{2.8}$$

where V_{td} and V_{tq} are related to V_{bd} and V_{bq} via the voltage drop in the transmission circuit. The d and q-axis components of the terminal voltage are thus given by:

$$\begin{aligned} V_{td} &= V_{bd} - R_{ex}\, i_d - \frac{X_{ex}}{\omega_0}\, \dot{i}_d - \omega\, \frac{X_{ex}}{\omega_0}\, i_q \\ V_{tq} &= V_{bq} - R_{ex}\, i_q - \frac{X_{ex}}{\omega_0}\, \dot{i}_q + \omega\, \frac{X_{ex}}{\omega_0}\, i_d \end{aligned} \tag{2.9}$$

2.1.3 Exciter Modelling

Different types of exciters are in use today and a detailed analysis of the models which can be used is given in an IEEE report [100]. Here, the excitation system assumed is a high initial response type which consists of a rotating ac exciter supplying a static controlled rectifier that feeds into the generator field. This corresponds to the IEEE type AC-4 system and has been modelled by a simple lag network with output limits as shown in Figure 2.2 [100]. It is assumed that positive as well as negative field forcing is allowed, but negative field current is not possible. The state space representation of the exciter model is given by:

$$\dot{V}_f = -\frac{1}{T_e}\, V_f + \frac{G_e}{T_e}\, V_e \tag{2.10}$$

The ceiling values of the exciter input voltage V_e and the field voltage V_f are assumed to be ± 3 times their rated load value.

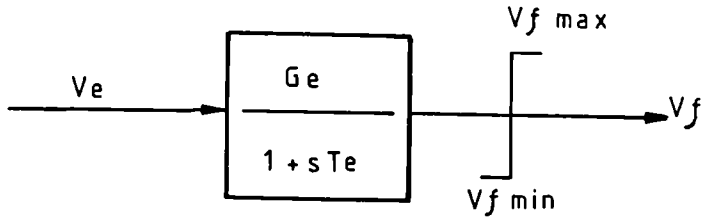

Fig. 2.2 The Exciter model.

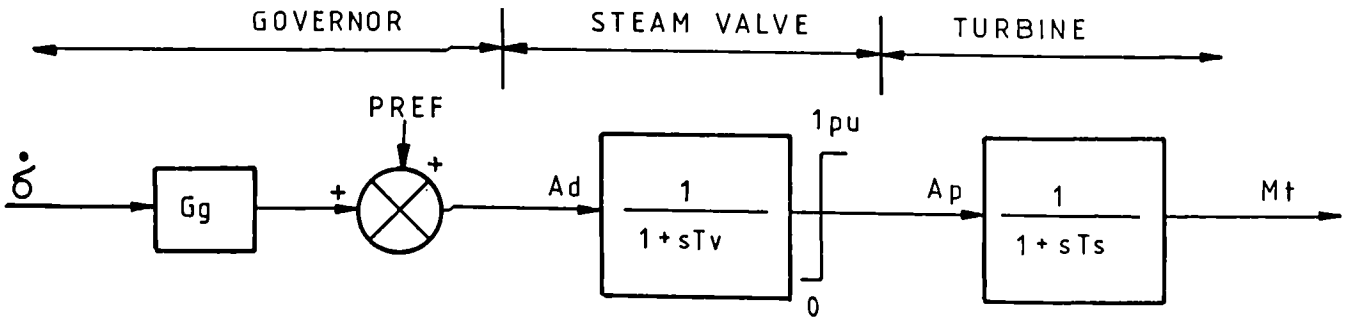

Fig. 2.3 The Governor, Steam Valve, and Turbine model.

2.1.4 Modelling of Governor / Turbine System

The modelling aspects of prime movers have been studied extensively and a detailed treatment is given in [101]. An accurate representation of the dynamics of the various turbine stages, hydraulic system and valves would require several state variables. However, for the sake of simplicity, a three stage governor / valve / turbine model with two of the stages represented by 1st order differential equations has been used in this work, see Figure 2.3.

The speed governor is a proportional controller with a gain of G_g with the speed error $\dot{\delta}$ as its input. P_{ref} is the load set point which is added to the speed loop output to produce A_d, the steam valve demand. The steam valve is assumed to be actuated by a high pressure hydraulic system and has a time constant of T_v. The output of the valve model is amplitude limited in the range of 0 to 1 pu to obtain the valve position A_p. The turbine is assumed to have a single lag of T_s and produces the mechanical torque M_t.

From Figure 2.3, the state equations for the governor / valve / turbine model are derived as:

$$\begin{aligned} \dot{A}_p &= -\frac{1}{T_v} A_p + \frac{1}{T_v} (P_{ref} + G_g \dot{\delta}) \\ \dot{M}_t &= -\frac{1}{T_s} M_t + \frac{1}{T_s} A_p \end{aligned} \tag{2.11}$$

2.1.5 Implementation of the Power System Model

The state equations of the various blocks of the power system as derived in Sections 2.1.1 to 2.1.4 can be combined to obtain the general model given by:

$$\dot{\boldsymbol{x}}_{ps} = \boldsymbol{A}_{ps} \boldsymbol{x}_{ps} + \boldsymbol{B}_{ps} \boldsymbol{u}_{ps} + \boldsymbol{N}_{ps}(x) \tag{2.12}$$

where $\boldsymbol{x}_{ps}$ represents the states of the power system in vector form, $\boldsymbol{A}_{ps}$ and $\boldsymbol{B}_{ps}$ are the state and control matrices respectively and the $\boldsymbol{N}_{ps}(x)$ vector accounts for the important system non-linearities. The control input vector $\boldsymbol{u}_{ps}$ contains the inputs to the power system model. Depending on the scope of the TG controller to be

tested using the model, the input variables in u_{ps} change. For example, if the controller to be tested is a self-tuning AVR, the part of the TG controller which is not under test, ie. the governor, is treated as part of the standard power system.

Combining (2.3), (2.6), (2.10) and (2.11) gives the state vector x_{ps} with 10 variables as:

$$x_{ps} = [\delta \quad \dot{\delta} \quad \omega_0\psi_d \quad \omega_0\psi_f \quad \omega_0\psi_{kd} \quad \omega_0\psi_q \quad \omega_0\psi_{kq} \quad V_f \quad A_p \quad M_t]^T \qquad (2.13)$$

The control input vector u_{ps} when the governor is excluded from the model is given by:

$$u_{ps} = [V_e \quad A_d]^T \qquad (2.14)$$

whereas it is given by:

$$u_{ps} = [V_e \quad P_{ref}]^T \qquad (2.15)$$

with the governor included. The non-zero elements of the matrices A_{ps} and B_{ps} and the vector $N_{ps}(x)$ are given in Appendix F.

The simple fourth order Runge-Kutta numerical integration method has been employed for digital simulation. Details of the method are given in Appendix G. The integration step length is taken as 1 msec. The non-linearities of the plant given by $N_{ps}(x)$ are evaluated and the state variables tested for constraint violation and limited if necessary at the end of each integration step. The numerical integration requires initial conditions of the system to be established. These are calculated based on a steady state phasor diagram of the generator as given in Appendix H, and the voltage, electrical power and reactive power at the machine terminals. The parameters of the synchronous generator and the transmission line used in the simulator are given in Appendix I.

The simulation software is written in the high level language 'C'. It is organised as a stand-alone function with the calling function, in this case the control algorithm, supplying the control input u_{ps} and receiving the variables and states of interest. The start of an abnormal power system operation such as a

short-circuit and its end are made known to the simulator function using flags which are passed in as arguments.

2.2 Laboratory Model Turbine Generator System

A convenient intermediate step between the use of a software simulator and a real full-size machine is a micro-alternator for power system control investigations. This approach has the advantage that the control system under test can be subjected to practical difficulties which can arise in the field such as noise, transducer lags, etc. and evaluated before the field trials are conducted. Another important benefit of using a 'real' system although scaled down is that the control algorithm will have to execute in real time. This 'on-line' test can reveal problems relating to timing and sampling period. The micro-alternator can provide a realistic scaled-down simulation of a typical large alternator in terms of its per unit parameters, hence its use can provide valuable information with regard to the controller's performance on a full-size machine [32,70].

The laboratory model turbine generator system which has been used extensively during this work is shown in a block schematic form in Figure 2.4. At the heart of the system is a 3-phase micro-alternator which is driven by a dc motor. The micro-machine can be synchronised to the busbar via the step-up transformer and the double circuit transmission line simulator. The set-up has facilities for modifying the field time constant of the alternator, monitoring variables such as voltages and currents and applying faults to the power system. The prime mover dynamics of a typical turbine generator system are represented by an electronic simulator which drives the dc motor. A detailed explanation of the set-up is given in the subsequent sub-sections.

2.2.1 The Micro-alternator

The micro-alternator is a 3 kVA, 220 V, 50 Hz machine manufactured by Mawdsley Ltd. [102]. The machine is designed to have similar per unit parameter values to typical turbine generator sets of large capacity. The parameter values of

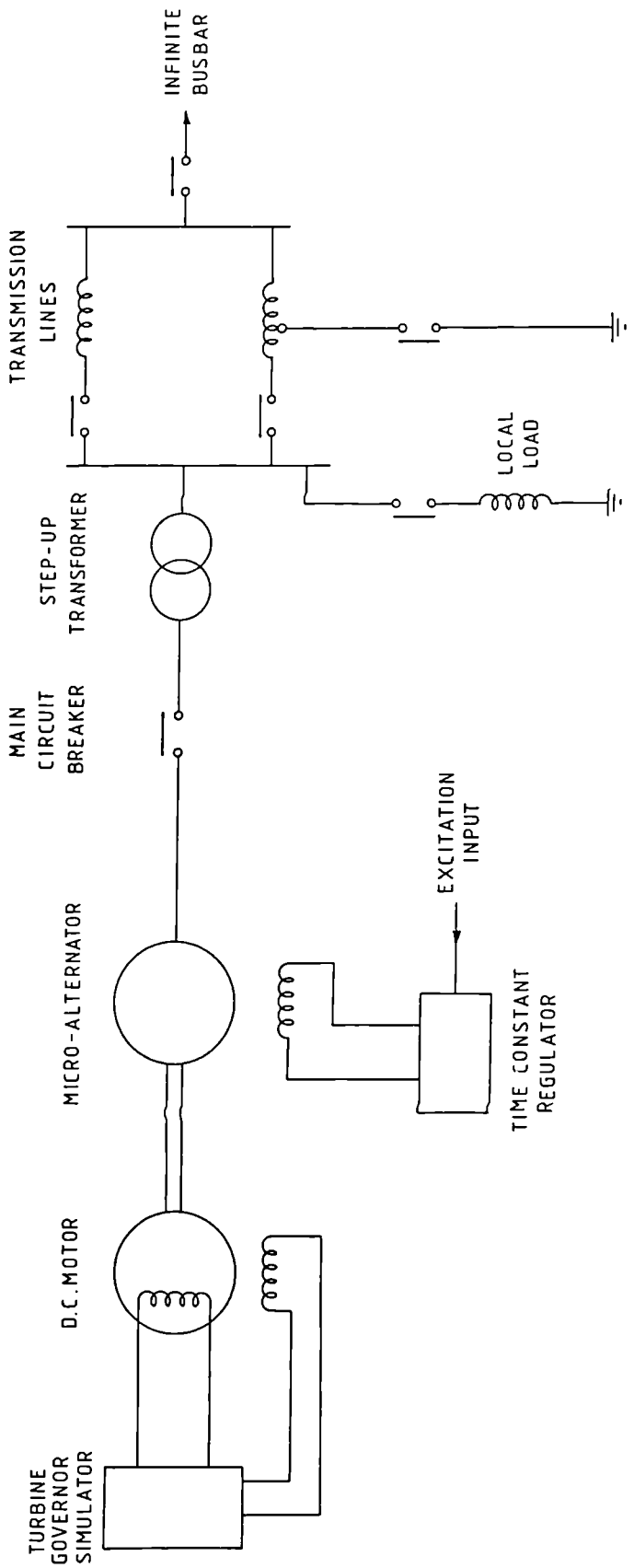

Fig. 2.4 Laboratory model turbine generator system.

the micro-alternator are given in Appendix I. The alternator is a 1500 rpm machine with a 4-pole cylindrical rotor. The field winding consists of a main winding and a shadow winding which are wound in parallel on the direct axis. A similar arrangement is provided for the damper windings on the direct and quadrature axes of the rotor. The shadow windings can be used for modifying the time constants of the micro-machine.

2.2.2 Time Constant Regulator

The achievement of per unit parameters in a micro-alternator which are similar to those of a typical turbine generator is at the expense of winding resistances which are invariably excessive compared with practical values [102]. This makes the micro-alternator respond differently to a full-size machine. This problem is tackled by the use of a Time Constant Regulator (TCR) which is fitted to the field of the machine. The TCR is regarded as an integral part of the micro-machine field and the excitation signal from the AVR is applied to the field through the TCR. The principle of operation of the TCR is to introduce a negative resistance characteristic to the field thereby increasing the field time constant. This is achieved by the use of the shadow field winding which is wound in the same slots as the main field and has the same number of turns, hence the same flux links both the field and the shadow winding.

The TCR is a high gain dc power amplifier which is used to derive the field of the machine. The induced voltage, due to the rate of change of main field flux linking the shadow winding, is fed back to the amplifier input together with the voltage dropped across a feedback resistor installed in series with the main field winding. For large amplifier gains, the open circuit field time constant of the micro-alternator with TCR is then inversely proportional to the feedback gain applied to the resistive drop due to the field current [70]. Transient open-circuit field time constants typically in the range of 5 to 8 sec are achieved using the TCR thus giving a response similar to a full-size turbine generator. A similar regulator for increasing the sub-transient time constant of the micro-alternator is possible by making use of the damper windings and their shadow windings, but this has not been incorporated in the present set-up.

2.2.3 Prime Mover Simulator

The sub-system consists of two parts. The dynamic behaviour of the governor, steam valves and the turbines is simulated by electronic circuits which form the modelling part of the simulator. The output of this part is power amplified to drive the armature of the dc motor which is mechanically coupled to the micro-alternator thus producing the desired mechanical torque. A block schematic diagram of the prime mover simulator is given in Figure 2.5.

The governor, steam valves and the turbines are modelled by analogue electronic circuits and a block schematic diagram of the same is given in Figure 2.6. The speed loop of the governor is a proportional controller with a droop setting of typically 4%. The load is regulated by a slow integrating loop the output of which is added to the speed loop output to form the power demand. The power demand signal is applied directly to the electronic circuit which models the governor valve dynamics. Since the intercept valve has to remain fully open even from a low value of load, the power demand signal is suitably adjusted inside the intercept valve gain / offset block before it is applied to the intercept valve dynamic model. Provision is given for applying external demand signals to the governor and intercept valves thus enabling the set-up to be used for the evaluation of a governor system.

The governor and intercept valve dynamic models are similar in structure. These blocks model the dead-band, primary actuator response, velocity limits, power piston response and the valve travel limit associated with a typical steam valve. The valve positions are fed into the turbine simulator which models the High Pressure (HP) and Intermediate / Low Pressure (IP / LP) stages of the turbine separately. The HP stage is represented by a low pass filter which has a time constant typically 0.1 sec. The contribution of the HP stage to the overall mechanical power output is modelled by a gain K_{HP} of typically 0.25.

The reheat storage is represented by a time constant T_{RH} which has a value of 8 sec. As the effect of the intercept valve movement is to alter the rate at

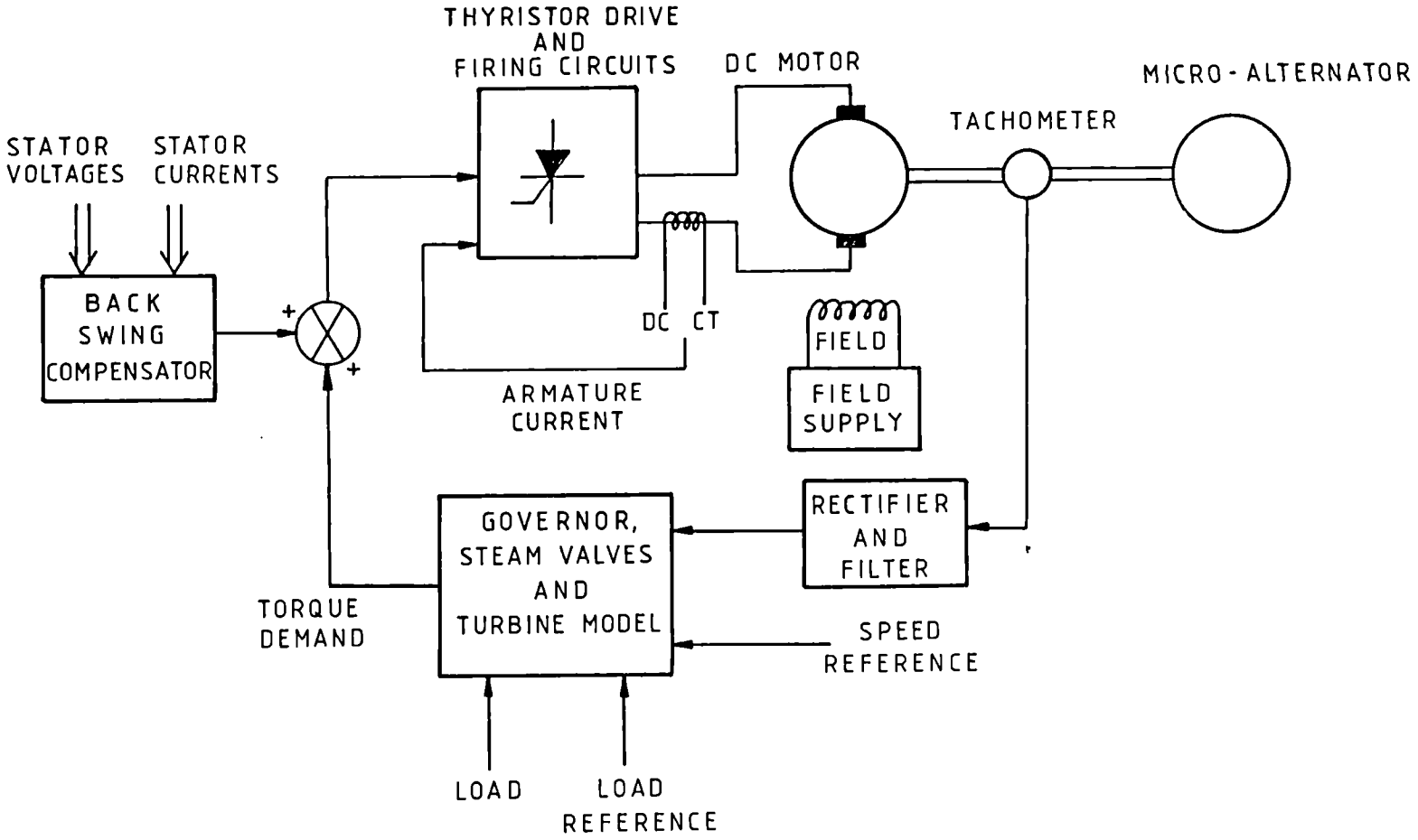

Fig. 2.5 The Prime Mover simulator block schematic.

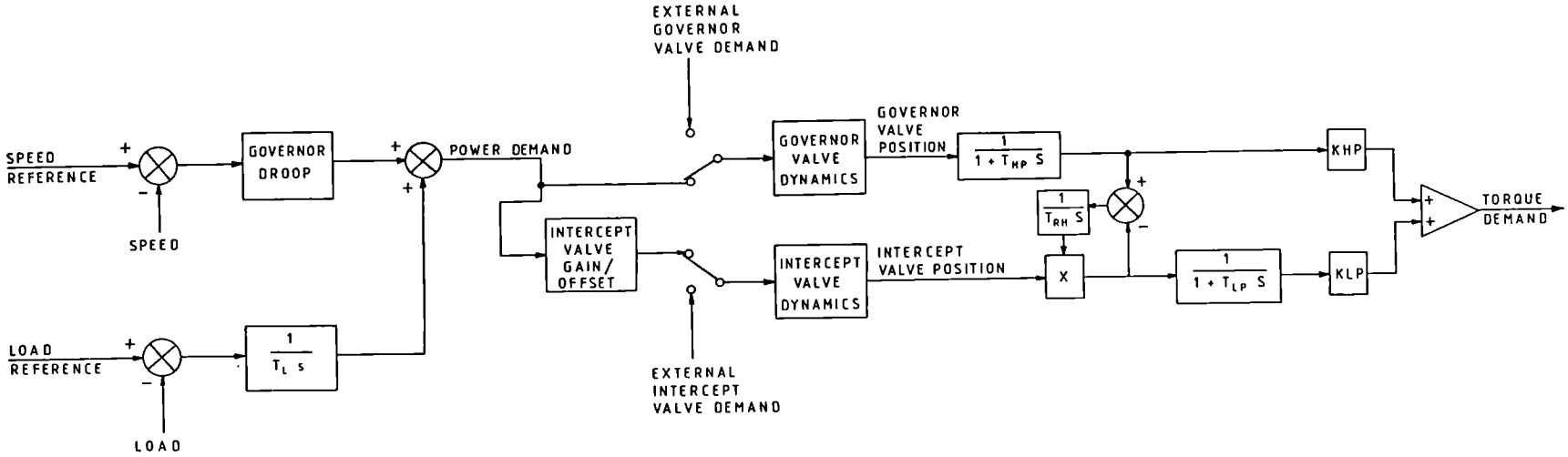

Fig. 2.6 The Governor, Steam Valve, and Turbine simulator.

which the reheat storage is discharged, the output of the reheat storage block is multiplied with the intercept valve position. The IP / LP turbine lag is modelled by a low pass filter of time constant (T_{LP}) 0.3 sec and its contribution to the overall mechanical power is represented by the gain block K_{LP} which is set to 0.75. The contributions from the HP and IP / LP stages of the turbine are summed together to produce the torque demand signal.

The torque demand signal controls the armature current of the dc motor by means of a thyristor bridge through its associated firing circuits. The dc motor is a 7.5 HP, 1500 rpm, 220 V machine whose field is excited by a constant current source. Since the field current of the dc motor is kept constant, the mechanical torque developed by it is directly proportional to the armature current which is regulated as per the torque demand signal. Thus the torque demand is converted to a proportional mechanical torque which is applied to the micro-alternator.

2.2.4 Back-Swing Compensator

Micro-alternators suffer from proportionately high winding resistances, stray load losses and core losses when compared with a full-size machine [102,104]. The effect of these losses can generally be ignored under normal operating conditions of the micro-alternator. These effects can become significant during abnormal / fault conditions of the system even to the extent of invalidating laboratory test results. One such case is the phenomenon of 'rotor back-swing' which can become unrealistically large on a micro-alternator during short-circuits and load rejection. This back-swing is the retardation of the rotor angle during the initial part of a short-circuit or load rejection.

The compensation for these excessive micro-alternator losses is achieved by increasing the driving torque developed by the dc motor in accordance with the alternator's stator phase voltage and current. Signals proportional to instantaneous phase voltages and currents are used to derive variables which are proportional to the instantaneous core, stray and armature losses within the micro-alternator. Experiments have shown that the core losses are proportional to the square of the

stator voltage whilst the stray losses are proportional to the square of the stator current and can be treated as armature losses [103,104].

The back-swing compensator has been built using a microprocessor-based intelligent analogue input / output board [46]. The board reads the instantaneous values of the stator phase voltages and currents every 4.44 msec and generates the loss compensation signals. The armature / stray loss compensation signal is generated as $k_1(i_a^2 + i_b^2 + i_c^2)$ where i_a , i_b and i_c are the stator currents and k_1 is the armature / stray loss compensation gain. Similarly, the core loss compensation signal is derived as $k_2(v_a^2 + v_b^2 + v_c^2)$ where v_a , v_b and v_c are the stator phase voltages and k_2 is the core loss compensation gain. The loss compensation signals are summed with the torque demand signal produced by the governor / valve / turbine simulator as shown in Figure 2.5 before it is applied to the thyristor drive which controls the armature current and hence the mechanical torque of the dc motor. The magnitudes of these compensation signals are adjusted by varying k_1 and k_2 based on a procedure given in [103] to achieve the desired loss compensation.

Figure 2.7 gives the response of the rotor in terms of its angle with resect to the infinite busbar voltage following a 3-phase short circuit near the sending end of the transmission line of the laboratory set-up. It can be observed that the rotor back-swing without loss compensation is more than 20 degrees. However the use of a properly tuned loss compensator has been able to reduce the rotor back-swing to about 3 degrees which is a realistic value for a typical full-size machine.

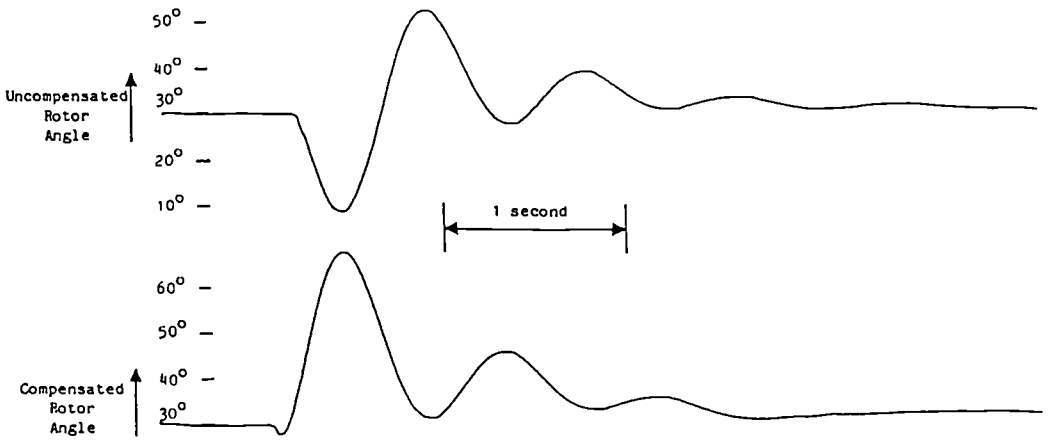

Figure 2.7. Effect of loss compensation on the rotor angle measurement during a 3-phase short-circuit on the micro-alternator.

2.2.5 Instrumentation and Test Facility

The laboratory model turbine generator system has conventional analogue instrumentation which has a small band-width suitable only for display purposes. The various parameters of the set-up such as voltages and currents at different parts of the system, real and reactive power etc. are displayed on digital panel meters.

A high speed data logging facility is also available as part of the test facility which is normally used for logging the variables of the system during tests. The data logging software is run on a Hewlett Packard 9000 series 320 desk-top instrument controller. It makes use of a 16 channel high speed analogue input card capable of sampling at 200 kHz. Facilities to save the collected data on a hard disc or a floppy disc, display it on a Visual Display Unit (VDU) and plot the results are available as part of the system. The parameters of interest are derived by means of hardware circuits and conditioned if necessary before applying to the data logger. The band-width of these signals is kept to the maximum possible to capture the dynamic behaviour of the laboratory model.

The test facility enables the simulation of various abnormal power system conditions involving fluctuations, faults etc. under which a turbine generator controller is required to be tested. This is achieved by means of circuit breakers which are installed at various parts of the laboratory model as shown in Figure 2.4. These circuit breakers are operated by sequencing units which are programmable for a particular requirement. Power system fault conditions such as short circuit, full load rejection, and transmission line switching can be simulated by this arrangement.

The circuit breaker sequencing unit is a microprocessor-based unit which controls the switching of circuit breakers over a defined time interval. The duration of switching and the point with respect to the system voltage waveform at which the switching has to take place are user-programmed into the sequencing unit by means of press buttons. This point-on-wave switching facility is useful for making the test conditions more precise thereby improving the repeatability of the test

results. The sequencing units can be cascaded so that they work on a master-slave basis. This enables the simulation of a sequence of events on the power system such as a short circuit followed by the isolation of the faulty transmission line.

CHAPTER 3

DESIGN AND IMPLEMENTATION OF A SELF-TUNING AUTOMATIC VOLTAGE REGULATOR

It is generally true that self-tuning control algorithms produce excellent results during simulation studies under ideal conditions. However, when a practical implementation of such a strategy is attempted, several potential problems will have to be tackled before a reasonable design can be evolved. Hence it is most important that sufficient care is taken during the design and implementation phases of the control system development so that the associated practical issues are given due consideration.

In 'real' systems, the quality of the plant signals used for feedback purposes in the controller is far from perfect. This can be attributed to several factors such as sensor noise, sensor lag, aliasing, quantisation error etc. Improving the quality of plant signals is most important for achieving enhanced performance with advanced control strategies such as self-tuning. Some plant variables may not be readily available for measurement, hence they have to be derived from other plant signals. The most effective way of computing these variables requires to be investigated during the design of the control system.

Another important consideration is the investigation into improving the robustness of the self-tuning algorithm. Although this topic has received some consideration from researchers in the self-tuning field, techniques most suitable for the particular application will have to be identified and chosen for implementation. Robustness of the controller during long term operation of the system is to be considered. Problems such as unmodelled dynamics, disturbances, steady state offsets and non-linearities associated with the plant can have a considerable effect on the robustness properties of the control system and hence need attention during the design. The popular assumption of a persistently exciting plant, either naturally or by artificial means through the control input, is generally not true in practice.

Hence ways to make the parameter estimator of the self-tuning controller handle those periods, during which very little dynamic information about the plant is available, should be considered.

This chapter explains the design and implementation considerations employed during the development of a Self-Tuning Automatic Voltage Regulator (STAVR) based on the GPC strategy. The techniques chosen to derive the turbine generator variables which are required in the controller are summarised in Section 3.1. This section also presents several practical ways in which the quality of these plant variables has been improved. Section 3.2 briefly describes the system design aspects of a prototype STAVR and the structure of its software. This is followed by a summary of the hardware configuration adopted for the prototype STAVR, Section 3.3. Techniques which have been used to improve the robustness of the parameter estimator in the self-tuning controller are presented in Section 3.4. Finally, Section 3.5 gives the design of a Generalised Predictive controller and the use of its various tuning 'knobs' to satisfy a typical customer specification on excitation system performance.

3.1 Measurement of Plant Signals

There are several plant quantities to be obtained for use either as feedback signals for control, for protection purposes, or for the evaluation of performance of the closed-loop system. They are the generator terminal voltage, real power, reactive power, system frequency, rotor / load angle, shaft speed, field current, steam valve position, steam pressure, shaft acceleration and the condenser vacuum. The terminal voltage is the main feedback signal from which the AVR calculates the excitation demand. Real power is used for power system stabilisation, locating the generator operating point and load control. Reactive power / volt-ampere (VAr) is used for leading VAr limitation and constant VAr control. System frequency is used for the detection of the overflux condition and subsequent limiting of the voltage-to-frequency ratio.

Rotor / Load angle is the most important parameter to be monitored during transient disturbances for evaluating the performance of a controller. This signal

can also be considered for feedback purposes. Shaft speed is the main feedback signal for the governor during the run-up of the turbine. Steam valve position is used in the valve controller. Field current is employed in the convertor controller for control and protection purposes. The steam pressure, shaft acceleration and condenser vacuum are used in the governor for limiting functions.

The traditional approach to plant signal measurement is to make use of specialised hardware. Although the hardware techniques presently in use are generally acceptable, it is worthwhile investigating whether improvements can be made in this area. Since the self-tuning AVR is a software based system, it is felt that measurement techniques implemented in software should be actively considered.

There are several advantages in using a software based approach to the measurement of terminal quantities in the STAVR. It gives flexibility in design and enables modifications and improvements to be incorporated easily. Inaccuracies in measurement due to offset, drift etc. can be minimised by the use of the software approach. The system can be configured using standard off-the-shelf hardware which is advantageous for testing and maintenance purposes. Reducing the dedicated hardware required for terminal quantity measurement can improve the overall system reliability and cost effectiveness.

This section briefly describes the techniques chosen for the derivation of generator terminal quantities such as real power, reactive power, terminal voltage and frequency. The implementation considerations are then explained and the performance of the software measurement system is evaluated in terms of bandwidth and signal-to-noise ratio. The method of measuring the load angle by a hardware circuit using a toothed wheel and probe arrangement is also briefly explained.

3.1.1. Real Power Measurement

Several techniques for the measurement of 3-phase power can be considered for software implementation in the STAVR [105]. The 3-wattmeter

2-wattmeter methods, sample and derivative method [106,107] and the technique based on the Fourier analysis algorithm [21] were compared before the final choice was made. All the methods considered are suitable for both balanced and unbalanced loads. However, the sample and derivative method and the technique based on the Fourier analysis algorithm are computationally complex when compared with the wattmeter approaches and require sampling of voltage and current waveforms at precise intervals in time to obtain good results. The sample and derivative method is sensitive to inaccuracies in the sample values because of the derivative calculation. The Fourier analysis algorithm requires special hardware to 'lock' the sampling rate with the system frequency [21]. The 2-wattmeter method is simple and accurate, hence it has been chosen for implementation in the STAVR.

The equation for average 3-phase power P over a period T for the 2-wattmeter method is given by:

$$P = \frac{1}{T} \int_0^T (v_{ba}\, i_b + v_{ca}\, i_c)\ dt \qquad (3.1)$$

where $(v_{ba}\, i_b + v_{ca}\, i_c)$ is the instantaneous real power of the 3-phase system with phases a, b and c. The components $v_{ba}\, i_b$ and $v_{ca}\, i_c$ are biased ac waveforms at twice the system frequency. These ac components are removed by the respective wattmeter in a traditional 2-wattmeter arrangement. It can be shown (Appendix J) that the ac components in $v_{ba}\, i_b$ and $v_{ca}\, i_c$ cancel each other when added together to produce the instantaneous power. Thus the use of $(v_{ba}\, i_b + v_{ca}\, i_c)$ to calculate the instantaneous 3-phase power in software gives a dc value under ideal conditions. The averaging in (3.1) is achieved by digitally low-pass filtering the instantaneous power in software.

3.1.2 Reactive Power Measurement

There are several techniques for deriving the reactive power / volt-ampere (VAr) in 3-phase systems [105]. The difference between the wattmeter readings in a 2-wattmeter method, a modified version of the 2-wattmeter equation [70], the sample and derivative method [106,107], the technique based on the Fourier analysis algorithm [21], and the derivation of VAr from the volt-ampere and real

power were considered for possible incorporation into the STAVR measurement software. The sample and derivative method and the Fourier analysis technique were rejected due to the reasons given in Section 3.1.1. The derivation of VAr from volt-ampere and real power requires rms values of voltage and current, the measurement of which can cause implementation difficulties. Hence that method was also rejected. Since the techniques based on the 2-wattmeter equation are simple to implement and do not require any special hardware, it was decided to follow this route.

Unlike the 2-wattmeter equation for the real power measurement, the method based on the difference between the components $v_{ba}\, i_b$ and $v_{ca}\, i_c$ for VAr measurement gives an ac component at twice the system frequency superimposed on the dc part which represents the VAr signal. The amplitude of this ac 'ripple' in comparison with the dc part is so large that special filters are required to remove it satisfactorily without affecting the dynamic response of the measurement system. The modified equation for VAr measurement proposed in [70] improves the ratio of the amplitude of the ac 'ripple' to the dc signal by a factor of 4. Although this is a considerable improvement, special filtering is still required.

Investigation into further improvement in the VAr signal-to-ripple ratio has led to the following equation [105]:

$$Q = \frac{1}{T}\int_0^T \frac{1}{\sqrt{3}}\left[(v_{ca} + v_{cb})\, i_b + (v_{cb} - v_{ba})\, i_c\right]\, dt \qquad (3.2)$$

where Q is the average VAr of the power system. Although (3.2) is marginally more complex in terms of computational load when compared with the equation proposed in [70], it has the advantage that the instantaneous VAr given by $[(v_{ca} + v_{cb})\, i_b + (v_{cb} - v_{ba})\, i_a]$ has no ac ripple under ideal conditions when the load is perfectly balanced (see Appendix K). The averaging in (3.2) is again achieved by low-pass filtering in software.

Accurate results are obtained when using (3.2) for VAr measurement under balanced conditions, but the accuracy is degraded as the unbalance in load increases. Since the unbalance at the generator terminals is always kept low, any ac ripple in the VAr signal will be small and can be removed by the low-pass filter

which is used for averaging. Hence the use of (3.2) for VAr measurement is considered acceptable for use in the STAVR measurement software.

3.1.3 Terminal Voltage Measurement

Terminal voltage is represented by a dc signal which is generally derived in hardware by rectifying the 3-phase ac voltage at the output of a voltage transformer connected to the generator stator terminals. The 3-phase voltage obtained is converted to a 6-phase voltage by a suitable transformer before rectification to reduce the ripple content in the rectified output. The rectified signal is then smoothed by a low-pass filter to produce the terminal voltage signal.

The scheme proposed for terminal voltage measurement in software makes use of the Root Mean Square (RMS) technique [105]. Using this method, the terminal voltage can be derived as:

$$V_t = \frac{1}{T}\int_0^T \frac{\sqrt{\Sigma v^2}}{\sqrt{3}}\ dt \qquad (3.3)$$

where V_t is the average value of terminal voltage, and Σv^2 is the sum of the squares of the instantaneous value of the 3-phase voltage signals. The main advantage with this technique apart from its simplicity is that the instantaneous value of the RMS terminal voltage given by $\sqrt{(\Sigma v^2)} / \sqrt{3}$ does not have any ripple content under ideal conditions. This is shown to be true in Appendix L. The averaging in (3.3) is achieved as before by means of a low-pass filter in software which also attenuates noise in the terminal voltage signal due to harmonics, unbalance etc. which are present in the power system.

3.1.4 System Frequency Measurement

Several methods to calculate the system frequency are given in [105]. These techniques can be summarised as:

a) Measurement of period of the system voltage waveform and calculation of its reciprocal,

b) Counting of repetitions of the system voltage signal during a large 'window' which can be fixed or moving,

c) Calculation of system frequency from the shaft speed which is used in electronic governors and is generally available from a dedicated hardware peripheral using a toothed wheel and probe arrangement [9], and

d) The use of angle difference relations in trigonometry utilising the system voltage signals [12].

Out of the four techniques considered above for system frequency measurement, the ones based on period measurement and repetition count require the detection of zero crossing of the system voltage waveform. This is a time consuming process when implemented in software and can prevent other software tasks from executing at the desired rate. The measurement of system frequency from shaft speed has the disadvantage that the dedicated hardware peripheral has to be shared with the governor system which is not a good practice in high integrity applications. Moreover, the availability of the hardware peripheral cannot always be guaranteed in older turbine generator systems. Since the angle difference method requires only the system voltage signals which are already available for the calculation of P, V_t and Q, this technique is chosen for software implementation in the measurement system of the STAVR.

System frequency by the angle difference method at any instant is given by [12]:

$$\omega = (a - b) / (t_a - t_b) \qquad (3.4)$$

in which ω is the angular frequency in radians / sec, a is the phase angle (in radians) of the system voltage waveform at any instant t_a and b is the phase angle (in radians) at a previous time t_b. The angle difference relations of the sine and cosine functions are used to derive the tangent function the inverse of which generates the angle difference *(a-b)* in (3.4). The derivation of the technique is given in Appendix M.

3.1.5 Practical Considerations during Implementation

Several practical aspects need to be considered. The measurement system should be robust and should tolerate unwanted characteristics in the power system such as harmonics, unbalance etc. The sampling frequency of the incoming signals should be chosen with care and the hardware should be able to cope with the sampling rate chosen. The measurement system should be numerically robust and be adjustable as well as fault-tolerant. These practical considerations are explained in the following sub-sections.

3.1.5.1 Robustness against Input Signals of Poor Quality

It is essential that the terminal quantity measurement is robust against imperfections in the 3-phase system. The techniques proposed for use in the STAVR assume an ideal balanced 3-phase system. In practice, the sine wave is distorted with higher order harmonics, and the power system is subjected to unbalanced loads. Any such unbalance results in negative sequence components in the voltages and currents. These corrupt the calculation of the terminal quantities thereby causing unwanted ripple to appear at the output. Low-pass filters have to be provided at the output to suppress this ripple. The integration / averaging required to produce the terminal quantities is also achieved using these filters. They are incorporated in software using Z - transforms and are of double repeated pole type. They have cut-off frequencies of 20 Hz for terminal volts and 10 Hz for all other derived signals.

A problem which has been noticed with modern high speed A / D converter boards is that they can occasionally produce a wrong digital value corresponding to an analogue signal being sampled. Although this is rare, its effect cannot always be satisfactorily removed by simple low-pass filtering, because the amplitude of the 'spike' can be large. This problem is generally tackled by some form of spike filtering. The popular methods to achieve spike filtering are logical filtering and median selection.

Logical filtering applies a high and low limit to the digitised input signal where the limit used is based on the maximum rate at which the analogue signal can change in practice. Median selection requires three successive samples of the input signal and selects the middle value of the three samples for calculation. Although median selection is generally considered to be a more effective technique for spike filtering, it requires three successive values for decision making. Since logical filtering is simpler to implement, it has been chosen.

3.1.5.2 Sampling Rate of the Measurement System

The rate at which the signals have to be sampled and the outputs updated is governed by various factors. From a functional point of view, it may be desirable to have a very fast update rate so that the STAVR software is presented with the most up-to-date values. But the processing power available in the system determines the execution speed and hence the update rate which is practically achievable with that hardware. In the case of the STAVR, it is found that a sampling rate of approximately 1 kHz can be achieved with standard off-the-shelf boards. This is considered acceptable since it is known that the STAVR software needs to have an update rate of only 50 to 100 Hz.

There are other factors to be considered while choosing the rate at which the voltage and current waveforms are to be sampled and processed. Higher order harmonics present in the signals will be aliased to frequencies below the Nyquist rate of sampling, thus appearing as low frequency components in the digitised waveform. Since the harmonic frequencies are known, a careful choice of the sampling rate can ensure that the aliased components are shifted away from the low frequency region as much as possible. Thus the effect of the output low-pass filters on these components is maximised. It can be shown that choosing a sampling frequency midway between two harmonic frequencies rather than coincident with one of them also gives an improvement.

In the STAVR, a sampling frequency of 925 Hz has been chosen for reading the analogue input signals. This does not cause any implementation problems as it is in the region of the 1 kHz seen to be possible above. Assuming

a 50 Hz power system, a sampling frequency of 925 Hz ensures that components up to the 9th harmonic (450 Hz) are reconstructed without any frequency shift since the Nyquist frequency of sampling is 462.5 Hz. Higher order harmonics are progressively mapped on to lower frequencies, but the lowest of these aliased frequencies, which is at 25 Hz, occurs for the 18th (900 Hz) and 19th (950 Hz) harmonics only and these are negligible. Thus the low-pass filtering employed at the output is able to attenuate the harmonics to an acceptable level since the harmonic content progressively reduces as the harmonic order increases. The analysis assumes that components above the 20th harmonic can be neglected.

3.1.5.3 Numerical Robustness of the Measurement System

For frequency measurement, the technique uses the tangent function which approaches infinity as the angle approaches π / 2 radians. Thus, numerical problems can arise during calculation if the sampling instants t_a and t_b are separated by approximately π / 2 radians of the sine wave at that frequency. Since the maximum frequency to be measured is generally specified as 60 Hz for a 50 Hz system, it is proposed to separate these sampling instants by approximately π / 4 radians at that frequency. Any lower frequency being measured will only cause lesser separation between t_a and t_b in terms of radians and hence does not cause any numerical problems.

3.1.5.4 Effect of Sequential Sampling

In the analysis of the various techniques for terminal quantity measurement, it is assumed that the voltage and current signals are sampled simultaneously. This cannot normally be achieved with standard off-the-shelf A / D boards since they can only read input channels sequentially which will introduce some phase error in the measurement. To minimise this error, the voltages and currents required for a calculation have to be read at the maximum speed possible. Even then, there will be a delay between the first and the last readings which is equal to the average A / D conversion time multiplied by the number of channels read. The effect of this delay on the derived terminal quantities can be reduced to

some extent by suitably selecting the order in which the signals are read. An optimum solution was arrived at by trial and error which gave a sequence order of i_c, v_c, v_b, v_a and i_b.

3.1.5.5 Calibration Facility and Fault Tolerance

The terminal quantities derived in software sometimes need fine-tuning to remove any small dc error due to inaccuracies in the voltage and current transformers. The facility to nullify this offset in software is a useful feature and will improve the overall accuracy of the measurement system. In the measurement system used, a facility for calibration is provided through the operator interface of the system. The calibration is performed by applying a gain term and an offset to the raw terminal quantities.

Another useful feature which has been incorporated in software is an intelligent front-end for the voltage and current signals which are sampled through the A / D board. This software checks the amplitude and phase of the voltage and current signals arriving during start-up and then finds correction factors if the signals do not confirm to the amplitude and phase relationship expected. During normal operation of the system, the raw voltage and current samples obtained are corrected by means of these factors before use in deriving the terminal quantities.

3.1.6 Performance Evaluation of the Measurement System

The performance of the software measurement system was evaluated using a 3-phase simulator and the micro-alternator system. The hardware set-up consisted of a BVME 380 CPU board [108] and BVME 650 analogue input / output board [109]. Details of the hardware are given in Section 3.3. This hardware is same as that used to implement the STAVR software measurement system. Hence these results are directly applicable.

The functional specification upon the software measurement system includes:

a) Terminal voltage should be measured with an accuracy of better than 0.25% with a bandwidth of typically 10 to 15 Hz.

b) Real power and VAr signals should have an accuracy of typically 0.5% and a bandwidth of 5 to 10 Hz.

c) System frequency signal should have an accuracy of 0.5% and a bandwidth of 2 to 5 Hz.

The terminal quantity measurement software was initially tested under various balanced load conditions using a 3-phase hardware simulator. The simulator consists of two 3-phase sine wave generators representing the voltage and current in the system. The amplitude of the sine waves and the phase angle between the two generators can be varied to represent the power system at various loads and power factors. The system behaved satisfactorily under laboratory conditions with an overall accuracy of better than 0.1% for terminal voltage and 0.25% for all other derived terminal quantities.

Further tests were conducted using signals from the micro-alternator system. This evaluated the performance of the measurement system under more realistic conditions. Figure 3.1 shows the frequency response characteristic of the real power signal from the micro-alternator system obtained using a Frequency Response Analyser (FRA) based on the swept sine wave technique. It is observed that a band-width of 6 Hz has been obtained with the software measurement system which is acceptable. Figure 3.2 illustrates the signal-to-noise ratio (SNR) of the real power signal from the micro-alternator system. This result has been obtained using a FFT analyser performing a power spectrum analysis of the real power signal. It is seen that the SNR is better than 60 dB which indicates that the noise in the real power signal is within 0.1% of its range. This too is considered to be an acceptable value. The overall accuracy of the real power signal was

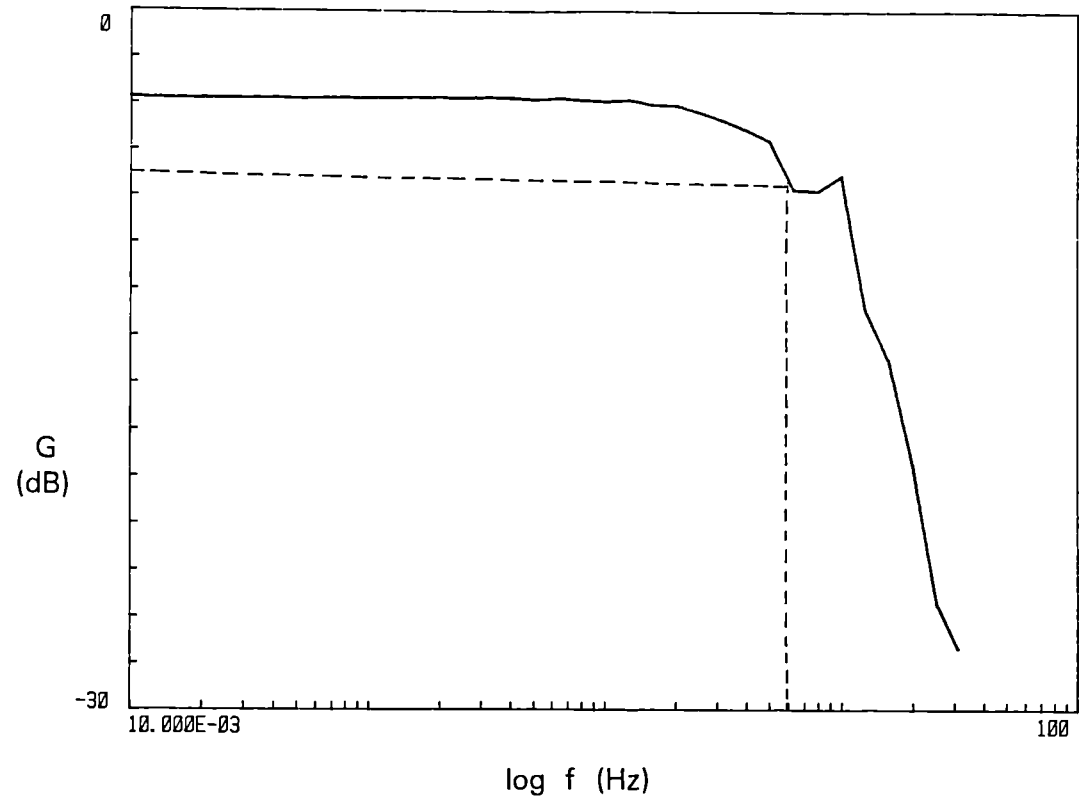

Fig. 3.1 Frequency response of real power signal using micro-alternator.

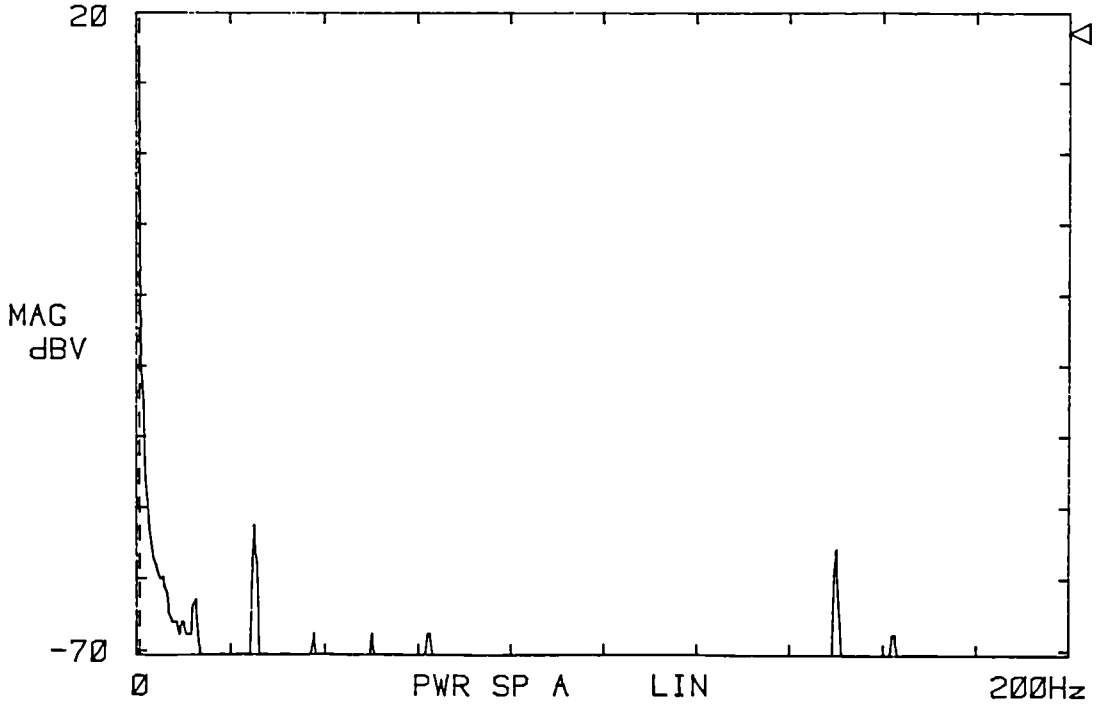

Fig. 3.2 Power spectrum of real power signal using micro-alternator.

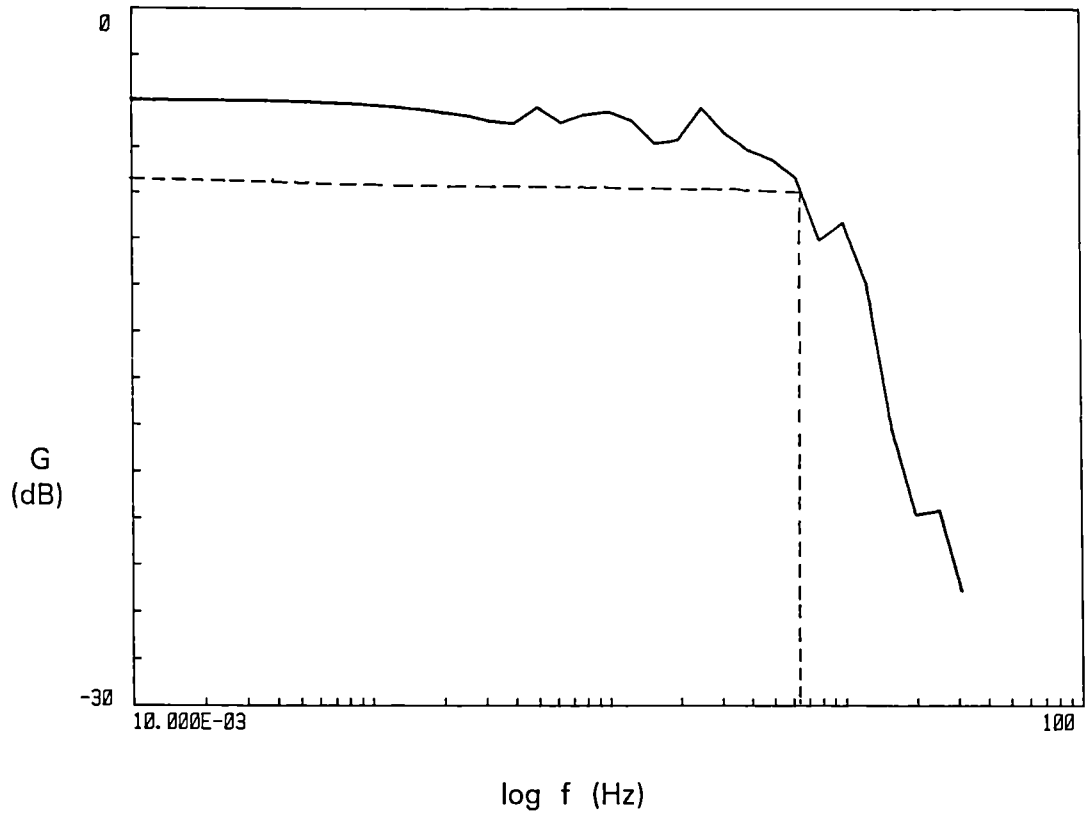

Fig. 3.3 Frequency response of reactive power signal using micro-alternator.

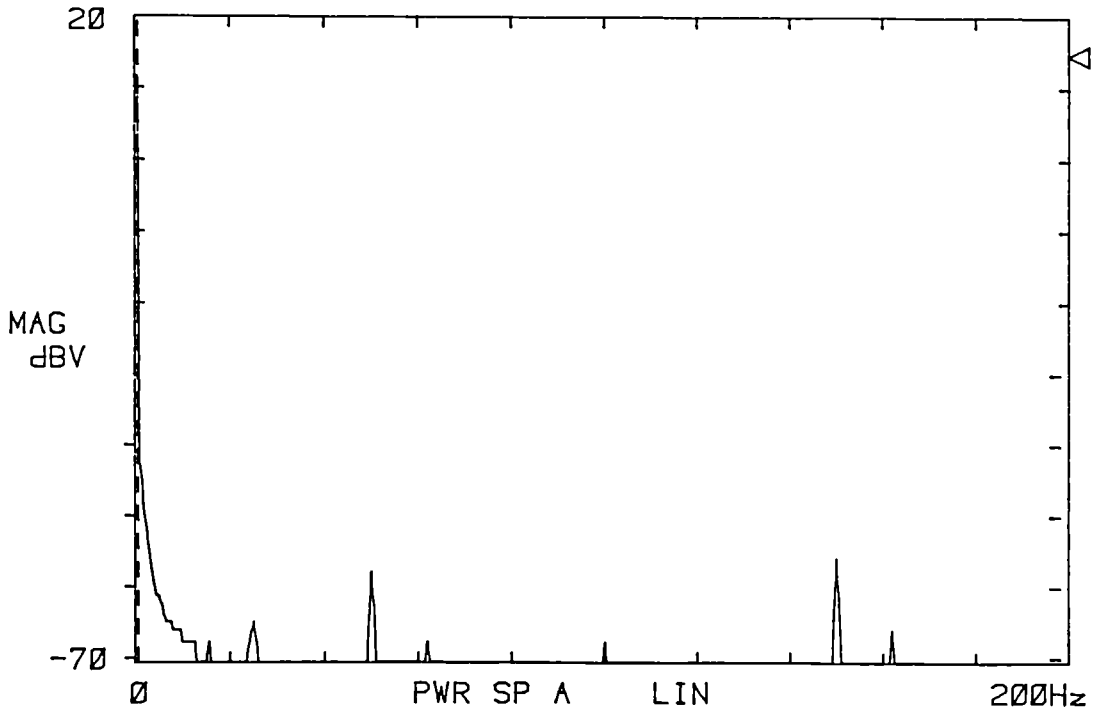

Fig. 3.4 Power spectrum of reactive power signal using micro-alternator.

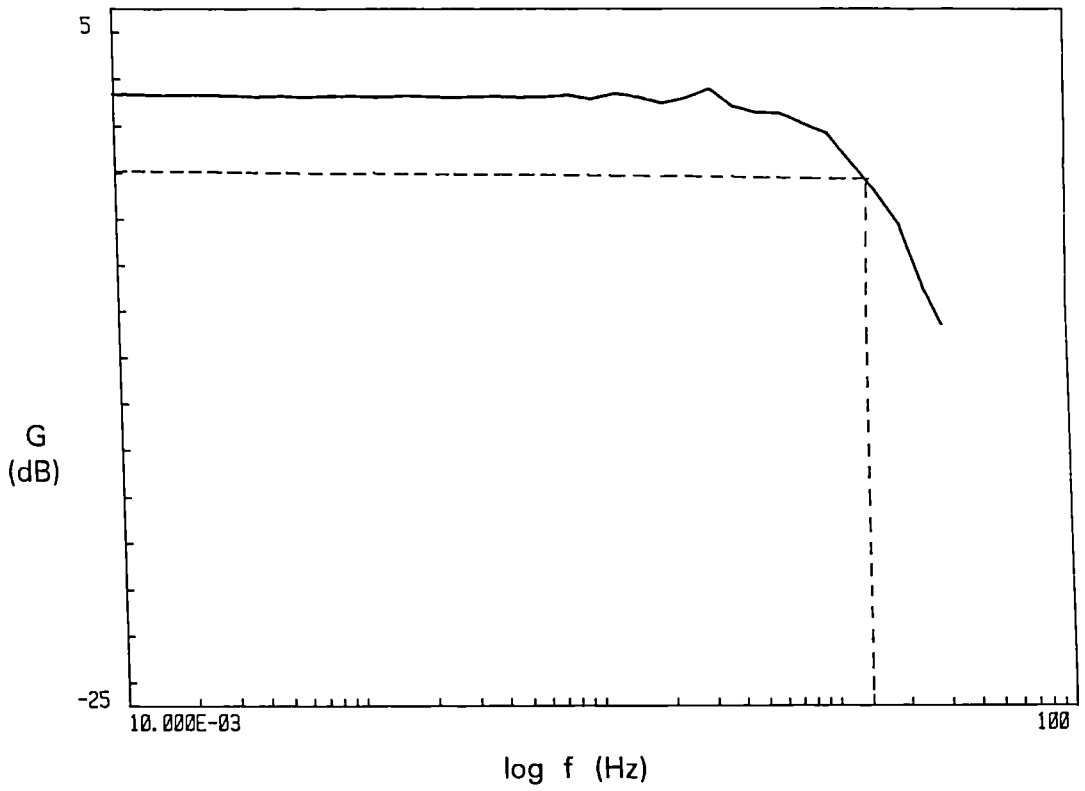

Fig. 3.5 Frequency response of terminal voltage signal using micro-alternator.

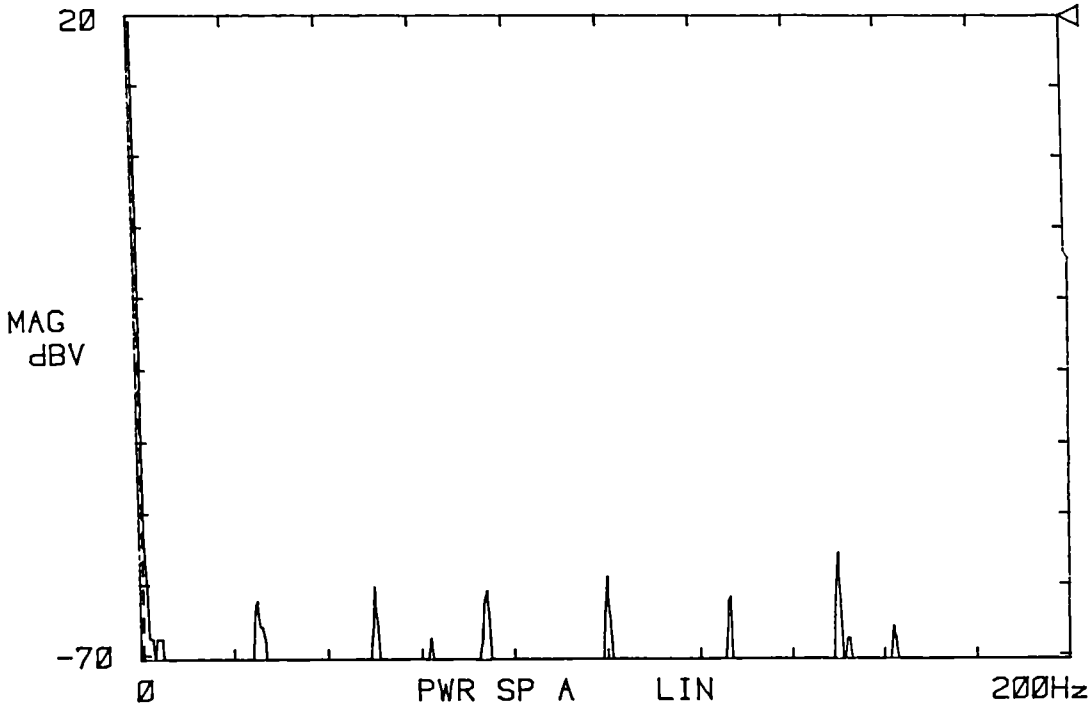

Fig. 3.6 Power spectrum of terminal voltage signal using micro-alternator.

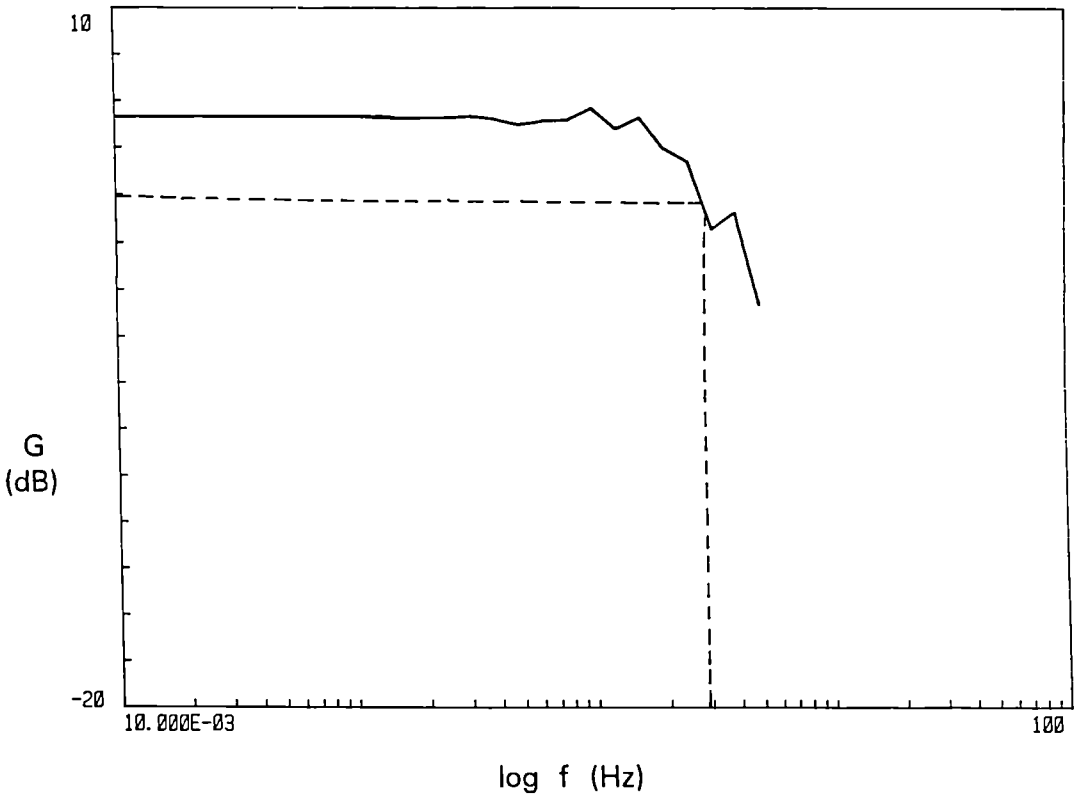

Fig. 3.7 Frequency response of system frequency signal using micro-alternator.

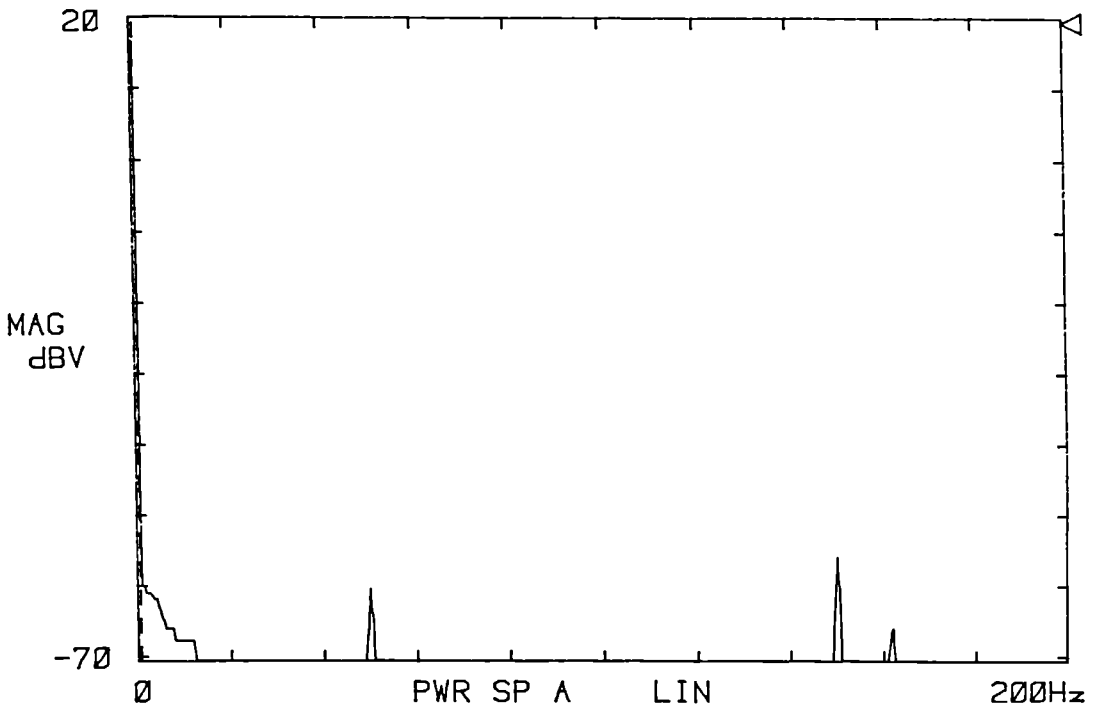

Fig. 3.8 Power spectrum of system frequency signal using micro-alternator.

verified to be within 0.5% by conducting 'spot' checks using a digital 3-phase wattmeter.

Figures 3.3 and 3 4 show the frequency response characteristic and the power spectrum respectively of the VAr signal from the software measurement system when input signals from the micro-alternator were used. It can be observed that a bandwidth of 6.5 Hz and a SNR of better than 60 dB are obtained which are acceptable. The dc accuracy of the signal was also found to be within acceptable limits.

The frequency response characteristic given by Figure 3.5 and the power spectrum by Figure 3.6 of the terminal voltage signal are observed to give a bandwidth of 13 Hz and a SNR of better than 60 dB. Similarly a bandwidth of better than 2.5 Hz and a SNR of better than 60 dB are obtained for the system frequency signal as shown in Figures 3.7 and 3.8 respectively. The dc accuracy of the terminal voltage and the system frequency signals from the software measurement system were also verified to be acceptable. Thus the software measurement system proposed for use in the STAVR is found to satisfy the requirements of a typical excitation control system.

3.1.7 Load Angle Measurement

Load angle is the electrical angle between the generator field mmf and the infinite busbar voltage. A study of the pattern of oscillation of the load angle following a fault in the power system gives a good indication of whether the system is transiently stable under fault conditions. Traditionally, the load angle is determined by measuring the phase difference between the infinite busbar voltage and the voltage from a tachogenerator mounted on the machine shaft. Zero-setting of the load angle transducer in this case is achieved by a cumbersome procedure.

The use of shaft encoders to derive the load angle is also a popular technique. Here, pulses from a toothed wheel which is mounted on the generator shaft have been used [46]. There are several advantages with the chosen toothed

wheel technique over the use of encoders to derive the load angle. Firstly, the accuracy of the measurement is determined by the basic clock of the transducer and not by the resolution of the encoder. Secondly, the pulses picked up from the toothed wheel are of considerably lower frequency than from an encoder and hence are more immune to noise. Toothed wheels of the type used for the load angle transducer are installed for the governor system to measure speed in modern turbine generators. This is also an important advantage over the use of encoders during field trials. Since the load angle is being measured primarily for monitoring purposes during the evaluation of the STAVR, a hardware approach to its derivation is considered to be acceptable.

The principle of operation of the load angle transducer built for the STAVR work is shown in Figure 3.9. The transducer makes use of pulses from a toothed wheel which is mounted on the prime mover shaft of the micro-alternator system and a phase voltage from the busbar. Pulses of two different frequencies are picked up from the wheel. One is a pulse per tooth and the other is a pulse per rotation of the shaft. These pulses are shaped and are used to derive a rotor shaft pulse train of nominally 10 mSec ON and 10 mSec OFF for a 50 Hz system. This pulse train is phase shifted through a precise angle such that the shifted signal is in phase with a similar pulse train derived from the busbar voltage on no-load. This zero-setting of the transducer is accomplished by means of a 12-bit digital switch. As the generator is progressively loaded, the rotor advances with respect to the reference frame produced by the busbar voltage and this advance is measured by the phase difference timer.

The accuracy of the measured load angle N_1 depends on the system frequency and can be corrected for frequency variations by using the output N_2 from the transducer which represents half the period of the busbar voltage. Hence the corrected load angle is given by $\pi N_1 / N_2$ radians.

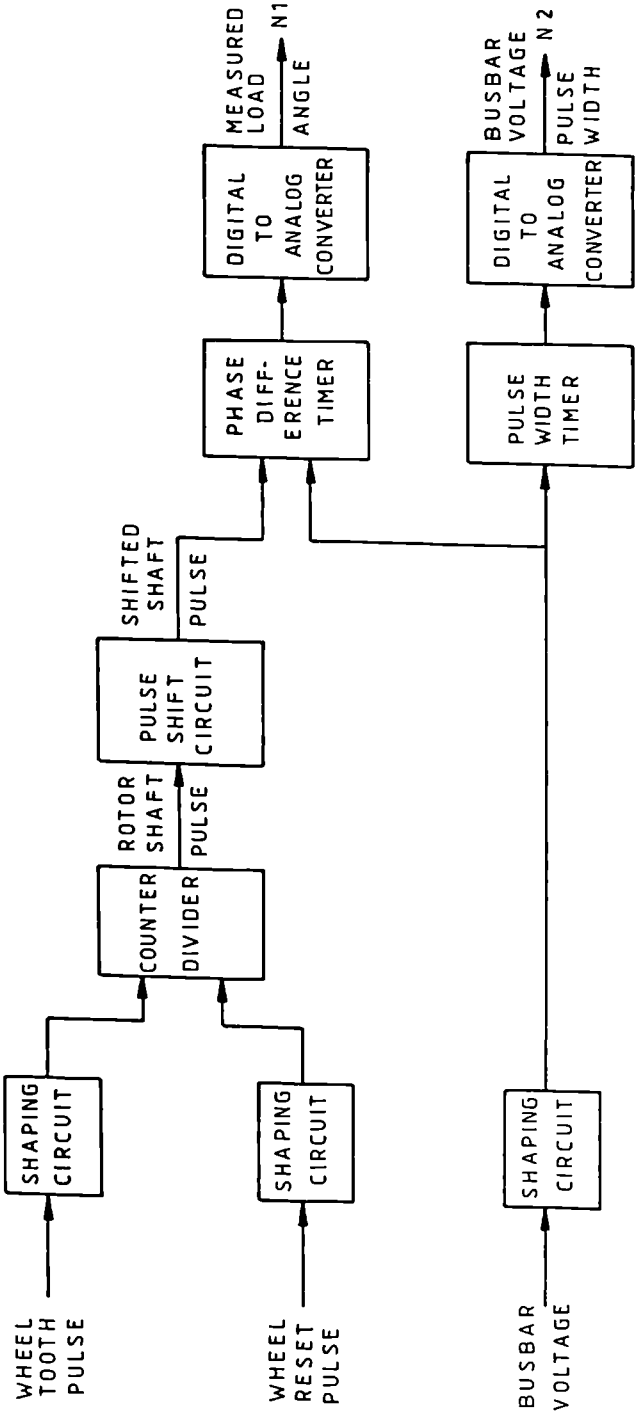

Fig. 3.9 Block diagram of the load angle transducer.

3.2 System / Software Design

It is desirable that the design methodology used for the STAVR considers the overall functional requirements as its starting point. This leads to a 'top-down' approach in system design and is favoured in many software based systems. The main advantage with this approach is that the resulting system would have a good structure leading to software which is easy to understand and maintain. This technique ensures that the overall functional specifications of the system are understood in sufficient detail during the design stage and that the system is documented as the design progresses.

The methodology used is called Structured Design [110]. This takes the form of an Implementation Model of the system which considers the requirements of the desired end-product and the constraints of the final hardware design. The Implementation Model consists of a structured set of Data Flow Diagrams (DFDs) which show the flow of data to and from one or more processes. Each process on a DFD is further represented by a more detailed DFD to show data flowing between sub-processes. This is repeated until, at the lowest level, each sub-process is described by a 'mini-specification'. Thus a 'top-down' structure is created for the system.

The Structured Design methodology could be followed only to a limited extent during the STAVR design. This was primarily due to the nature of the work which required a moderate amount of 'software prototyping'. Hence only higher level DFDs were produced during the design of the system. The mini-specification for each process was written as a file header in the respective source code file.

The important processes from two of the higher level DFDs have been combined to show a conceptual DFD of the STAVR, Figure 3.10. The concept of the system 'database' and how the various processes use parts of this database are shown by directional data flow lines in the figure. A 'window' of the database to the outside world has been provided through the 'Communicate with MMI and Data Logger' process which enables the modification of 'system parameters' and

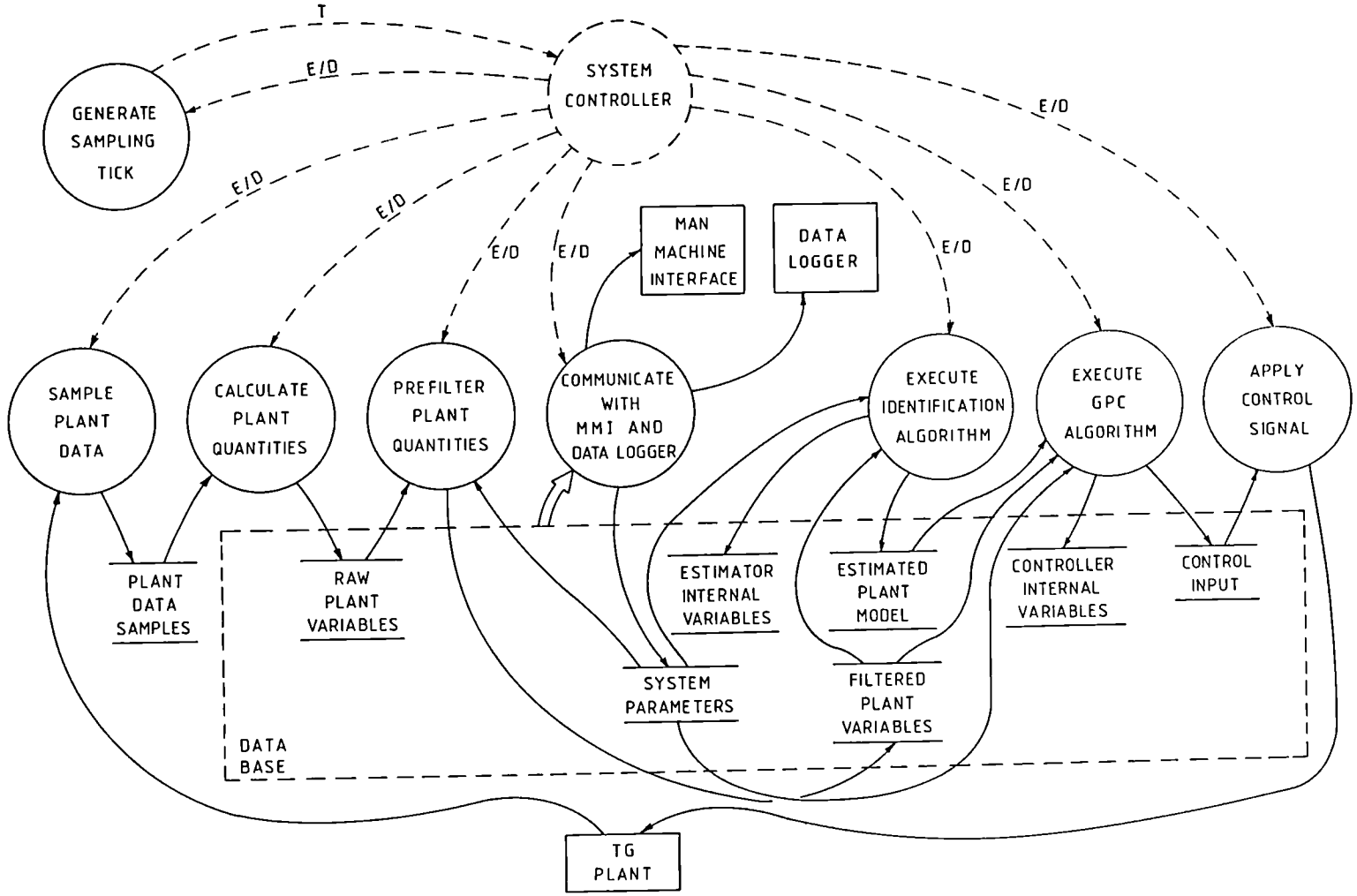

Fig. 3.10 Conceptual Data Flow Diagram of the self-tuning AVR.

monitoring of variables in the database. Processes which collect and pre-process plant data supply these variables to the identification and control processes through the database. The identification process estimates the coefficients of the chosen plant model and passes it to the GPC process. The GPC process computes the control input and supplies it to the 'Apply control signal' process which sends it to the TG plant.

The various processes in the system are enabled / disabled for execution through the 'E/D' control flow lines by the 'System Controller'. The System Controller activities are triggered (T) by the 'Generate sampling tick' process which signals the start of the sampling instant. In the case of the STAVR, the main program from which the various software modules are invoked can be regarded as the system controller.

The use of the Structured Design methodology for software development has enabled the generation of 'modular' software. The software modules have been coded using a high level language 'C' [111] which gives execution efficient code. Execution efficiency in real time control applications is an important consideration, especially when using a computationally intense self-tuning algorithm such as GPC [26]. The software development was carried out on a Motorola 1131 Development System [112] under the UNIX Operating System environment. The 'object' modules were generated and 'linked' using the development system and downloaded to the 'target' prototype STAVR through a RS-232 serial link where it was executed under the control of a Debug Monitor FBUG+ [113].

3.3 Hardware Description of the STAVR

The prototype STAVR uses a multiprocessor architecture for the execution of its software. The system is constructed from a range of commercially available computer modules. The hardware is built using 'VMEbus' compatible modules in a 19" rack which communicate with each other through the VME backplane. The CPU modules are designed using the M68000 family of microprocessors.

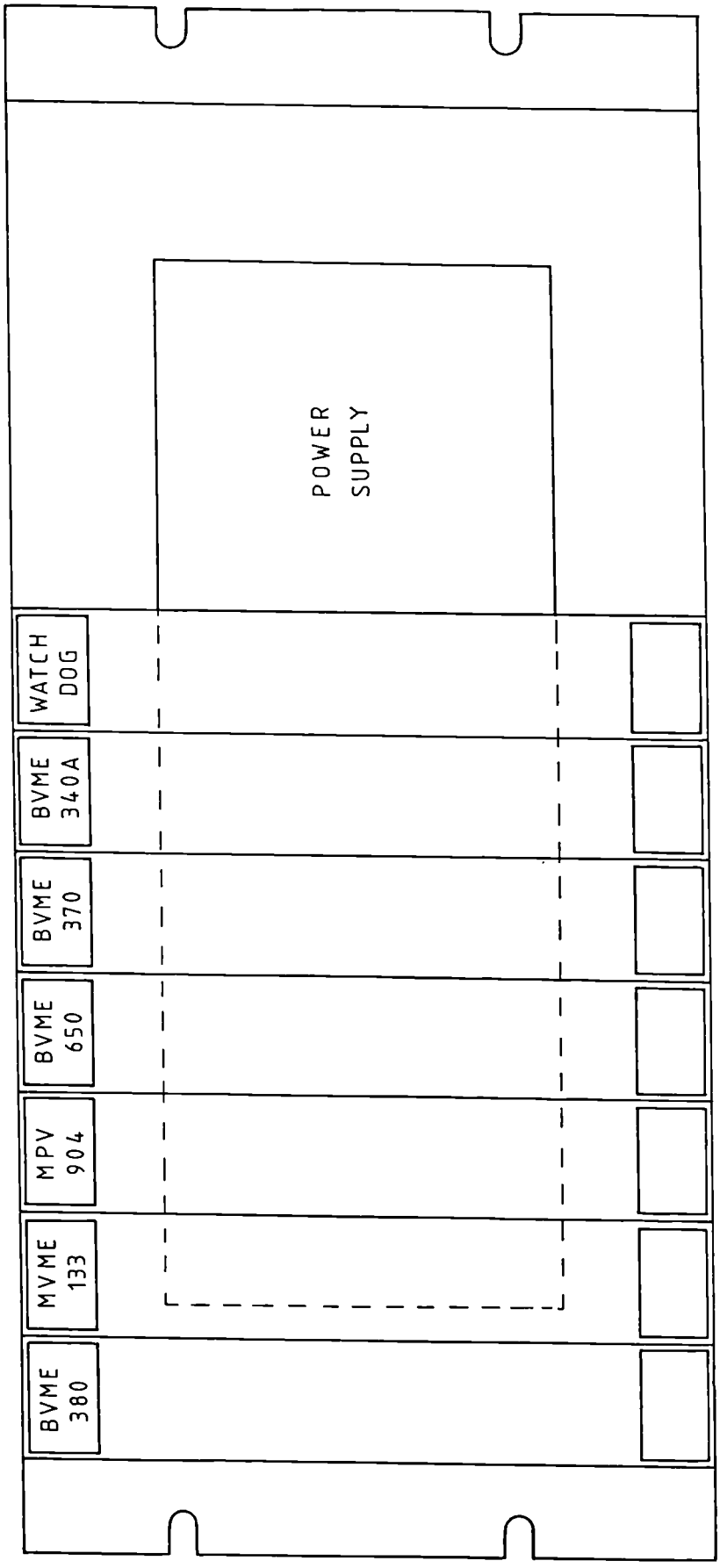

Fig. 3.11 Hardware layout of the prototype self-tuning AVR.

The hardware layout of the STAVR system is given in Figure 3.11. It consists of a 19" sub-rack with a power supply and VME backplane into which the various modules are plugged in. The system has been designed such that it has a moderate amount of spare processing power. This enables the implementation of more complex control systems such as a multivariable TG controller (See Chapter 6) using the same hardware. The hardware is designed for distributed processing whereby the overall system is split into various high level tasks which are executed on different CPU modules.

The prototype STAVR makes use of 3 CPU boards, viz. BVME 380 [108], BVME 370 [108], and MVME 133 [114]. The BVME 370 module has been designed using the Motorola MC68030 32-bit CPU with a clock rate of 40 MHz. The board is equipped with a hardware Floating Point Unit (FPU) MC68882 for faster floating point operations and has 4 MBytes of dual-ported dynamic RAM for shared memory functions. The BVME 380 CPU module is similar to the BVME 370 board except that it runs at 25 MHz and has 1 MByte of dual-ported dynamic RAM. The MVME 133 CPU module is based on a MC68020 32-bit CPU running at 12.5 MHz. It also has a FPU MC68881 and has 1 MByte of dynamic RAM. The modules communicate through the VMEbus and share the system database by means of the global memory arrangement. The CPU modules interrupt each other by a 'mailbox' interrupt scheme to initiate the execution of the tasks assigned to them.

All the 'background' tasks such as the managing of the Man Machine Interface (MMI), updating of system parameter database, passing of data to the logger and the generation of the sampling 'tick' are handled by the MVME 133 module. The MMI of the prototype STAVR is shown in Figure 3.12. The interface panel provides facilities for adjustment of set-point, selection and indication of automatic / manual control modes of operation, display of plant variables and internal parameters of the controller, as well as the adjustment of control input in 'manual' mode and controller presets. The MVME 133 CPU communicates with the MMI panel through the digital input / output module MVME 340A [115].

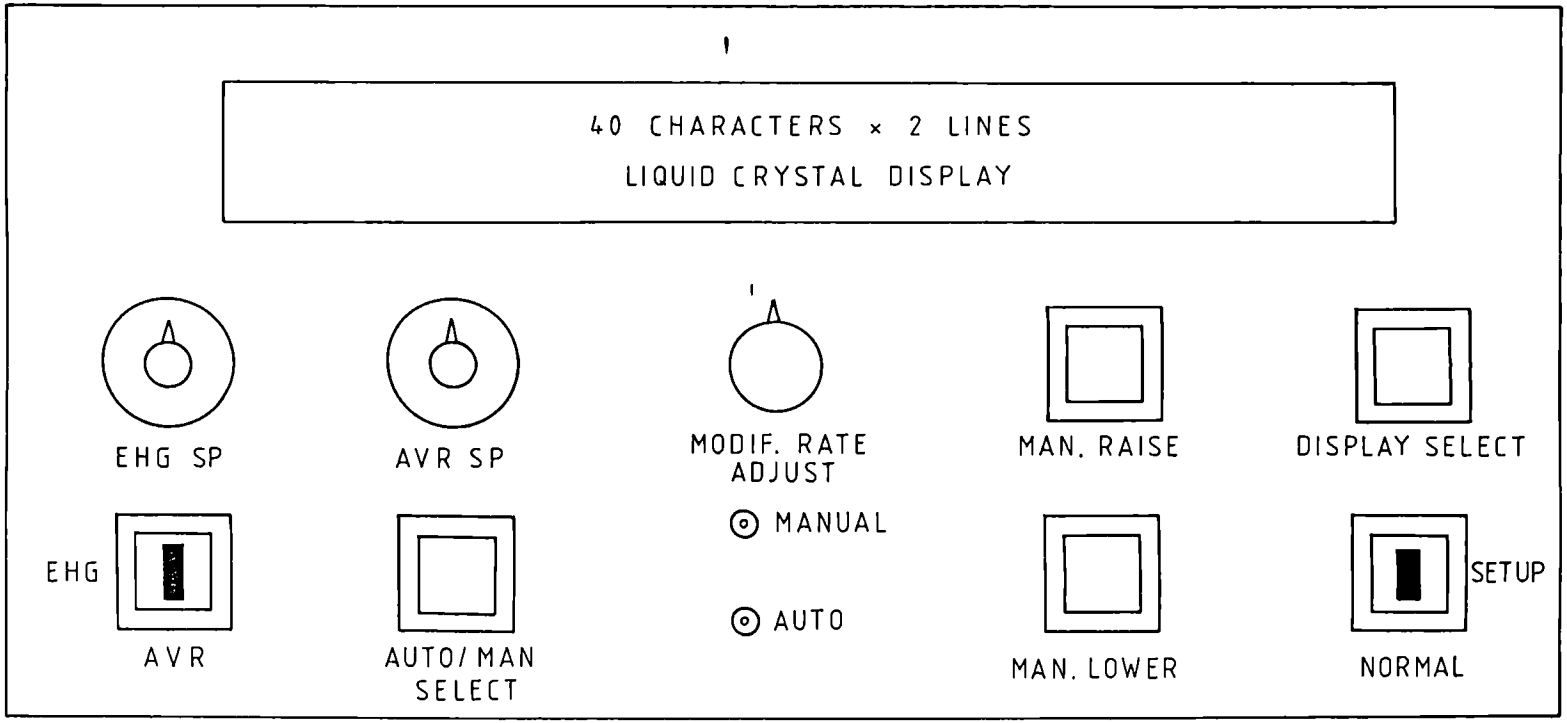

Fig. 3.12 Man Machine Interface of the prototype self-tuning AVR.

The MVME 133 CPU is responsible for updating the system parameter database in accordance with the commands received from the MMI. The updating is done only when the other CPU modules have finished executing their tasks so that the integrity of the database is maintained at all times. The data logging function of the system is intended for diagnostic purposes only and enables the monitoring of system variables, controller parameter etc. as analogue signals if required. This function is achieved by the use of a 16-channel analogue output module MPV904 [116] which is driven by the MVME 133 CPU board based on values obtained from the system database.

The plant data is acquired by the BVME 650 analogue input / output module [109]. Signal conditioning at the input of the BVME 650 board is achieved by voltage and current transformers which are designed to measure phase voltages and currents of up to 1.5 times their rated value. The BVME 650 board has a limited 'intelligence' on-board in the form of timers and Direct Memory Access (DMA) facility. This enables the board to be programmed for collecting plant data samples at regular intervals and storing them in its dual-ported memory without the help of a CPU.

The controller sampling 'ticks' generated by the MVME 133 CPU by means of its timers trigger the BVME 380 CPU through the 'mailbox' interrupt scheme. On receipt of this interrupt, the BVME 380 starts executing its task of collecting and preparing the plant data for control purposes. The BVME 380 retrieves the plant data samples collected by the BVME 650 board during the previous sampling period and processes them to derive plant variables such as the terminal voltage and power. The BVME 380 then prefilters before making them available in the system database and interrupts the BVME 370 module through the 'mailbox'.

The BVME 370 is the fastest CPU in the system and hence the computationally intense self-tuning control algorithm is assigned to it. It executes the identification and control algorithms using plant data supplied by the BVME 380 module through the database and the system parameters / presets made available in the database by the MVME 133 module. When the control input has been

calculated, the BVME 370 CPU applies the signal to the plant through the analogue output port of the BVME 650 module.

A hardware Watchdog module has been incorporated in the system which requires its input to be 'toggled' at regular intervals to prevent a 'time-out'. The toggling of the Watchdog input is done by the BVME 370 CPU. In the unlikely event of a Watchdog time-out, the system gets automatically reset and a 'safe' value of control input is applied to the plant through a relay until the Watchdog is once again made 'healthy'.

3.4 Robustness Improvement in the Parameter Estimator

A robust parameter estimator is central to the performance of a self-tuning controller. This requirement has been acknowledged for some time now, and several methods to improve the robustness in the estimator have been proposed [47,39,117]. This section briefly describes the techniques employed for this purpose.

3.4.1 Washout Filtering of Plant Data

The STAVR is based on the GPC strategy which employs a CARIMA plant model. This model requires the use of differential data in the parameter estimator. Although this is a convenient way of avoiding biased estimates in the presence of dc offsets and load disturbances, it generally leads to poor estimates of parameters in situations where the plant is in a steady-state condition for a long time. This is because the CARIMA model tends to over-emphasise the high frequency dynamics of the system, making it difficult for the estimator to produce a good match on the low frequency part of the response.

In the STAVR, the use of a CARMA model with positional data will lead to biased parameter estimates due to the presence of dc offsets in the input / output data during synchronised operation of the generator as well as due to load disturbances. Hence a CARMA plant model with the input / output data pre-filtered by a 'washout' function has been used in the parameter estimator of the

STAVR. The 'washout' filter is essentially a high-pass filter of the form $sT_w / (1 + sT_w)$ where T_w is the washout time constant which is made adjustable. The advantage of this approach is that it eliminates the undesirable effects of offsets and load disturbances on the parameter estimates, but allows more effective use of the low frequency dynamic information.

In the STAVR, a sampled data version of the washout filter is used with the time constant T_w set to 10 Sec; thus dynamic information above 16 mHz is passed into the estimator without any attenuation. The provision to modify the washout filter to a band-pass filter as proposed in [89] is made in the STAVR, but has been found to offer no additional advantage in practice. It should be noted that the bandwidth of the input / output signals in combination with the washout filter performs the band-pass function in the STAVR.

3.4.2 The Use of a Variable Forgetting Factor

The advantage of using a variable forgetting factor scheme in the estimator have been explained in Chapter 1. In the STAVR, the desired asymptotic memory length of the estimator N_m of the variable forgetting factor scheme is set to 10^4. The expected noise variance of the plant σ^2 is set to 10^{-5}. Thus the amount of dynamic information $(N_m \sigma^2)$ which the variable forgetting factor scheme aims to preserve in the estimator is set to 0.1. This was observed during STAVR trials to be a reasonable value which gave the required sensitivity to the estimator. However, a provision has been made to automatically adjust this value by the estimator depending on the condition of the covariance matrix, should the need arise. The lower limit of the variable forgetting factor is set to 0.3 in the STAVR.

3.4.3 The Use of Random Walk

The facility of a 'random walk' is useful when it is required to increase the dynamic information content in the estimator with the system under closed-loop control. It involves artificially perturbing the plant during normal control operation by modulating the control signal with a noise signal. In the STAVR, the random walk signal is a binary sequence which toggles between 0 and 0.05 pu and has a

random duration of between 5 to 10 sample periods. The random walk sequence lasts for 100 sample periods. This facility can be invoked either manually by the operator or automatically by the estimator when it detects a need to improve its dynamic information content. Another situation where a random walk is performed is when it is known that the dynamics of the system have changed considerably, for example, when the main circuit breaker of the generator has changed state.

3.4.4 Dynamic Information Monitoring and Estimator Freeze

Although the parameter estimator is working continuously to track the varying dynamics of the system, it is recommended that the estimation process is suspended when little dynamic information about the plant is available from its input / output data. This condition arises when the turbine generator is operating without any perturbation and a 'freeze' on the estimator during this period helps to conserve the dynamic information already available in the estimator. This 'freeze' facility is commonly recommended in parameter estimators and helps to further improve the performance of the variable forgetting factor scheme.

Another operating condition during which an estimator freeze is highly desirable is when the plant is subjected to severe disturbances [46,47,39]. These abnormal conditions occasionally arise in turbine generators due to sudden load changes and faults in the power system. However they are transient in nature and typically persist only for a few machine cycles. The system dynamics will be considerably different during these abnormal conditions, but since the faults generally are cleared very quickly, it is better for robustness in the parameter estimator that it is frozen during these 'glitches'.

The dynamic information content in the input / output data of the plant can be checked against a 'window' to freeze the estimator. A measure of the information can be obtained from the expression, $\epsilon^2(t) / [1 + \mathbf{d}^T(t)\, \mathbf{P}(t-1)\, \mathbf{d}(t)]$, where $\epsilon(t)$ is the estimation error, $\mathbf{d}(t)$ is the data vector and $\mathbf{P}(t-1)$ is the covariance matrix of the estimator [81]. When the information content in the data vector is outside a pre-specified window, the estimator is frozen. This feature is not invoked

when the plant is artificially perturbed through the controller in situations such as the estimator start-up or the random walk.

The use of a window to freeze the estimator requires the mean value of dynamic information that can be expected from the turbine generator during normal operating conditions. Since this can only be obtained after extensive field trails, an estimate of the same was produced by low-pass filtering with a large time constant the instantaneous values of the measure of information content in the data vector. The filter time constant was chosen to be 20 Sec and the freeze facility was invoked only after the first 10,000 samples to enable the mean value of the information content to be available for the freeze operation. This approach provides a moving window arrangement for the freeze facility since the mean value of the measure of information content is constantly updated through the low-pass filter.

The size of the window is made adjustable and during the STAVR tests, it was found that choosing the upper threshold of the window to be 100 times the mean value of the measure of dynamic information and the lower threshold to be 1/10th of the mean value gives satisfactory results. The duration of freeze when the instantaneous measure of information content goes below the lower threshold is only for 1 sample while the same when the upper threshold is exceeded is set to 25 samples. This assumes that the effect of a sudden disturbance in the plant disappears within 0.5 Sec for a sampling period of 0.02 Sec which is true for the majority of disturbances.

3.4.5 Covariance Matrix Trace Monitoring

The state of a parameter estimator is reflected in its covariance matrix. The sum of the diagonal elements of the covariance matrix, ie. its trace, can be effectively used to determine whether some corrective action should be taken to improve the condition of the estimator. A very low value of the trace indicates that the estimator is conserving too much information about the plant and hence the adaptability of the estimator to a change in the plant dynamics is very poor. A very high value of the trace signifies that there is too little information about the plant

in the estimator leading to a very sensitive estimator. Both the above conditions should be avoided to achieve a robust estimator.

In the STAVR, the trace of the covariance matrix is monitored and if it goes below a user-defined low limit, all the diagonal elements of the matrix are replaced by the low limit. This gives an artificial boost to the covariance matrix thus making it more sensitive to variations in the plant dynamics. The memory length of the estimator N_m used by the variable forgetting factor scheme is simultaneously reduced to 90% of its value to indicate to the forgetting scheme that it should conserve only a lesser amount of the dynamic information of the plant in the future. This scheme helps to keep the trace higher than its low limit thus leading to a more sensitive estimator.

If the trace is found to exceed a pre-defined high limit indicating that there is too little information about the plant in the estimator, a 'random walk' is invoked. This will bring more dynamic information to the parameter estimator thus reducing the trace of its covariance matrix. At the same time the memory length of the estimator used by the variable forgetting factor scheme is increased to 110% of its value, which will eventually make the forgetting scheme conserve more dynamic information. This helps to keep the trace at a lower value thus reducing the sensitivity of the estimator.

The low and high limits of the trace of the covariance matrix should be chosen such that the parameter estimator has an acceptable level of sensitivity. In the STAVR, trials on the micro-alternator system have shown that values of 10^3 and 10^4 for the low and high limits of the trace respectively give acceptable adaptability to the parameter estimator. It should be noted that the monitoring of the trace is not invoked at start-up of the estimator nor during the 'random walk'.

3.4.6 Plant Gain Boosting

It is observed in many 'real' systems that the coefficients of the $B(z^{-1})$ polynomial of the plant model are very small. This may be due to a low plant gain, the presence of large time constants in the plant, or the choice of a fast sampling

rate. These small B coefficients can sometimes adversely affect the performance of the estimator in terms of its robustness and ability to converge. A solution to this problem is to artificially 'boost' the dc gain of the plant so that the B coefficients are increased by the same factor. In this case the control input signal used for the estimation and control algorithms will be small when compared with the actual signal applied to the plant, by a factor equal to the 'boost'.

This procedure of artificially increasing the plant gain by a factor 'boost' changes the real weighting provided by the 'move suppression' factor λ in the GPC cost function. To obtain the original weighting of the control increment due to λ in the cost function, a modified value λ' has to be used in the control law where λ' is given by $(\lambda\ Boost^2)$. A proof of this is given in Appendix N. In the STAVR a boost value of 100 has been found to give the best results.

3.4.7 Start-up of the Parameter Estimator

The parameter estimation of the STAVR is started with zero initial estimates. To reflect the uncertainty in the initial parameter values, the covariance matrix is initiated with a large value $10^8 \boldsymbol{I}$ where $\boldsymbol{I}$ is an identity matrix of the required size. Random values of control input are applied for the first 100 sample periods to enable the estimator to produce reasonable parameter values before invoking the control law calculation. The maximum amplitude of the random signal is set to 0.1 pu and the pulse width is randomly chosen to be between 5 and 25 sample periods. The numerically robust U-D factorised covariance update method described in Chapter 1 has been used in the parameter estimator.

3.5 Design of Controller Parameters

At the present time, there is no 'off-the-shelf' complete performance specification for large turbine driven generators and their excitation systems [4]. The relevant IEEE standard [6] gives a range of dynamic performance indexes for excitation control which are so wide that it is rather difficult to derive a single set of typical specifications for the design of the STAVR. One of the guidelines given in the IEEE standard is that an acceptable transient response for an excitation

system can be considered as one having no more than two overshoots with a maximum overshoot of 5% to 15%. Power Utilities in the past have given several different specifications for the response of the AVR. These are generally based on performance during a step response with the generator on open-circuit.

One of the reasons why a wide variation in the AVR specification exists is because of the type of response of the excitation system required for a particular application. Some Utilities require a high initial response excitation system to improve the transient stability of their power system, while others who have this problem to a lesser degree require only a moderate response system. The latest trend has been to specify that the excitation system should have an adequate range of continuous adjustment so that the preferred damping can be obtained for the undamped natural frequency chosen for a particular application on a 2nd order system basis. The recommended undamped natural frequency is about twice the electromechanical frequency of the turbine generator for faster response applications and half the electromechanical frequency for moderate response systems. The preferred damping for the high initial response excitation systems is greater than 0.7 whereas for the moderate response systems, lower values of damping typically greater than 0.5 are often tolerated.

In the absence of a well established specification for the AVR, two sets of small signal dynamic performance indexes have been derived from the recent customer enquiry documents for the design of the STAVR. The purpose of this exercise is to demonstrate how the controller's design parameters can be set up to meet a particular specification. For the first set of performance indexes, the damping factor ξ is taken as 0.7 and the undamped natural frequency ω_n of the closed-loop system as 25 radians / sec. This can be regarded as a typical high initial response excitation system. The second set which is for a typical moderate response excitation system uses $\xi = 0.55$ and $\omega_n = 7$ radians / sec.

The other specifications which are common to both the sets are:

Rise time to 100%	< 0.5 Sec
Settling time to 5% of change	< 2 Sec
Dead time	< 0.025 Sec
Steady state regulation	< 0.5%

Since GPC uses an integral control law, the specification on steady state regulation is automatically satisfied. It is known that the TG plant does not possess a time delay, hence the dead time specification can be met if the sampling period is chosen to be smaller than 0.025 Sec. The rise and settling times are specified in terms of their upper limits, so they can be verified when the design is tried out. The 'approximate model following' characteristic of GPC is used to satisfy the specification on ω_n and ξ. This is achieved by calculating the coefficients of the P_n polynomial based on ξ and ω_n.

A desired continuous-time closed-loop model specified in terms of ξ and ω_n can be discretized to obtain the coefficients of a 2nd order P_n polynomial for use in the STAVR. The polynomial and its coefficients are given by [118]:

$$\begin{aligned} P_n &= 1 + p_1 z^{-1} + p_2 z^{-2} \\ p_1 &= -2\, e^{-(\xi\, \omega_n\, T_k)} \cos\left(T_k\, \omega_n \sqrt{1-\xi^2}\right) \\ p_2 &= e^{-(2\, \xi\, \omega_n\, T_k)} \end{aligned} \tag{3.5}$$

where T_k is the sampling period of the system.

For $\xi = 0.7$, $\omega_n = 25$ radians / sec, and $T_k = 0.02$ Sec, the desired pole polynomial P_n is given by:

$$(P_n)_1 = 1 - 1.32\, z^{-1} + 0.50\, z^{-2} \tag{3.6}$$

For $\xi = 0.55$, $\omega_n = 7$ radians / sec, and $T_k = 0.02$ Sec, P_n is given by:

$$(P_n)_2 = 1 - 1.84\, z^{-1} + 0.86\, z^{-2} \tag{3.7}$$

The model following properties of the STAVR will be affected by the controller de-tuning factors such as the control horizon N_u and the control weighting factor λ. Hence using the values of P_n given above can only satisfy the specifications on ξ and ω_n approximately. The practical approach taken is to use the design value of P_n as a default value and fine-tune it if required during trails. Although the specifications on rise and settling times do not conflict with those of ξ and ω_n, these too need verification during trials.

There are several factors to be considered for the choice of the sampling period T_k. The knowledge of the fastest dynamics of the plant to be controlled is an important consideration in this context. As the sampling frequency increases, faster system dynamics can be captured in the estimated plant model and thus controlled. For the turbine generator excitation system, the fastest dynamics of interest is in the region of 0.05 to 0.1 sec. In the case of an AVR, a very fast response is essential during transient disturbances, this is the reason for specifying a maximum dead time of 0.025 sec. For the STAVR, a sampling period of 0.02 sec has thus been chosen. It has been shown that under normal system conditions, a higher value of sampling period such as 0.04 sec does not make any difference to the performance of the excitation control system [60,22]. The computation power of the hardware used for the implementation of the STAVR is in line with the sampling period chosen.

The order of the continuous-time plant can help towards deciding the number of poles and zeros to be estimated in the self-tuning controller. Over-estimation of the number of parameters of the plant model increases the computational burden, while under-estimation can prevent the parameter estimates from converging. In the case of the turbine generator, although the system is known to be of a high order, studies have indicated that low-order models identified using a parameter estimator can represent the real plant accurate enough to be used for self-tuning control [32,17]. For the STAVR, the order of A and B polynomials in the plant model is taken as 3 and 2 respectively.

The output predication horizon N_y of the controller is to be chosen to exceed the degree of the B polynomial in the plant model. A rather large value of

N_y which is in line with the rise time of the plant is desirable [30], but such a choice can increase the computational burden of the control algorithm considerably. N_y has been set to 10 in the STAVR which satisfies all the essential requirements.

The choice of the control horizon N_u plays a significant role in de-tuning the controller. N_u should be chosen such that unnecessary liveliness of the controller is minimised. The guideline proposed is that N_u should be chosen to be at least equal to the number of unstable or poorly damped poles of the plant for acceptable control [30]. Since the turbine generator does not have such a dynamic behaviour, a value of 1 has been initially chosen for N_u in the STAVR. Moreover, this choice is beneficial from the point of view of the computational load imposed by the GPC algorithm. The control weighting factor λ which acts as a fine-tuning knob for controller liveliness is set to zero unless otherwise stated. The P_d polynomial which specifies the zeros of the desired closed-loop model has been set to unity in the STAVR.

The plant disturbance tailoring polynomial $T(z^{-1})$ is a very useful 'knob' in altering the disturbance rejection properties of the closed-loop without affecting the set-point following characteristics of the controller [30]. The role of the T polynomial in improving the robustness of the controller has been studied in some detail and certain guidelines for its choice have been provided in [89] and [87]. Although the guidelines indicate the use of a high order T polynomial, in practice a simple first order polynomial as an observer is quite adequate [89]. Hence a first order function of the form $T = 1 - 0.8\, z^{-1}$ has been chosen for use in the STAVR. It can be seen that the low-pass filter characteristic given by $1 / T$ corresponds to a cut-off frequency of 1.8 Hz. This is an acceptable value for the turbine generator excitation system since the electromechanical frequency of the system is typically in the range of 1.5 to 2.0 Hz.

CHAPTER 4

PERFORMANCE EVALUATION OF THE SELF-TUNING AVR

There is little doubt that an advanced control strategy such as GPC is theoretically superior to a lag-lead compensator. Hence, in principle, its use in the AVR should lead to improvements in the system performance in comparison with the conventional compensator based AVR. Performance evaluation studies of the self-tuning AVR are essential to adequately verify the extent to which this improvement can be achieved as well as its significance in a practical implementation.

The benefits of using an advanced control system are generally assessed using criteria such as increased efficiency, reduction in energy consumption, tighter product tolerance etc. which are easily measurable. However, these 'yard-sticks' are not applicable in the case of an excitation control system. Quantifying the improvement achieved with a self-tuning AVR is therefore a rather difficult exercise. The task is further complicated by the fact that the specification of an excitation system with regard to its control performance is generally not laid down in detail.

The basic approach chosen here for the evaluation of the self-tuning AVR is to study its performance over a wide range of operating points and conditions of the generator. This will enable the assessment of how much the characteristics of the closed-loop system can vary under different operating conditions of the system. This is an important consideration since the predictability of control performance of the closed-loop system is a key factor in deciding the controller stability margins to be used during its design. An excitation control system which can have a wide variation in its control performance can lead to unnecessary restrictions in the range in which the generator can be permitted to operate.

Any undesirable characteristic of the self-tuning AVR needs to be identified and its effect on the overall system performance evaluated. In this context, one of the areas which needs special attention is power system stability. One of the functions of an AVR is to increase the synchronising torque of the

turbine generator which helps to keep the generating set in synchronism with the rest of the power system during a disturbance. In achieving this objective, the AVR can inadvertently reduce the damping torque which damps out the rotor oscillations following a system disturbance [6]. A self-tuning AVR is inherently a fast-acting controller and can boost the synchronising torque of the turbine generator to a level that can result in an unacceptable reduction in its damping torque. This aspect of the system should be assessed during the evaluation of the self-tuning AVR.

The success of a self-tuning AVR depends greatly on the performance of its parameter estimator. It is therefore essential that the parameter estimation algorithm is evaluated extensively under various operating conditions of the generator. This is done using the turbine generator simulation software as well as the micro-alternator system and is documented in section 4.1.

The performance of the self-tuning AVR is evaluated firstly with the generator disconnected from the power system and then connected to it and supplying power. These are regarded as the normal operating conditions of the generator and the results of the tests under these operating modes are compared with those of a conventional AVR in section 4.2. There are also abnormal power system conditions such as momentary short circuit on the output and transmission line switching, under which the excitation control system should function satisfactorily. The tests to assess the performance of the self-tuning AVR during these situations have been carried out using the software simulator and the micro-alternator system and the results are compared with those of a conventional AVR under similar disturbances in section 4.3.

4.1 Performance of the Parameter Estimator of the Self-tuning AVR

It has been widely acknowledged that the most critical part of any self-tuning controller is the parameter estimator [89,39]. Although a considerable amount of theoretical work has been done to establish its convergence properties and ways to make it robust, the parameter estimator continues to remain as the 'weak link' in the self-tuning controller. Hence it is imperative that the performance of the parameter estimation algorithm is assessed in detail. The most important

properties of a parameter estimator are convergence, adaptation and robustness. These aspects of the parameter estimator used in the self-tuning AVR are examined in the following sub-sections.

4.1.1 Verification of Parameter Convergence in the Estimator

The parameters of the plant model used in the estimator are considered to have converged when the estimation error is at its minimum. Unfortunately, satisfying this requirement alone cannot always guarantee parameter convergence. This is because even when the estimated parameters have not converged to their true values, the estimation error can be at its minimum under certain system conditions such as the plant operating in the steady state. Hence the approach adopted here is to compare the frequency response of the plant model, which uses the estimated parameters, with the frequency response of the plant itself. The frequency response of the plant is obtained using a Dynamic Signal Analyser (DSA) [119] which performs this measurement by the Fast Fourier Transform (FFT) technique.

Convergence of parameters of the plant model used in the estimator is affected by various factors. It primarily depends on the amount of dynamic information available in the plant input / output data which is used by the parameter estimator. This in turn is a function of the extent of perturbations present in the plant resulting from set point changes, noise and liveliness of the controller. Hence the convergence property of the parameter estimator should be verified under various plant operating modes such as the generator on open circuit and on load, controllers with varying degree of liveliness etc.

4.1.1.1 Parameter Convergence with the Generator on Open-circuit

The micro-alternator system has been used for the verification of parameter convergence of the estimator with the generator on open-circuit. The micro-alternator has been operated at rated speed and its terminal voltage regulated at its rated value by the self-tuning controller during this test. The open-circuit field time constant of the machine has been set to 6.0 sec. which is typical of a large

turbine generator system. A third order plant model has been used in the parameter estimator during this test. It should be noted that in this operating mode of the generator, there are no d.c. offsets in the plant input and output, hence the use of a washout pre-filter on the plant's input / output data will not improve the performance of the parameter estimator.

The first 2 minutes of operation of the parameter estimator is given in Fig. 4.1(a). It can be observed that the 3 parameters of each of the A and B polynomials of the plant model after their initial 'swing' reach near-steady values within the first 2 minutes. The start-up 'swing' of the parameters is unavoidable in the case of an estimator with zero initial estimates, but it does not affect the performance of the self-tuning controller since it happens during the first few samples when only random inputs are applied to the plant. The dominant pole of the plant model at the end of the 2 minute period corresponds to 6.8 sec. and the steady state gain is 1.85, both of which have been calculated using the A and B polynomials. These are close to the respective values of 6.0 sec and 1.95 directly measured on the micro-alternator in this operating mode.

The convergence of parameters to their true values is further illustrated in Fig. 4.1(b) where the frequency response of the digital plant model with the estimated parameters at the end of the 2 minute period is given in solid lines while the frequency response of the micro-alternator in this operating mode measured by the DSA is shown in dotted lines. It can be seen that a close match between the two curves exists in both the magnitude and phase plots which is a further confirmation of the convergence of the parameter estimator of the self-tuning AVR.

Fig. 4.2(a) shows the evolution of the estimated parameters when a 2nd order plant model has been used in the estimator. It is observed that the parameters reach near-steady values within the first 2 minutes of operation of the estimator with a steady state gain of 1.88 and a dominant time constant corresponding to 6.7 sec. A further confirmation of the convergence of the estimated parameters to their true values is obtained in Fig. 4.2(b) where a comparison of the frequency response similar to Fig. 4.1(b) is given.

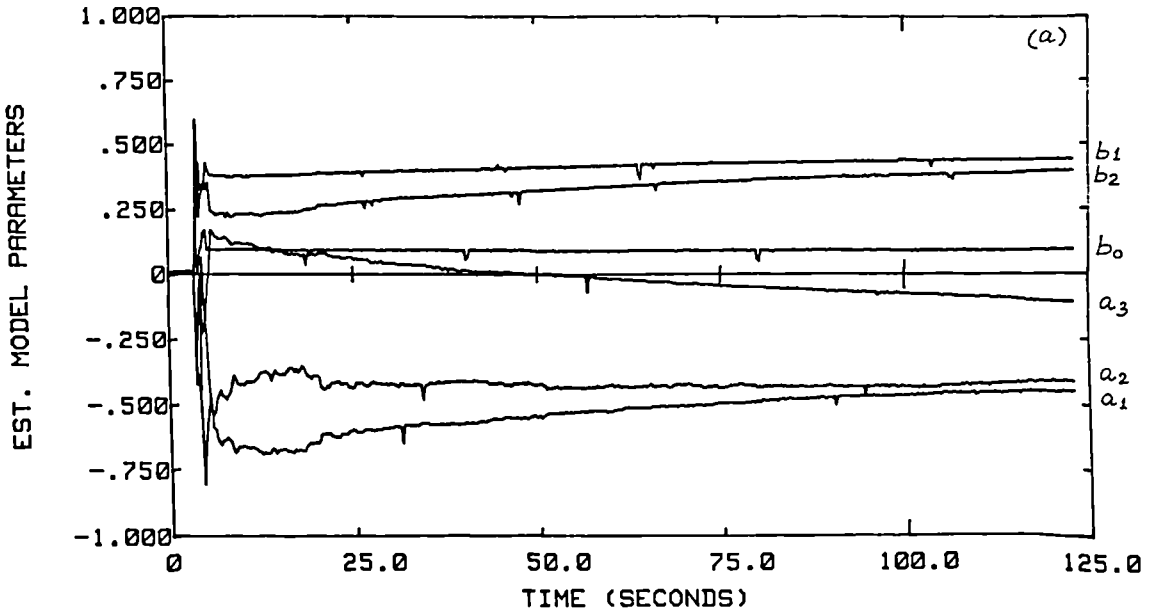

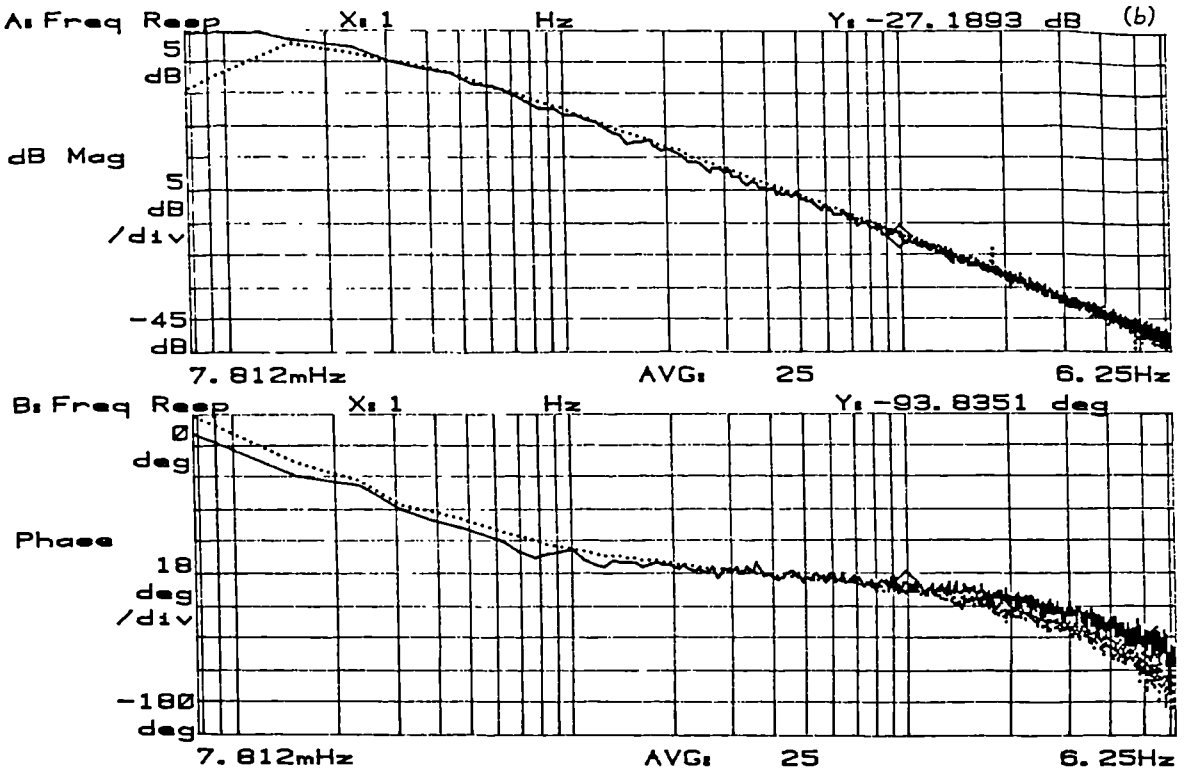

Fig. 4.1 Convergence of parameter estimator with micro-alternator on open-circuit (third order plant model).
F.R. Dotted - real plant; F.R. Solid - estimated plant model.

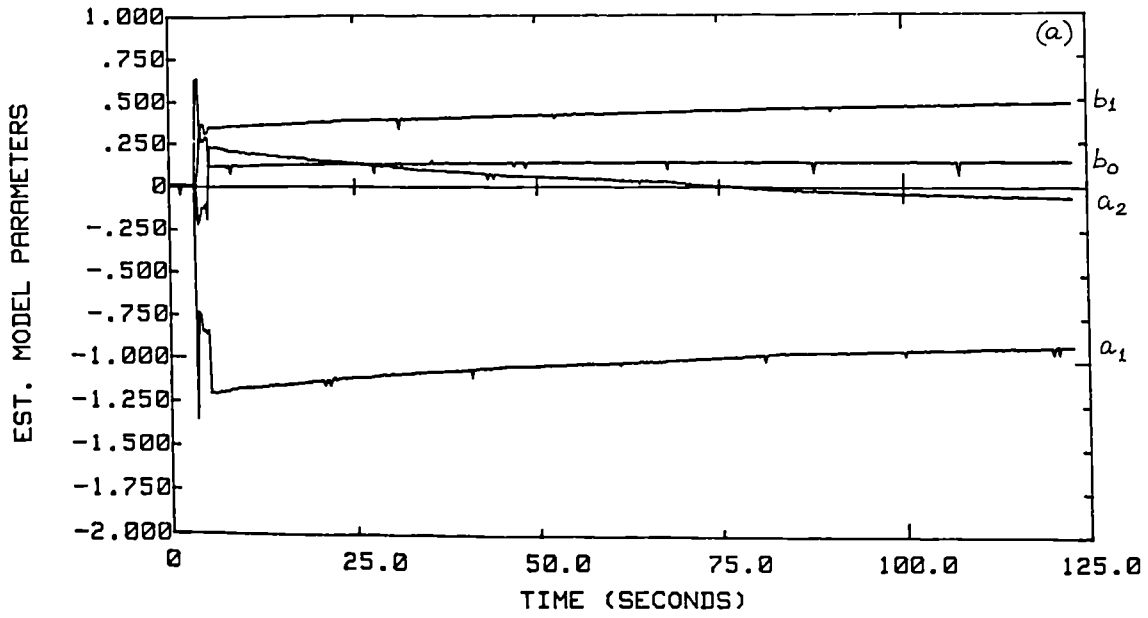

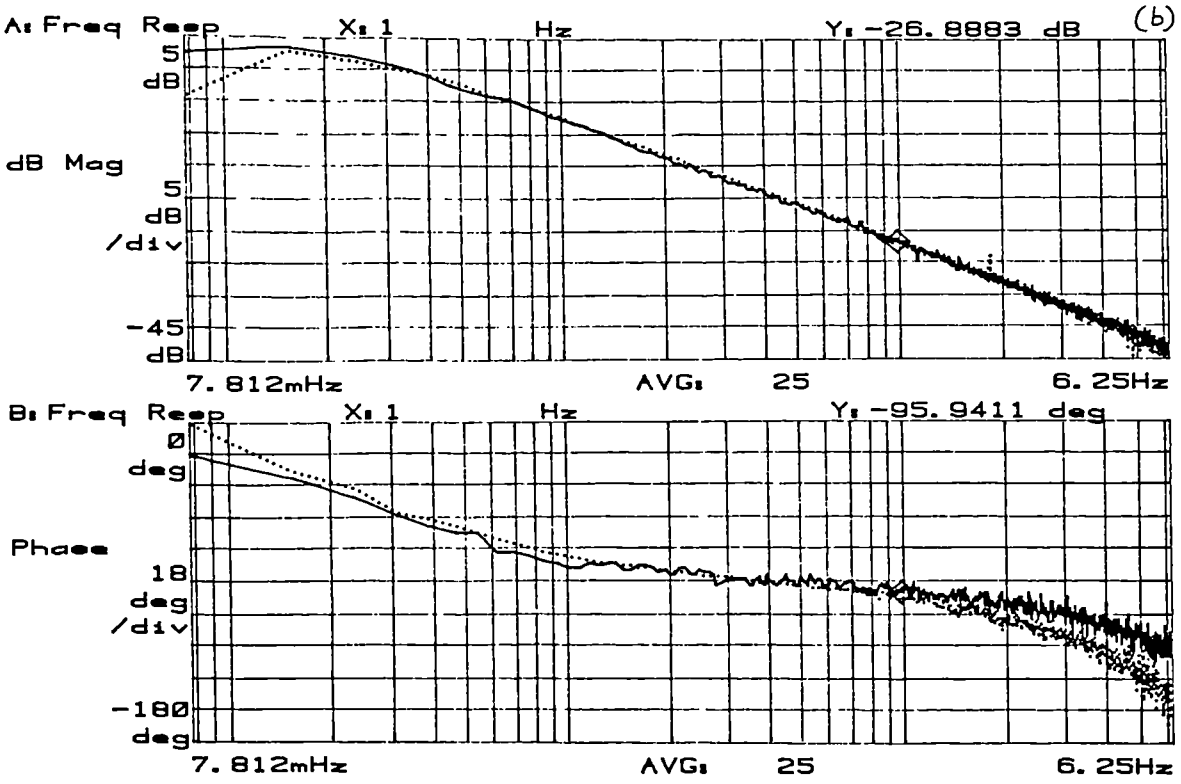

Fig. 4.2 Convergence of parameter estimator with micro-alternator on open-circuit (second order plant model).
F.R. Dotted - real plant; F.R. Solid - estimated plant model.

4.1.1.2 Parameter Convergence with the Generator on Load

During most of its operating life, a turbine generator is on load. In this operating mode of the generator, the plant between the field and the stator has a dc offset since the magnitude of the terminal voltage is mainly determined by the busbar voltage due to the connection to the rest of the power system. The use of a washout pre-filter for the plant I / O data in the parameter estimator of the self-tuning AVR will prevent the problem of biased estimates in the presence of this offset. Another important point to note is that the steady state gain and the dominant pole of the plant are considerably different from their open-circuit values in this mode.

4.1.1.2.1 Investigation using the Micro-alternator System

Parameter convergence is affected by the 'richness' of the plant I / O data in terms of its dynamic information content. Hence it is necessary to verify that convergence of sufficient rapidity can be achieved under varying degrees of liveliness of the self-tuning AVR. This is investigated by observing the performance of the parameter estimator under a fast-acting and sluggish controller. The operating point of the micro-alternator during this test has been chosen to be P = 1.5 kW (0.5 pu) and Q = 0, this being a point near the centre of the P-Q diagram of the machine.

Fig. 4.3(a) shows the evolution of the estimated parameters of a 3rd order plant model during the first 2 minutes of its operation when the 'fast' controller given by (3.6) is used. It is observed that the parameters reach near-steady values very quickly with the 'fast' controller. The steady state gain of the estimated plant model at the end of the 2 minute period is calculated as 0.29 and its dominant pole as 2.6 sec. which are close to the corresponding values of 0.32 and 2.8 sec directly measured on the micro-alternator. As mentioned earlier, it can be observed that these are considerably different from the corresponding open-circuit values.

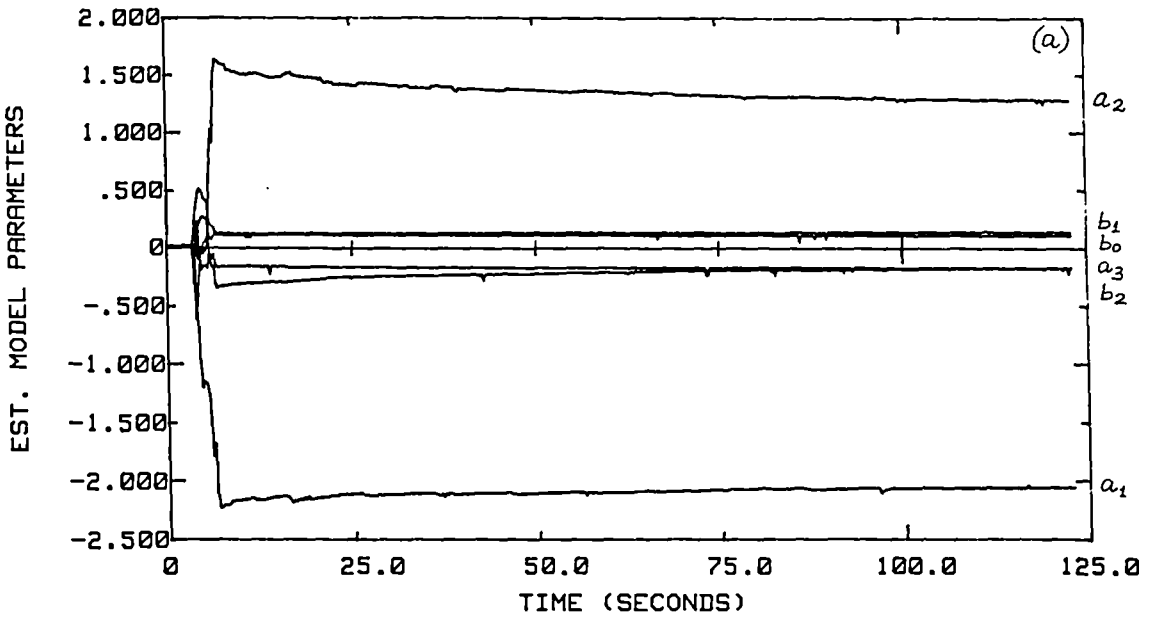

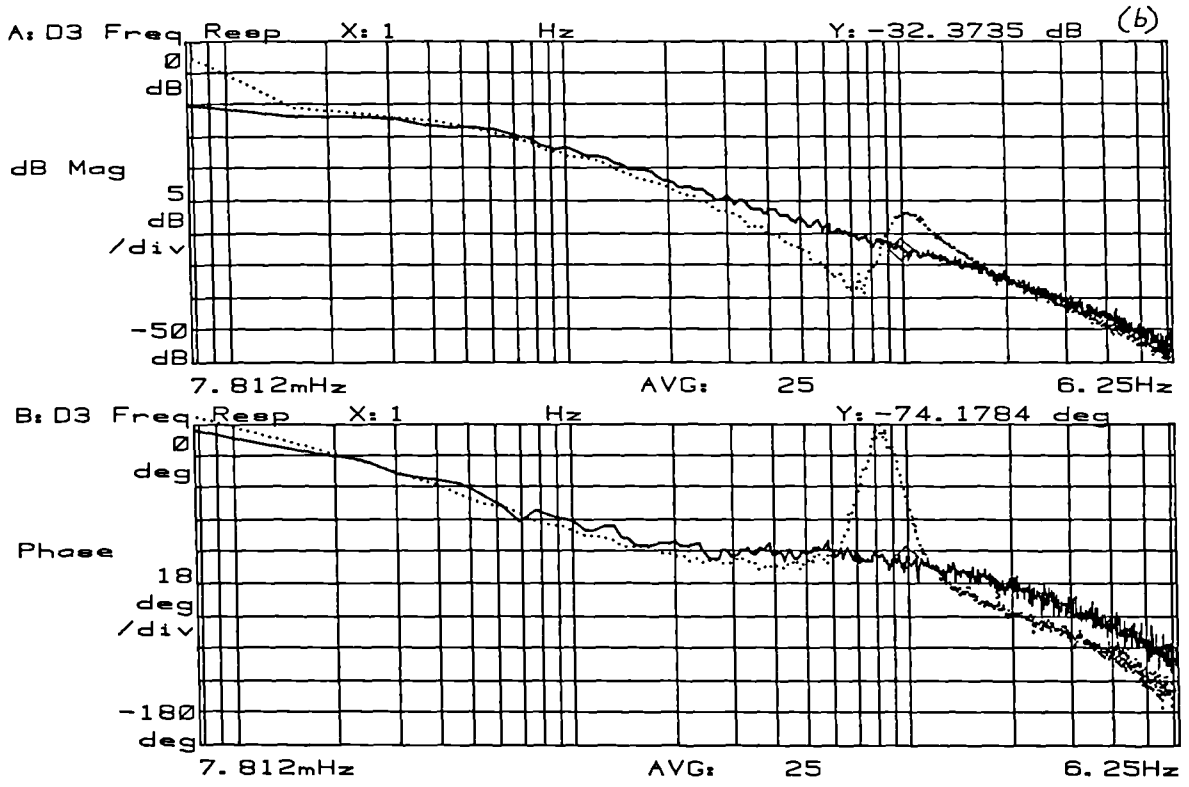

Fig. 4.3 Convergence of parameter estimator with micro-alternator on load (third order plant model; active control).
F.R. Dotted - real plant; F.R. Solid - estimated plant model.

The frequency response of the digital plant model using the estimated parameter values at the end of the 2 minute period is shown in solid lines in Fig. 4.3(b), while the dotted curves show the frequency response of the micro-alternator at this operating point obtained using the DSA. It can be observed that the two responses are sufficiently close to one another except at the resonance in the 0.7 to 1.0 Hz region where the estimated plant model does not exhibit this behaviour. It is generally accepted that the parameter estimator is unable to 'observe' a characteristic such as the resonance which happens in a very small frequency range unless sufficiently rich excitation is available in that range on a continuous basis which is not the case here. This does not however cause a significant problem in the self-tuning AVR since it is the accurate estimation of the steady state gain and the dominant time constant of the plant that dictates the controller performance to a great extent.

The convergence of the estimated parameters when a sluggish controller given by (3.7) is used is shown in Fig. 4.4(a). It can be observed that the parameters especially a_1 and a_2 have not yet converged fully within the 2 minute period. However, the steady state gain and the dominant pole of the estimated plant model at the end of the 2 minute period are 0.30 and 2.02 sec. respectively which are reasonably close to their true values. It is worth noting that although the individual estimated parameter values are considerably different from those obtained using a 'fast' controller, the steady state gain and dominant pole in both cases are similar. This is the reason why limits on individual estimated parameters have not been imposed in the estimator to improve its robustness as proposed elsewhere [39]. The comparison of frequency response is shown in Fig. 4.4(b) which further illustrates that an acceptable estimated parameter set can be obtained with a sluggish controller also.

Similar to the open circuit case, a 2nd order plant model has also been tried out in the parameter estimator of the self-tuning AVR. For this test, a sluggish controller has been used and the parameters during the first 2 minutes of operation of the estimator are shown in Fig. 4.5(a). The steady state gain and dominant pole of the estimated plant model at the end of the 2 minute period are 0.30 and

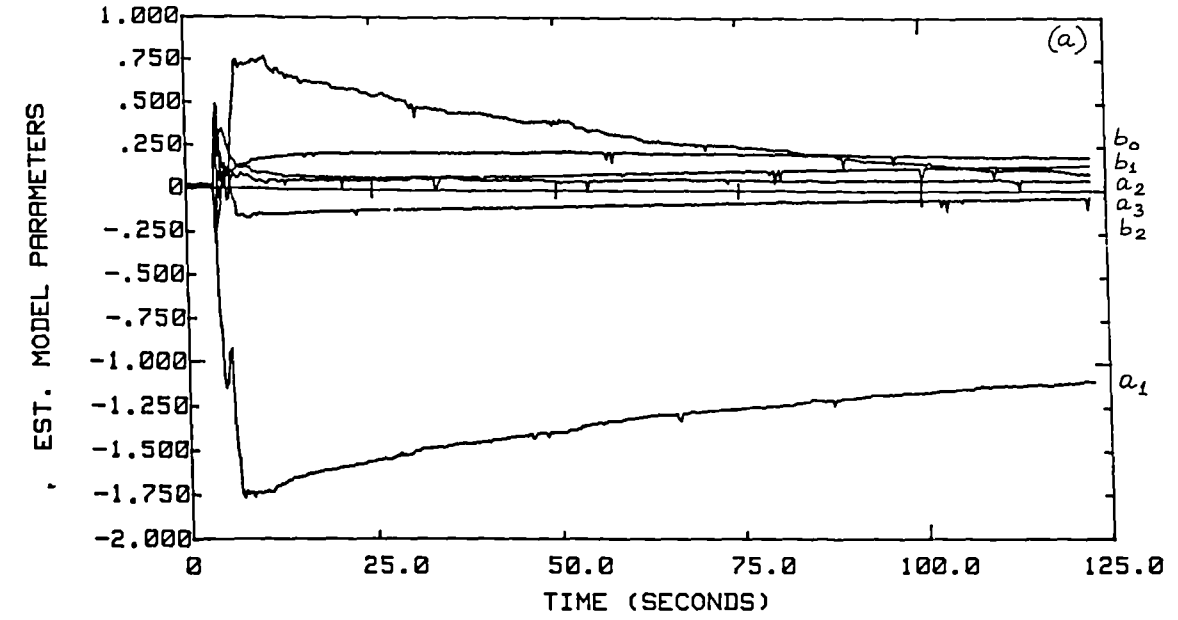

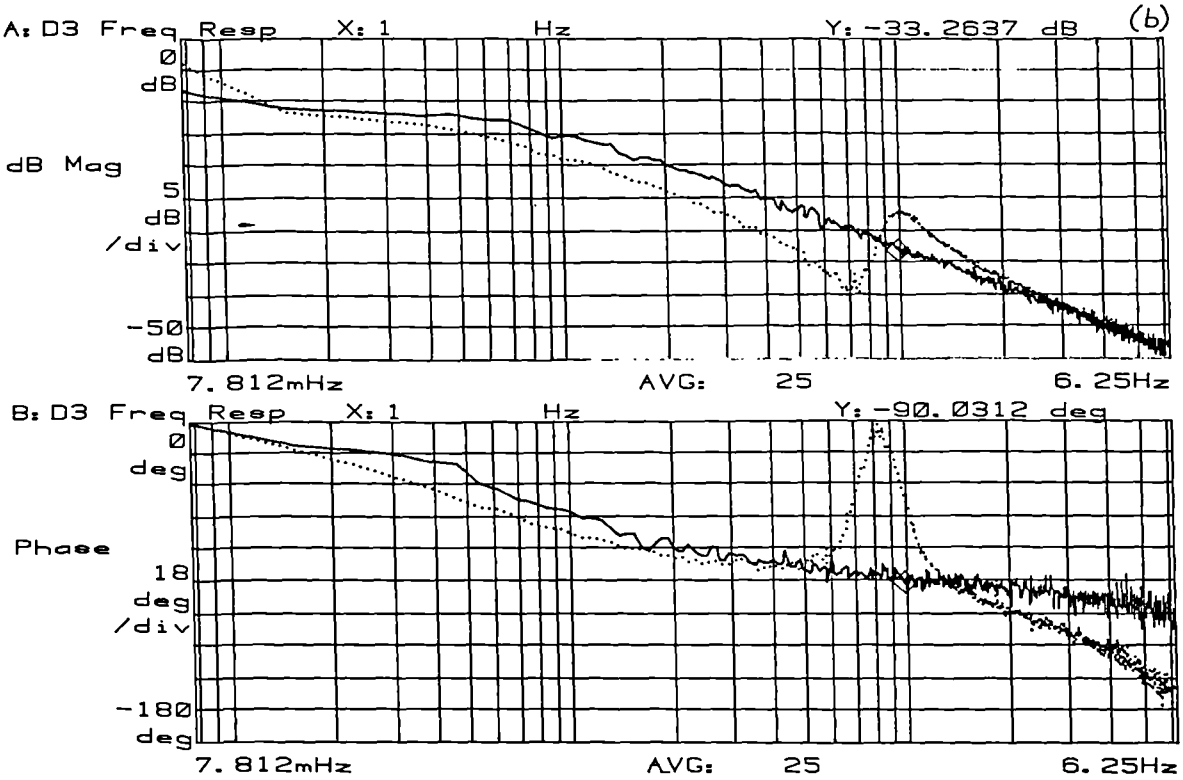

Fig. 4.4 Convergence of parameter estimator with micro-alternator on load (third order plant model; sluggish control).
F.R. Dotted - real plant; F.R. Solid - estimated plant model.

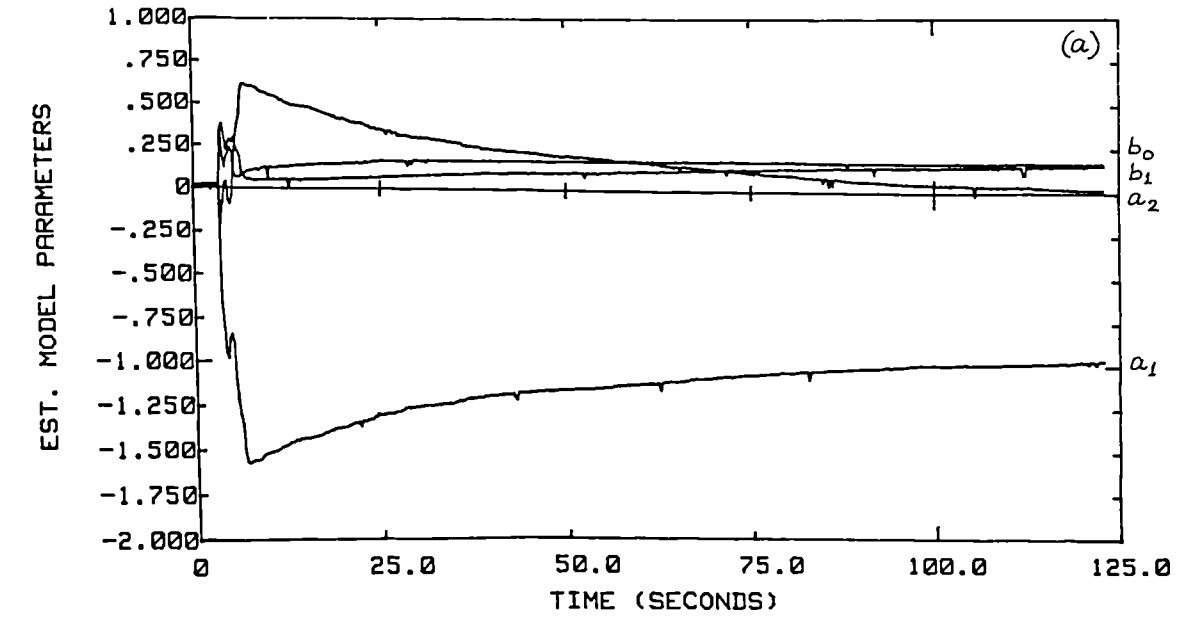

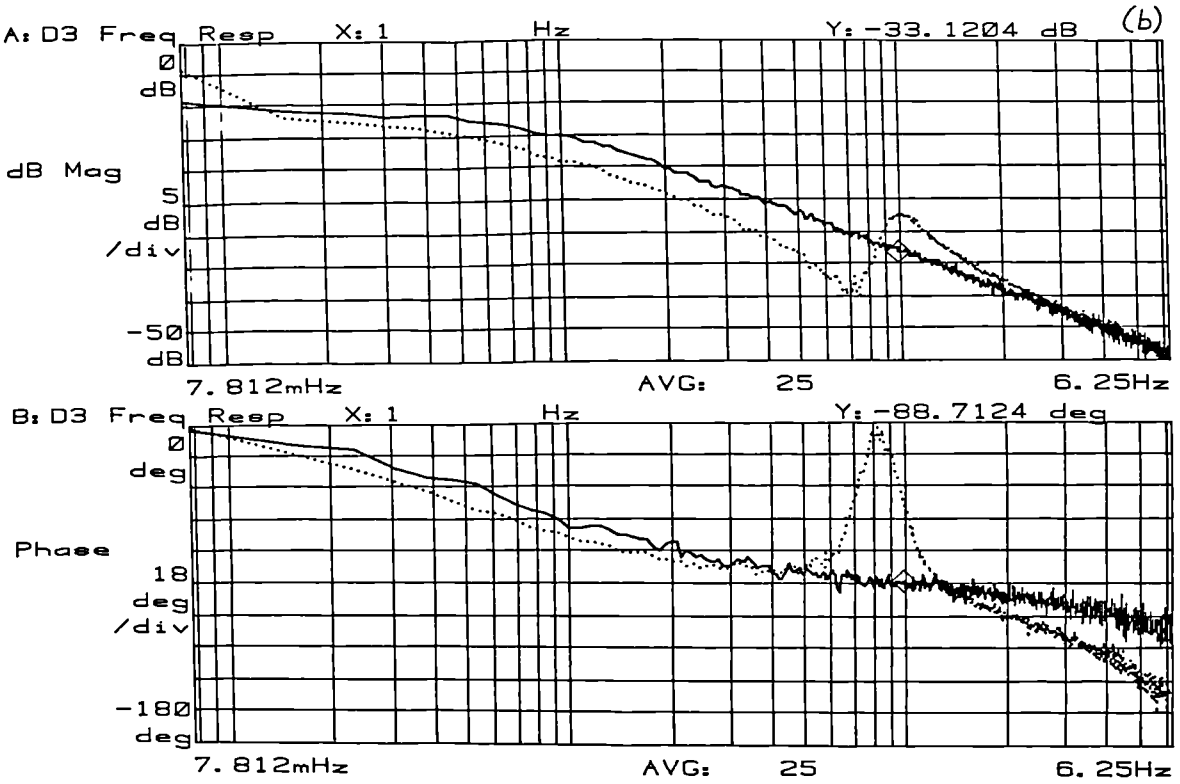

Fig. 4.5 Convergence of parameter estimator with micro-alternator on load (second order plant model; sluggish control).
F.R. Dotted - real plant; F.R. Solid - estimated plant model.

2.06 sec respectively which are similar to the values obtained during the previous test. An acceptable frequency response is also obtained as illustrated by Fig. 4.5(b). This indicates that a reduction in the order of the estimated plant model can be considered if problems in achieving the required sampling rate arise in the future.

4.1.1.2.2 Investigation using the TG Simulator

The convergence of the parameter estimator has also been tried out using the TG simulator. The simulator has been set up to represent a typical 660 MW turbine generator and its operating point has been chosen as P = 0.8 and Q = 0. A 3rd order plant model has been assumed in the estimator and the sluggish controller has been used. Since the TG simulator produces a 'clean' output ie. without any noise, the main perturbation is provided by the liveliness of the controller which in this case is low. This test is thus aimed at investigating the convergence of the estimator under very low perturbation conditions which to some extent is unrealistic in real life.

Fig 4.6(a) shows the performance of the parameter estimator during the first 10 minutes of the simulation run. This corresponds to 1 minute of 'real' time as the simulator is running 10 times slower. It can be observed that acceptable convergence is achieved during this time. The steady state gain and the dominant time constant are 1.48 and 4.5 sec. respectively. Fig. 4.6(b) gives the parameter convergence with a 2nd order plant model with all other conditions remaining the same. The steady state gain and the dominant time constant in this case are found to be 1.27 and 4.4 sec. respectively which are close to the values obtained earlier. These results show that the parameter estimator works satisfactorily with 'no noise' conditions, provided that some perturbation is available in the plant through control action.

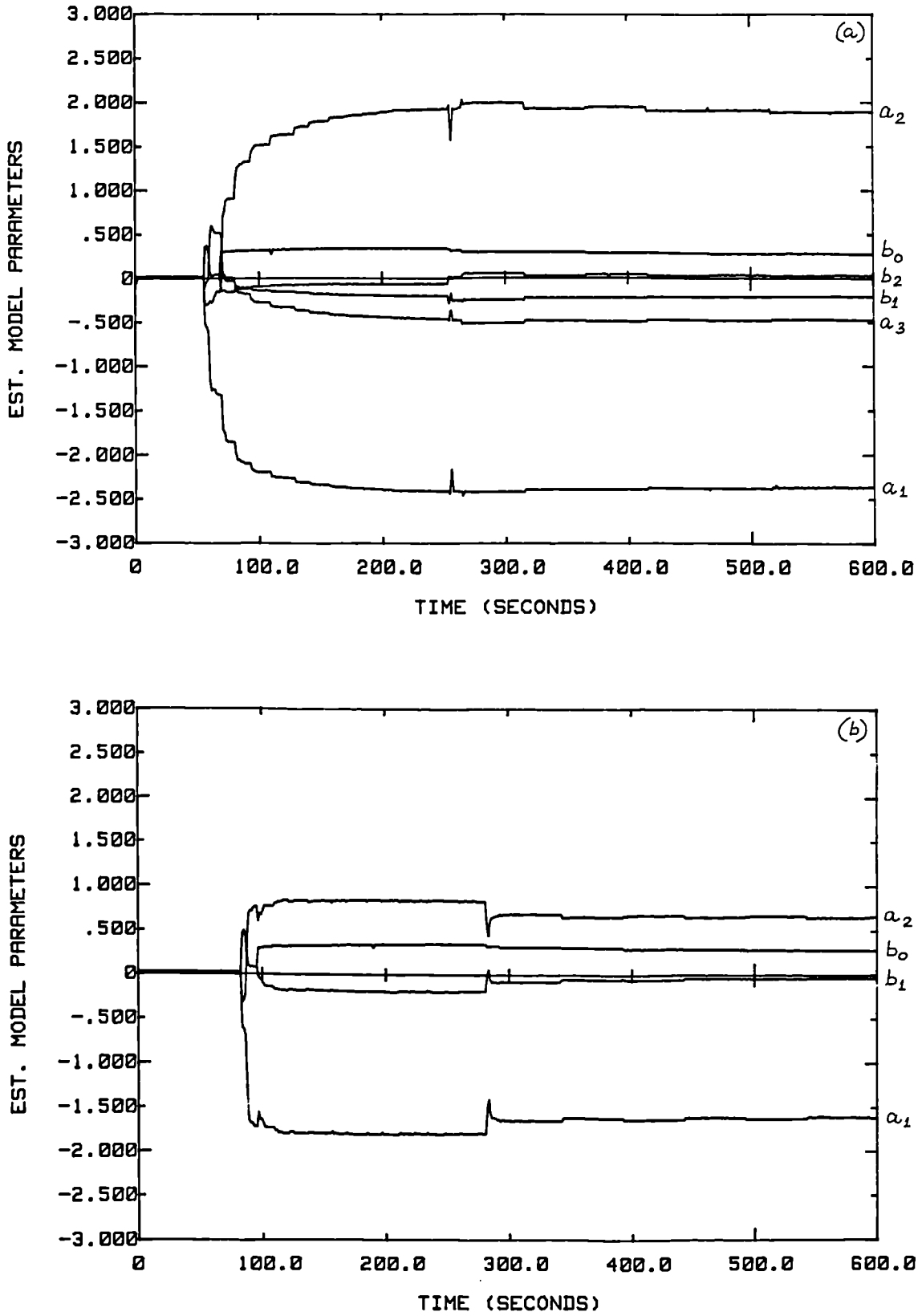

Fig. 4.6 Convergence of parameter estimator with TG simulator.
(a) Third order plant model; (b) Second order plant model.

4.1.2 Verification of Parameter Adaptation

A self-tuning controller is expected to track changes in the dynamic behaviour of the plant if those variations are slow in nature. This aspect of the parameter estimator of the self-tuning AVR is verified by observing the estimated parameters during system changes. Fig. 4.7(a) shows the parameter adaptation when an abrupt system change is made by synchronising the micro-alternator at t = 48 sec. Similarly, the effect of another system change by reducing the load of the micro-alternator from 1.5 kW to 0.25 kW is given in Fig. 4.7(b). In both cases, it can be observed that rapid adaptation of the estimated parameters has been achieved. A further improvement in the adaptation capability of the estimator is possible if the system change can be detected and a random walk is invoked at that time, but this has not been attempted here.

4.1.3 Verification of the Parameter Estimator Robustness

It is widely acknowledged that a recursive parameter estimator needs some form of 'software jacketing' to improve its robustness. The two schemes which are incorporated in the estimator of the self-tuning AVR are the parameter freeze and covariance trace monitoring facilities. The parameter freeze facility enables the stopping of the estimation process when either too little or too much dynamic information is arriving from the plant. The former happens when the plant is hardly perturbed while the latter is an indication of a transient disturbance in the plant. Both these conditions necessitate the freezing of the estimator for improved robustness [47].

Fig. 4.8(a) shows the amount of dynamic data in the pre-filtered plant signals which typically enters the parameter estimator of the self-tuning AVR under closed-loop control. The mean dynamic data which is obtained by low-pass filtering these instantaneous values is shown in Fig. 4.8(b). It can be seen that the mean dynamic data settles to a near-steady value soon after start-up. The instantaneous dynamic data during a 3-phase short circuit on the micro-alternator at t = 9 sec. is given in Fig. 4.9(b). It can be noted that the dynamic data increases a few

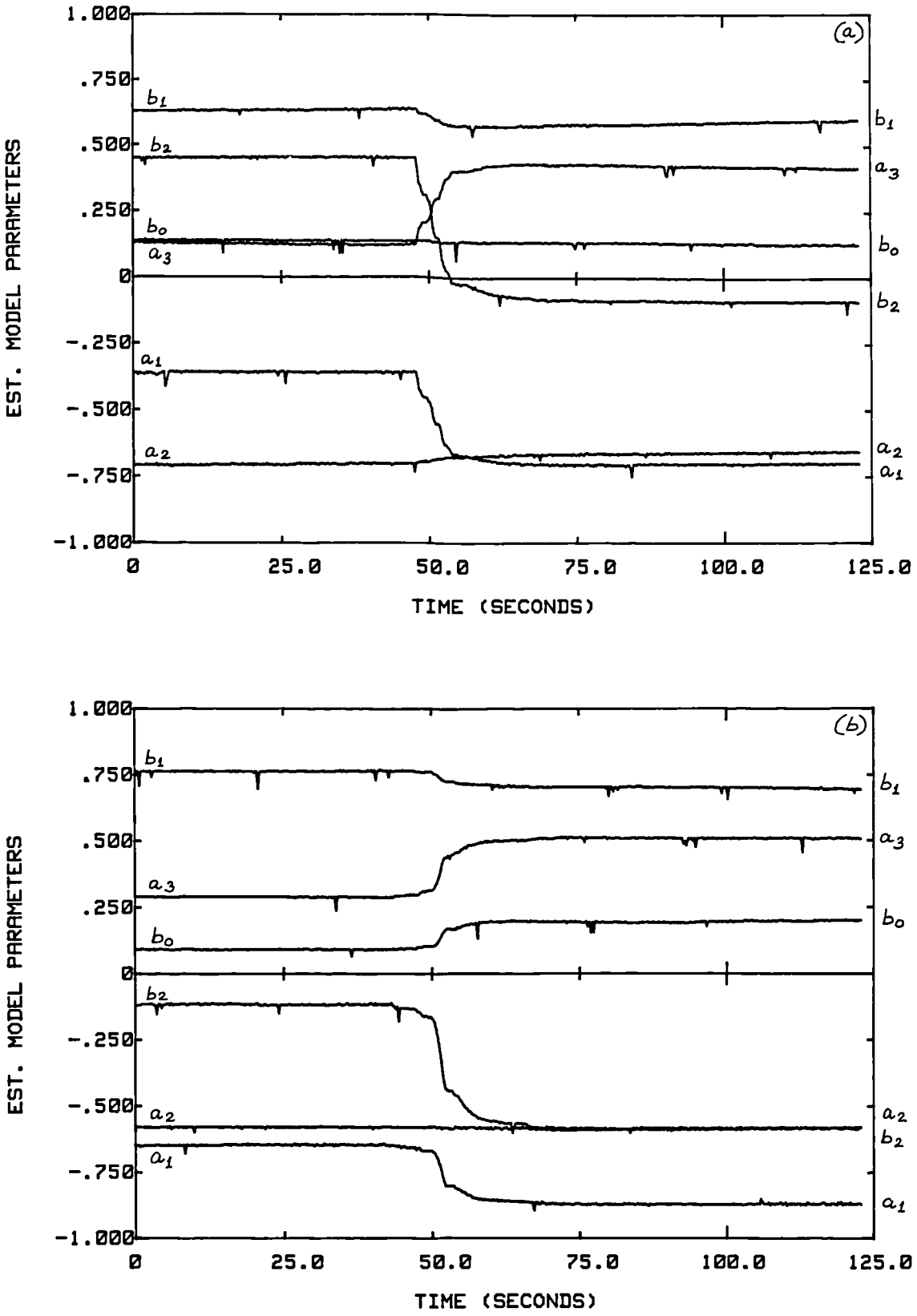

Fig. 4.7 Adaptation of parameter estimator with the micro-alternator.
(a) During synchronisation; (b) During load change.

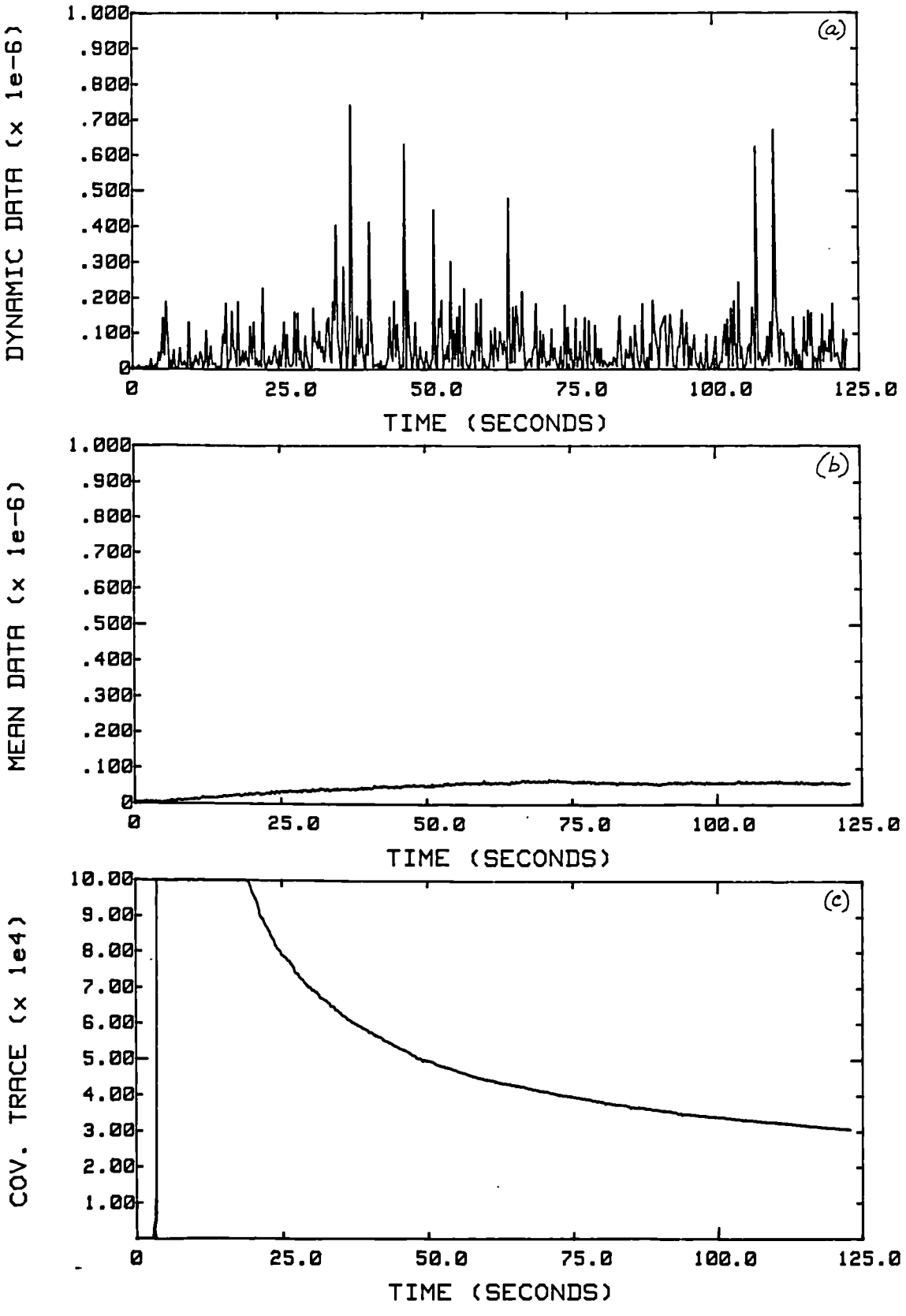

Fig. 4.8 Start-up of parameter estimator with micro-alternator.

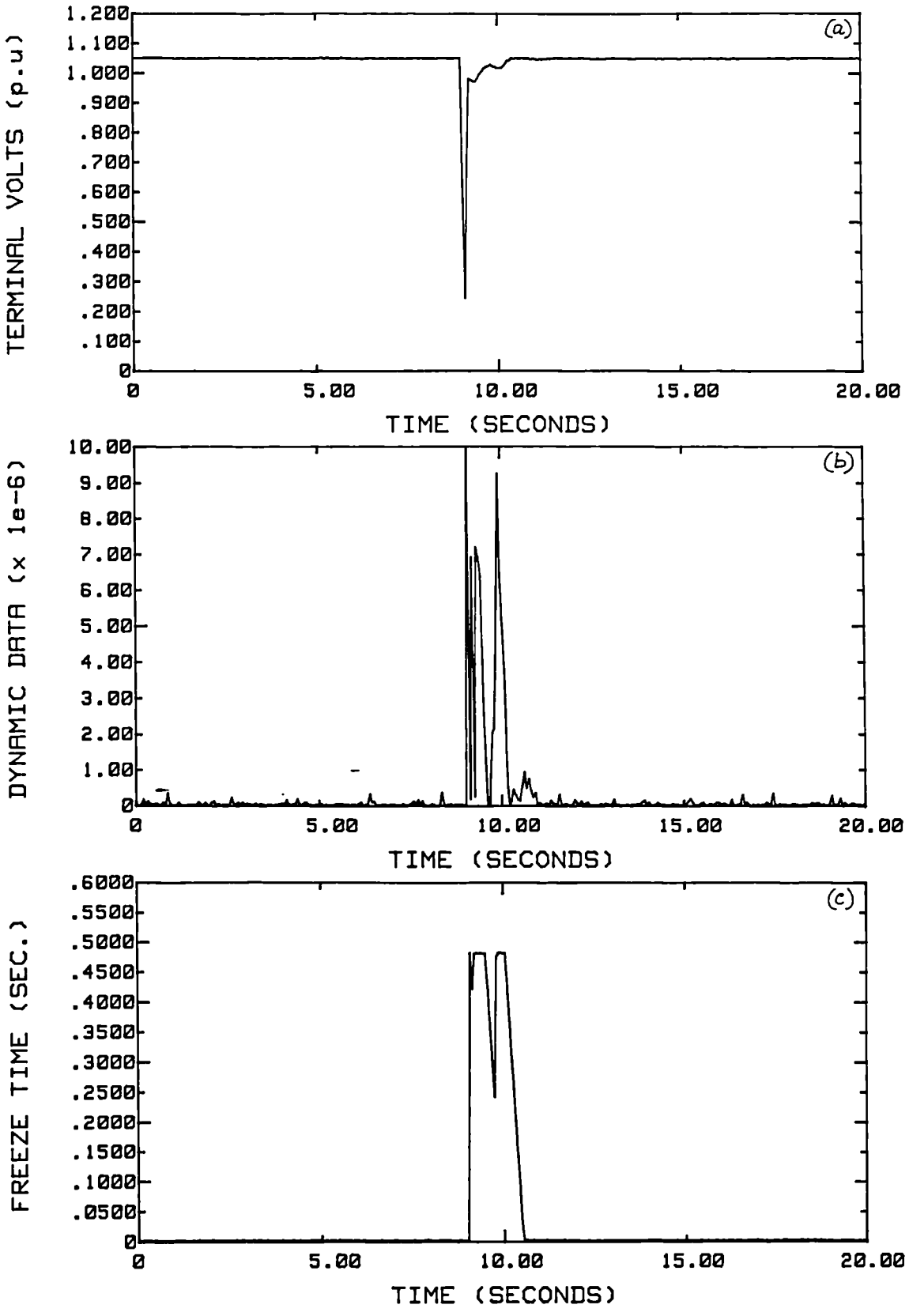

Fig. 4.9 Parameter estimator during a 3-phase short-circuit on the micro-alternator.

hundred times during this disturbance which is considerably above the upper limit of 100 times set in the estimator. The timer value which determines for how many samples the estimator should be frozen is shown in Fig. 4.9(c), together with the terminal voltage (Fig. 4.9(a)). It is observed that the estimator remains frozen from the start of the short circuit till the terminal voltage settles down after the fault, which is sufficient to provide the required estimator robustness.

Another feature which has been incorporated is the covariance matrix trace monitoring and automatic adjustment of the speed of adaptation. The initial decay of the covariance matrix trace during start-up is shown in Fig. 4.8(c). The trace eventually settles to a value corresponding to the amount of dynamic information which the variable forgetting factor aims to preserve in the estimator. This aspect has been verified by observing the operation of the estimator for 30 to 45 minutes. If the final settling value of the trace is within its pre-defined limits of 1000 and 10000, the estimator would have the desirable speed of adaptation. However, if the trace exceeds one of these limits, the algorithm adjusts the desired dynamic information content in small steps until the trace remains inside the limits. This is a very slow process and depends primarily on the long-term liveliness of the controller. This automatic adjustment has also been verified by trials on the micro-alternator lasting several hours. It is also observed that invoking the random walk when the covariance matrix trace hits one of its limits and the variable forgetting factor scheme help to collect and conserve the required amount of dynamic information about the plant throughout the operation of the self-tuning AVR.

4.2 Performance Evaluation of the Self-tuning AVR under Normal Operating Modes of the Generator

The self-tuning AVR has been designed to satisfy the desired step response characteristic of the turbine generator system. Hence it is logical that the resulting controller is evaluated using step response tests. A step size of 3% has been chosen for these tests this being small enough to prevent the saturation of the excitation demand, but large enough to make accurate measurements.

4.2.1 Evaluation of Step Response with the Generator on Open-circuit.

The step response specification used for the controller design applies to a turbine generator on open-circuit. Hence it is reasonable that the design is verified under this operating mode of the generator. The micro-alternator system has been used for this validation. The operating condition of the machine has been set to rated speed and terminal voltage during the tests. The open-circuit field time constant of the generator has been set to 6.0 sec. using the TCR.

The 'fast' self-tuning AVR design given by (3.6) has been evaluated by applying a 3% positive step and the response of terminal voltage and excitation demand are given in Fig. 4.10(a) and (b) respectively. It may be noted that the control horizon, N_u used in this test is unity as proposed in Chapter 3. The overshoot, rise time and settling time obtained are 0%, 500 msec. and 500 msec. against design values of 4.3%, 130 msec. and 230 msec. respectively. The frequency response of the closed-loop system measured by the DSA is shown in Fig. 4.10(c) from which the bandwidth is given as 1.45 Hz whereas the design value is 4.0 Hz.

It can be observed that the self-tuning AVR is considerably slower than expected. The primary reason for the difference between the actual and expected response is the choice of unity control horizon since this value can produce only a sluggish control action. This point is verified by repeating the step response test with N_u = 2 and 3 the results of which are shown in Fig. 4.11 and 4.12 respectively. For N_u = 2, the overshoot, rise time, settling time and the bandwidth are found to be 1%, 180 msec., 300 msec. and 3.0 Hz respectively. These figures for Nu = 3 are obtained as 6.5%, 140 msec., 350 msec. and 3.8 Hz respectively. As expected, this indicates that as N_u approaches the prediction horizon, the step response gets closer to the design values.

It is observed that N_u = 2 gives a reasonably 'fast' response which is not considerably different from the design values. Although N_u = 3 gives a response which is closer to the design values, this is not proposed for use in the

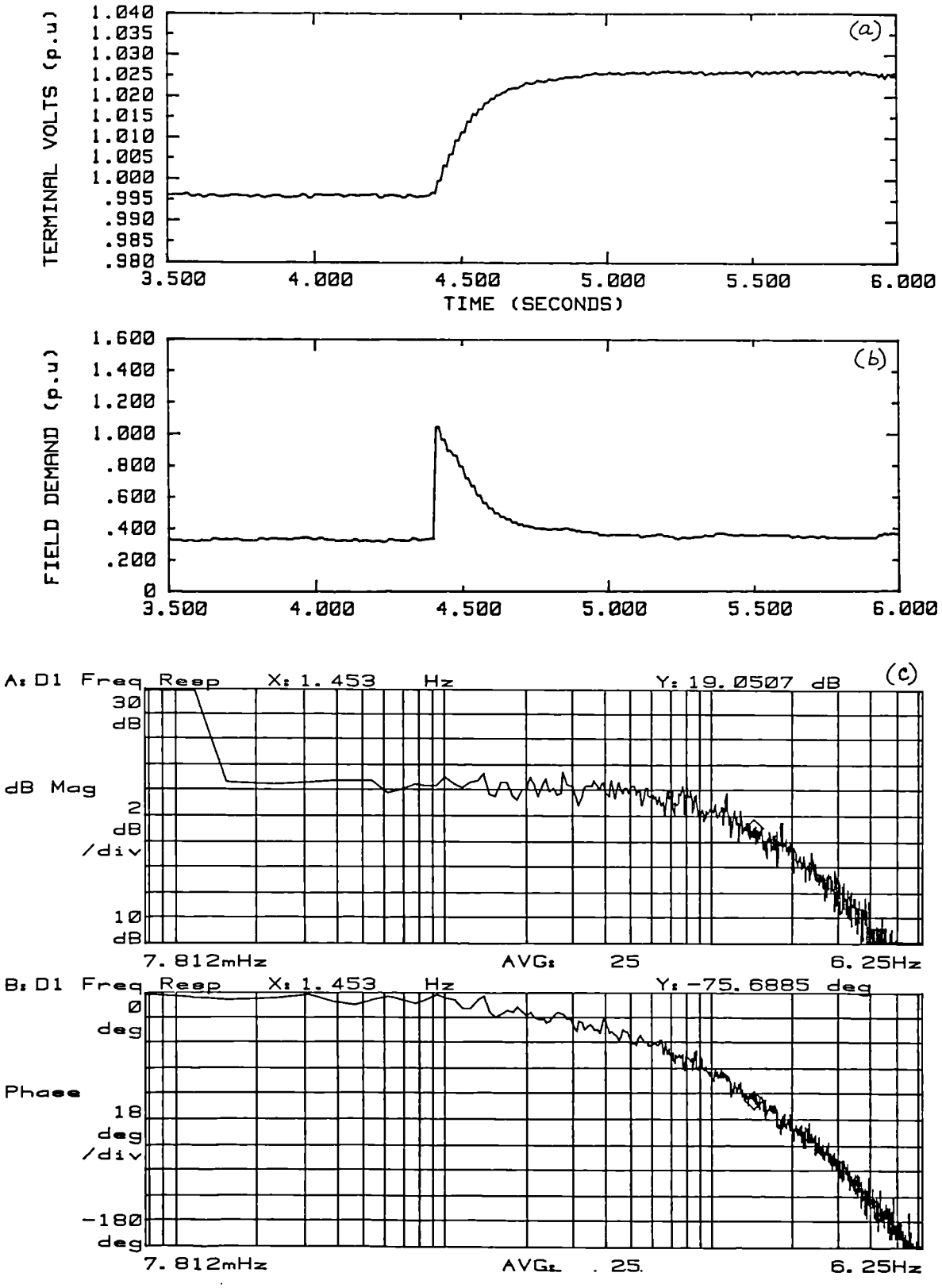

Fig. 4.10 Step response with micro-alternator on open-circuit (STAVR-F; N_u = 1).

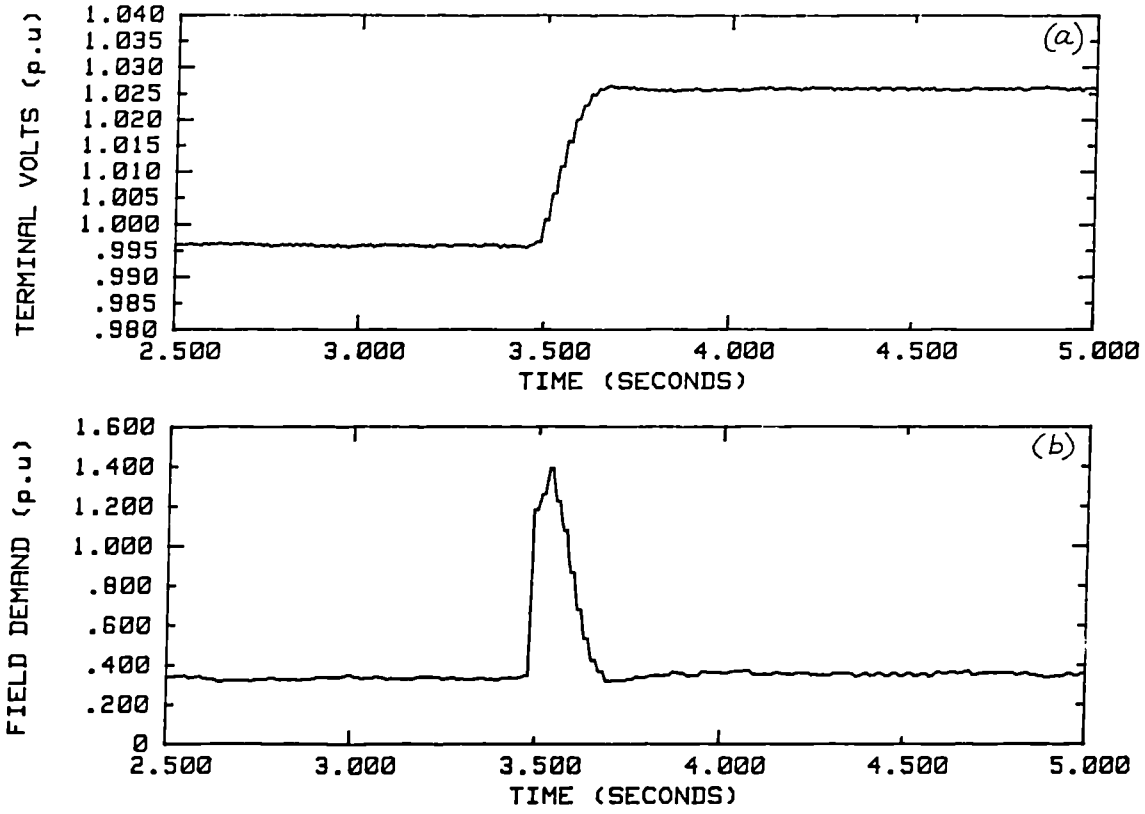

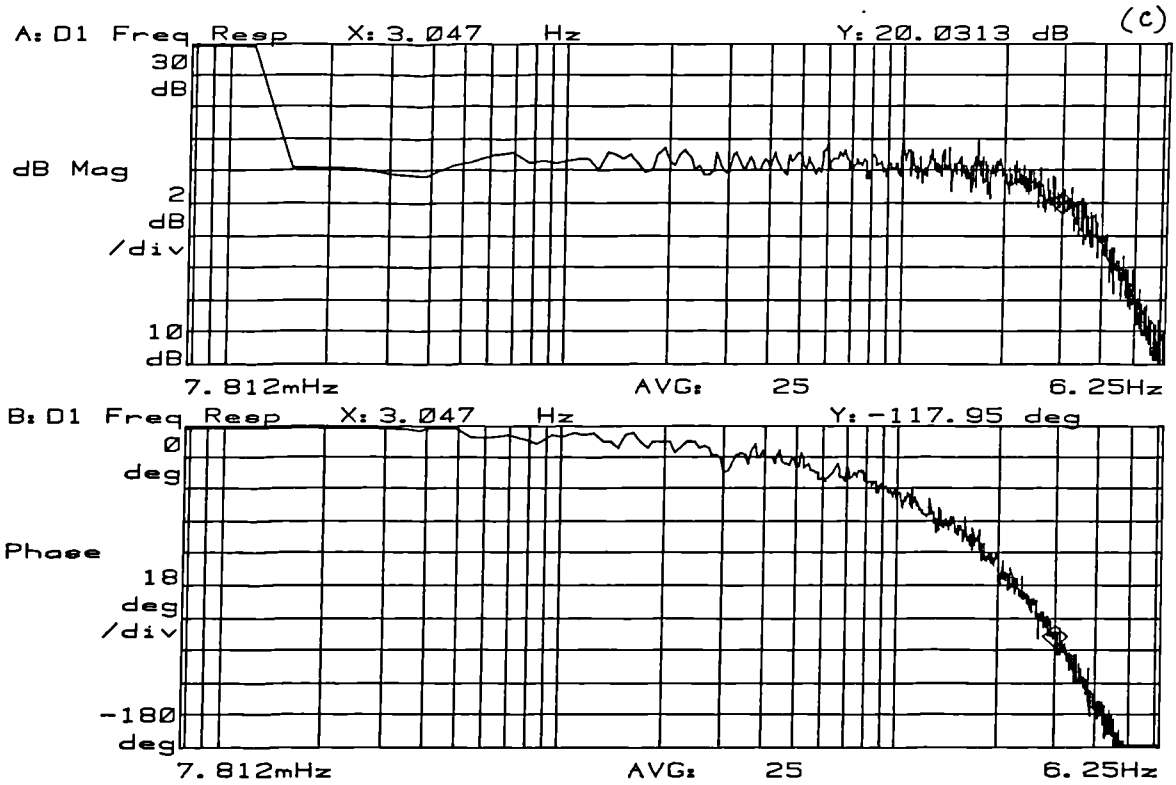

Fig. 4.11 Step response with micro-alternator on open-circuit (STAVR-F; N_u = 2).

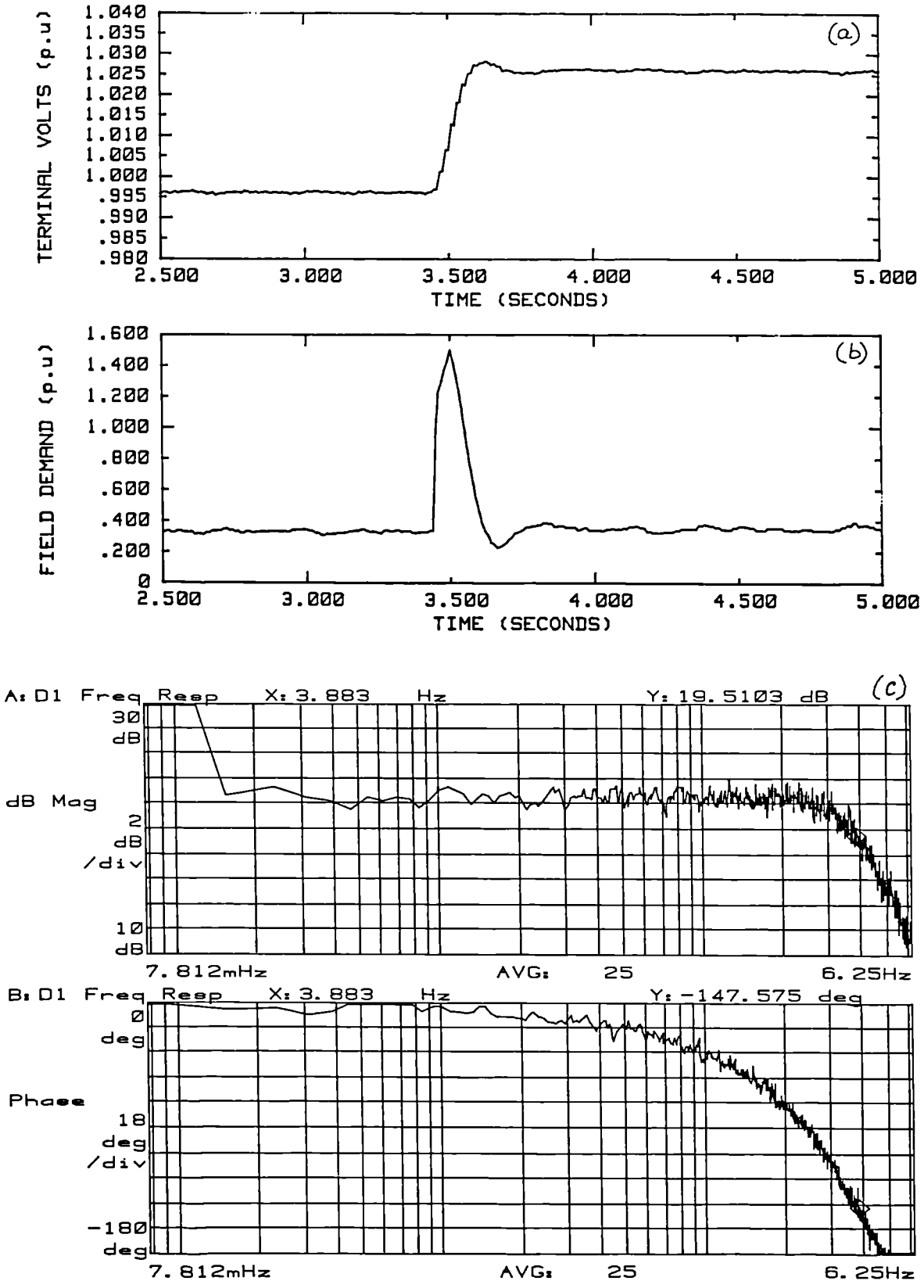

Fig. 4.12 Step response with micro-alternator on open-circuit (STAVR-F; N_u = 3).

self-tuning AVR due to the possible reduction in the controller robustness and the additional computational burden imposed by the algorithm. For future reference, let this design which uses $N_u = 2$ be called STAVR-F.

A conventional digital AVR which satisfies the design specification for the 'fast' excitation control system has been produced for comparison with STAVR-F. An approximate design using simulation studies fine-tuned by trial and error on the micro-alternator gave the parameters of the digital AVR as: Loop gain with generator on open-circuit = 325; Lag time constants = 9.0, 0.064, 0.025 sec.; Lead time constants = 3.0, 0.064 sec. For future reference, let this design be called DGAVR-F. The step response of this AVR under conditions identical to the previous test is given in Fig. 4.13. The overshoot, rise time, settling time and bandwidth are found to be 4%, 175 msec., 350 msec. and 2.8 Hz respectively which are close to those of STAVR-F.

The step response test under identical conditions to the above has been tried out using the 'slow' self-tuning AVR design given by (3.7). During this test N_u has been progressively increased from 1 to 3 and the response with Nu = 3 is shown in Fig. 4.14. It has been found that even with $N_u = 3$, the overshoot, rise time, settling time and bandwidth obtained are 1%, 430 msec., 430 msec. and 1.1 Hz only, as opposed to the design values of 12.6%, 370 msec., 1.04 sec. and 1.35 Hz respectively.

Since provision to increase N_u further has not been made in the algorithm, the prediction horizon, N_y has been reduced from 10 to 5 to prove the validity of the basic design. The step response with the resulting controller is shown in Fig. 4.15. The overshoot, rise time, settling time and bandwidth are obtained as 10%, 345 msec., 625 msec. and 1.5 Hz respectively which are close to the design values. This indicates that GPC designs for slower responses are affected more by the choice of N_u than for the faster responses.

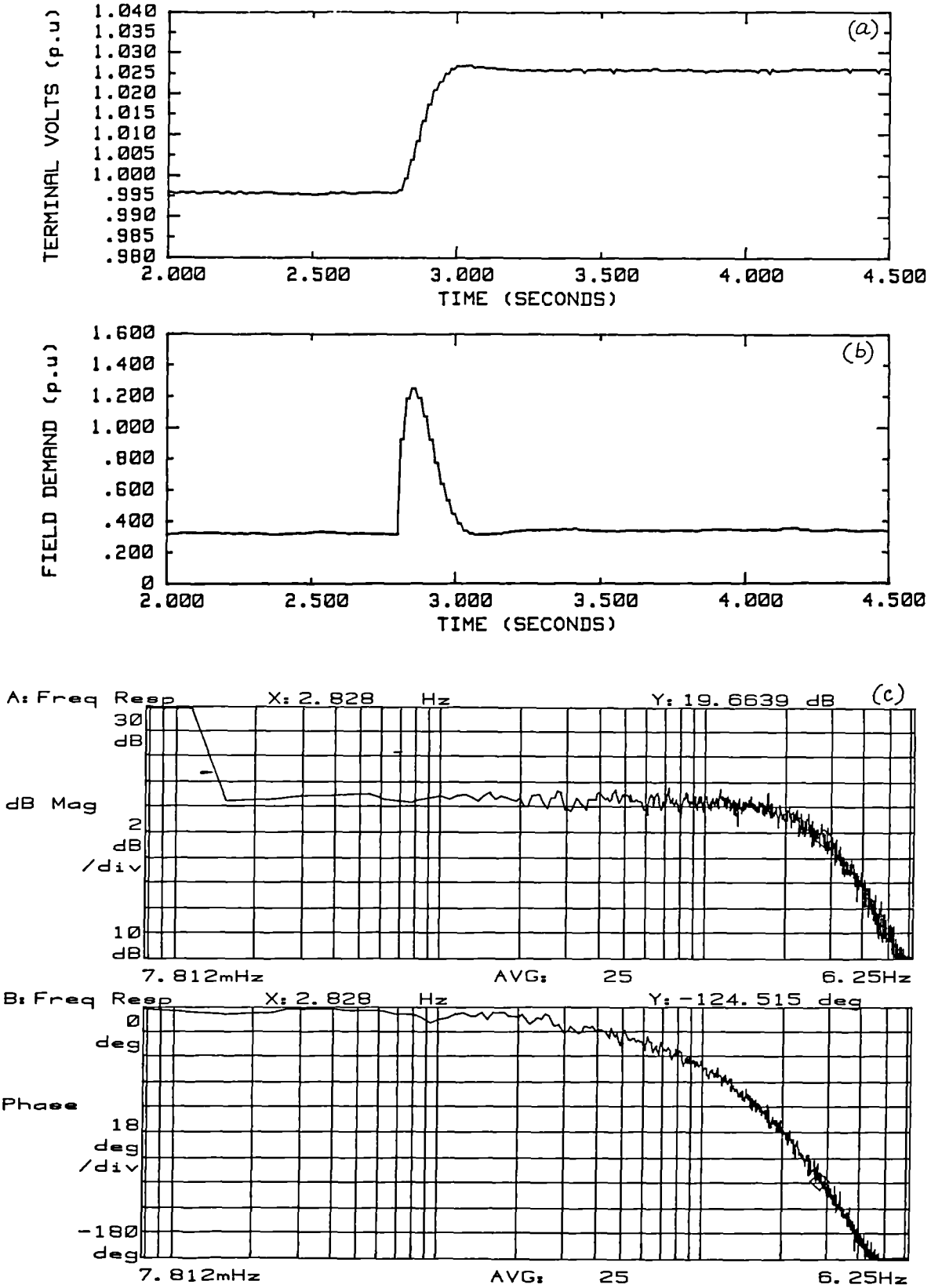

Fig. 4.13 Step response with micro-alternator on open-circuit (DGAVR-F).

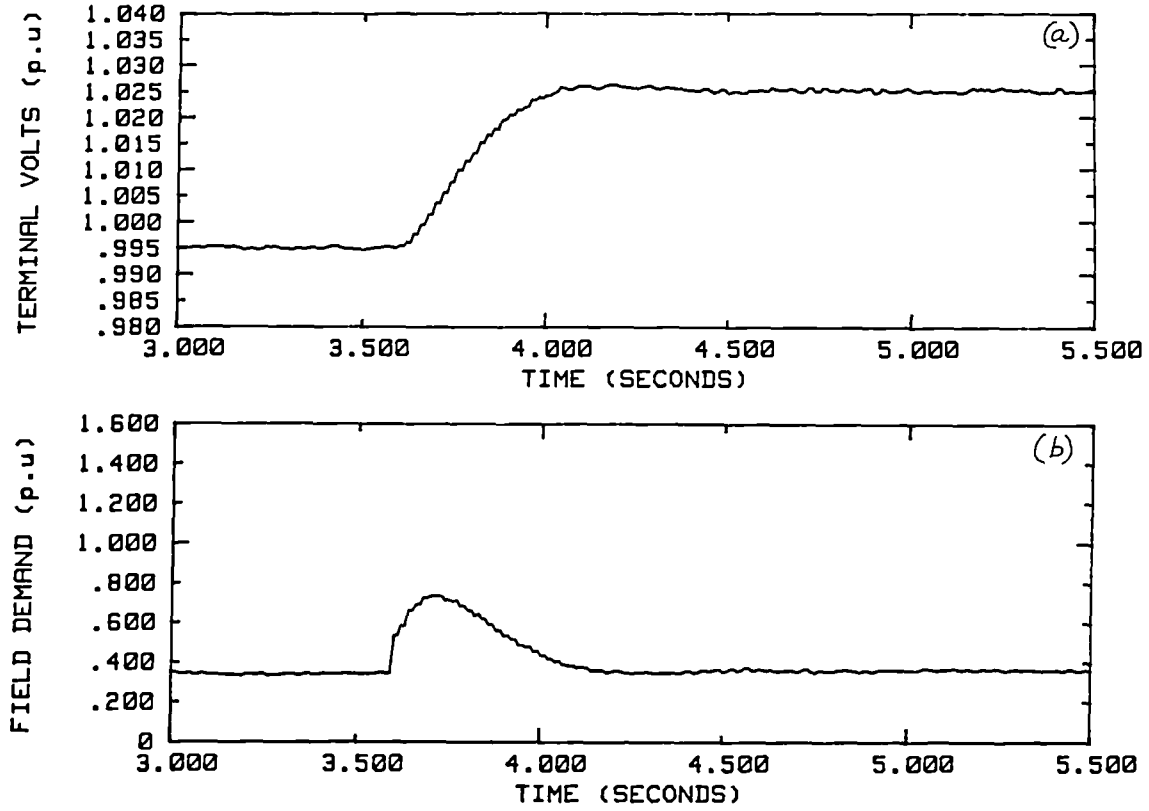

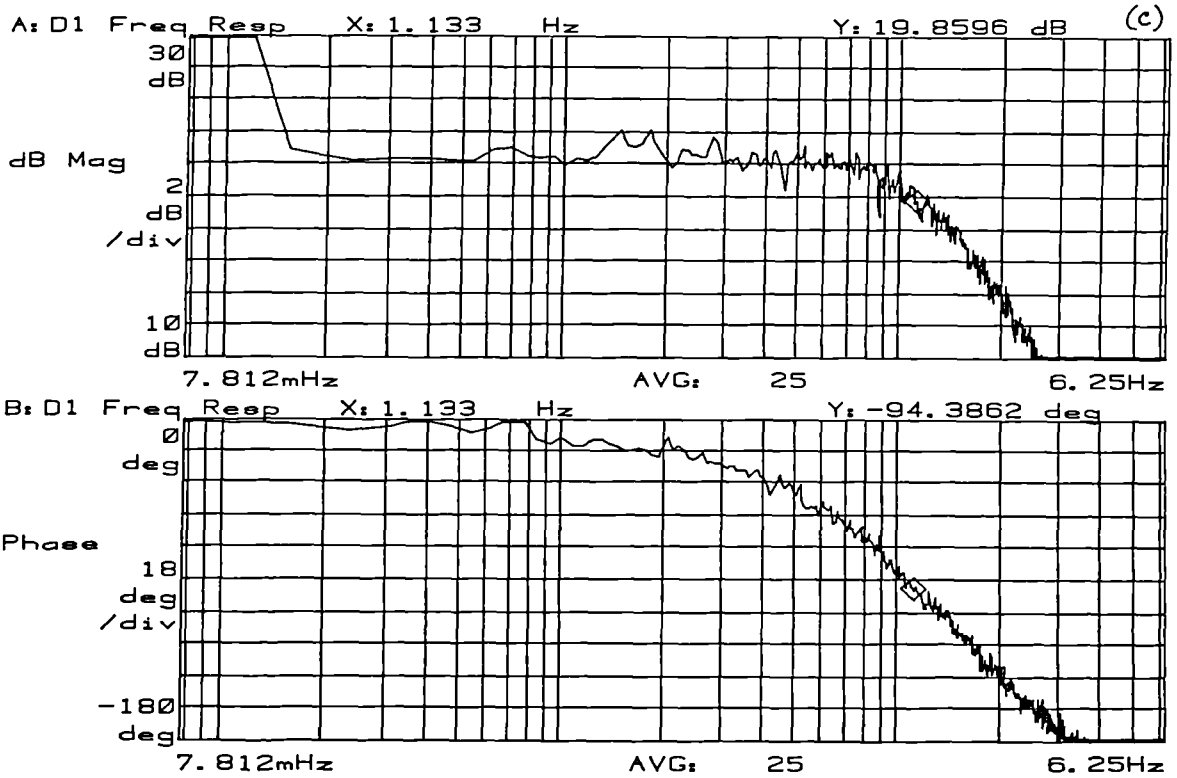

Fig. 4.14 Step response with micro-alternator on open-circuit (STAVR-S; N_u = 3; N_u = 10).

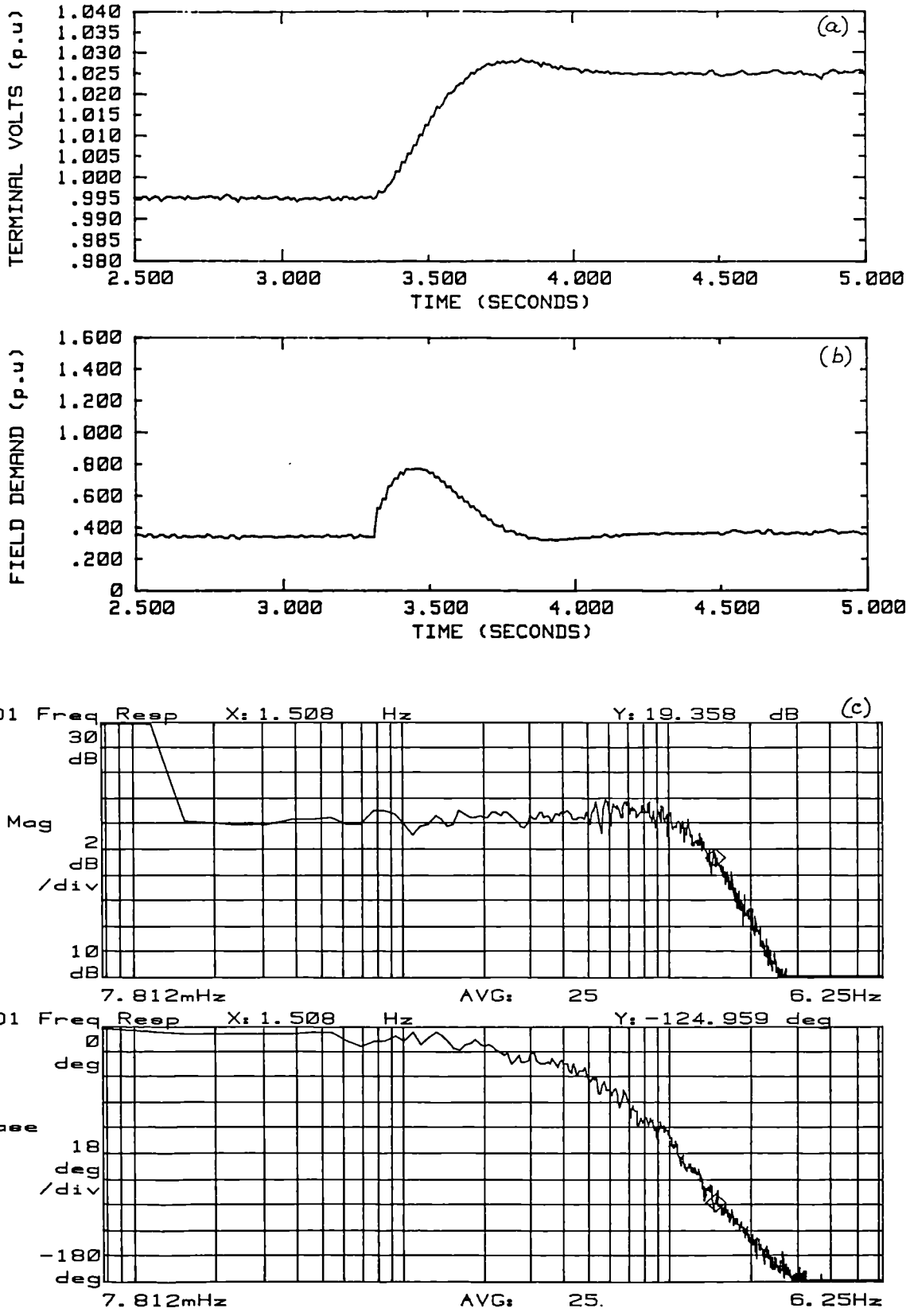

Fig. 4.15 Step response with micro-alternator on open-circuit (STAVR-S; $N_u = 3$; $N_y = 5$).

Since it is better not to reduce N_y from 10 which is already a slightly low value, it was decided to modify the pole polynomial of the 'slow' self-tuning AVR to achieve the required step response. This has been done using trial and error and the step response for $P_n = 1 - 1.914\ z^{-1} + 0.923\ z^{-2}$ with $N_u = 2$ is given in Fig. 4.16. The overshoot, rise time, settling time and bandwidth are obtained as 11%, 450 msec., 950 msec. and 1.15 Hz which are close to the corresponding design values for a 'slow' controller. Let this design be called STAVR-SO (slow and oscillatory) while the original design as per (3.7) with $N_u = 2$ be called STAVR-S.

A conventional digital AVR which has been designed for the 'slow' controller response for comparison purposes is given by the following parameters: Loop gain with the generator on open-circuit = 400; Lag time constants = 18.0, 0.94, 0.064 sec.; Lead time constants = 3.0, 0.6 sec. The step response of this AVR is shown in Fig. 4.17 and the overshoot, rise time, settling time and bandwidth are obtained as 12%, 425 msec., 1.6 sec. and 1.05 Hz respectively which are similar to the corresponding values of STAVR-SO. For future reference, let this design be called DGAVR-SO.

4.2.2 Evaluation of Step Response with the Generator on Load

The response of the excitation control system when the turbine generator is on load is very important since the system operates in this mode most of its life. The responses of the various types of AVR obtained on open-circuit in the previous section cannot normally be achieved when the generator is on load. This is due to the significant changes that the generator characteristics undergo when the operating mode is changed from open-circuit to loaded state. As observed during the evaluation of the parameter estimator, the steady state gain and dominant time constant in the loaded state are considerably lower than their open-circuit values and the system can exhibit some degree of oscillatory behaviour at high load conditions.

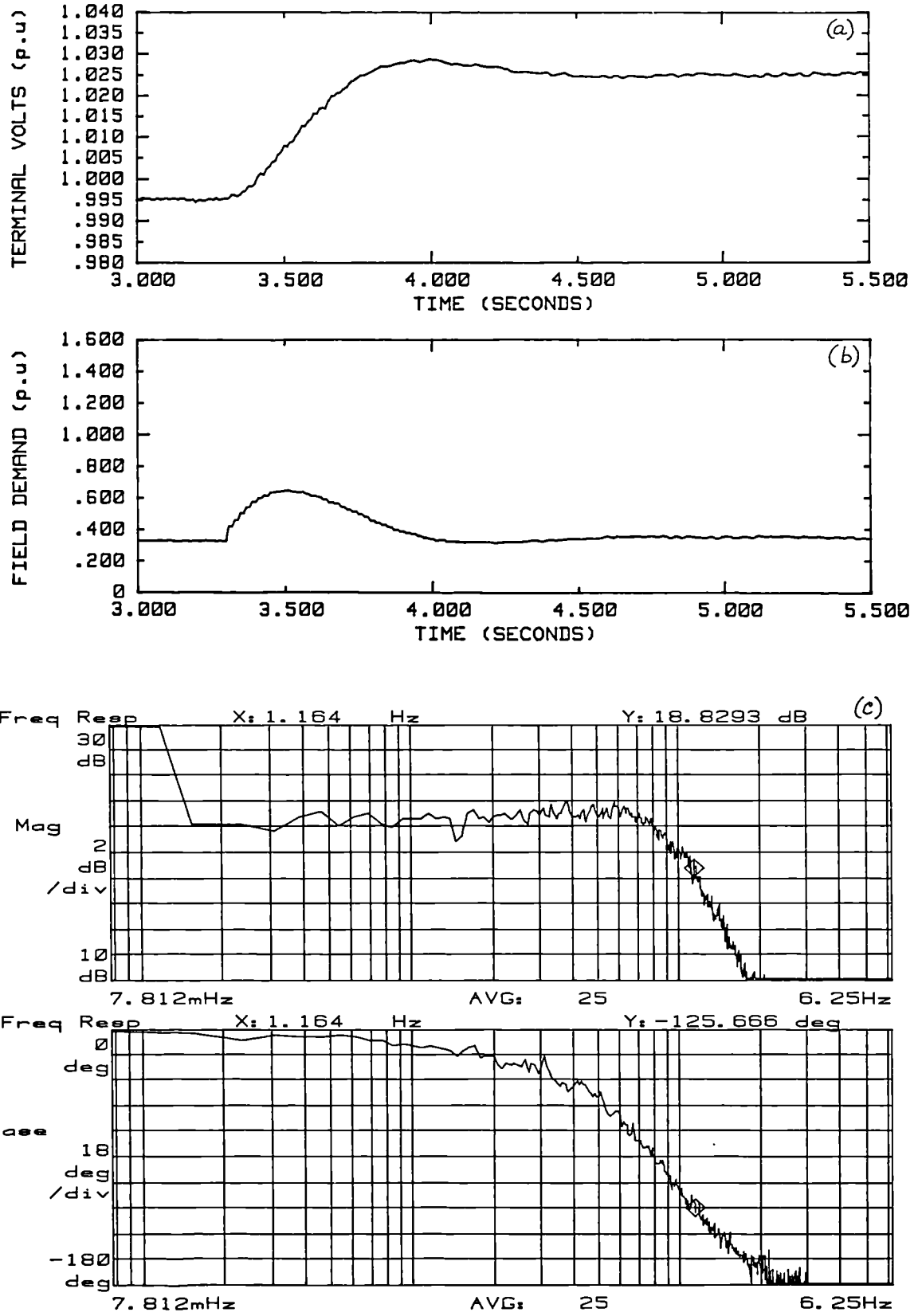

Fig. 4.16 Step response with micro-alternator on open-circuit (STAVR-SO; $N_u = 2$).

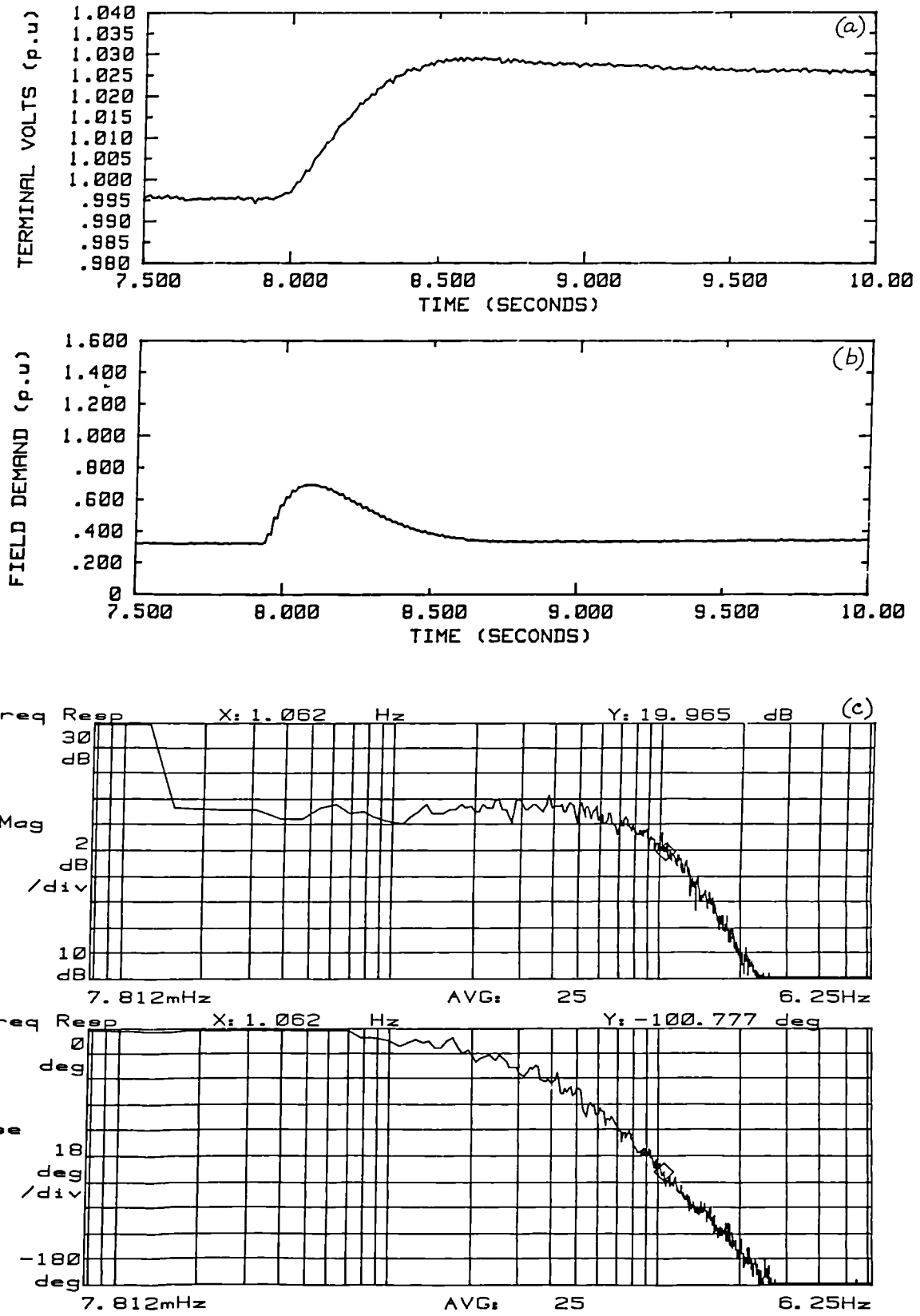

Fig. 4.17 Step response with micro-alternator on open-circuit (DGAVR-SO).

4.2.2.1 Step Response using the Micro-alternator System

The on-load step responses of the various types of AVR identified in the previous section have been evaluated using the micro-alternator system. As before, a step size of 3% has been chosen for these tests. Since a turbine generator is likely to work at its Continuous Maximum Rating (CMR) operating point for a significant part of its life, this point for the micro-alternator viz. P = 2.4 kW; Q = 1.8 kVAr lag, has been chosen for evaluation.

Fig 4.18(a) gives the step response characteristic of the system when STAVR-F has been used with the micro-alternator. It is observed that the over-shoot, rise and settling times achieved are 3.5%, 500 msec. and 500 msec. respectively. The significant change from the corresponding open-circuit values is the rise time which can be attributed to the reduction in the steady state gain of the micro-alternator by a factor of 4 to 6. The frequency response of the closed-loop system is shown in Fig. 4.18(c) which indicates a bandwidth of 3.6 Hz which is similar to the open-circuit case.

The step response of the micro-alternator system when a conventional AVR of type DGAVR-F is used is given in Fig. 4.19 for comparison purposes. It is found that the overshoot, rise and settling times obtained are 3%, 840 msec. and 840 msec. respectively and the bandwidth given by the frequency response plot is 1.7 Hz. These values are considerably different from the corresponding open-circuit values. This shows that the extent of variation in the response of the conventional digital AVR between open-circuit and on-load operation is significantly more than the corresponding variation with the self-tuning AVR.

Fig. 4.20 gives the step and frequency responses of the micro-alternator system when a 'slow' self-tuning AVR of type STAVR-S is used. The overshoot, rise time, settling time and bandwidth in this case are found to be 7.5%, 660 msec., 1.05 sec. and 1.5 Hz respectively. The corresponding values when the 'slow and oscillatory' self-tuning AVR of type STAVR-SO is used are obtained from Fig. 4.21 as 14%, 610 msec., 1.23 sec. and 1.57 Hz respectively. In both the

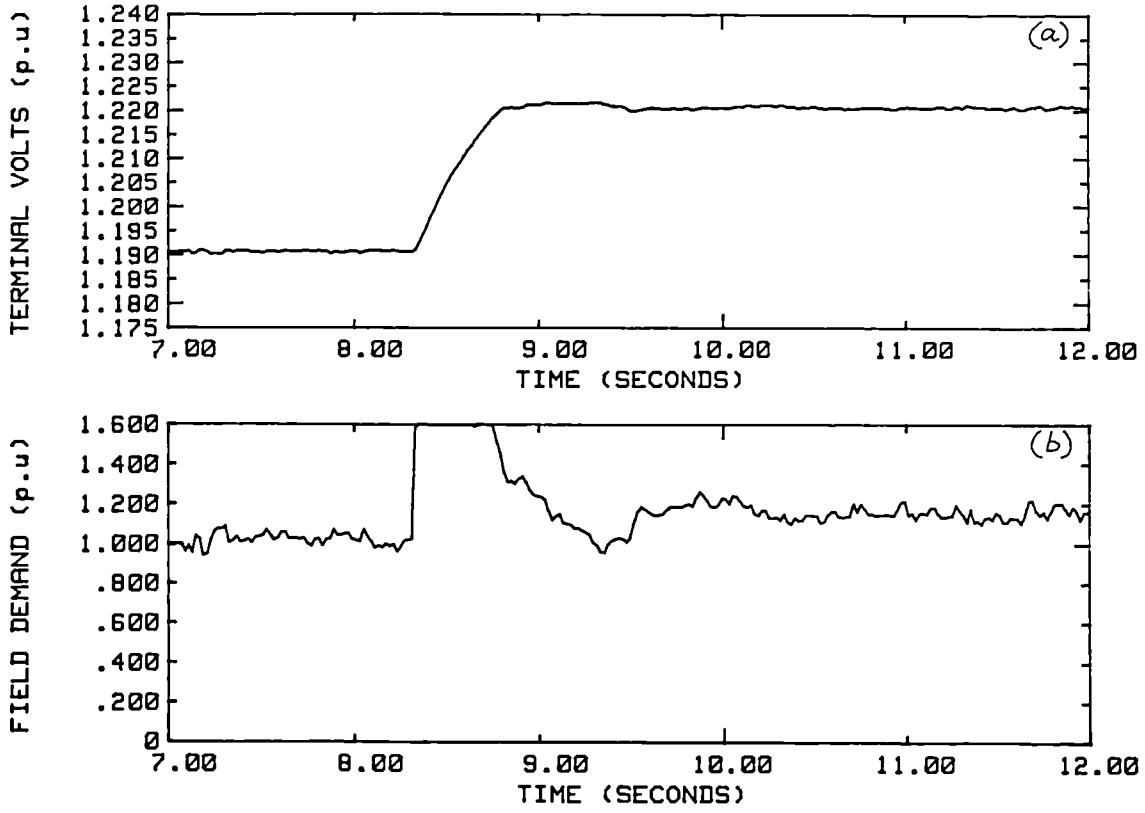

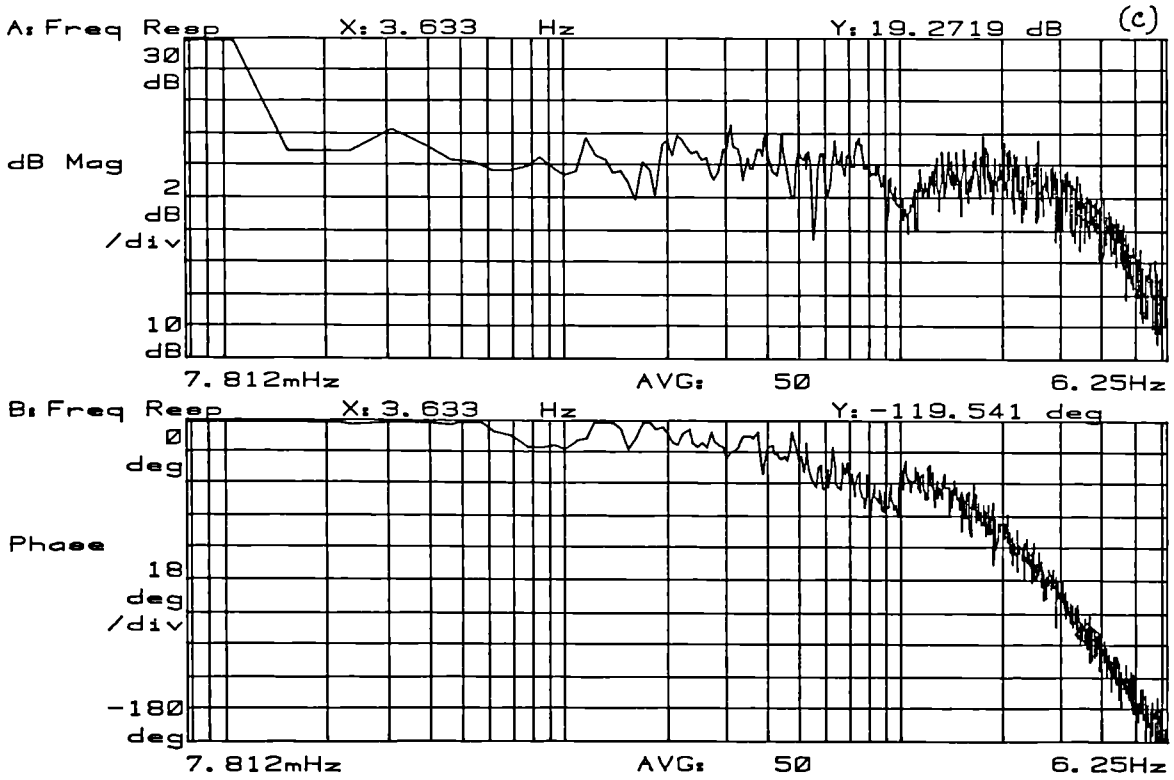

Fig. 4.18 Response with micro-alternator on load (STAVR-F).
(a), (b) Step response; (c), (d) Frequency response.

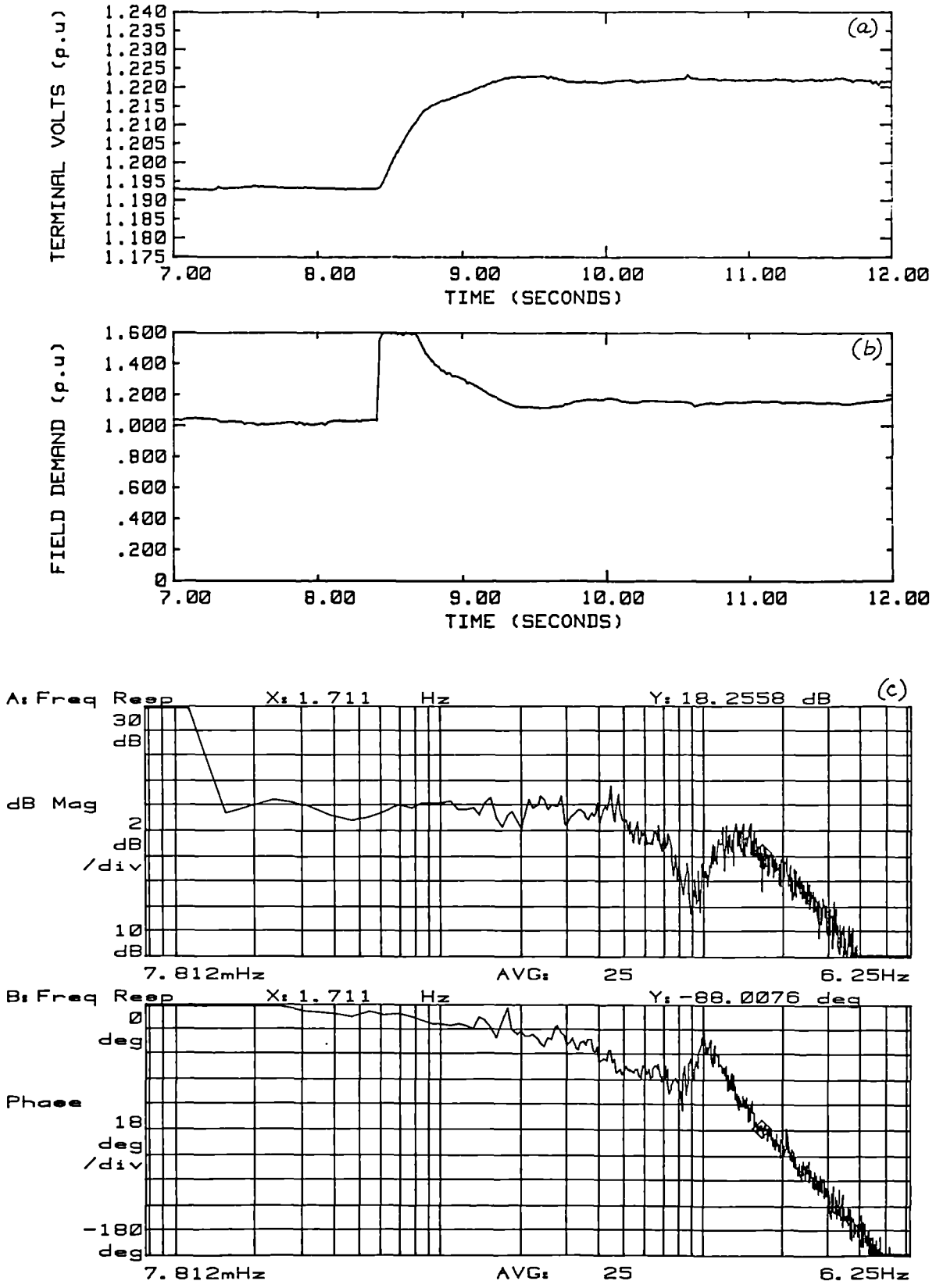

Fig. 4.19 Response with micro-alternator on load (DGAVR-F).
(a), (b) Step response; (c), (d) Frequency response.

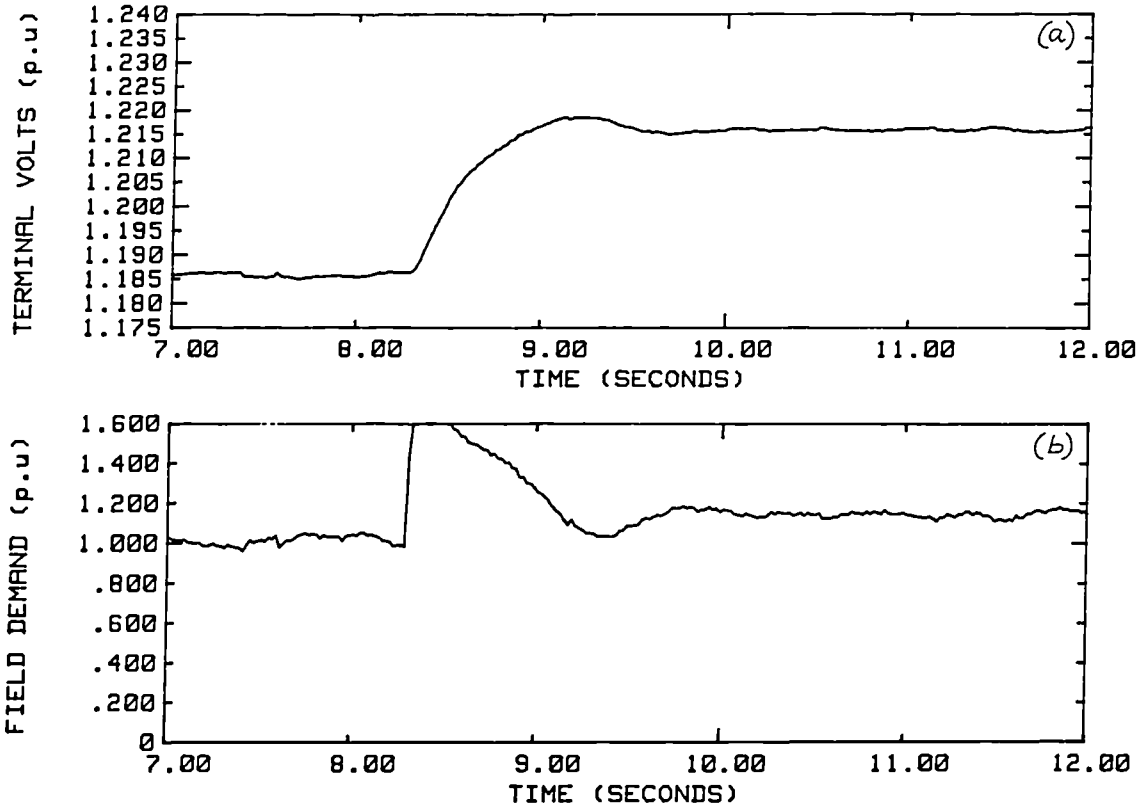

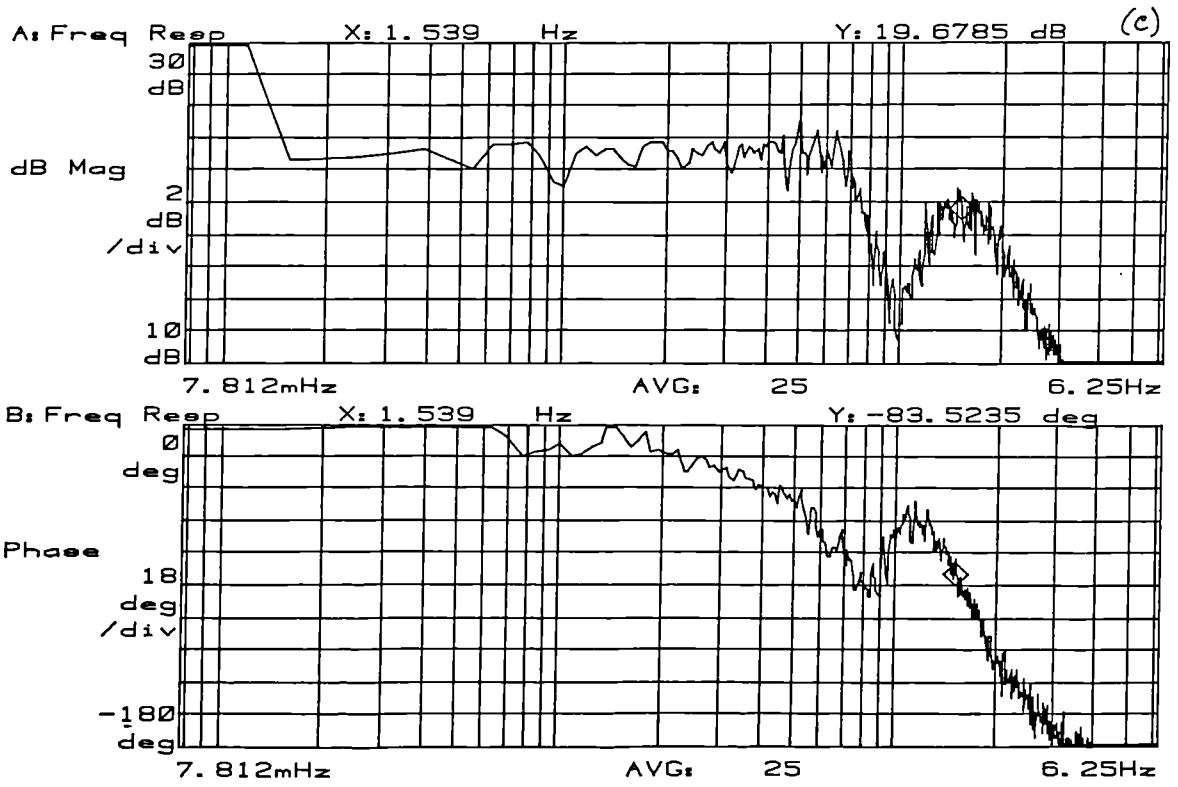

Fig. 4.20 Response with micro-alternator on load (STAVR-S).
(a), (b) Step response; (c), (d) Frequency response.

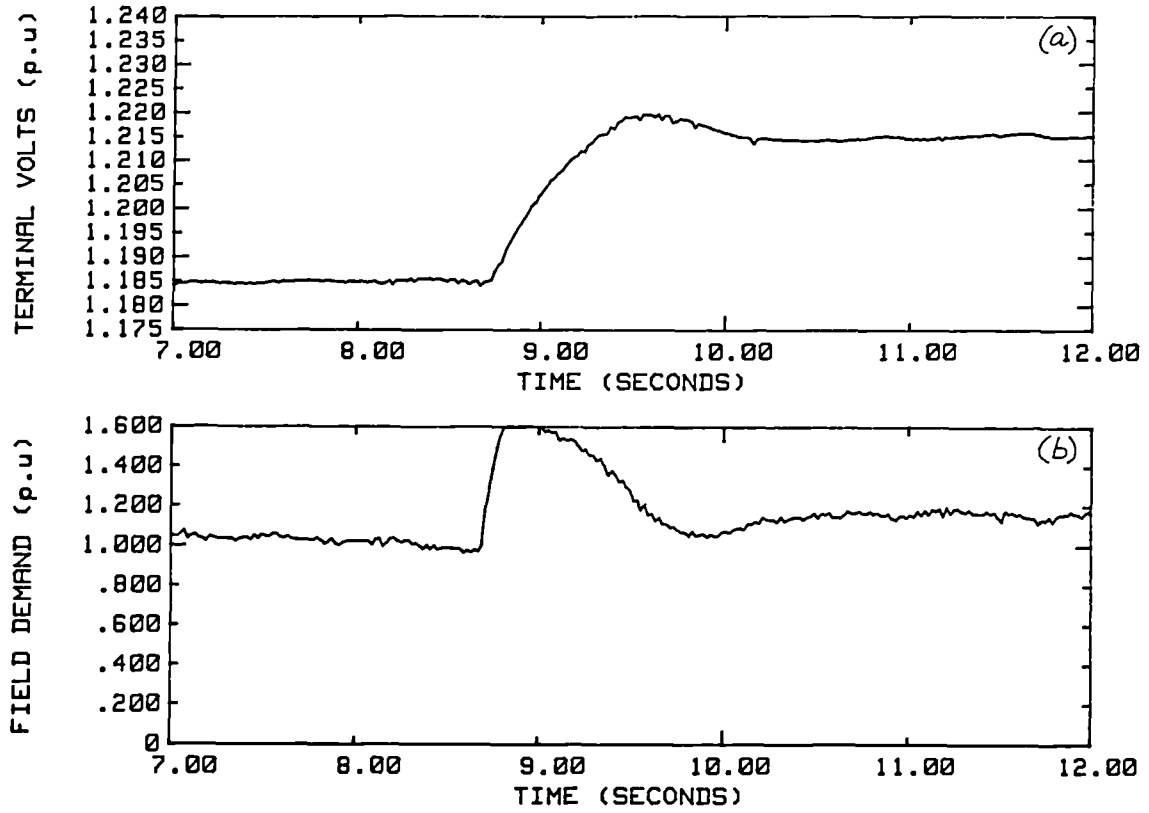

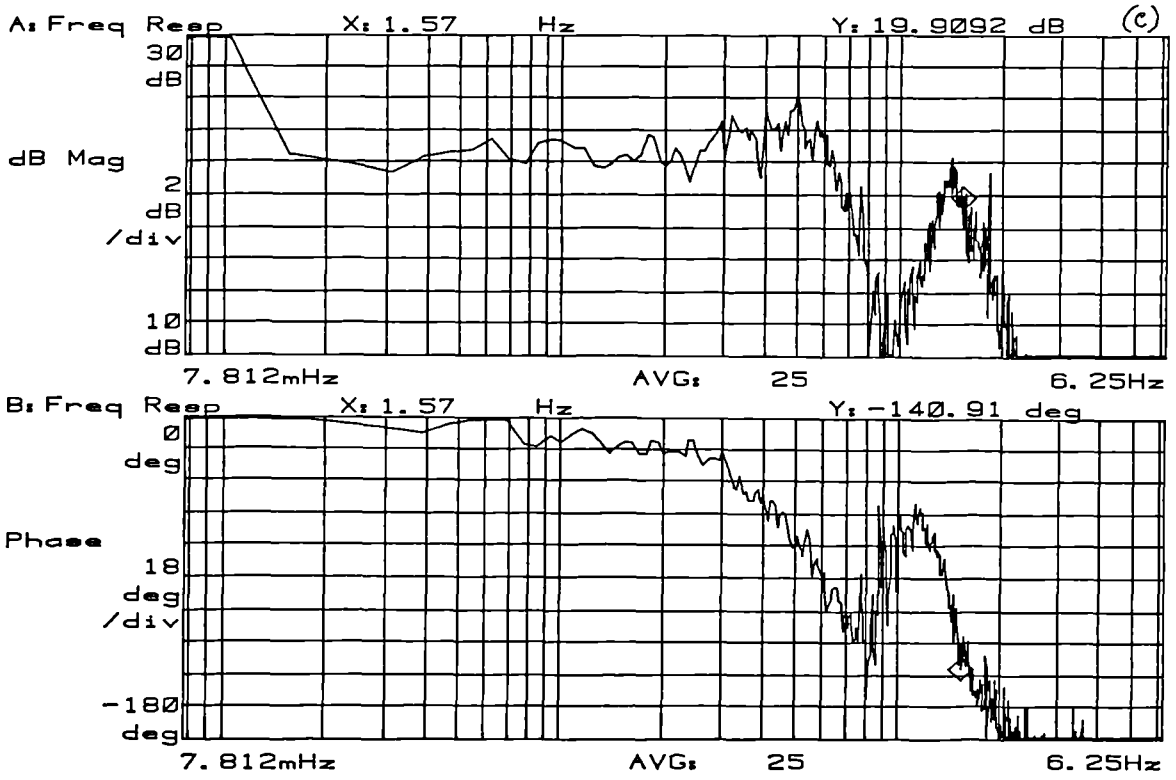

Fig. 4.21 Response with micro-alternator on load (STAVR-SO).
(a), (b) Step response; (c), (d) Frequency response.

cases, the extent of variation in the responses is similar to that when using the 'fast' self-tuning AVR of type STAVR-F.

For comparison purposes, the performance of a 'slow' conventional digital AVR of type DGAVR-SO has been evaluated at the CMR operating point of the micro-alternator system. The step and frequency responses obtained are shown in Fig. 4.22 from which the overshoot, rise time, settling time and bandwidth are calculated as 0%, 1.12 sec., 1.12 sec. and 0.5 Hz respectively. As observed with the 'fast' AVR, the values obtained in this case are also considerably different from the corresponding open-circuit values.

To assess the variability in performance over the complete operating range of the generator, a number of points at different parts of the P-Q diagram of the micro-alternator have been chosen for step and frequency response evaluation. The results obtained are tabulated in Table 4.1 for the 'fast' AVR and Table 4.2 for the 'slow' AVR designs. It can be observed from these tables that the performance of the excitation control system varies significantly over the operating range of the micro-alternator.

The maximum and minimum values when using the 'fast' AVR design given in Table 4.1 are summarised in Table 4.3 to assess the extent of variation when different types of AVR are used. It can be clearly seen from Table 4.3 that the variability in performance and closeness to the design values are significantly better for the self-tuning AVR than for the conventional one. The variability is less for the self-tuning AVR by a factor of at least 2 and the mean values are considerably closer to the design figures than those of the conventional AVR.

Table 4.4 is a summary of the performance of the 'slow and oscillatory' design of the AVR and is derived from Table 4.2. Once again, the observations made for the 'fast' AVR regarding the variability of values and closeness to design figures are found to be valid here also. From these, it can be concluded that the self-tuning AVR is superior to the conventional lag-lead based digital AVR because its repeatability of performance over the whole operating range of the generator is considerably better.

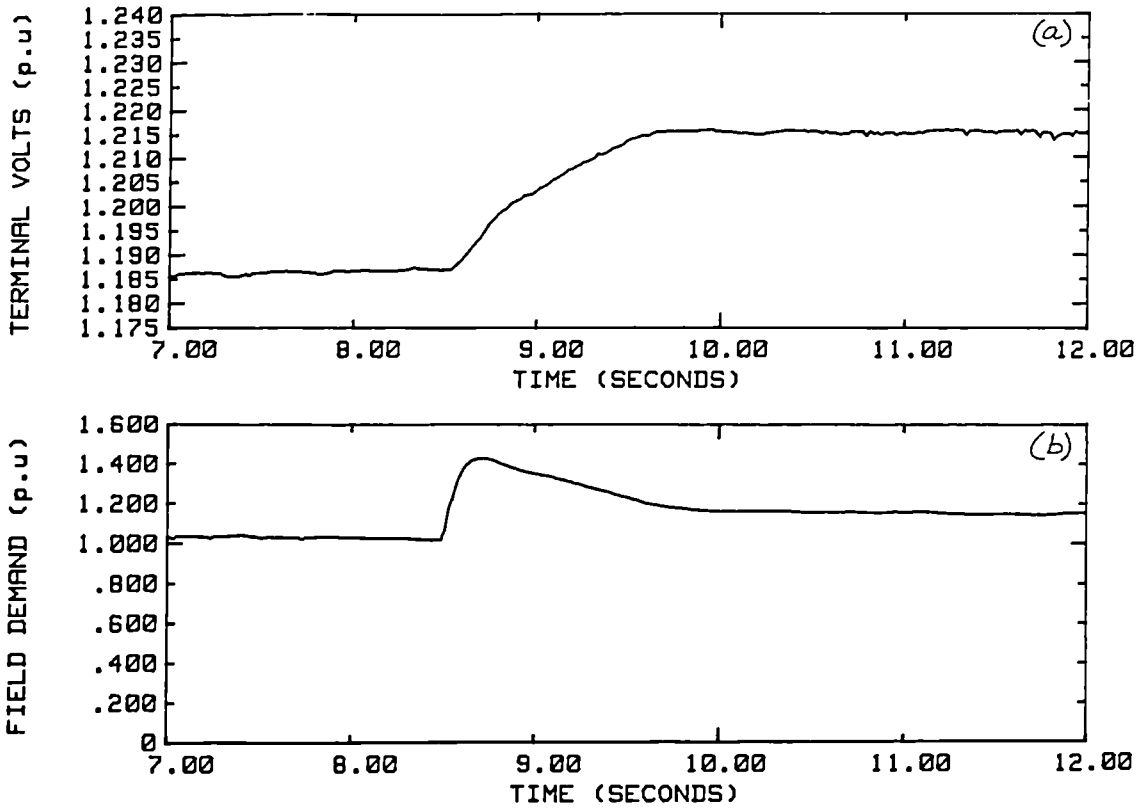

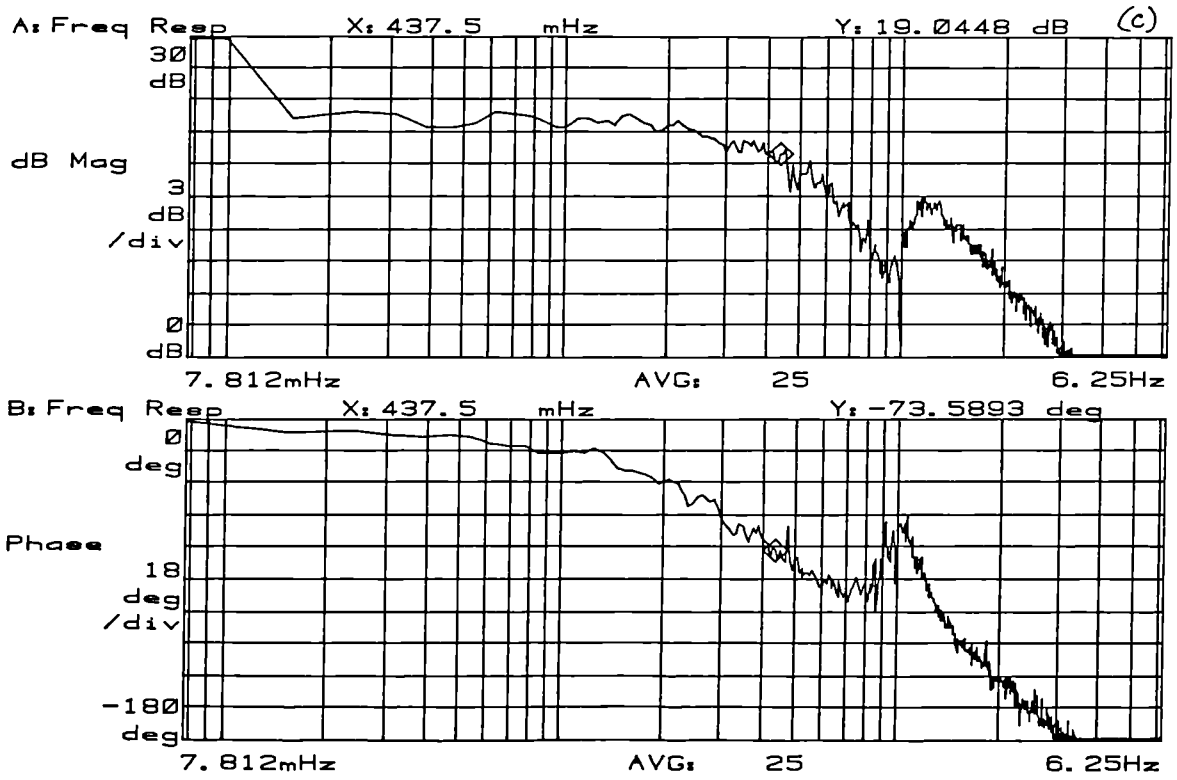

4.22 Response with micro-alternator on load (DGAVR-SO).
(a), (b) Step response; (c), (d) Frequency response.

P (kW); Q (kVAr)	V_t Over-shoot (%)	V_t Rise time (sec)	V_t Settling time (sec)	Bandwidth (Hz)	AVR Type
2.40; 0	4 0	0.400 0.900	0.400 0.900	4.6 1.3	STAVR-F DGAVR-F
2.40; 0.75 lag	4 6	0.475 0.900	0.475 1.200	4.1 1.4	STAVR-F DGAVR-F
2.40; 0.75 lead	1 0	0.500 0.975	0.500 0.975	4.1 0.6	STAVR-F DGAVR-F
2.40; 1.80 lag	4 3	0.500 0.840	0.500 0.840	3.6 1.7	STAVR-F DGAVR-F
1.50; 0	0 8	0.275 1.000	0.275 2.000	4.8 1.4	STAVR-F DGAVR-F
1.50; 0.75 lag	0 6	0.350 0.900	0.350 1.200	4.7 1.5	STAVR-F DGAVR-F
1.50; 0.75 lead	0 0	0.350 1.150	0.350 1.150	4.7 1.2	STAVR-F DGAVR-F
0.60; 0	2 7	0.400 1.000	0.400 1.500	4.7 1.5	STAVR-F DGAVR-F
0.60; 1.00 lag	0 0	0.165 0.950	0.165 0.950	4.3 1.4	STAVR-F DGAVR-F
0.60; 1.00 lead	0 6	0.225 1.860	0.225 3.800	4.9 1.3	STAVR-F DGAVR-F
0.25; 0	0 0	0.225 1.270	0.225 2.500	4.6 1.5	STAVR-F DGAVR-F
0.25; 1.00 lag	0 0	0.275 0.680	0.275 0.680	4.2 1.5	STAVR-F DGAVR-F
0.25; 1.00 lead	0 6	0.240 1.600	0.240 2.500	4.7 1.6	STAVR-F DGAVR-F

Table 4.1. Comparison of performance of the 'fast' AVR designs.

P (kW); Q (kVAr)	V_t Over-shoot (%)	V_t Rise time (sec)	V_t Settling time (sec)	Bandwidth (Hz)	AVR Type
2.40; 0	11 11	0.615 1.500	1.130 4.000	1.7 0.3	STAVR-SO DGAVR-SO
2.40; 0.75 lag	10 4	0.635 1.300	1.090 3.000	1.6 0.4	STAVR-SO DGAVR-SO
2.40; 0.75 lead	8 16	0.685 1.600	1.130 4.500	1.3 0.3	STAVR-SO DGAVR-SO
2.40; 1.80 lag	14 0	0.610 1.120	1.230 1.120	1.6 0.5	STAVR-SO DGAVR-SO
1.50; 0	9 6	0.610 1.350	1.200 2.700	1.6 0.3	STAVR-SO DGAVR-SO
1.50; 0.75 lag	12 4	0.640 1.250	1.250 1.250	1.5 0.4	STAVR-SO DGAVR-SO
1.50; 0.75 lead	7 0	0.525 2.140	0.840 2.140	1.5 0.2	STAVR-SO DGAVR-SO
0.60; 0	10 6	0.735 1.300	1.300 2.500	1.5 0.4	STAVR-SO DGAVR-SO
0.60; 1.00 lag	12 3	0.525 1.100	1.300 1.100	1.4 0.5	STAVR-SO DGAVR-SO
0.60; 1.00 lead	6 17	0.490 2.250	0.960 7.000	1.5 0.4	STAVR-SO DGAVR-SO
0.25; 0	7 7	0.515 1.130	1.350 1.900	1.3 0.5	STAVR-SO DGAVR-SO
0.25; 1.00 lag	7 0	0.500 1.350	1.150 1.350	1.3 0.5	STAVR-SO DGAVR-SO
0.25; 1.00 lead	12 17	0.465 1.880	0.990 5.000	1.5 0.9	STAVR-SO DGAVR-SO

Table 4.2. Comparison of performance of the 'slow' AVR designs.

Description	V_t Overshoot (%)	V_t Rise time (sec)	V_t Settling time (sec)	Bandwidth (Hz)
STAVR-F	0 to 4	0.165 to 0.50	0.165 to 0.50	3.6 to 4.9
DGAVR-F	0 to 8	0.68 to 1.86	0.68 to 3.80	0.6 to 1.7
Design	4.3	0.13	0.23	4.0

Table 4.3. Summary of performance of the 'fast' AVR designs.

Description	V_t Overshoot (%)	V_t Rise time (sec)	V_t Settling time (sec)	Bandwidth (Hz)
STAVR-SO	6 to 14	0.47 to 0.74	0.84 to 1.35	1.3 to 1.7
DGAVR-SO	0 to 17	1.10 to 2.25	1.10 to 7.00	0.2 to 0.9
Design	12.6	0.37	1.04	1.35

Table 4.4. Summary of performance of the 'slow and oscillatory' AVR designs.

4.2.2.2 Step Response using the TG Simulator

The step response when using the various types of AVR on the TG simulator has also been investigated. The simulator has been set up to represent a typical 660 MW turbine generator system and a positive step of 3% has been used during these tests. The operating point has been chosen to be P = 0.8 pu; Q = 0 pu for the simulator. The purpose of these tests is to confirm that performance similar to the ones obtained with the micro-alternator can be repeated with the TG simulator also.

Fig. 4.23(a) gives the step response with the 'fast' self-tuning AVR type STAVR-F. The overshoot, rise and settling times in this case are found to be 1%, 0.205 sec. and 0.205 sec. respectively. The corresponding values for the conventional AVR type DGAVR-F obtained from Fig. 4.23(c) are 0%, 0.950 sec. and 0.950 sec. respectively. The responses obtained are comparable to those on the micro-alternator system.

The step response with the 'slow' self-tuning AVR type STAVR-S is given in Fig. 4.24(a) from which it can be calculated that the overshoot, rise and settling times achieved are 2%, 0.420 sec. and 0.420 sec. respectively. The corresponding values for STAVR-SO obtained from Fig. 4.24(c) are 10%, 0.465 sec. and 1.02 sec. which are very close to the mean values obtained on the micro-alternator. Fig. 4.24(e) shows the step response for the conventional DGAVR-SO in which the response values are found to be 8%, 1.2 sec. and 2.66 sec. respectively. Thus responses similar to the ones obtained with the micro-alternator system are achieved for the TG simulator also.

4.3 Performance Evaluation during Abnormal Operating Conditions of the Generator

Major disturbances that occur in the power system from time to time can seriously affect the smooth operation of the excitation control system. These disturbances which are transient in nature are classed as abnormal operating conditions of the generator. Although the occurrence of these abnormal operating conditions are very infrequent, the performance of an AVR during these events should be evaluated to assess whether the controller is able to cope with such situations satisfactorily.

In the case of the self-tuning AVR, the GPC cost function considers only the deviations of the terminal voltage from its set point and the liveliness of the control signal. However, during major disturbances the rotor / load angle of the generator is disturbed significantly and can take some time to settle down following the event. It is generally thought that a fast acting AVR such as the self-tuning

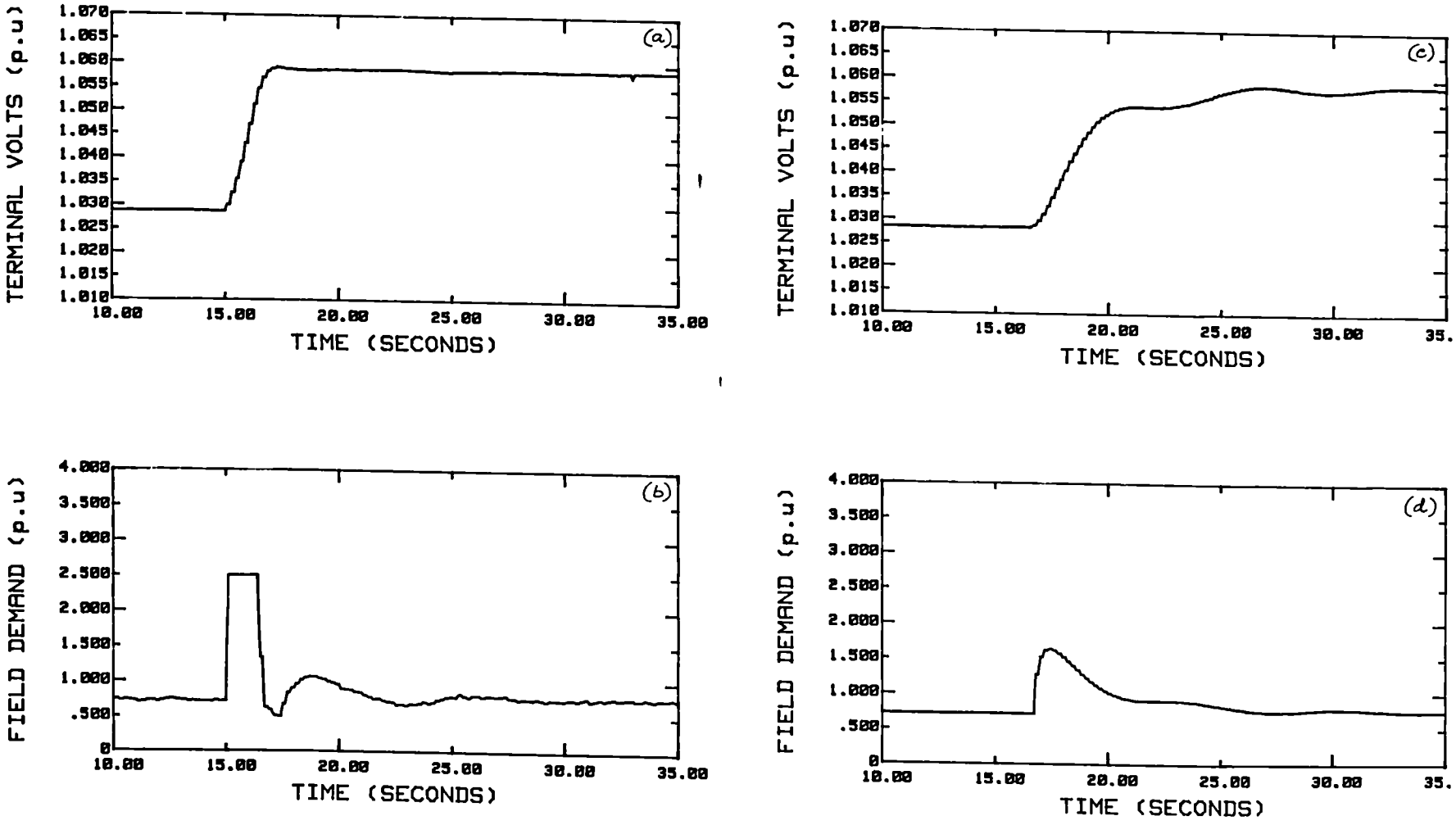

Fig. 4.23 Step response with TG simulator.
(a), (b) - STAVR-F; (c), (d) - DGAVR-F.

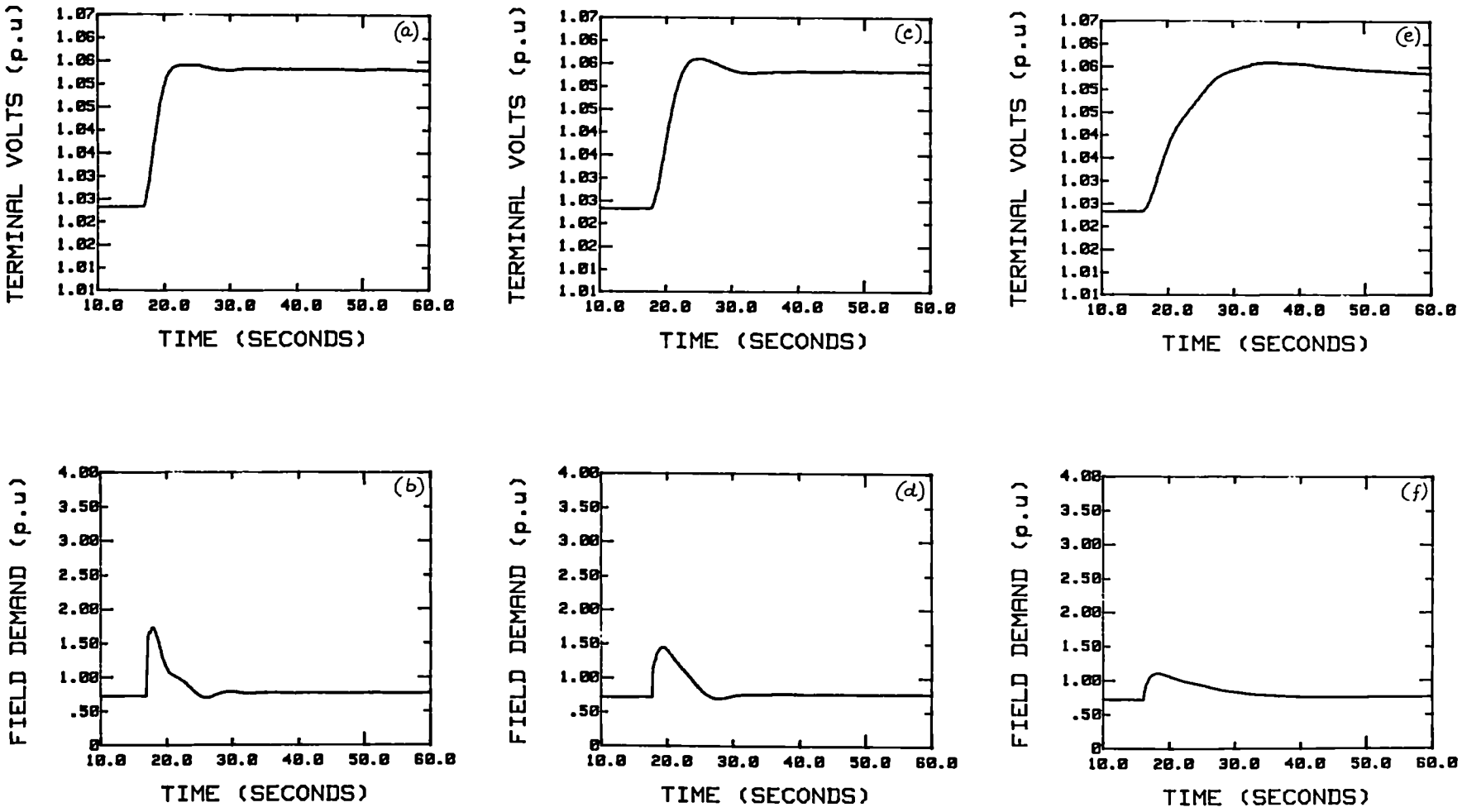

Fig. 4.24 Step response with TG simulator.
(a), (b) - STAVR-S; (c), (d) - STAVR-SO; (e), (f) - DGAVR-SO.

controller can reduce the damping torque of the generator if it uses only the terminal voltage as its feedback signal. The consequence of this is the reduction in the damping of rotor oscillations following a major disturbance. This aspect should therefore be examined in detail to ensure that sufficient damping of rotor oscillations is provided by the self-tuning AVR.

4.3.1 Evaluation using the TG Simulator

The response of a turbine generator to severe disturbances depends very much on its severity as well as the conditions of the power system at which the disturbance occurs. Since various power system conditions under which a turbine generator is required to operate can be easily created by the TG simulator, it is a convenient way of evaluating the performance of the excitation control system under these conditions. Two of the most severe disturbances that a turbine generator can be subjected to are the 3-phase short-circuit and short-circuit followed by a transmission line switching. The performance of the various types of AVR evaluated earlier are examined under these conditions in the following sub-sections using the TG simulator.

4.3.1.1 Three-phase Short-circuit

During this test, a sudden short-circuit is applied to the stator terminals of the generator and is removed after a period of 100 msec. The operating point of the generator has been chosen as P = 0.8 pu; Q = 0 pu and the load angle is 68.5 deg. The greater the load angle the more severe is the test since the stability margin of the rotor is lesser in that case. To measure and compare the damping available to the rotor during the disturbance, a factor called the 'Effective Damping Ratio' (EDR) has been used. This factor is widely used in the industry for similar applications and is defined as the ratio of the peak-to-peak amplitude between the first undershoot of a signal following a disturbance and the second over-shoot, to the peak-to-peak amplitude between the first undershoot and the first overshoot [14]. A lower value of the EDR indicates a higher value of damping.

Fig. 4.25 gives the response of the terminal voltage, excitation demand and load angle of the system during the 3-phase short-circuit test when a 'fast' self-tuning AVR of the type STAVR-F has been used with the simulator. It may be noted that the TG simulator is running 10 times slower than 'real' time and hence this factor should be applied to the X-axis for conversion purposes. The EDR of the load angle in this case is found to be 0.64 and the settling time of the signal to +/- 2 deg. within 1.25 sec. The terminal voltage is seen to settle down in 0.390 sec. The self-tuning AVR is found to perform satisfactorily during this test and the damping of the rotor is adequate. The response of a conventional digital AVR type DGAVR-F under similar conditions is also shown in Fig. 4.25 which gives an EDR of 0.73, settling times for load angle and terminal voltage of 2.14 sec. and 0.60 sec. respectively. In this case, STAVR-F is seen to perform better than DGAVR-F.

The 3-phase short-circuit test has been repeated with the 'slow' AVR designs, viz. STAVR-S, STAVR-SO and DGAVR-SO. The responses obtained when using these controllers are given in Fig. 4.26. The EDR of the load angle for each case is calculated as 0.53, 0.61 and 0.59 respectively. The settling time of the load angle is found to be 1.040, 0.900 and 2.21 sec. respectively. It is seen that the terminal voltage settles down after the fault in 0.490, 0.410 and 1.35 sec. respectively. The self-tuning AVR is found to be similar in the damping of the rotor, but faster in terms of settling when compared with the corresponding conventional AVR.

4.3.1.2 Three-phase Short-circuit Followed by the Switching of a Transmission Line

The isolation of the faulty transmission line following a short-circuit in the transmission network is a possible occurrence in power systems. This can increase the line reactance considerably in some power systems and hence cause a worse disturbance compared with a simple 3-phase short-circuit. In the TG simulator, this test is carried out by applying a short-circuit for 100 msec. at the end of which the transmission line reactance is increased from 0.25 pu to 0.50 pu

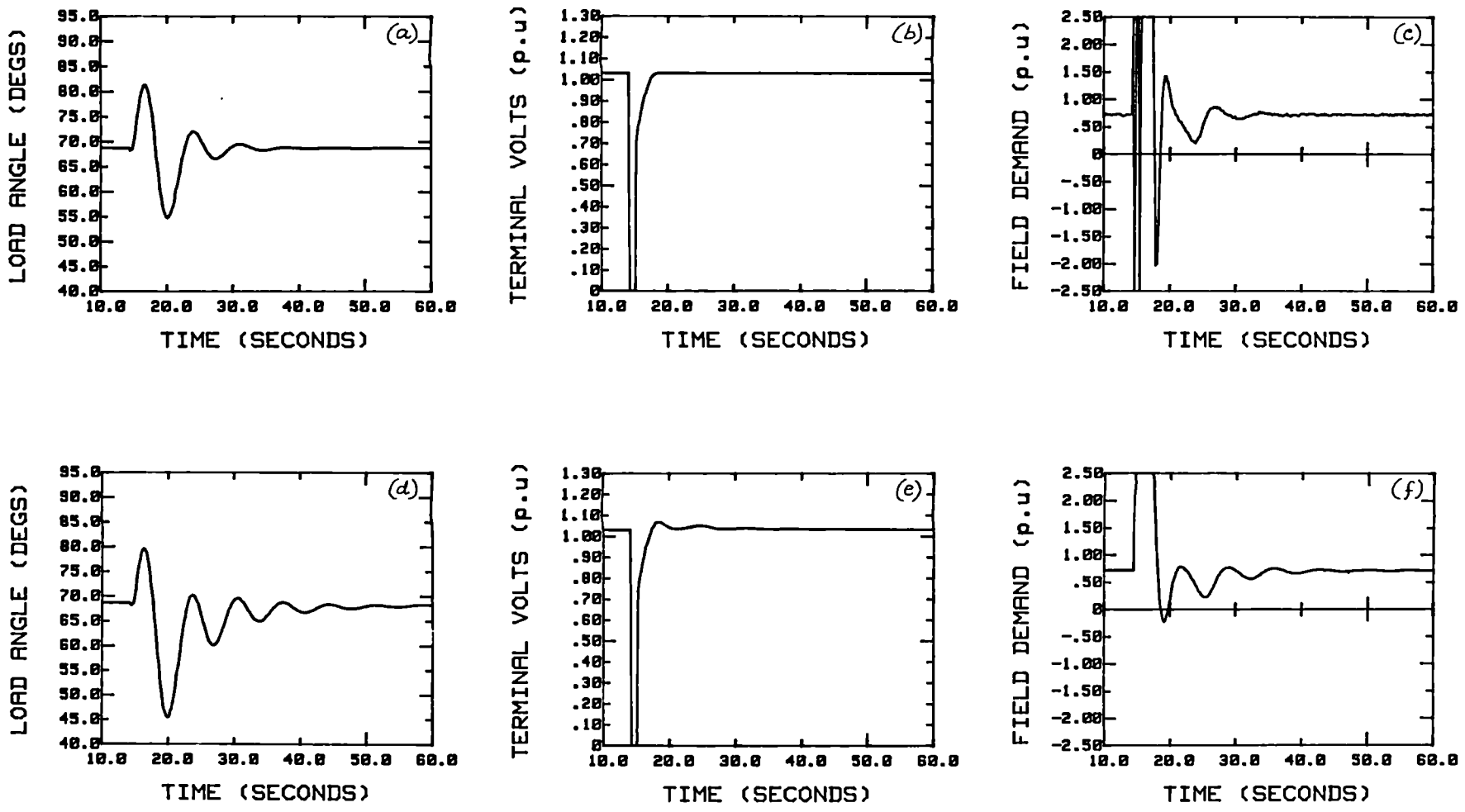

Fig. 4.25 Three phase short circuit test with TG simulator.
(a), (b), (c) - STAVR-F; (d), (e), (f) - DGAVR-F.

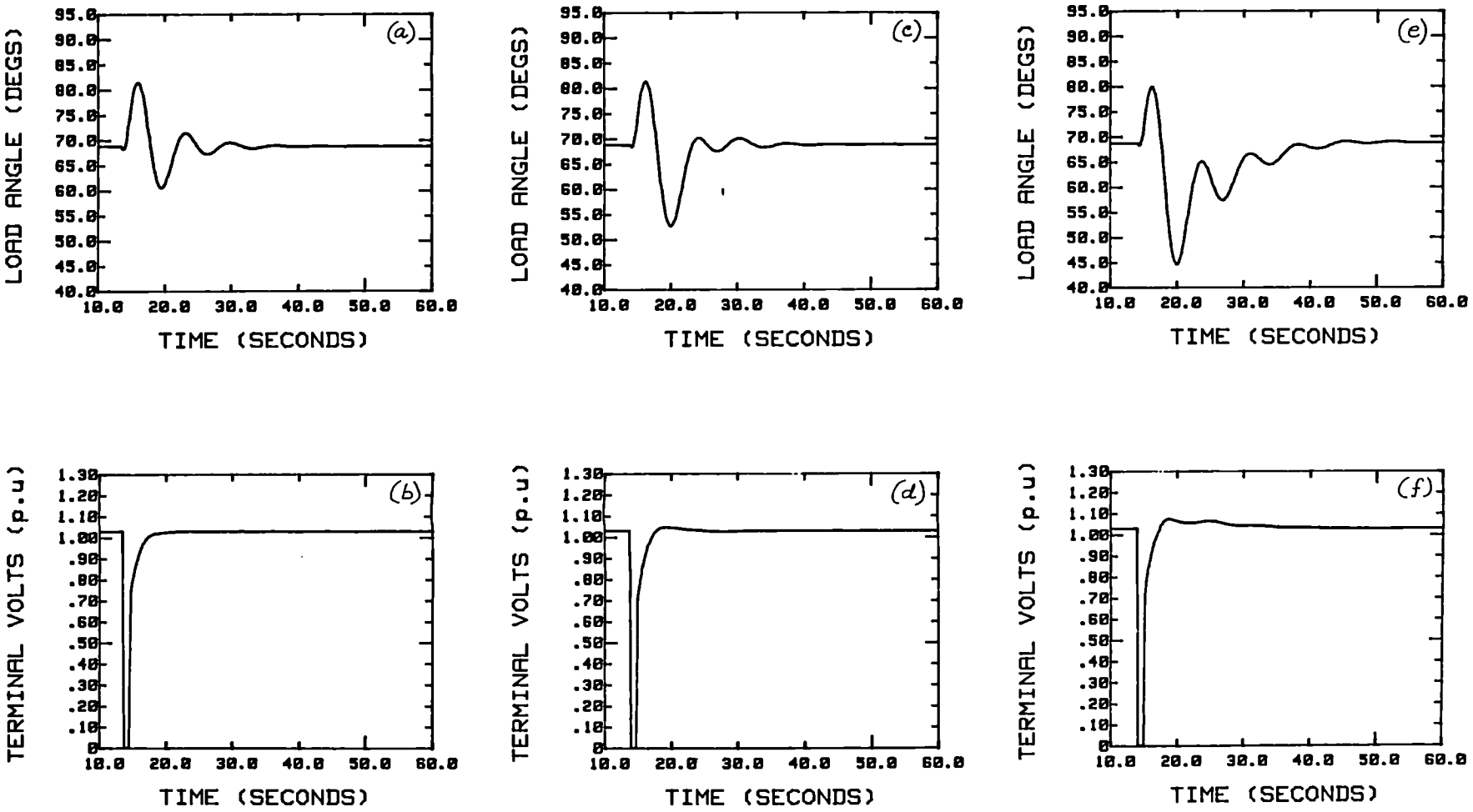

Fig. 4.26 Three phase short circuit test with TG simulator.
(a), (b) - STAVR-S; (c), (d) - STAVR-SO; (e), (f) - DGAVR-SO.

to simulate the removal of a line. This causes the load angle to settle to a higher value after the fault which results in a further reduction in the rotor stability margin.

The response of the system when using a 'fast' self-tuning AVR of type STAVR-F is shown in Fig. 4.27. The operating point of the generator before the fault is the same as the one used in the previous test and the new load angle after the fault is 84.5 deg. The EDR of the load angle and its settling time are 0.73 and 1.9 sec. respectively, while the settling time of the terminal voltage is 0.50 sec. Although the damping of the rotor is not as good as in the previous case, it is justified considering the severity of the test. The response of the system when using a conventional AVR of type DGAVR-F is also given in Fig. 4.27. The rotor damping is very light in this case with an EDR of 0.96 and a settling time of 5.1 sec. The terminal voltage is found to settle down in 2.4 sec. The self-tuning AVR is able to perform better in this test also.

Fig. 4.28 illustrates the performance of the 'slow' AVR designs, viz. STAVR-S, STAVR-SO and DGAVR-SO during the above test. The EDR of the load angle is obtained as 0.70, 0.74 and 0.84, and its settling times as 2.15, 2.58 and 3.6 sec. respectively. The terminal voltage is found to settle down in 0.56, 0.80, and 2.28 sec. respectively. In this case too the self-tuning AVR designs are found to cope with the disturbance better than the corresponding conventional AVR.

4.3.2 Evaluation using the Micro-alternator System

The performance of the various types of AVR identified earlier needs to be evaluated during abnormal operating conditions of the micro-alternator system. This exercise helps to validate the results obtained using the TG simulator in similar operating conditions. It is difficult to achieve an exact match in the test conditions between the TG simulator and the micro-alternator and the situation is further complicated by schemes such as the back-swing compensation. Hence, results identical to the ones obtained with the TG simulator are generally not achieved on the micro-alternator system. However, the measurement of EDR, settling times etc. can provide the required assessment of the performance of the AVR.

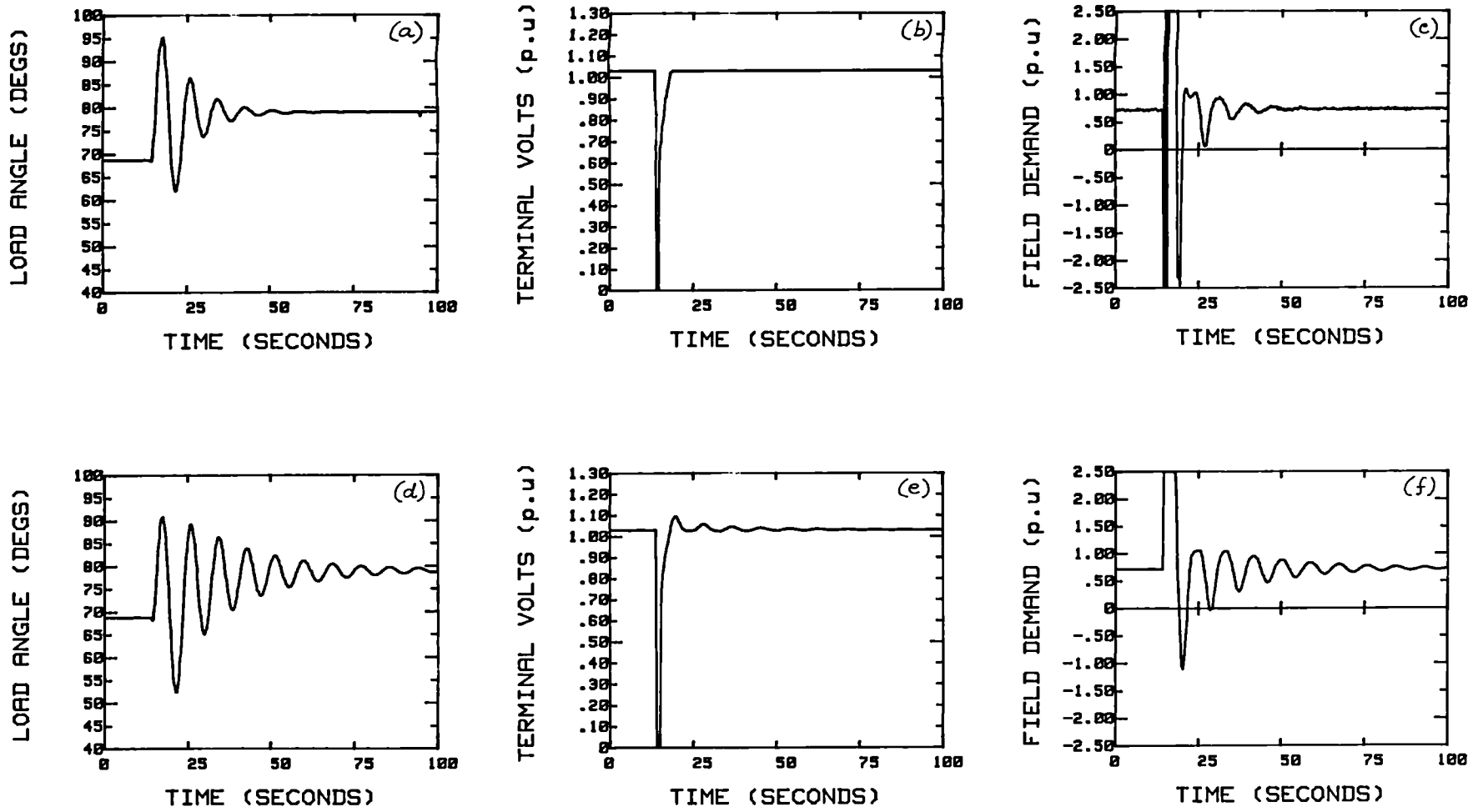

Fig. 4.27 Three phase short circuit and line switch test with TG simulator.
(a), (b), (c) - STAVR-F; (d), (e), (f) - DGAVR-F.

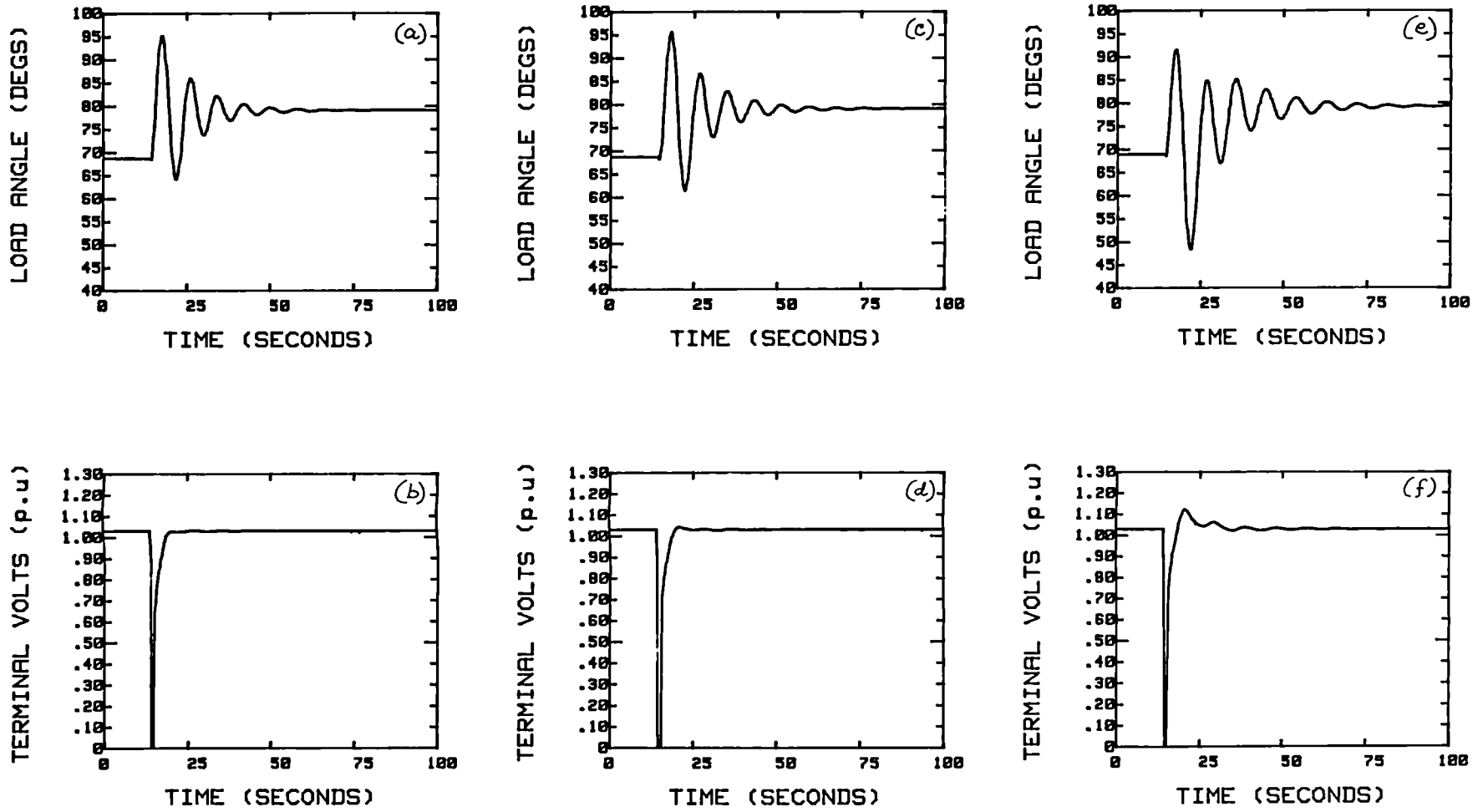

Fig. 4.28 Three phase short circuit and line switch test with TG simulator.
(a), (b) - STAVR-S; (c), (d) - STAVR-SO; (e), (f) - DGAVR-SO.

4.3.2.1 Three-phase Short-circuit

The 3-phase to neutral short-circuit test has been carried out on the micro-alternator at P = 2.4 kW (0.8 pu) and Q = 0. The load angle corresponding to this operating point is found to be 68 deg. The short-circuit has been applied at the sending end of the transmission line simulator and is performed using the point-on-wave switching unit which acts through a set of thyristors and contactors.

Fig. 4.29 gives the response of the micro-alternator system to the short-circuit when a 'fast' self-tuning AVR of the type STAVR-F has been used. The EDR of the load angle signal and its settling time are found to be 0.34 and 3.35 sec. respectively and the terminal voltage settles in 1.02 sec. It is observed that the performance obtained with the self-tuning AVR is satisfactory. The test has been repeated with a conventional AVR of the type DGAVR-F and the response obtained is also shown in Fig. 4.29 for comparison purposes. It is observed that the EDR and settling time of the load angle are 0.42 and 3.1 sec. respectively and the settling time of the terminal voltage is 1.53 sec. It can be seen that the performance of STAVR-F and DGAVR-F are similar which indicates that the self-tuning AVR has not reduced the damping of the rotor in this case.

The 3-phase short-circuit test has been performed on the micro-alternator using the 'slow' AVR designs also. The responses obtained with STAVR-S and STAVR-SO are shown in Fig. 4.30. It can be seen that the EDRs of the load angle signal are 0.26 and 0.27, and that its settling times are 2.32 and 1.2 sec. respectively. The terminal voltage signal is found to settle in 1.2 and 1.31 sec. respectively. Both types of the 'slow' self-tuning AVR are seen to perform satisfactorily with no significant reduction in the damping of the rotor. Fig. 4.30 also gives the response when a conventional AVR of the type DGAVR-SO is used in the system. The EDR, load angle settling time and terminal voltage settling time in this case are 0.41, 3.71 sec. and 2.45 sec. respectively. The self-tuning AVR is found to perform better than the corresponding conventional AVR in this case too.

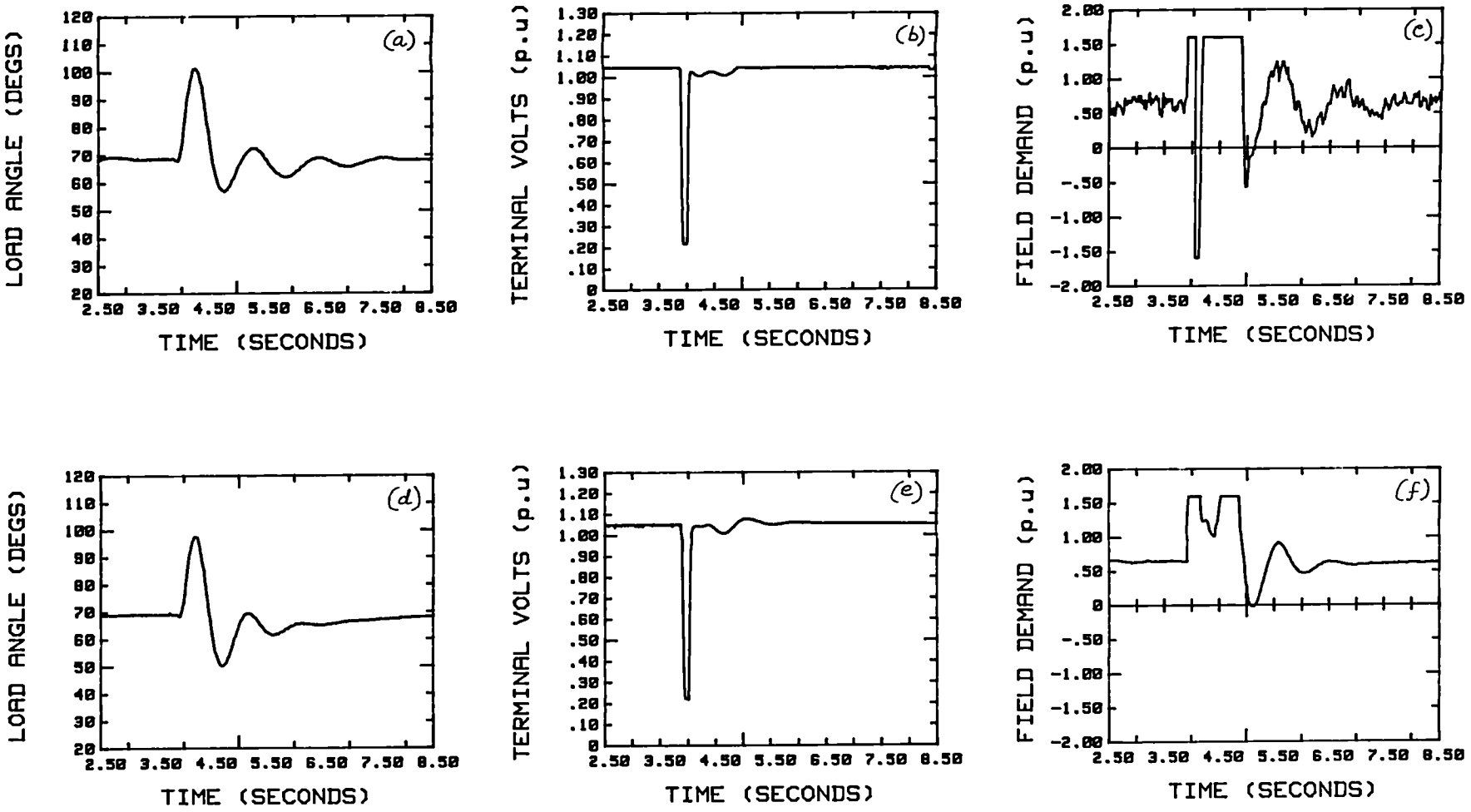

Fig. 4.29 Three phase short circuit test with micro-alternator on load.
(a), (b), (c) - STAVR-F; (d), (e), (f) - DGAVR-F.

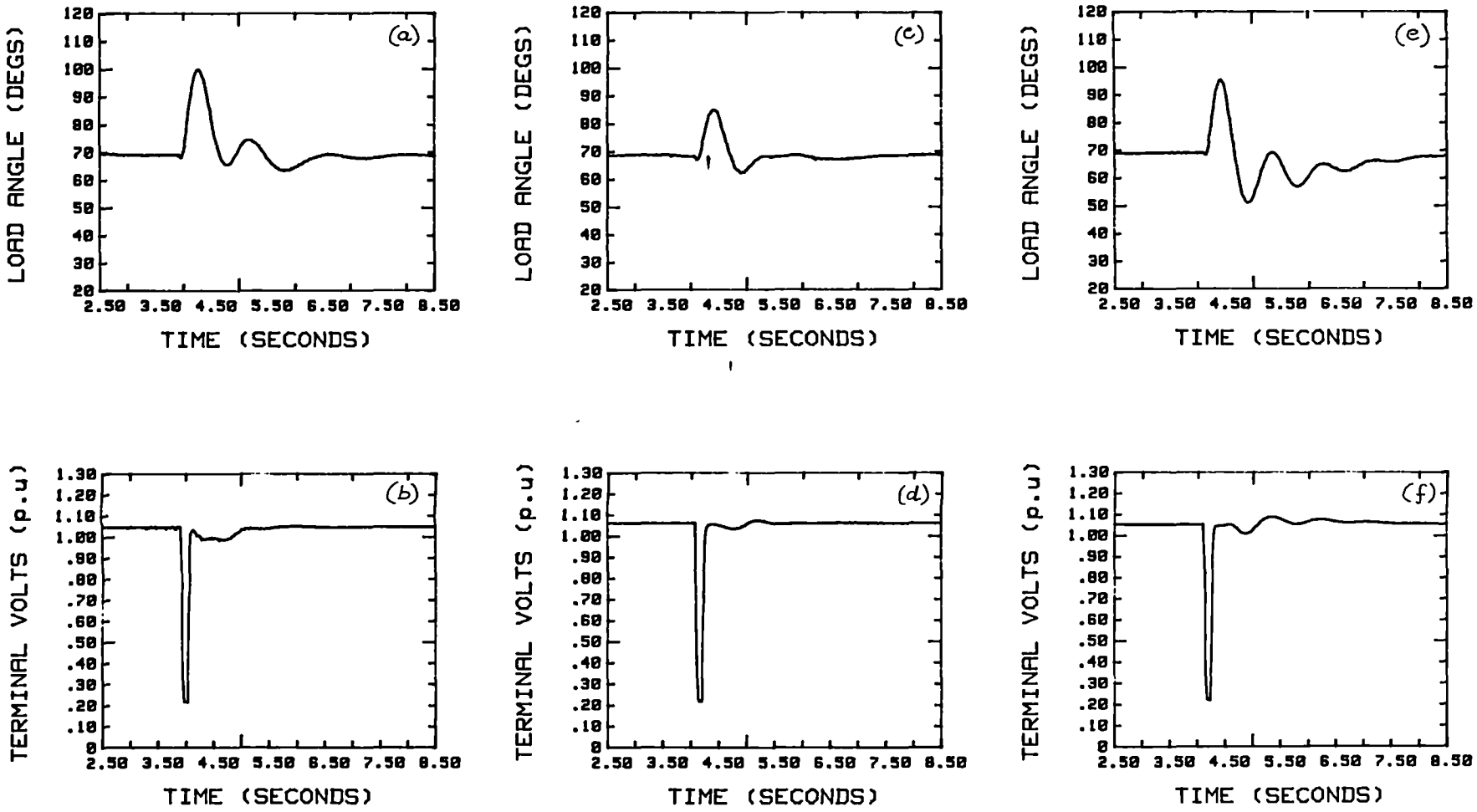

Fig. 4.30 Three phase short circuit test with micro-alternator.
(a), (b) - STAVR-S; (c), (d) - STAVR-SO; (e), (f) - DGAVR-SO.

4.3.2.2 Three-phase Short-circuit Followed by a Transmission Line Outage

A 3-phase short-circuit with one of the transmission line simulators disconnected at the end of the fault has been applied to the micro-alternator system. This test is not as severe as the one conducted using the TG simulator since the reactance of a transmission line simulator is only 0.250 pu. Thus the line reactance is switched from 0.125 to 0.250 pu at the end of the short-circuit during this test. The test has been done with 2 point-on-wave switching units connected in a master slave arrangement. The master applies the short-circuit and signals the slave at the end of the short-circuit to disconnect one of the transmission line simulators. The duration of the short-circuit is set to 100 msec. and the operating point is P = 2.4 kW; Q = 0. The load angle before the fault is 60 deg. and its final settling value at the end of the test is 64 deg.

Fig. 4.31 gives the response of the micro-alternator system when a 'fast' self- tuning AVR of the type STAVR-F has been used during this test. The EDR and the settling time of the load angle to its new value are obtained as 0.52 and 2.33 sec. respectively, and the terminal voltage is found to settle within 0.96 sec. These values indicate that acceptable performance is obtained with the 'fast' self-tuning AVR even under a severe abnormality in the system. The performance of a conventional AVR of type DGAVR-F is also given in Fig. 4.31 for comparison purposes from which the EDR, settling of load angle and settling of terminal voltage are found to be 0.38, 4.3 sec. and 4.0 sec. respectively. It can be observed that although the EDR is better than that of the self-tuning AVR, the rotor in this case reaches its final settling value only slowly which indicates a reduced synchronising torque.

The response of the 'slow' AVR designs have also been evaluated during the short-circuit and line switch test on the micro-alternator and the results are given in Fig. 4.32. The EDRs of the self-tuning AVR designs are found to be 0.43 and 0.32 respectively which compares well with the value of 0.40 obtained for the conventional AVR. The rotor settles in 2.40 and 1.14 sec. respectively for the self-tuning AVRs while it takes 2.88 sec. for the conventional one to settle. The

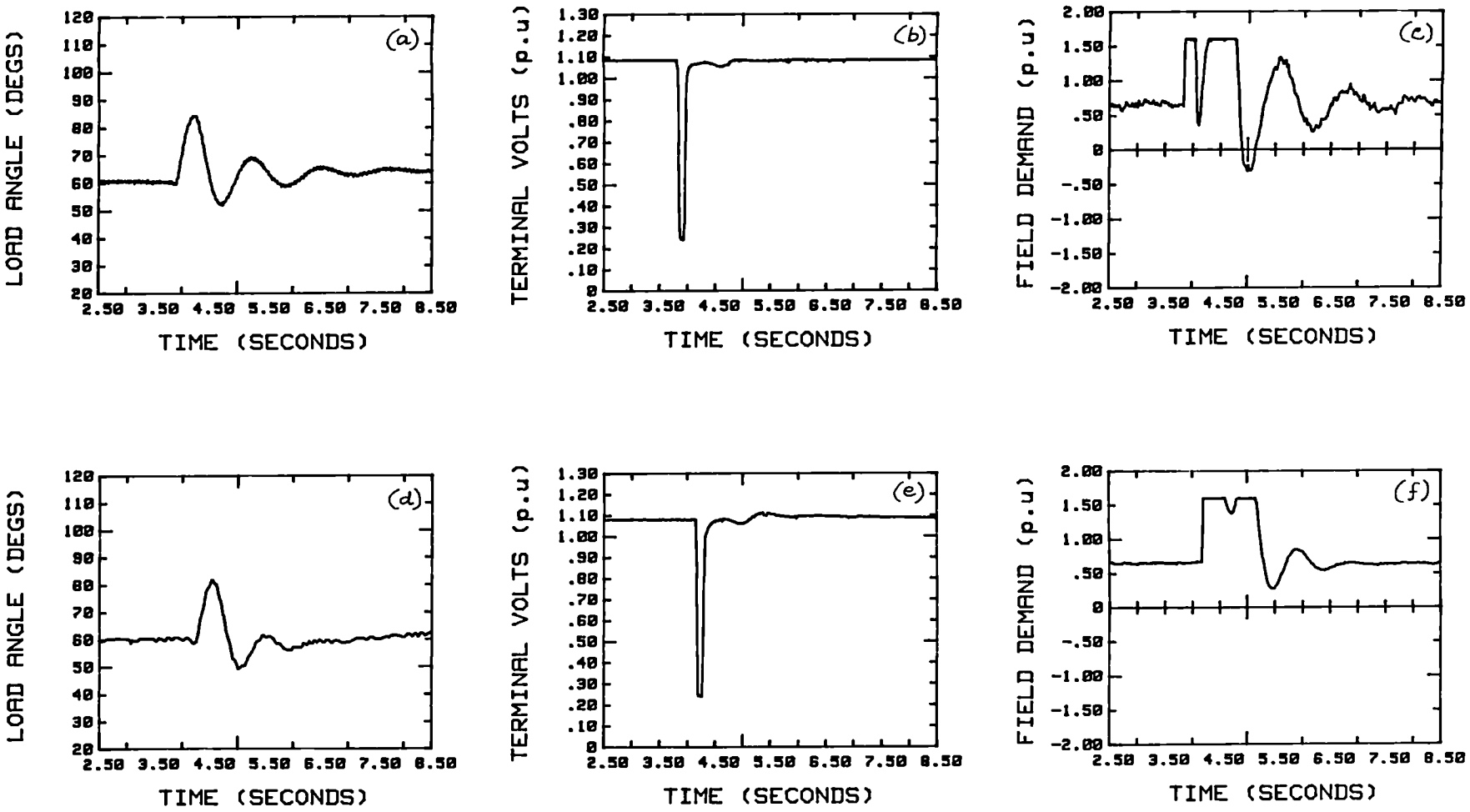

Fig. 4.31 Three phase short circuit and line switch test with micro-alternator.
(a), (b), (c) - STAVR-F; (d), (e), (f) - DGAVR-F.

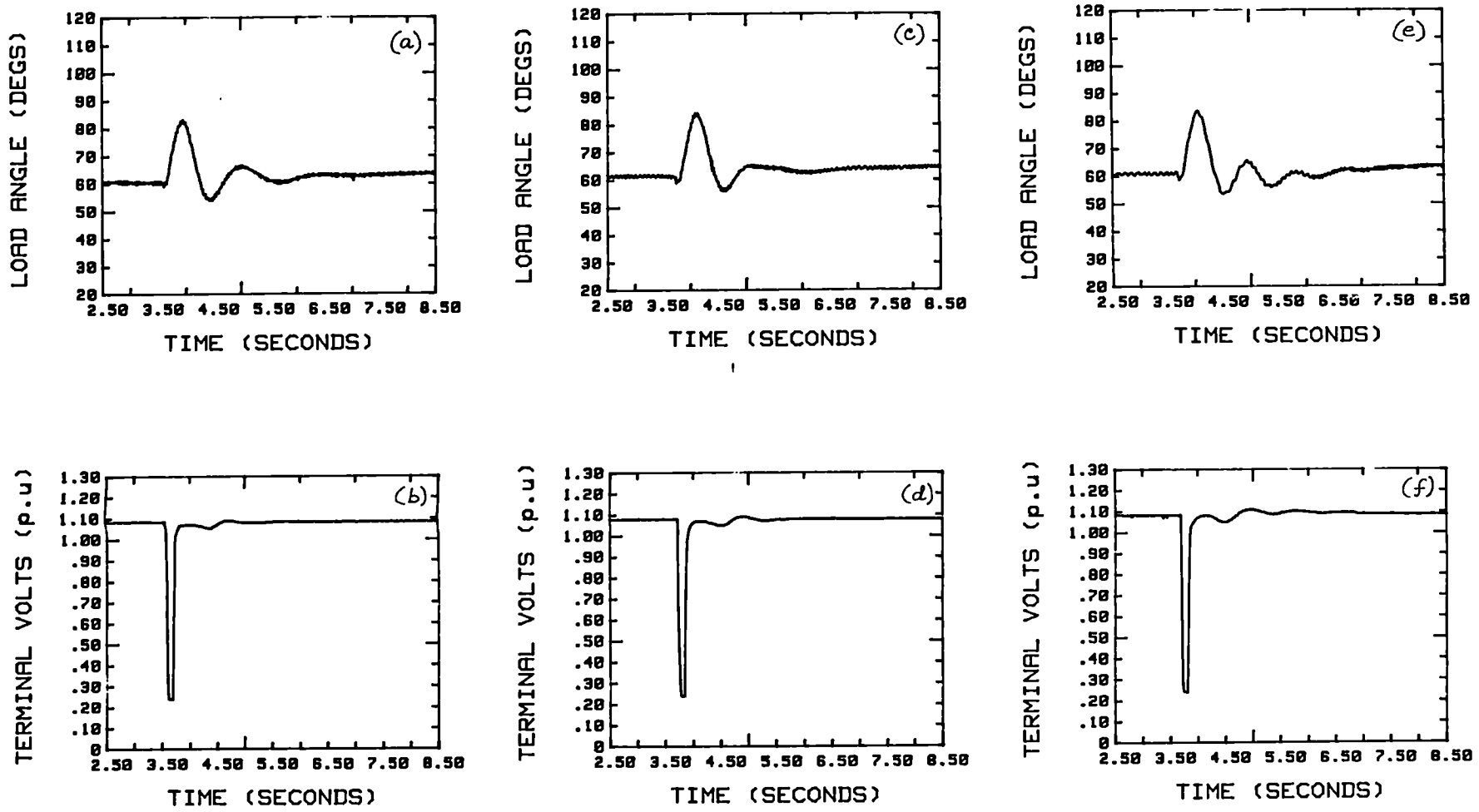

Fig. 4.32 Three phase short circuit and line switch test with micro-alternator.
(a), (b) - STAVR-S; (c), (d) - STAVR-SO; (e), (f) - DGAVR-SO.

terminal voltage settles to its final value in 0.975 and 1.34 sec. for STAVR-S and STAVR-SO respectively, but DGAVR-SO is considerably slower and takes 2.46 sec. Once again, the self-tuning AVR designs are found to be at least as good if not better than the conventional digital AVR in coping with a severe abnormality caused by the power system.

4.3.2.3 Full Load Rejection

Another major disturbance which the turbine generator system can be subjected is a full load rejection. This happens when the protection logic of the system detects a trip condition and opens the Main Circuit Breaker (MCB). This disturbance is most severe when the generator is operating at its Continuous Maximum Rating (CMR) point because the level of excitation in this case is maximum. When the MCB opens, the generator terminal voltage and the rotor speed momentarily increase and these are brought down to their rated values by the AVR and the Governor respectively. The speed with which the terminal voltage settles to its rated value is a good indication of the response of the AVR.

Fig. 4.33 gives the response of the 'fast' AVR designs to a full load rejection on the micro-alternator operating at its CMR point. It can be seen that the self-tuning controller is able to make the terminal voltage settle quickly to its set point value in 0.255 sec. A similar test with the corresponding conventional AVR (DGAVR-F) settles the terminal voltage only in 1.75 sec. The full load rejection test has been repeated with the 'slow' AVR designs also and the results are shown in Fig. 4.34 for the types STAVR-S, STAVR-SO and DGAVR-SO. It can be observed that the settling times of the terminal voltage for the self-tuning types are 0.615 and 1.2 sec. respectively whereas for the conventional type, it is 2.5 sec.

Although both the conventional and self-tuning types have been designed using similar performance criteria, the latter is able to perform considerably better during a severe system disturbance such as the full load rejection. This is due to the cost function minimising control strategy employed in the self-tuning AVR which enables the rapid regulation of the terminal voltage when sudden changes in the system conditions force it to deviate considerably from its set point.

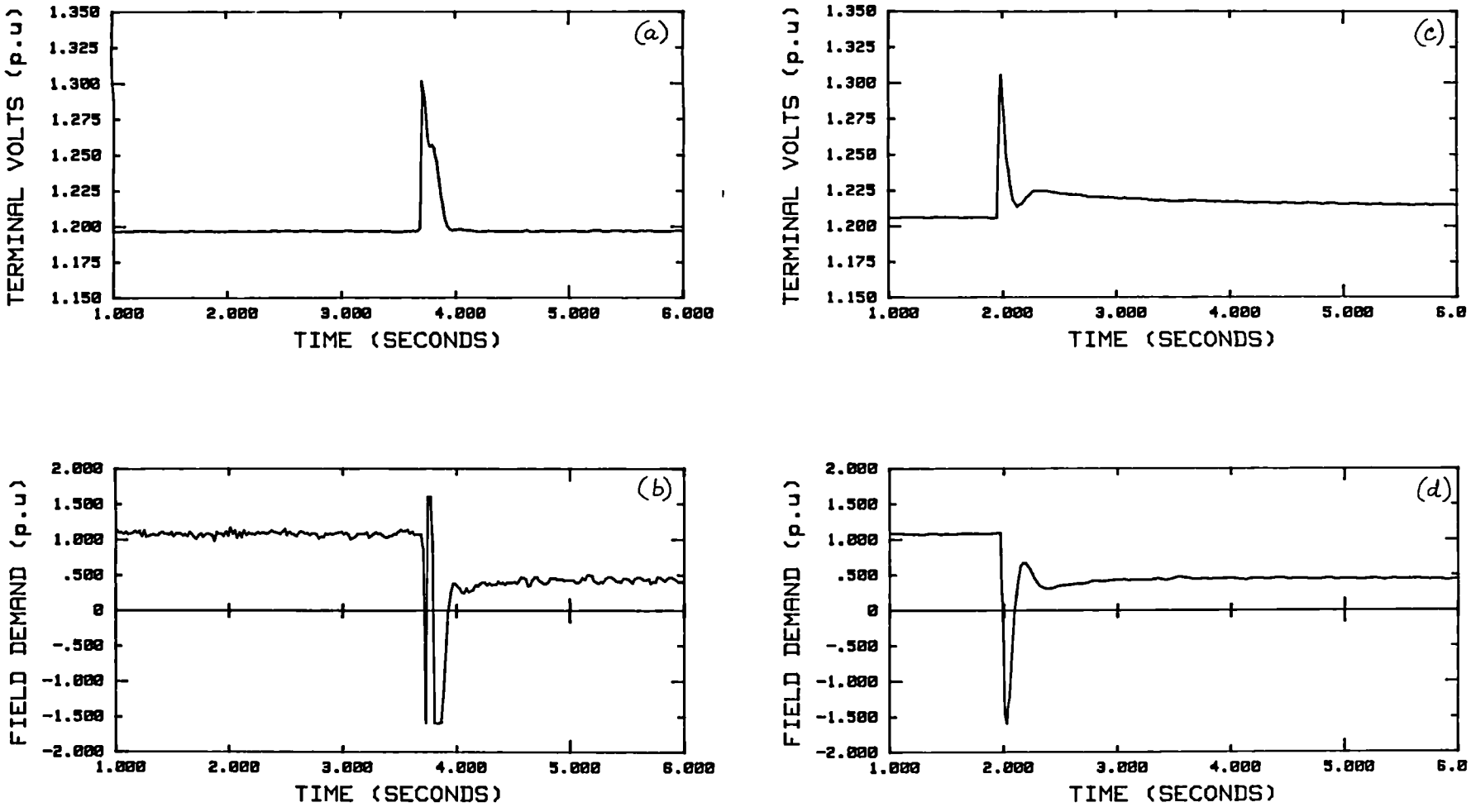

Fig. 4.33 Full load rejection test with micro-alternator.
(a), (b) - STAVR-F; (c), (d) - DGAVR-F.

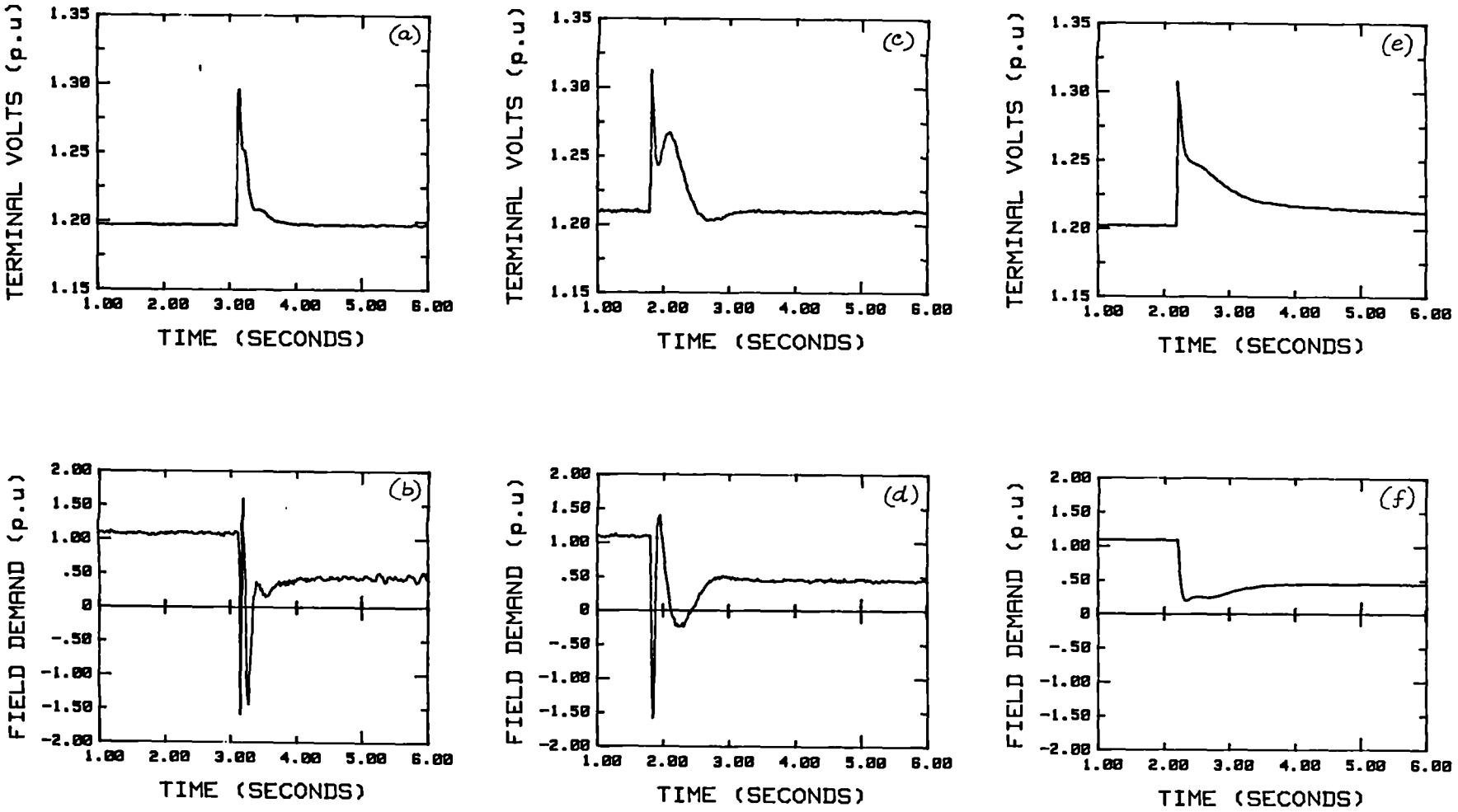

Fig. 4.34 Full load rejection test with micro-alternator.
(a), (b) - STAVR-S; (c), (d) - STAVR-SO; (e), (f) - DGAVR-SO.

CHAPTER 5

POWER SYSTEM STABILISED SELF-TUNING AUTOMATIC VOLTAGE REGULATOR

The problem of dynamic instability in power systems has become significant with the advent of large interconnected electric power systems. The role of the excitation system of the generator to improve stability has been the subject of intense research ever since the problem has been observed [2,120]. The AVR characteristic which tailors the response of the excitation system of the turbine generator is a critical factor in the stability of the power system.

In a multi-generator power system, the AVR through its voltage regulating action attempts to maintain machine rotor angle and therefore assists in maintaining a stable power system [1]. It has been long realised that an AVR in trying to improve the margin for a certain type of instability can inject negative damping into the system causing a different type of instability [121]. The use of a Power System Stabiliser (PSS) to derive a supplementary stabilising signal which acts through the AVR has been accepted as a standard practice to overcome this problem.

This chapter is divided into three sections. A brief introduction covering the various types of instability in power systems, their causes and the use of a PSS for stability improvement is given in Section 5.1. Section 5.2 highlights the need for the use of a suitable supplementary signal in the self-tuning AVR to overcome instability and shows how the AVR control law can be modified to achieve this objective. Finally, the effectiveness of the modified self-tuning AVR in improving the power system stability is evaluated using the TG simulator as well as the micro-alternator system and is documented in Section 5.3.

5.1 Power System Stability

The concept of power system stability relates to the ability of generators on a system to maintain synchronism and the tendency to return to and remain at

a steady-state operation point following a system disturbance [16]. There are several factors which affect power system stability. The operating point of the generator, its short-circuit ratio, transmission line reactance, and the response of the excitation system and the governor are some of them.

5.1.1 Classifications of Power System Stability

The stability of a turbine generator in a power system is generally classified into steady-state, dynamic, and transient depending on the nature of the disturbance acting on the system. It should be mentioned that there are no clear-cut boundaries for these classifications, however the general guideline used is that steady-state and dynamic instability are due to small disturbances, while transient instability is caused by large disturbances.

Historically, it was the instability due to small disturbances that was studied in detail first. Then, it was recognised that large disturbances such as short circuits were the most severe hazard to stable operation of the turbine generator, hence attention was directed to transient stability and its improvement. The progress that has been achieved in the last few decades in the field of power system protection as well as the need to work with reduced stability margins in recent years has switched the emphasis back to the analysis and improvement of stability in the presence of small disturbances [120].

5.1.1.1 Steady-State Stability

In the steady-state, a turbine generator is generally subjected to small and gradual changes in load, and drifts in the terminal voltage and frequency. Steady-state stability enables the turbine generator to remain synchronised to the power system under these conditions. The use of a continuously-acting AVR (ie. no dead band) greatly assists in maintaining steady-state stability since it acts as a maintainer of rotor angle and makes possible the stable operation of the machine at large rotor angles even in excess of the theoretical stability limit [1].

5.1.1.2 Dynamic Stability

Sudden disturbances of moderate intensity can cause electro-mechanical oscillations in the turbine generator and the power system. Dynamic stability refers to the ability of the system to provide sufficient damping to these oscillations. The oscillations include resonances between the turbine generator shaft and the rest of the power system as well as oscillations caused by linking two or more interconnected systems. The former are known as 'local machine-system oscillations' and the latter 'inter-area oscillations' [6]. The oscillating frequency for the local mode is in the range of 0.7 to 2.5 Hz while the inter-area oscillations have a much lower frequency typically 0.2 to 0.5 Hz. A third category is the 'torsional oscillations' with frequencies ranging from 4 Hz and above which are caused by relative angular motion between the rotating elements of a turbine generator.

Oscillations of small magnitude and low frequency often persisting for long periods of time in power systems are clearly indicative of dynamic instability. This in many cases presents limitations on the power transfer capability of a turbine generator. This is one of the most serious stability problems in modern power systems.

5.1.1.3 Transient Stability

Transient stability is defined as the ability of the machine to maintain synchronism following a sudden large disturbance. It covers events such as three-phase faults, unbalanced line-line or line-neutral faults, and sudden application of a large load. It is well known that the excitation system can improve transient stability appreciably even when facilities such as high-speed clearing of faults and fast-valving are available. The faster the excitation system responds to correct a low voltage condition caused by a transient fault, the more effective it is in improving the stability [120].

5.1.2 The use of a Power System Stabiliser for Dynamic Stability Improvement

One of the most important stability problems observed in large-scale electric power systems is the low-frequency dynamic oscillations of interconnected sub-systems. The frequency of these oscillations is of the order of a fraction of 1 Hz to a few Hz. At any given oscillation frequency, braking torques are developed in the system due to changes in 'slip'. The braking torque T_b thus produced can be resolved into two components, see Fig. 5.1. The component of braking torque which is in phase with the machine rotor angle is called the synchronising torque and that which is in phase with the machine rotor speed is termed the damping torque. Positive synchronising torque forces the rotor back to its original position while positive damping torque minimises the duration of rotor oscillations. Thus both torque components contribute to dynamic stability improvement.

As can be observed from Fig. 5.1, the voltage regulating action of an AVR improves the synchronising torque during system oscillations by increasing the magnitude of the torque vector T_b by the forcing action F_a. However, in doing so it reduces the natural damping torque of the machine which is already small [2]. This undesirable effect is due to the phase lag in the excitation system of the turbine generator as can be seen from the figure. A solution to this problem is to have just enough regulator gain to provide the necessary synchronising torque without cancelling all of the inherent machine damping, but this is not practical in many situations.

Since the control action of an AVR can act to reduce the damping of dynamic oscillations by sensing terminal voltage, it is reasonable to assume that a supplementary signal to the AVR derived from a suitable quantity can increase the system damping. In doing so, not only can the undamping effect of voltage regulator control be cancelled, but damping can be increased so as to allow safe operation even beyond the steady-state stability limit [16]. This is the basic principle of a PSS.

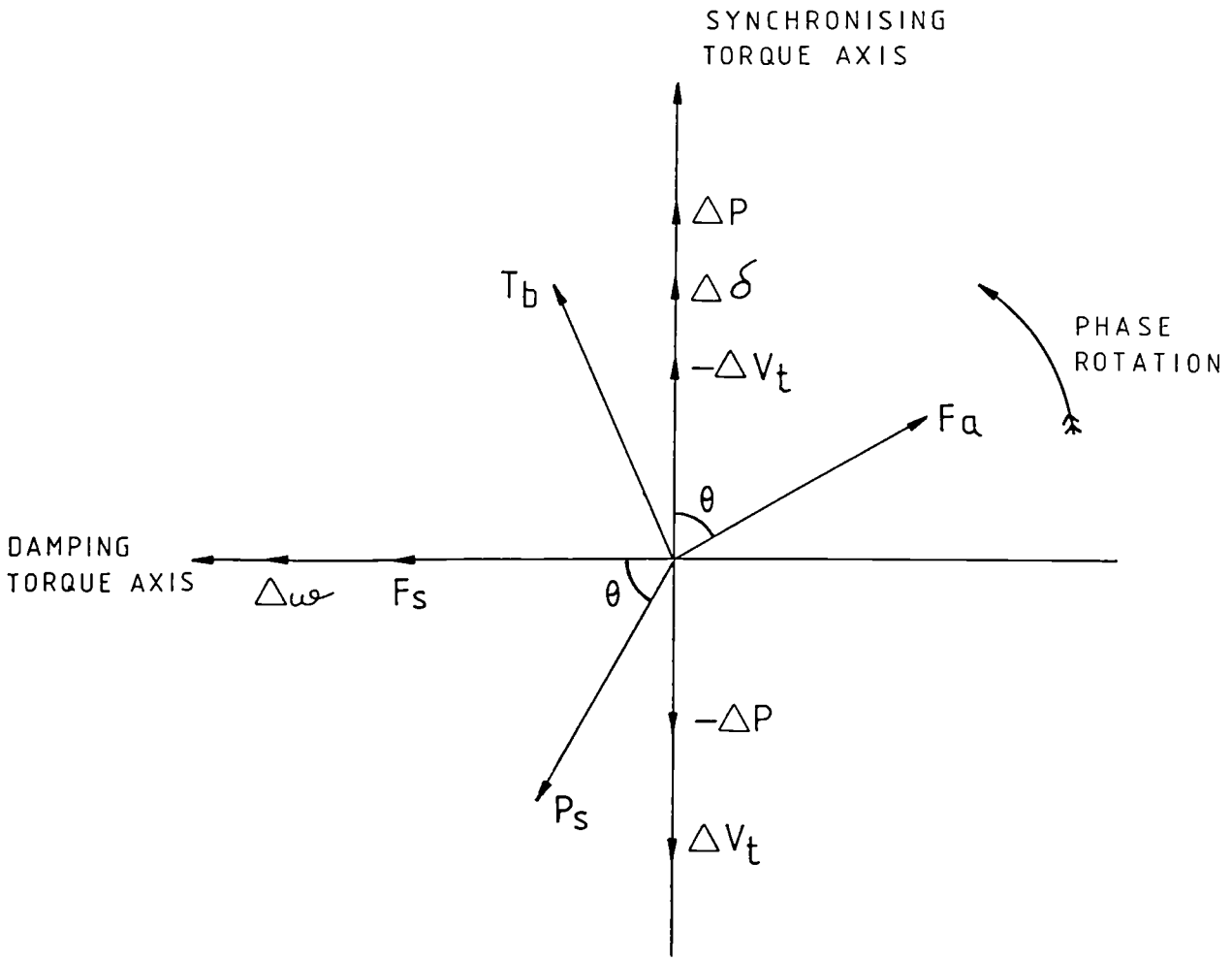

△δ - CHANGES IN ROTOR ANGLE

△P - CHANGES IN ELECTRICAL POWER

△ω - CHANGES IN ROTOR SPEED

T_b - NATURAL BRAKING TORQUE OF THE TURBINE GENERATOR

P_s - STABILISING SIGNAL INTO THE AVR

F_s - FORCING ACTION DUE TO P_s

F_a - FORCING ACTION DUE TO VOLTAGE FEED BACK

θ - PHASE LAG IN THE EXCITATION SYSTEM

△V_t - CHANGES IN TERMINAL VOLTS

Fig. 5.1 Relative phase positions of signals and torque components in a turbine generator.

The supplementary signal produced by a PSS may be derived from such quantities as shaft speed, generator frequency, electrical power or accelerating power. Although shaft speed was preferred for input to the PSS at one time due to its ease of measurement and the fact that the signal is in phase with the damping torque axis, its use can excite the torsional modes of the system unless special precautions are taken [13,16]. The electrical power or the accelerating power is the more popular choice as input to the PSS in recent designs [11].

Tuning of a PSS to maximise the dynamic stability margin of the turbine generator has received considerable attention in the past and several methods to do it are in use today [11,14,122]. Irrespective of the method used, the objective of PSS tuning is to apply a supplementary signal P_s to the AVR input which leads the damping torque axis by an angle equal to the phase lag of the excitation system at the frequency of the dynamic oscillation, as shown in Fig. 5.1. Thus the forcing action F_s produced by the PSS through the AVR will be in phase with the positive damping torque axis which increases the damping torque without reducing the synchronising torque.

5.2 Design of a Self-Tuning AVR for Improved Power System Stability

The use of an AVR which combines fast response and high gain can give a significant improvement to transient and steady-state stability margins of a turbine generator [1,120]. Since self-tuning controllers in general are fast-acting systems and possess a high value of gain, their use for excitation control is beneficial for power system stability. However, as pointed out earlier, one of the drawbacks of a fast-acting AVR is that it has the potential of introducing negative damping which can cause undamped modes of dynamic oscillations. Direct evidence of this has been seen by the fact that sustained oscillations on power systems have been stopped simply by switching the AVR from automatic to manual mode of operation [16]. Hence it is highly desirable that the self-tuning AVR algorithm is capable of utilising a supplementary feedback signal which can enhance the dynamic stability margin of the system.

The need for supplementary feedback even in AVRs employing advanced control strategies such as self-tuning has been identified for some time now [37,3]. The most popular signals for this purpose are rotor speed and electrical power. Since the use of the rotor speed signal can give rise to torsional oscillations as mentioned earlier, it has been decided to use the electrical power signal for stabilisation in the self-tuning AVR.

The control law for the power system stabilised self-tuning AVR can be derived by defining a modified GPC cost function J'' as:

$$J'' = \sum_{j=1}^{N_y} [\phi(t+j) + P_s(t) - w(t+j)]^2 + \sum_{j=1}^{N_u} \lambda[\Delta u(t+j-1)]^2 \qquad (5.1)$$

in which an additional term $P_s(t)$ has also been costed. $P_s(t)$ is defined as:

$$P_s(t) = G_p P'(t) \qquad (5.2)$$

where G_p is a weighting function and $P'(t)$ is the electrical power at time t which has been 'washed-out' using a high-pass filter of the form $sT_w / (1+sT_w)$. T_w is the washout time constant which in this case has been set at 2 sec. Thus variations in the electrical power signal given by $P'(t)$ are costed in (5.1) which leads to the damping of dynamic oscillations in the system. This approach prevents the occurrence of any dc bias in the terminal voltage due to the use of a stabilising signal in the self-tuning AVR.

Minimising the modified cost function J'' in the usual way leads to the power system stabilised control law as:

$$\bar{\boldsymbol{u}} = (\bar{\boldsymbol{G}}^T \bar{\boldsymbol{G}} + \lambda \boldsymbol{I})^{-1} \bar{\boldsymbol{G}}^T (\boldsymbol{w} - \boldsymbol{s} - \boldsymbol{P}_s) \qquad (5.3)$$

where $\boldsymbol{P}_s$ is a N_y-column vector whose elements are equal to $P_s(t)$. It may be noted that the polarity of the power signal is negative in the control law given by (5.3) thus achieving a phase lead of 90° over the positive damping torque axis.

The weighting function G_p associated with the washed-out electrical power signal can be a simple scalar value in which case it can be viewed as a weighting factor in the cost function. In the more general case, G_p can be a

transfer function which contains a weighting factor and a signal conditioning filter block to pre-filter the stabilising signal. This is most useful in applications where a fixed phase shift to the stabilising signal is required to be applied to get the forcing action due to the stabilising signal exactly in phase with the positive damping torque axis at the frequency of concern.

In the self-tuning AVR, the function G_p is taken as a scalar weighting factor for simplicity. This is acceptable since it is known from frequency response studies that the use of the washed-out power signal without any additional phase adjustment can produce a forcing action near the positive damping torque axis. The combined phase lag of a fast-acting excitation system and the electrical power transducer is generally in the region of 90° for frequencies of 1.0 to 1.5 Hz where dynamic oscillations are experienced. Since the phase-inverted electrical power signal is 90° ahead of the positive damping torque axis, its use without any additional phase adjustment can thus produce a forcing action close to that axis. The guideline generally used is that as long as the forcing action due to the stabilising signal is within $\pm 30°$ of the positive damping torque axis for the frequency spectrum of concern, acceptable results are obtained [2,11].

The scalar weighting factor G_p used in the self-tuning AVR should be chosen with care. A very low value of G_p can produce only a small increase in the damping torque of the system, while too high a value can destroy the voltage regulating property of the self-tuning AVR. A compromise value of 0.1 for G_p has been arrived at by trial and error for use in the self-tuning AVR. This is equivalent to giving 10 times more importance to voltage regulation than damping torque improvement in the cost function of the controller. This value is found to provide sufficient improvement to the damping torque without significantly affecting the voltage regulation of the self-tuning AVR.

It should be emphasised that the use of the power signal in the self-tuning AVR is intended to provide damping for small excursions about a steady-state operating point, and not to enhance transient stability, ie. the ability to recover from a severe disturbance. However, the use of the power signal can sometimes have an unwanted effect on transient stability by attempting to pull the

generator field voltage out of ceiling too early in response to a severe fault [10]. This undesirable effect should be minimised since the contribution made by a high performance self-tuning AVR towards transient stability is equally important and should not be reduced.

Any effort to damp oscillations following a fault clearance should not sacrifice the benefits derived from voltage regulator action in the early part of the transient [123]. This consideration necessitates limiting the magnitude of the stabilising signal so that voltage errors can effectively override the stabilising signal if the terminal voltage drops below some predetermined value. In the case of the self-tuning AVR, this limit has been set to 5% which is considered adequate for improving the dynamic stability without significantly affecting the transient stability of the system [13]. The provision of this limit also prevents the stabilising signal from causing excessive terminal voltage excursions during power variations which are not caused by dynamic instability such as during scheduled load changes [14].

5.3 Performance Evaluation of the Power System Stabilised Self-Tuning AVR

The performance of the power system stabilised self-tuning AVR has been evaluated using the TG simulator as well as the micro-alternator system. The tests were aimed at verifying the following:

a) to show that a significant improvement in the dynamic stability margin of the system is achieved,

b) to verify that the regulation of the terminal voltage is not significantly affected, and

c) to confirm that the transient stability of the system is not adversely affected.

The performance of the improved self-tuning AVR has also been compared with that of a conventional digital AVR equipped with a PSS.

5.3.1 Evaluation using the TG Simulator

The TG simulator was used to compare the improved performance of the power system stabilised self-tuning AVR with that of a standard self-tuning AVR and that obtained when using a PSS with a conventional digital AVR. As in the previous chapter, fast as well as slow AVR designs have been tried to assess the extent of enhancement in the dynamic stability of the system in each case. The results obtained during a step input, transmission line switch, and 3-phase short-circuit are analysed in the following sub-sections.

5.3.1.1 Step Response Test On Load

For this test, an operating point of P = 0.8 pu and Q = 0 has been chosen in the TG simulator. A positive step of 3% has been applied to the input of the AVR to create a moderate disturbance in the power system. The parameter estimator of the self-tuning AVR has been allowed to converge to some reasonable values before the test was conducted.

Fig. 5.2 shows the step response of a 'fast' self-tuning AVR of type STAVR-F defined in Chapter 4 with and without the power signal input. The Effective Damping Ratio (EDR) of the electrical power signal is found to reduce from 0.63 to 0.43 when using the power signal in the self-tuning AVR which is a significant improvement. As expected, the response of the terminal voltage when using the power signal has degraded to some extent. The rise and settling times of terminal voltage have been found to increase from 0.25 and 0.25 sec. to 0.36 and 0.87 sec. respectively.

The effect of varying the weighting factor G_p of the stabilising signal is shown in Fig. 5.3 which indicates that for a weighting factor of 0.05, the EDR of the power signal is 0.50 whereas for a value of 0.15, the EDR is 0.40. This shows that as the weighting factor is increased, the damping of the electrical power of the system is improved.

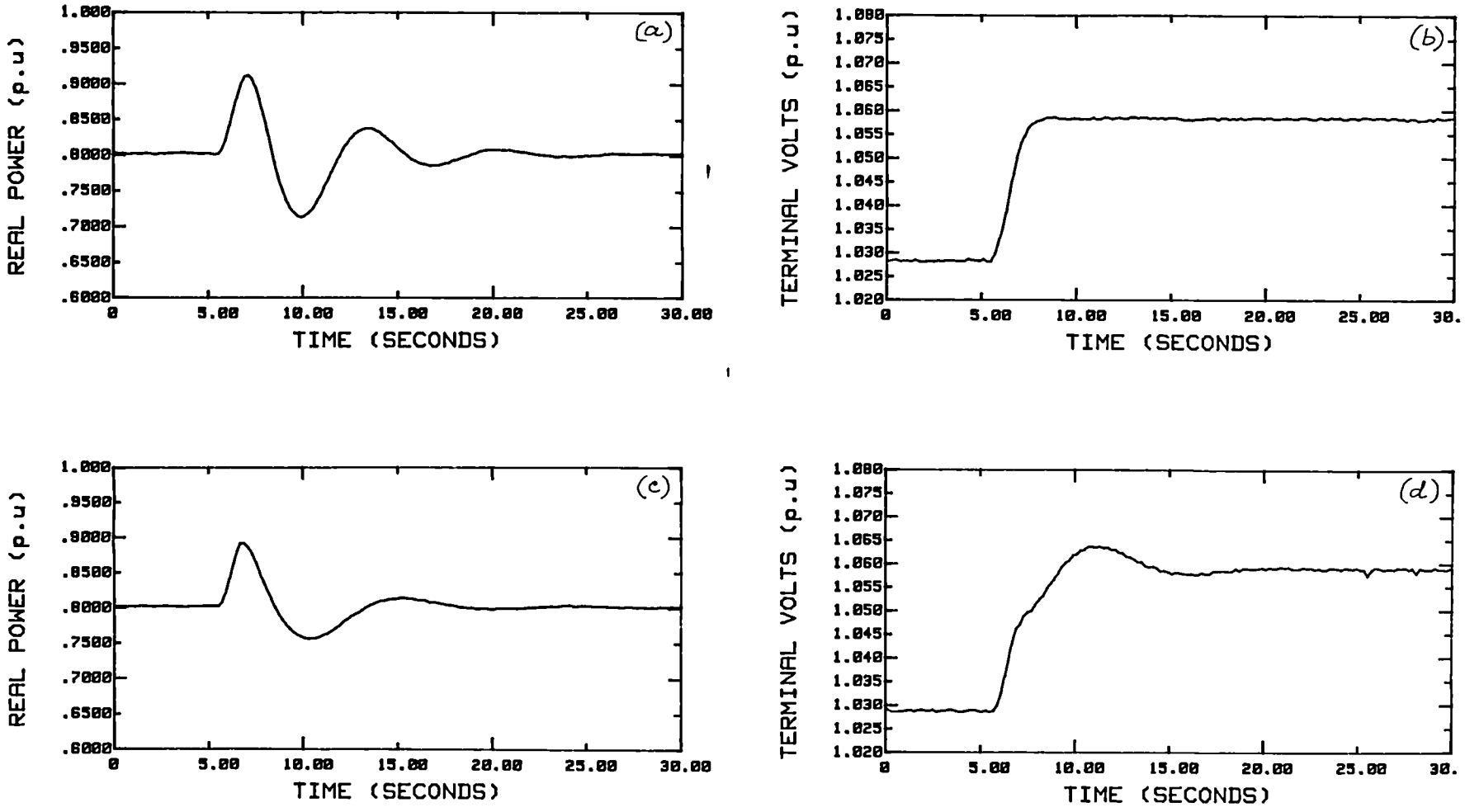

Fig. 5.2 Step response of the self-tuning AVR type STAVR-F using the TG simulator with and without the power signal. (a), (b) - without power signal; (c), (d) - with power signal.

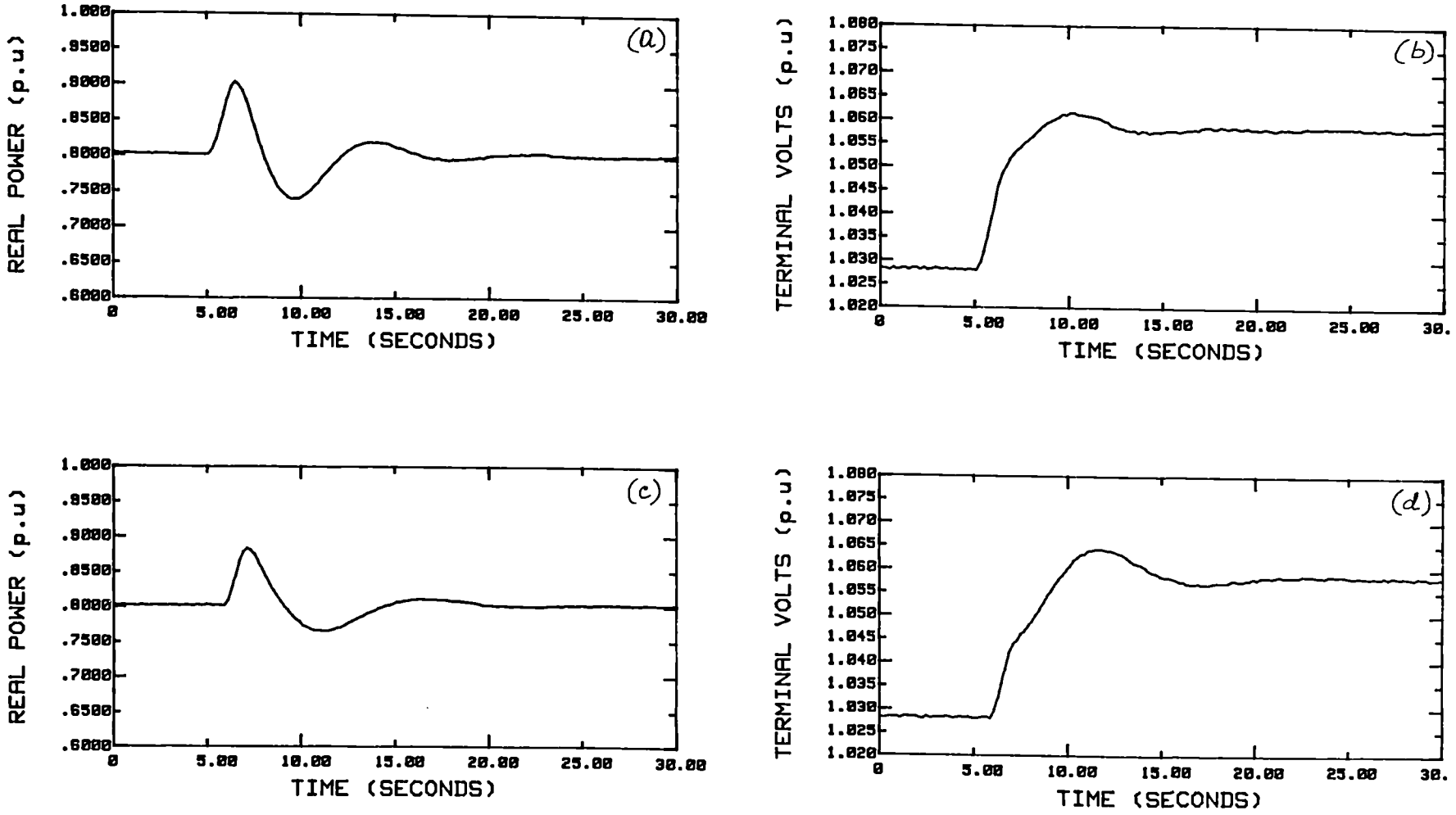

Fig. 5.3 Step response of the self-tuning AVR type STAVR(P)-F using the TG simulator with different weighting factors. (a), (b) - power weighting factor 0.05; (c), (d) - power weighting factor 0.15.

The performance of the corresponding conventional digital AVR type DGAVR-F with and without a PSS is given in Fig. 5.4 for comparison purposes. In this case, the EDR of the power signal is found to improve from 0.74 to 0.49 which indicates that the improvement obtained with the power system stabilised self-tuning AVR is at least as good as that obtained with a conventional digital AVR employing a PSS. The rise and settling times of the terminal voltage in the case of the digital AVR are found to increase from 0.93 to 1.0 sec. each respectively.

Figures 5.5 and 5.6 illustrate the step response of the 'slow' self-tuning AVR designs STAVR-S and STAVR-SO respectively, while Fig. 5.7 gives the response for the conventional 'slow' digital AVR with and without a PSS for comparison purposes. The results obtained are tabulated in Table 5.1. It can be observed from the table that the performance of the power system stabilised self-tuning AVR in terms of the EDR of the power signal is significantly better than that obtained with a standard self-tuning AVR. This improvement has been achieved with only a minor change in the response of the terminal voltage of the machine. It is also seen that the improvement obtained is comparable with that of a PSS acting through a conventional digital AVR. Thus the derivation of the Generalised Predictive Control law using the power signal in the cost function improves the damping of power oscillations during small disturbances caused by events such as a step change in the terminal voltage of the generator.

5.3.1.2 Transmission Line Switch Test

The operating point of the generator has been chosen as P = 0.8 pu and Q = 0 in the TG simulator for this test. The transmission line reactance of the power system has been switched from 0.25 pu to 0.375 pu to create a moderate disturbance. As before, the parameter estimator of the self-tuning AVR has been allowed to converge to a reasonable set of values before the test was conducted.

Fig. 5.8 shows the effect of this disturbance on the electrical power and terminal voltage of the system when the 'fast' self-tuning AVR of type STAVR-F has been used with and without the power input. It can be observed that the EDR

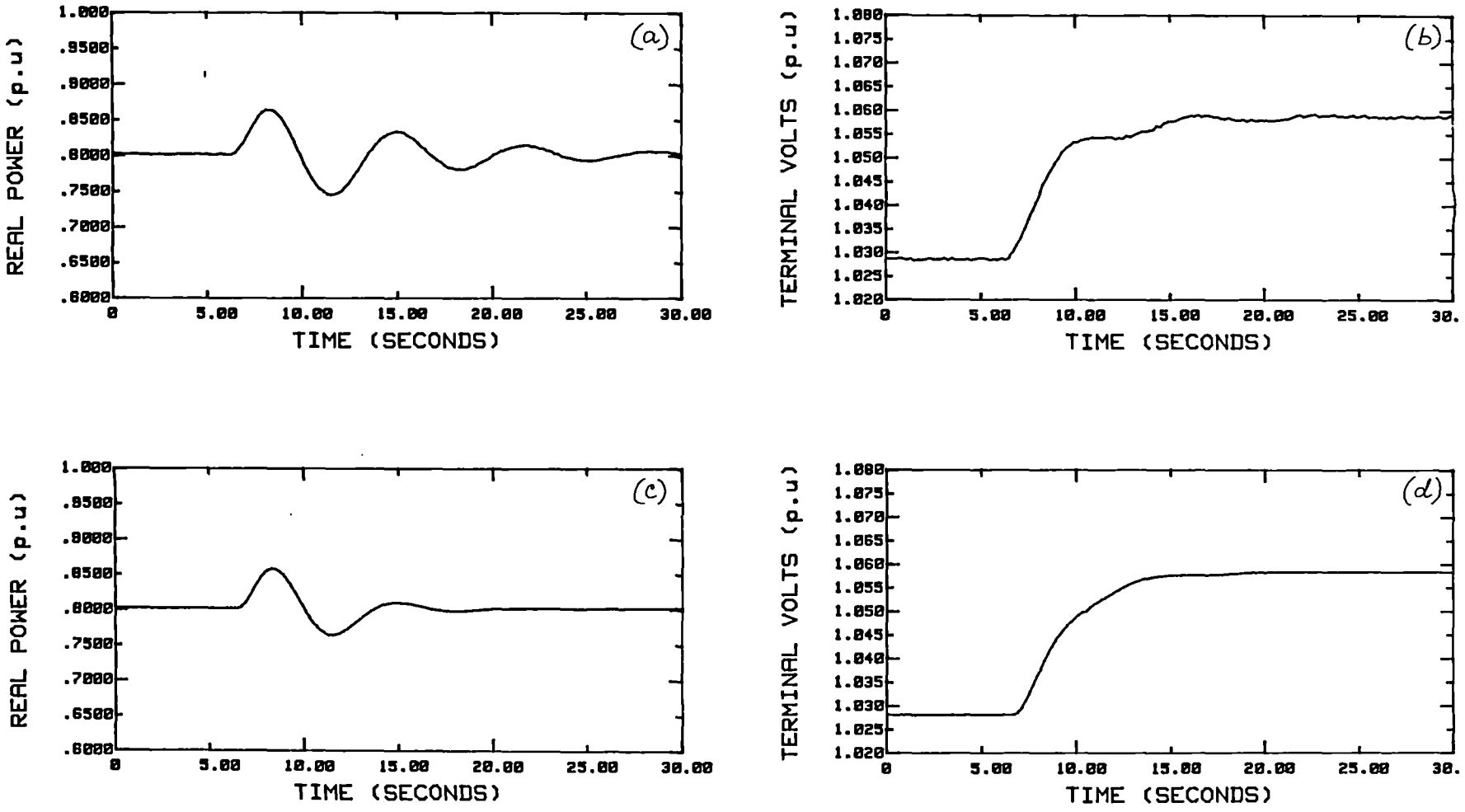

Fig. 5.4 Step response of a conventional digital AVR type DGAVR-F using the TG simulator with and without the PSS. (a), (b) - without PSS; (c), (d) - with PSS.

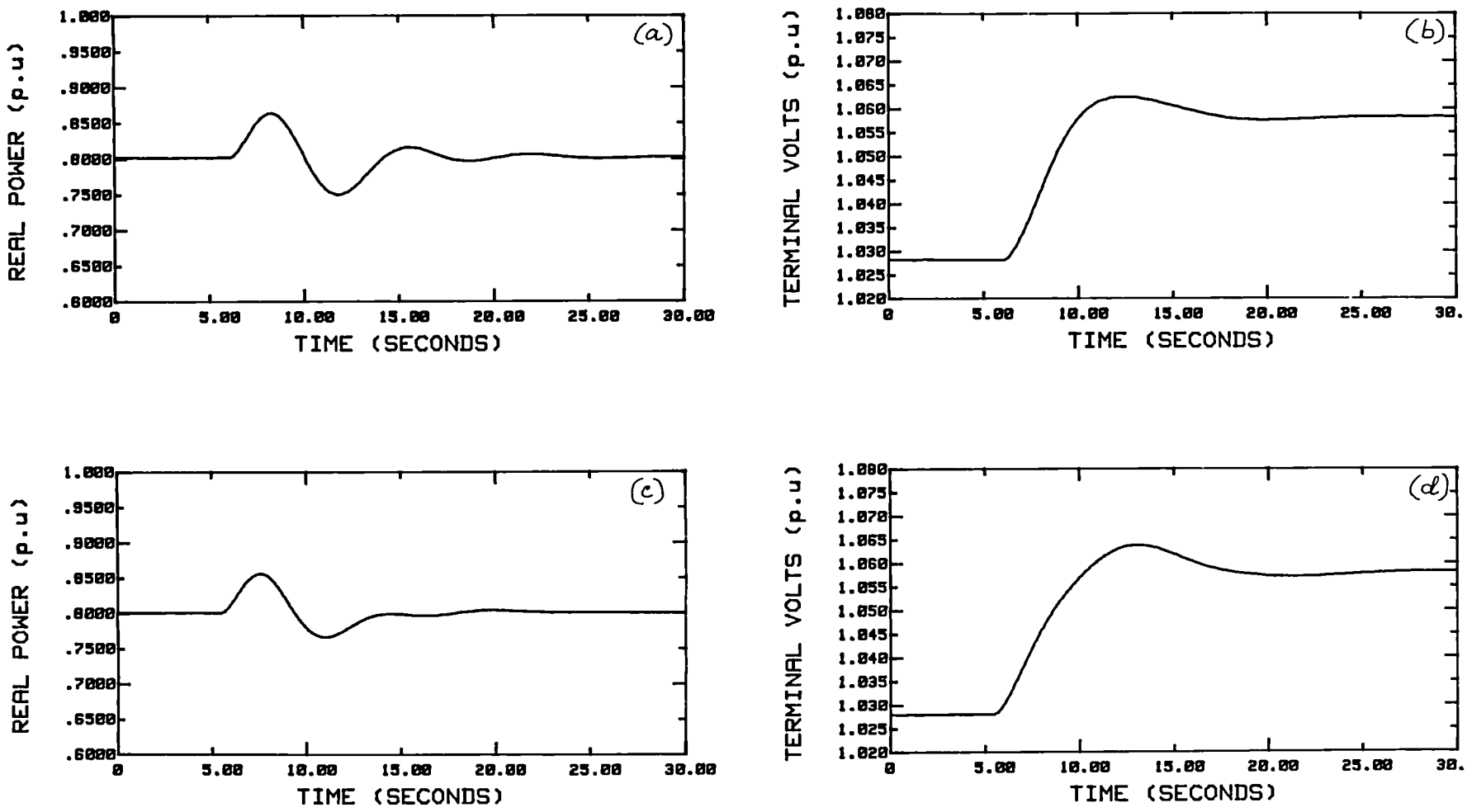

Fig. 5.5 Step response of the self-tuning AVR type STAVR-S using the TG simulator with and without the power signal. (a), (b) - without power signal; (c), (d) - with power signal.

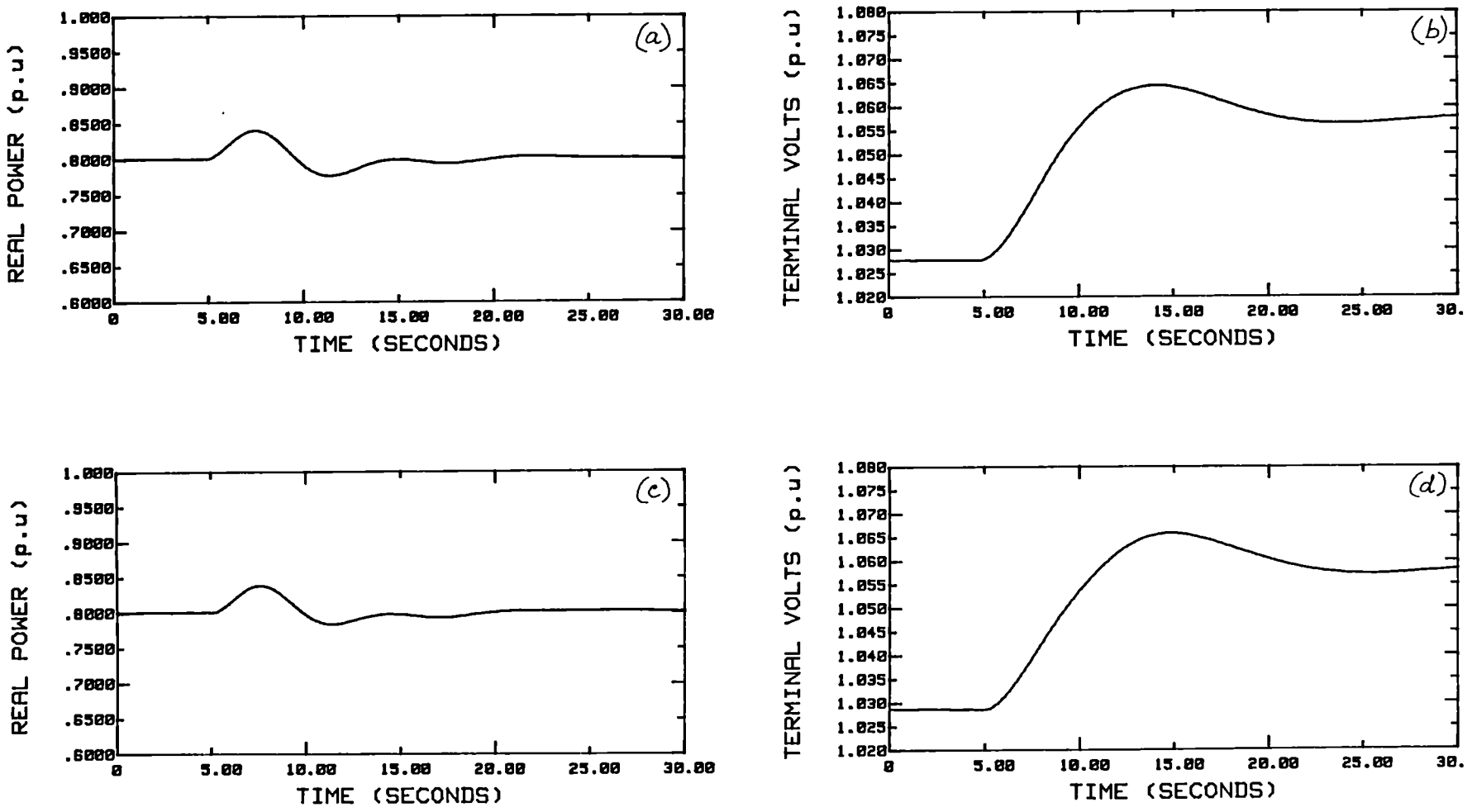

Fig. 5.6 Step response of the self-tuning AVR type STAVR-SO using the TG simulator with and without the power signal. (a), (b) - without power signal; (c), (d) - with power signal.

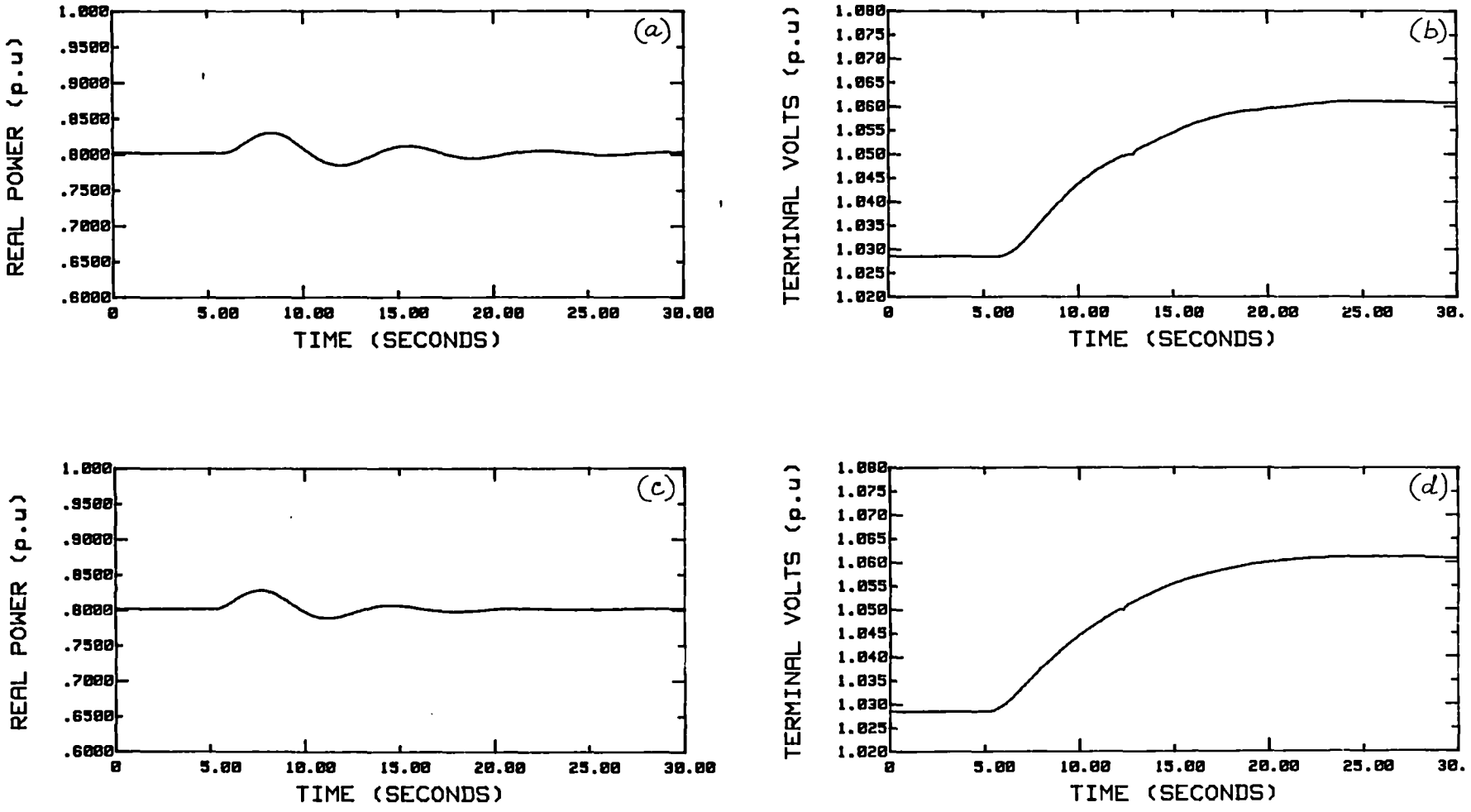

Fig. 5.7 Step response of a conventional digital AVR type DGAVR-SO using the TG simulator with and without the PSS (a), (b) - without PSS; (c), (d) - with PSS.

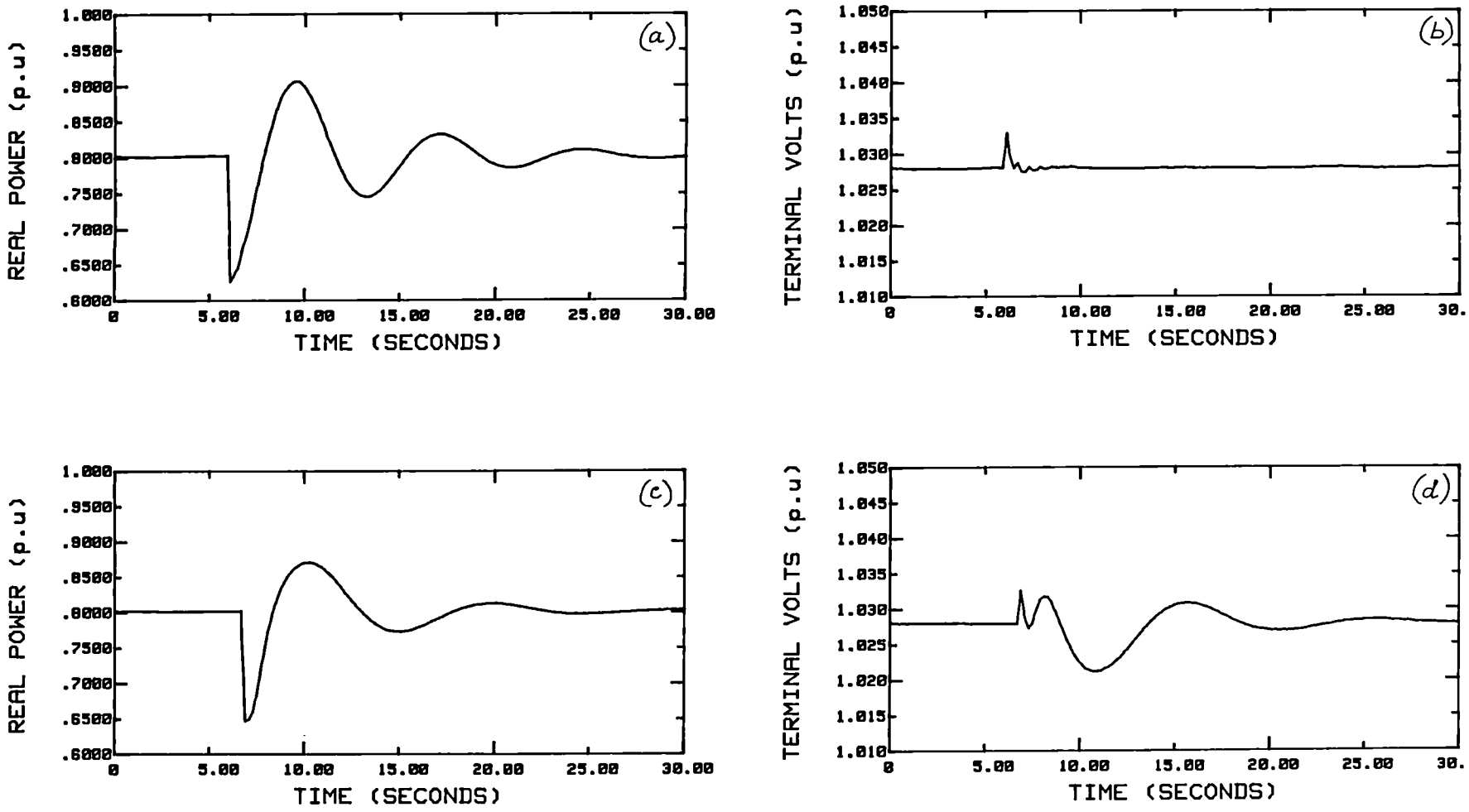

Fig. 5.8 Response of the self-tuning AVR type STAVR-F during transmission line switching using the TG simulator with and without the power signal. (a), (b) - without power signal; (c), (d) - with power signal.

AVR Type	EDR of Elec. Power	Rise Time (Vt) (sec.)	Settling (Vt) (sec.)
STAVR-F STAVR-F(P)	0.63 0.43	0.25 0.36	0.25 0.87
DGAVR-F DGAVR-F(P)	0.74 0.49	0.93 1.00	0.93 1.00
STAVR-S STAVR-S(P)	0.58 0.38	0.41 0.48	1.11 1.14
STAVR-SO STAVR-SO(P)	0.34 0.28	0.57 0.61	1.44 1.59
DGAVR-SO DGAVR-SO(P)	0.58 0.44	1.20 1.30	3.60 3.80

Table 5.1. Response of various types of AVRs with and without stabilising feedback on the TG simulator for a step input.

of the electrical power signal has improved from 0.56 to 0.42 with the use of the stabilising signal. As expected, the maximum variation in terminal voltage due to the disturbance as well as its settling time are seen to increase with the use of the power input. However, it should be noted that the terminal voltage deviates from its steady state value only by 0.7% which is rather small and can be tolerated. Fig. 5.9 shows that an improvement in the EDR of the power signal from 0.75 to 0.51 is achieved with a PSS working through a conventional AVR of type DGAVR-F. This is comparable with that obtained in the case of the self-tuning AVR.

Figures 5.10 and 5.11 illustrate the response of the 'slow' self-tuning AVR designs STAVR-S and STAVR-SO respectively during the transmission line switch test, while Fig. 5.12 gives the response for the conventional 'slow' digital AVR with and without a PSS for comparison purposes. The EDRs of the power signal obtained are tabulated in Table 5.2. It can be observed from the table that

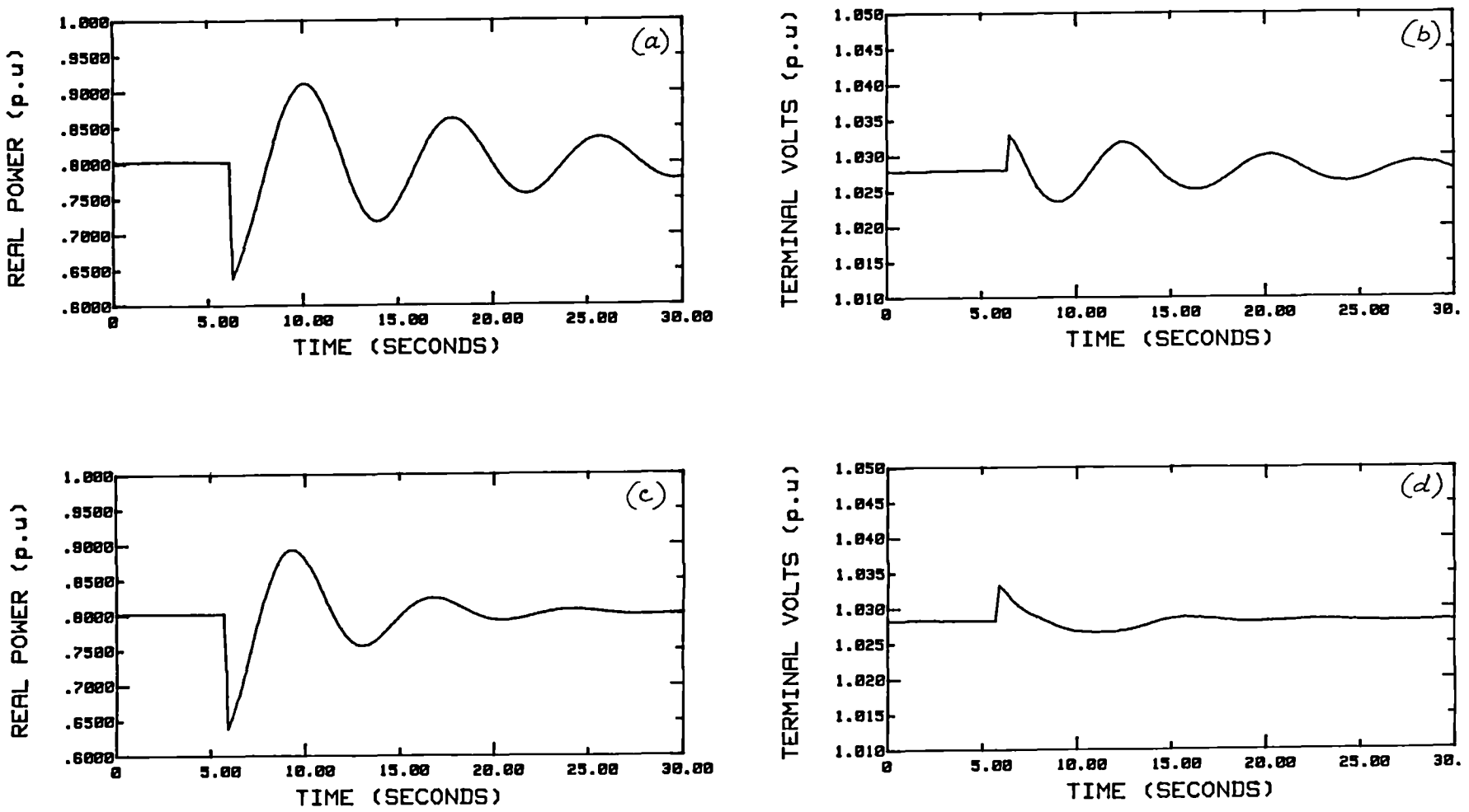

Fig. 5.9 Response of a conventional digital AVR type DGAVR-F during transmission line switching using the TG simulator with and without the PSS. (a), (b) - without PSS; (c), (d) - with PSS.

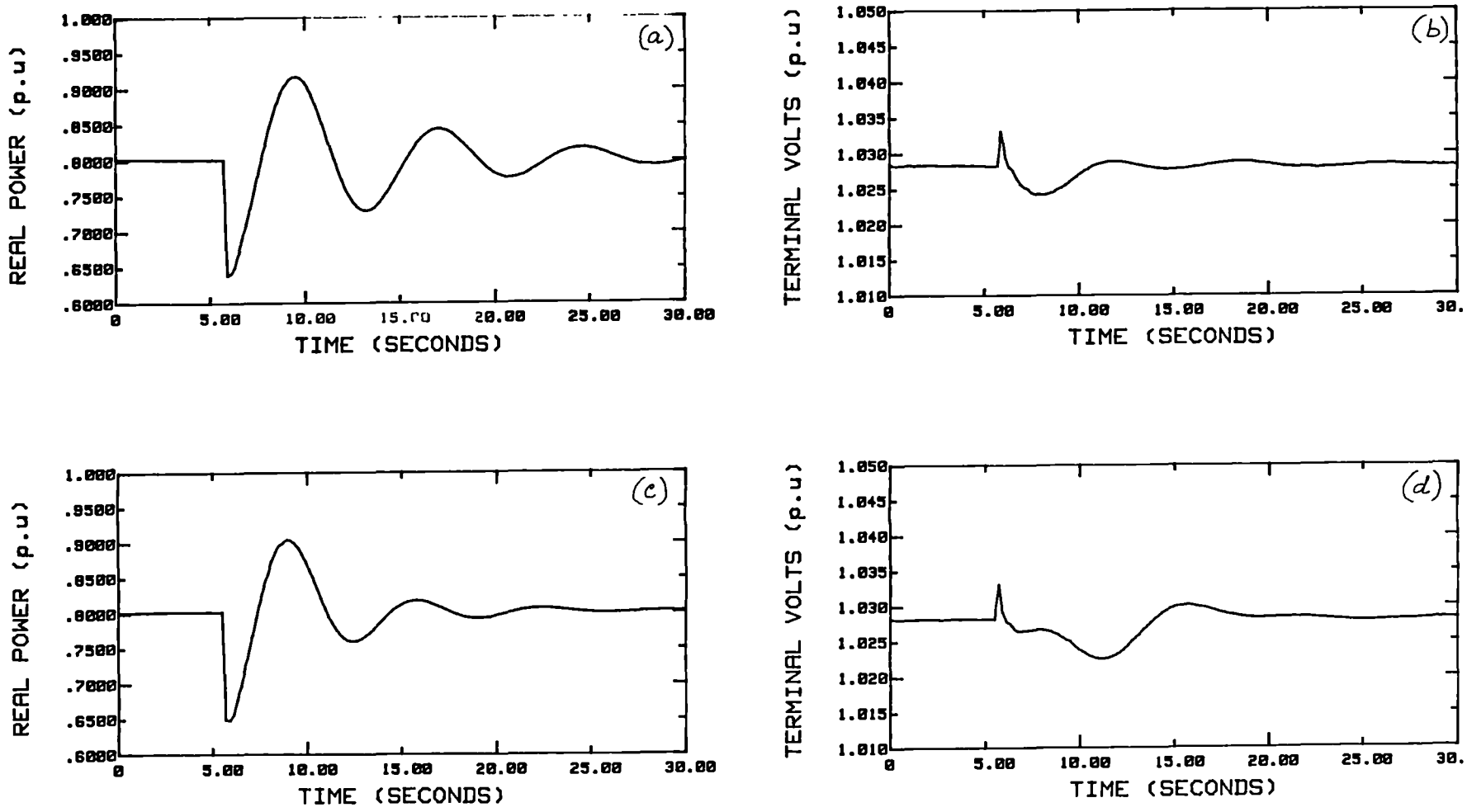

Fig. 5.10 Response of the self-tuning AVR type STAVR-S during transmission line switching using the TG simulator with and without the power signal. (a), (b) - without power signal; (c), (d) - with power signal.

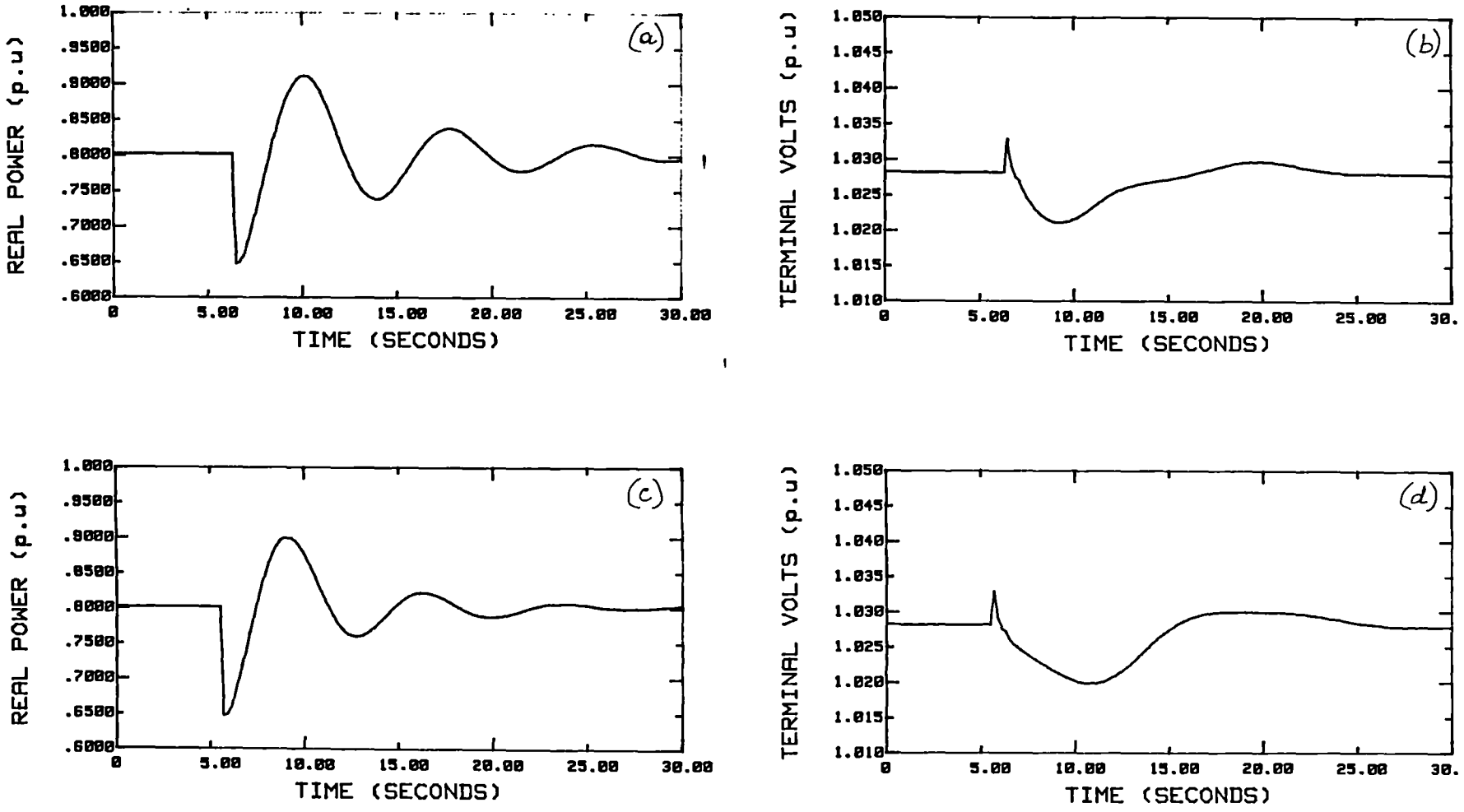

Fig. 5.11 Response of the self-tuning AVR type STAVR-SO during transmission line switching using the TG simulator with and without the power signal. (a), (b) - without power signal; (c), (d) - with power signal.

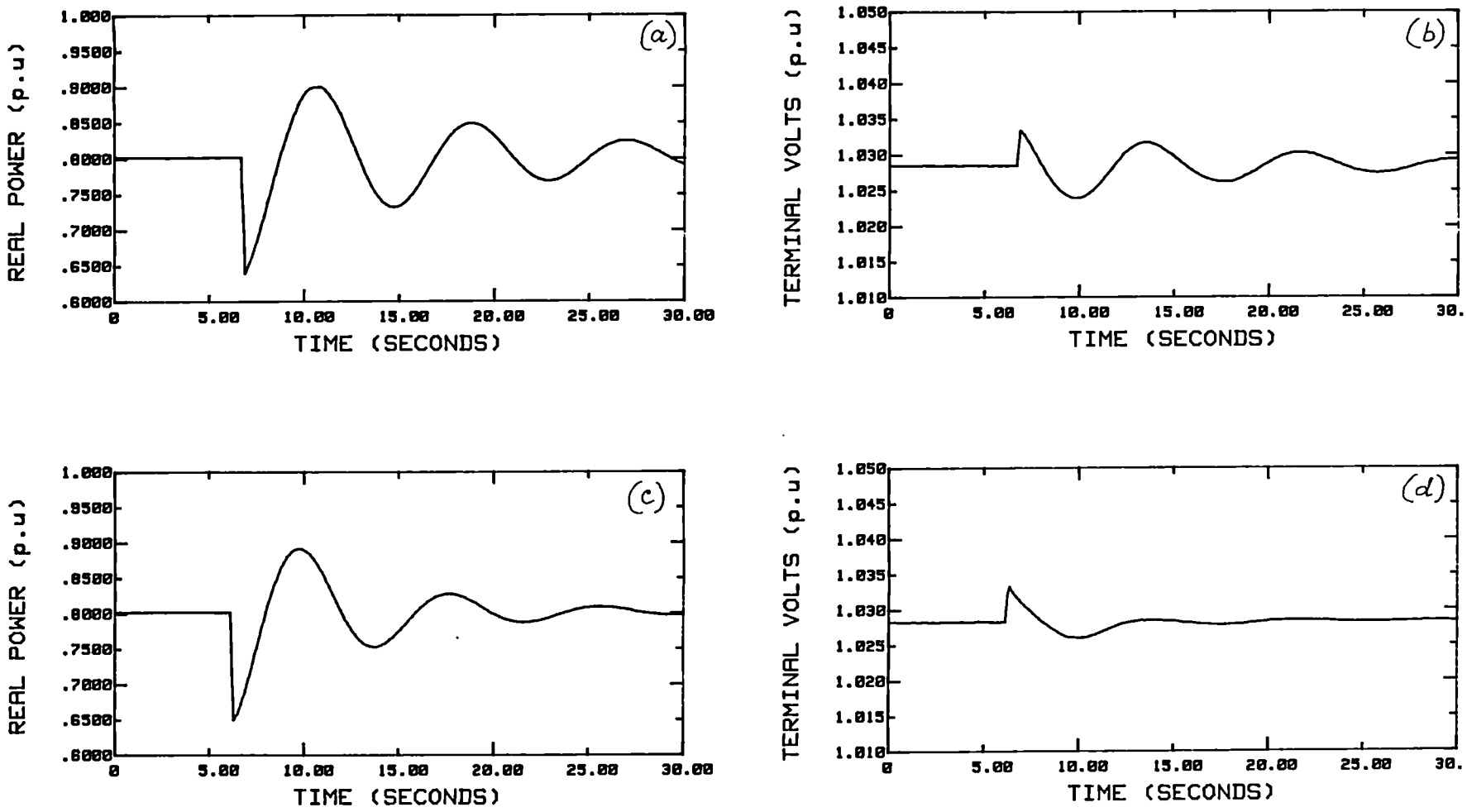

Fig. 5.12 Response of a conventional digital AVR type DGAVR-SO during transmission line switching using the TG simulator with and without the PSS. (a), (b) - without PSS; (c), (d) - with PSS.

AVR Type	EDR of Elec. Power
STAVR-F STAVR-F(P)	0.56 0.42
DGAVR-F DGAVR-F(P)	0.75 0.51
STAVR-S STAVR-S(P)	0.62 0.41
STAVR-SO STAVR-SO(P)	0.58 0.44
DGAVR-SO DGAVR-SO(P)	0.70 0.54

Table 5.2 Response of various types of AVRs with and without stabilising feedback on the TG simulator for a transmission line switch.

the performance of the power system stabilised self-tuning AVR has significantly improved and the extent of improvement is comparable with that of a PSS acting through a conventional digital AVR.

5.3.1.3 Three Phase Short Circuit Test

A 3-phase to neutral short-circuit test has been simulated at P = 0.8 pu and Q = 0 with the stabilised self-tuning AVR in operation using the TG simulator. The duration of the short which was located at the generator terminals has been set to 100 msec. The parameter estimator has been allowed to settle to some reasonable values before the test was conducted.

Fig. 5.13 shows the response of the electrical power, load angle, and the terminal voltage during the test with and without the use of the power signal in the self-tuning AVR which has been set-up to give a 'fast' response (type STAVR-F). The results show that an improvement from 0.63 to 0.37 in the EDR and 1.77 sec.

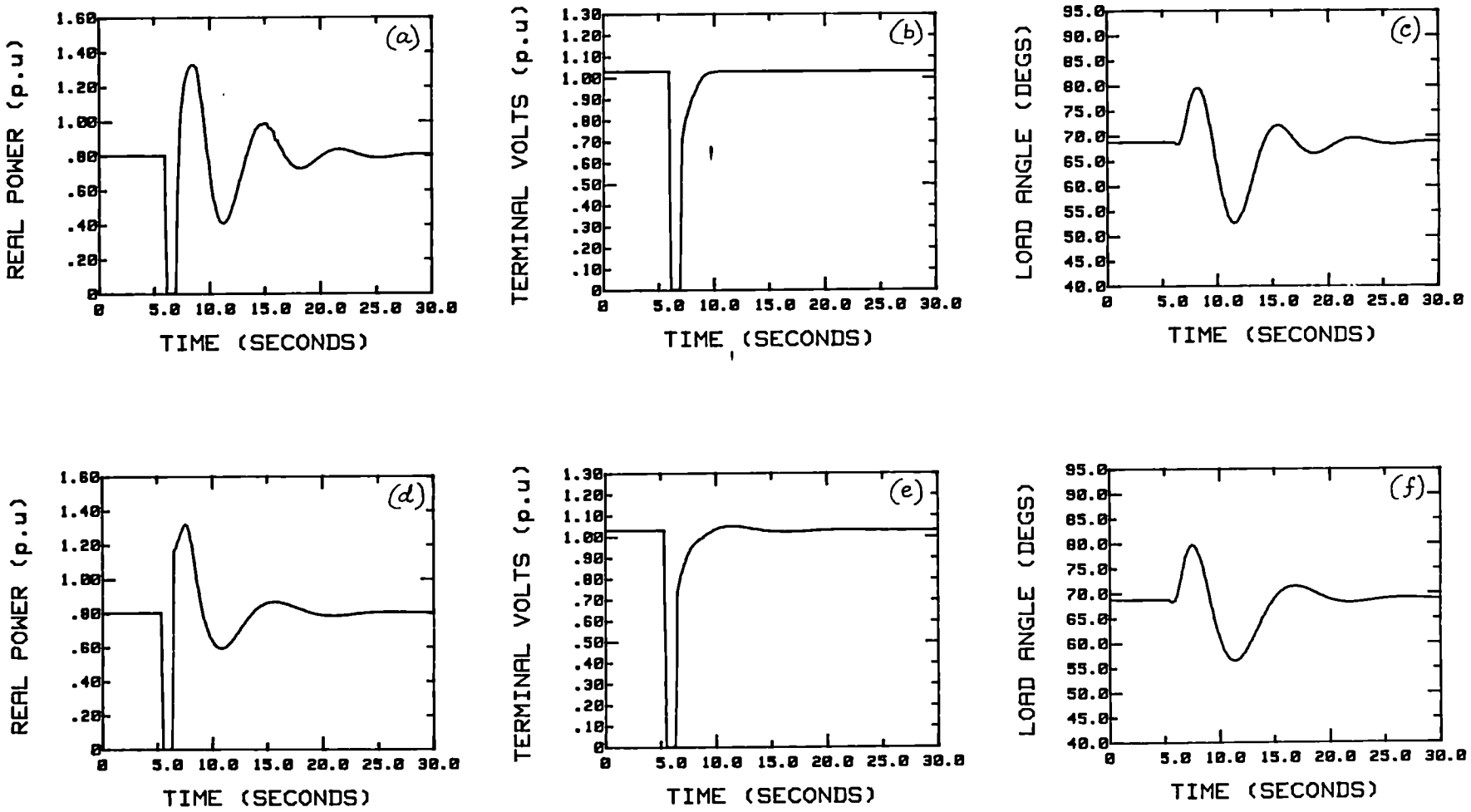

Fig. 5.13 Response of the self-tuning AVR type STAVR-F during short circuit using the TG simulator with and without the power signal. (a), (b), (c) - without power signal; (d), (e), (f) - with power signal.

to 1.3 sec. in the settling time of the electrical power signal has been achieved with the use of the supplementary feedback in the self-tuning AVR. The load angle damping has also been improved which is indicated by a reduction in its EDR from 0.72 to 0.64. These improvements have been achieved with a tolerable increase in the rise and settling times of the terminal voltage of the generator.

Fig. 5.14 illustrates the performance improvement obtainable with a conventional digital AVR (DGAVR-F) when it has been equipped with a PSS. The values of EDR etc., for this test are given in Table 5.3 for comparison purposes with the self-tuning AVR. Although the use of the power signal in the self-tuning AVR has not matched the improvement in performance achieved with the PSS, it has been able to give a significant contribution to the damping of dynamic oscillations. It can be seen that the primary reason for the PSS to perform better in this case is that there is more scope for improvement when using a fixed parameter digital AVR than when using a standard self-tuning AVR.

The performance improvement obtainable with 'slow' self-tuning AVR designs when using power input are illustrated in Fig. 5.15 and 5.16 and are summarised in Table 5.3 together with the results obtained for the corresponding fixed parameter digital AVR with a PSS (Fig. 5.17). It can be seen that significant improvement comparable with that obtained when using a PSS has been achieved with the power system stabilised self-tuning AVR. The results obtained with the fast and slow self-tuning AVR designs thus prove that the use of the power signal can make a useful contribution during conditions of transient instability also.

5.3.2 Evaluation using the Micro-Alternator System

The power system stabilised self-tuning AVR performance has been evaluated and compared with that of a standard self-tuning AVR using the micro-alternator system also. As with the TG simulator, the improvement in performance has been compared with that obtained when using a PSS with a conventional fixed parameter digital AVR. Fast as well as slow AVR designs have been tried out to ensure that a significant enhancement in the dynamic stability of the system is

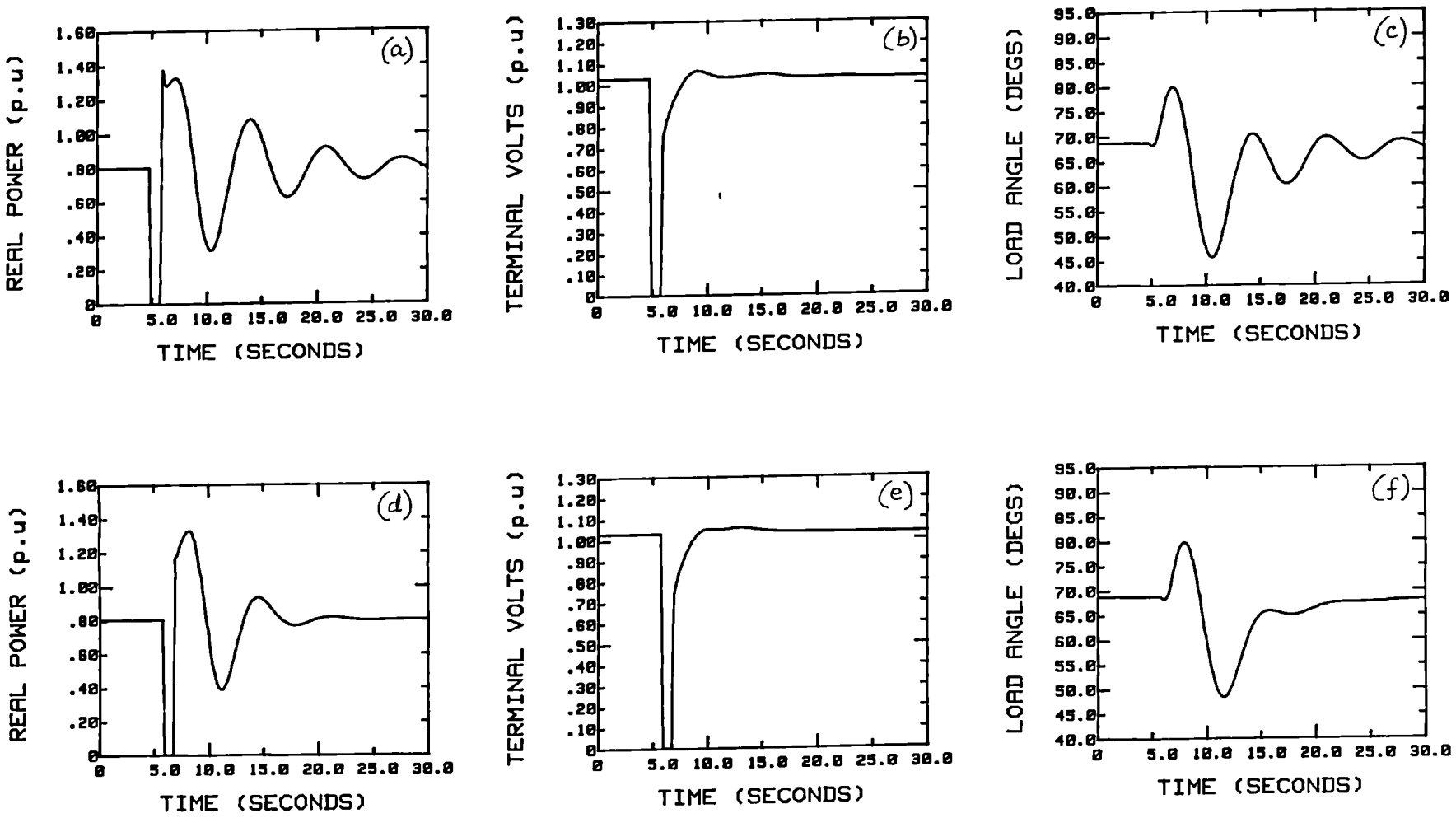

Fig. 5.14 Response of a conventional digital AVR type DGAVR-F during short circuit using the TG simulator with and without the PSS. (a), (b), (c) - without PSS; (d), (e), (f) - with PSS.

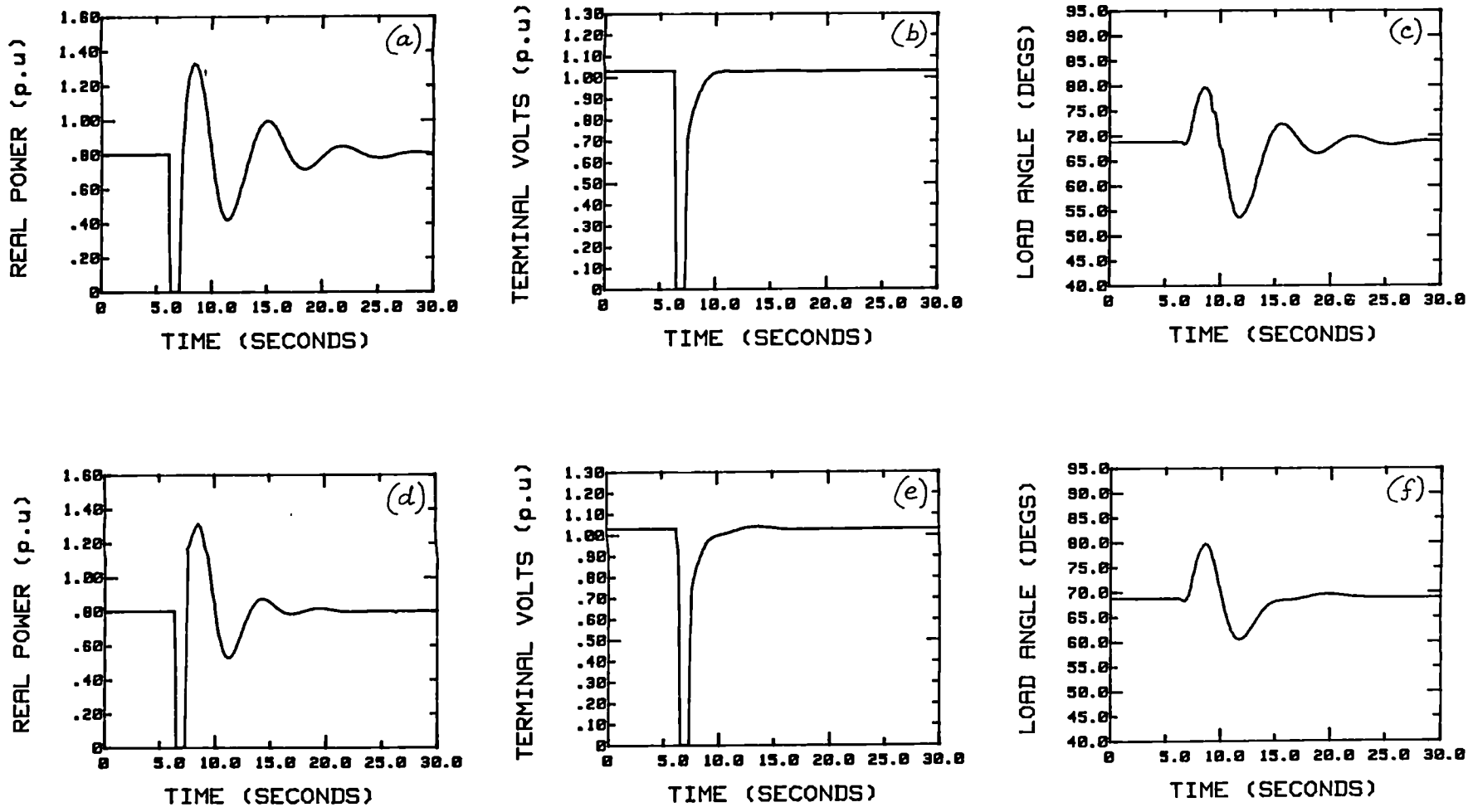

Fig. 5.15 Response of the self-tuning AVR type STAVR-S during short circuit using the TG simulator with and without the power signal. (a), (b), (c) - without power signal; (d), (e), (f) - with power signal.

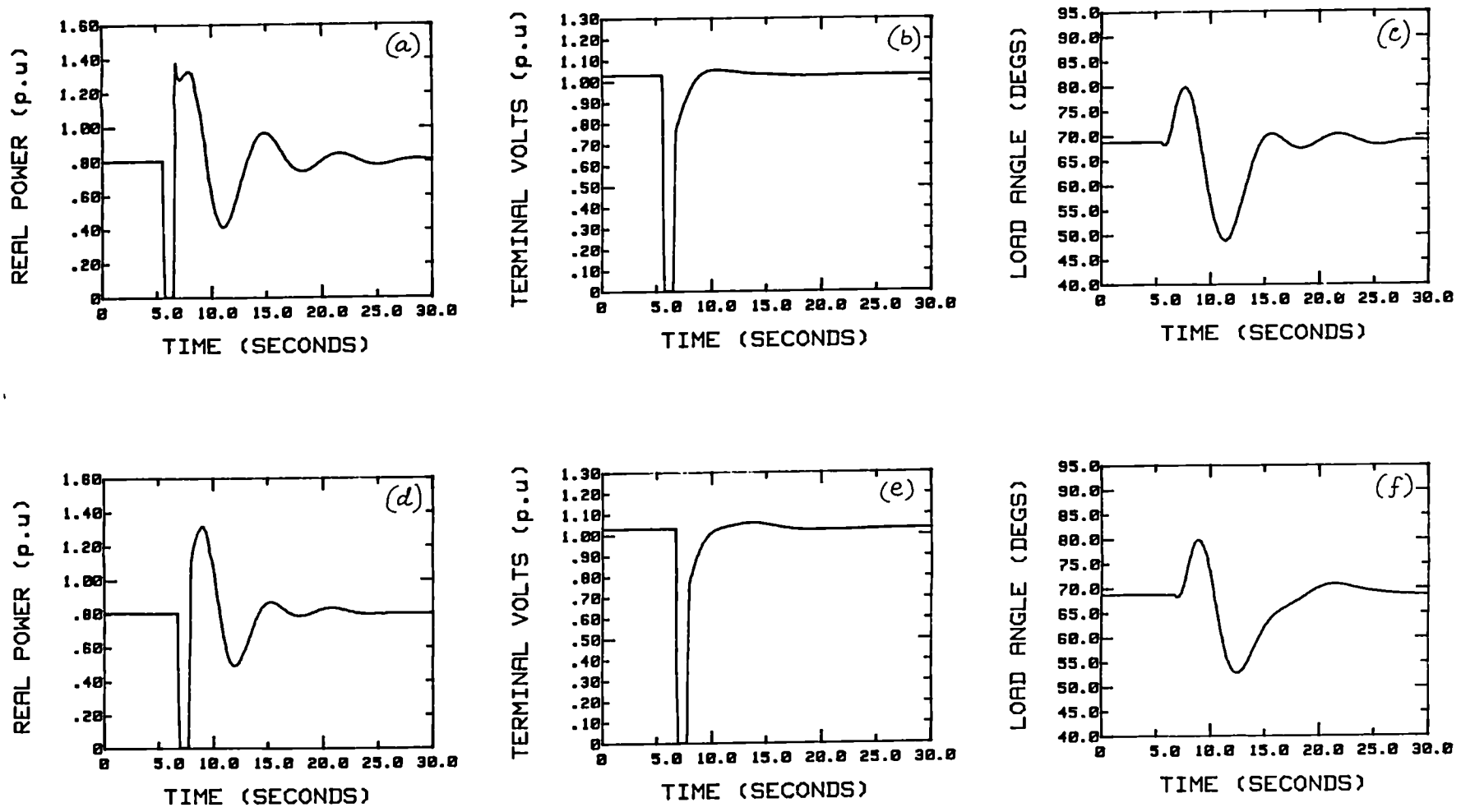

Fig. 5.16 Response of the self-tuning AVR type STAVR-SO during short circuit using the TG simulator with and without the power signal. (a), (b), (c) - without power signal; (d), (e), (f) - with power signal.

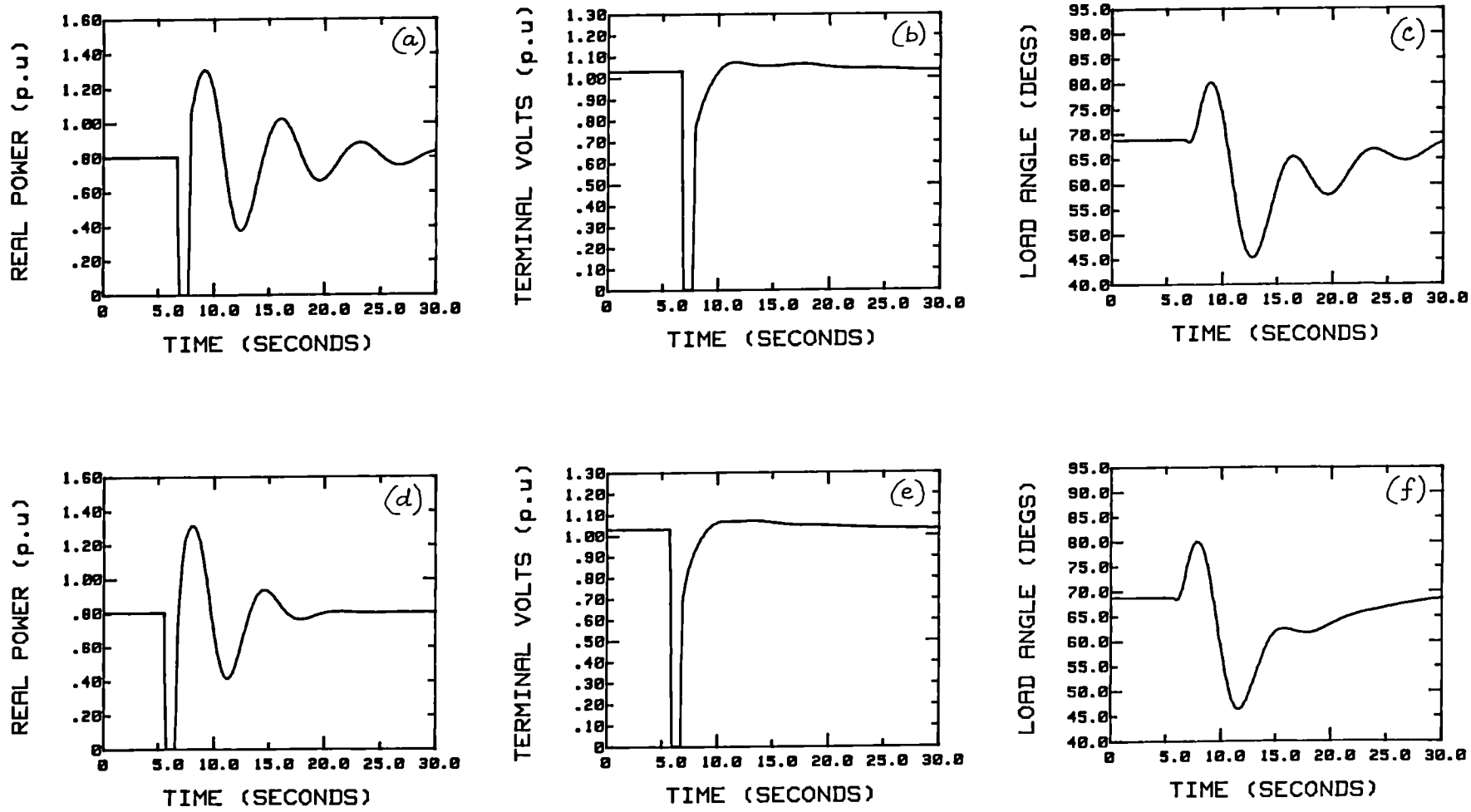

Fig. 5.17 Response of a conventional digital AVR type DGAVR-SO during short circuit using the TG simulator with and without the PSS. (a), (b), (c) - without the PSS; (d), (e), (f) - with the PSS.

AVR Type	EDR of Elec. Power P	Settling Time (P) (sec.)	Rise time (Vt) (sec.)	Settling time (Vt) (sec.)	EDR of Load Angle δ	Settling time (δ) (sec.)
STAVR-F STAVR-F(P)	0.63 0.37	1.77 1.30	0.36 0.45	0.36 0.78	0.72 0.64	1.46 1.38
DGAVR-F DGAVR-F(P)	0.77 0.58	3.48 1.74	0.34 0.37	1.29 1.05	0.73 0.56	2.88 1.53
STAVR-S STAVR-S(P)	0.64 0.45	2.03 1.16	0.39 0.57	0.39 0.86	0.72 0.40	1.41 0.93
STAVR-SO STAVR-S(P)	0.60 0.46	2.14 1.60	0.35 0.39	0.75 0.95	0.70 0.44	1.78 1.85
DGAVR-SO DGAVR-SO(P)	0.69 0.57	2.93 1.41	0.34 0.36	1.45 1.65	0.59 0.48	2.93 2.31

Table 5.3. Response of various types of AVRs with and without stabilising feedback on the TG simulator for a 3-phase short circuit.

achieved with the various designs. The results obtained during a step input, and 3-phase short-circuit are analysed in the following sub-sections. The transmission line switch test was not done with the micro-alternator system since the switching was not capable of producing a significant system disturbance. This is due to the low reactance of the transmission line simulators used in the micro-alternator system.

5.3.2.1 Step Response On Load

The micro-alternator system has been operated at P = 2.4 kW (0.8 pu) and Q = 0 kW during this test. The field time constant of the machine has been set to 6 sec. using the Time Constant Regulator and the governor has been set at 4% droop. The self-tuning AVR has been allowed to operate for a short period of time before the tests have been conducted to ensure that the parameter estimates are reasonably steady. A 3% positive step has been used to create a minor disturbance in the micro-alternator system.

Fig. 5.18 shows the performance of the 'fast' self-tuning AVR (STAVR-F) with and without the power signal, while Fig. 5.20 and 5.21 give the corresponding information for the 'slow' designs, viz. STAVR-S and STAVR-SO respectively. Fig. 5.19 and 5.22 illustrate for comparison purposes the performance improvement achievable with a PSS when used with the corresponding 'fast' and 'slow' designs of a fixed parameter digital AVR. The values of EDR of the power signal and the rise and settling times of terminal voltage are tabulated in Table 5.4.

AVR Type	EDR of Elec. Power	Rise Time (Vt) (sec.)	Settling (Vt) (sec.)
STAVR-F	0.72	0.50	0.50
STAVR-F(P)	0.28	0.62	1.50
DGAVR-F	0.57	1.05	1.05
DGAVR-F(P)	0.36	1.05	1.05
STAVR-S	0.52	0.68	2.02
STAVR-S(P)	0.31	0.64	1.76
STAVR-SO	0.34	0.71	2.60
STAVR-SO(P)	0.20	0.79	1.99
DGAVR-SO	0.56	1.70	1.70
DGAVR-SO(P)	0.38	1.65	1.65

Table 5.4. Response of various types of AVRs with and without stabilising feedback on the micro-alternator for a step input.

It can be observed from the table that improvement similar to that seen with the TG simulator are achieved by the self-tuning AVR with the power input on the micro-alternator system also. Once again, the use of the stabilising power input in the self-tuning AVR is found to compare favourably in performance with a PSS acting through a fixed-parameter digital AVR thus validating the results obtained using the TG simulator.

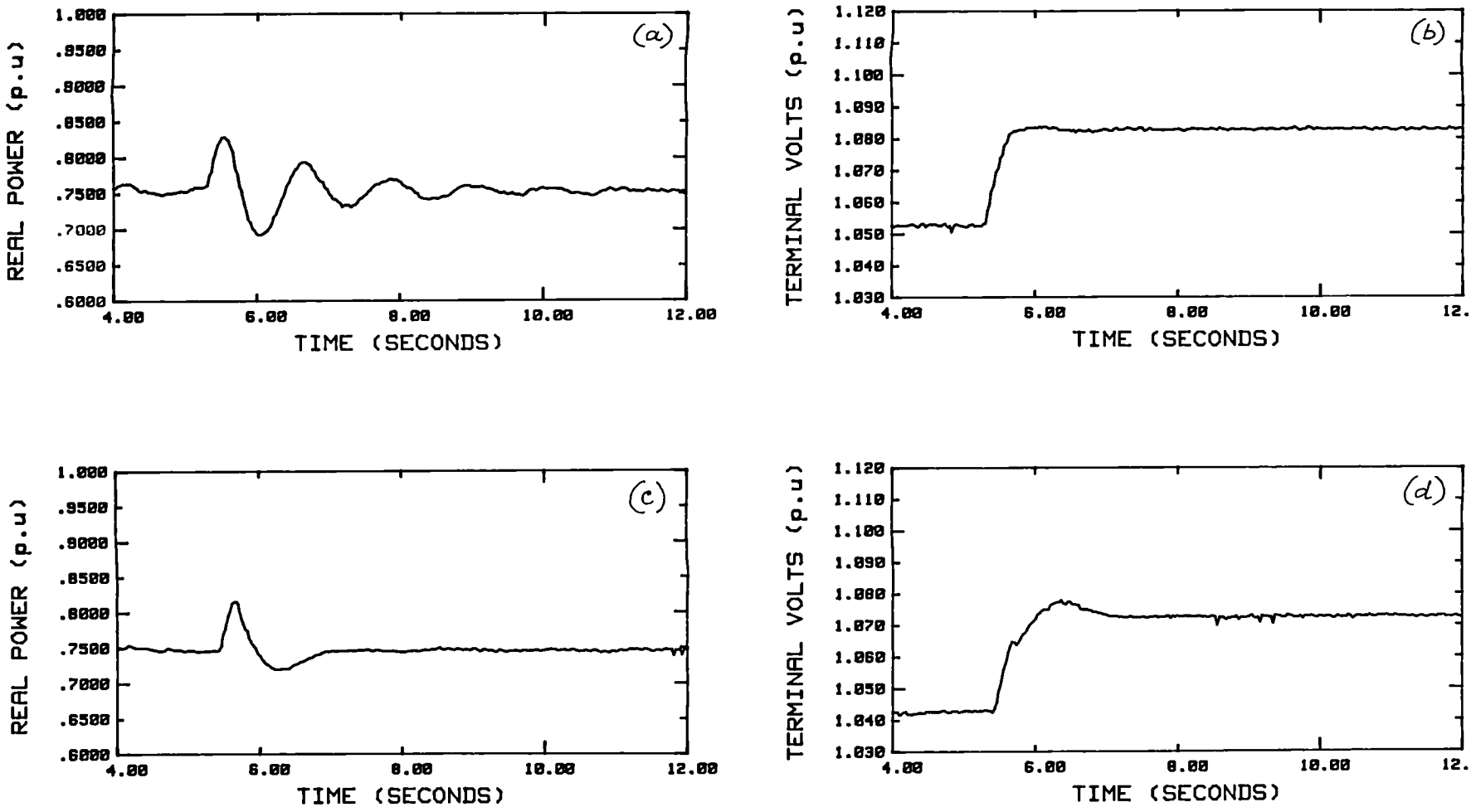

Fig. 5.18 Step response of the self-tuning AVR type STAVR-F using the micro-alternator with and without the power signal. (a), (b) - without power signal; (c), (d) - with power signal.

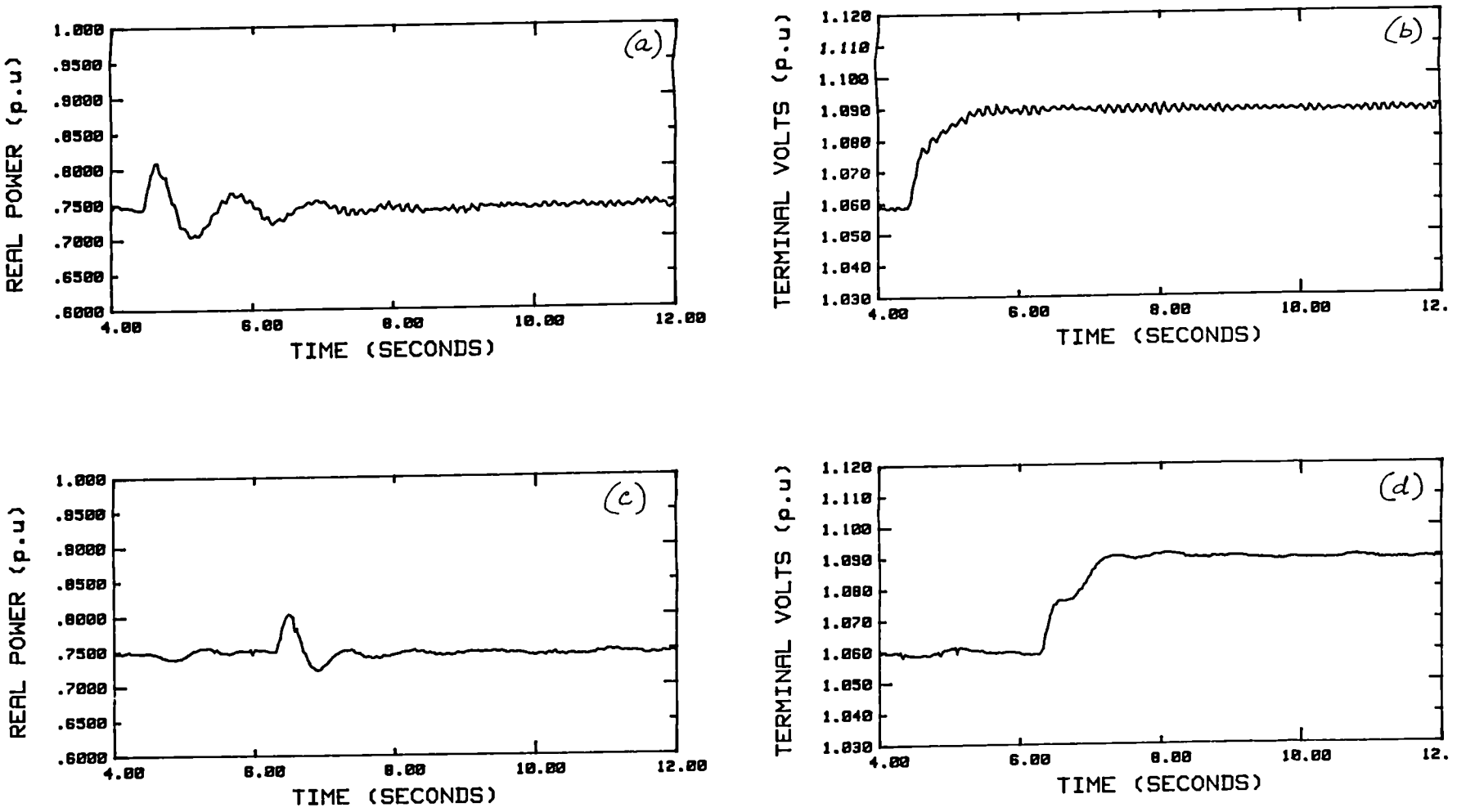

Fig. 5.19 Step response of a conventional digital AVR type DGAVR-F using the micro-alternator with and without the PSS. (a), (b) - without the PSS; (c), (d) - with the PSS.

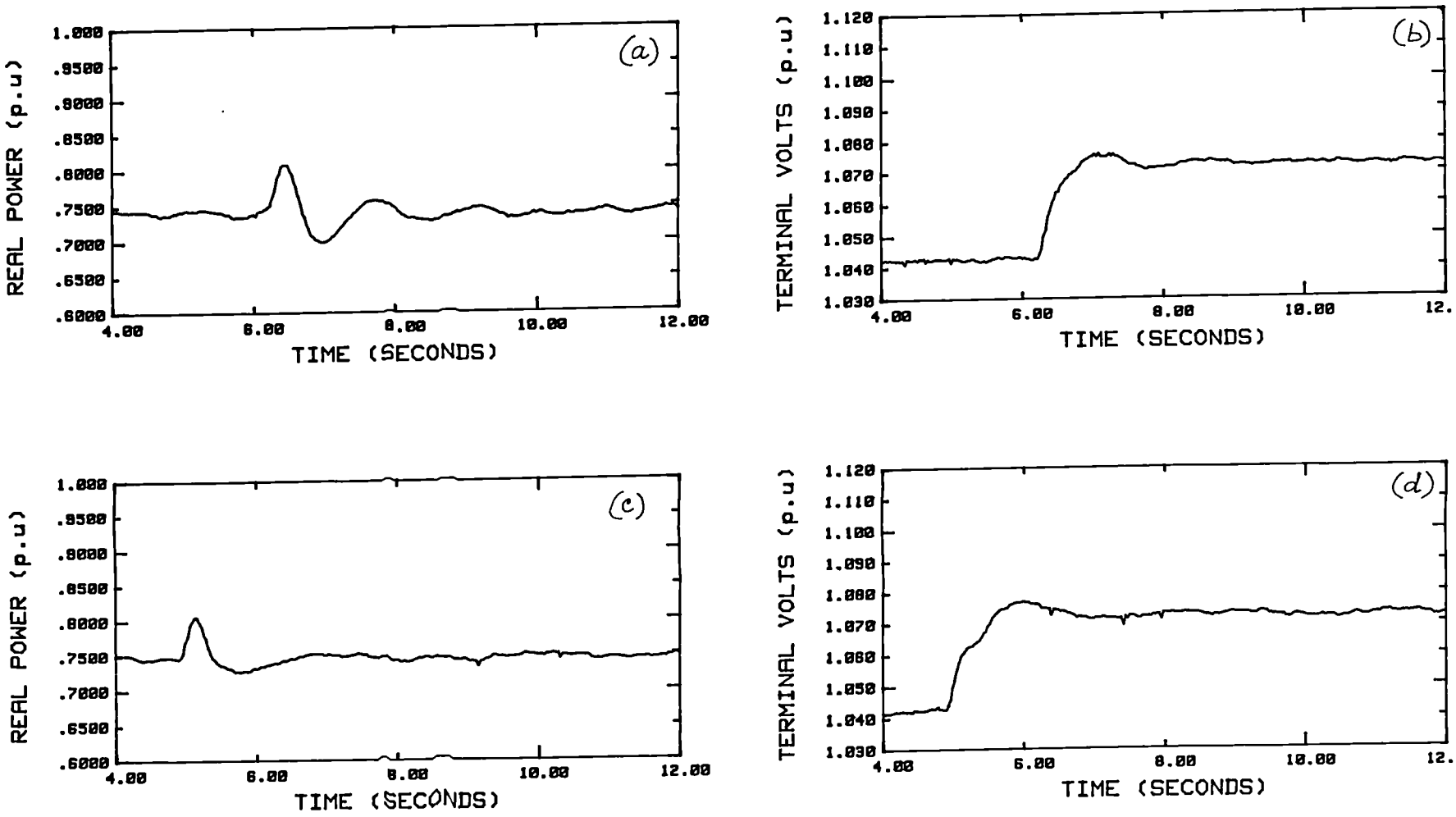

Fig. 5.20 Step response of the self-tuning AVR type STAVR-S using the micro-alternator with and without the power signal. (a), (b) - without power signal; (c), (d) - with power signal.

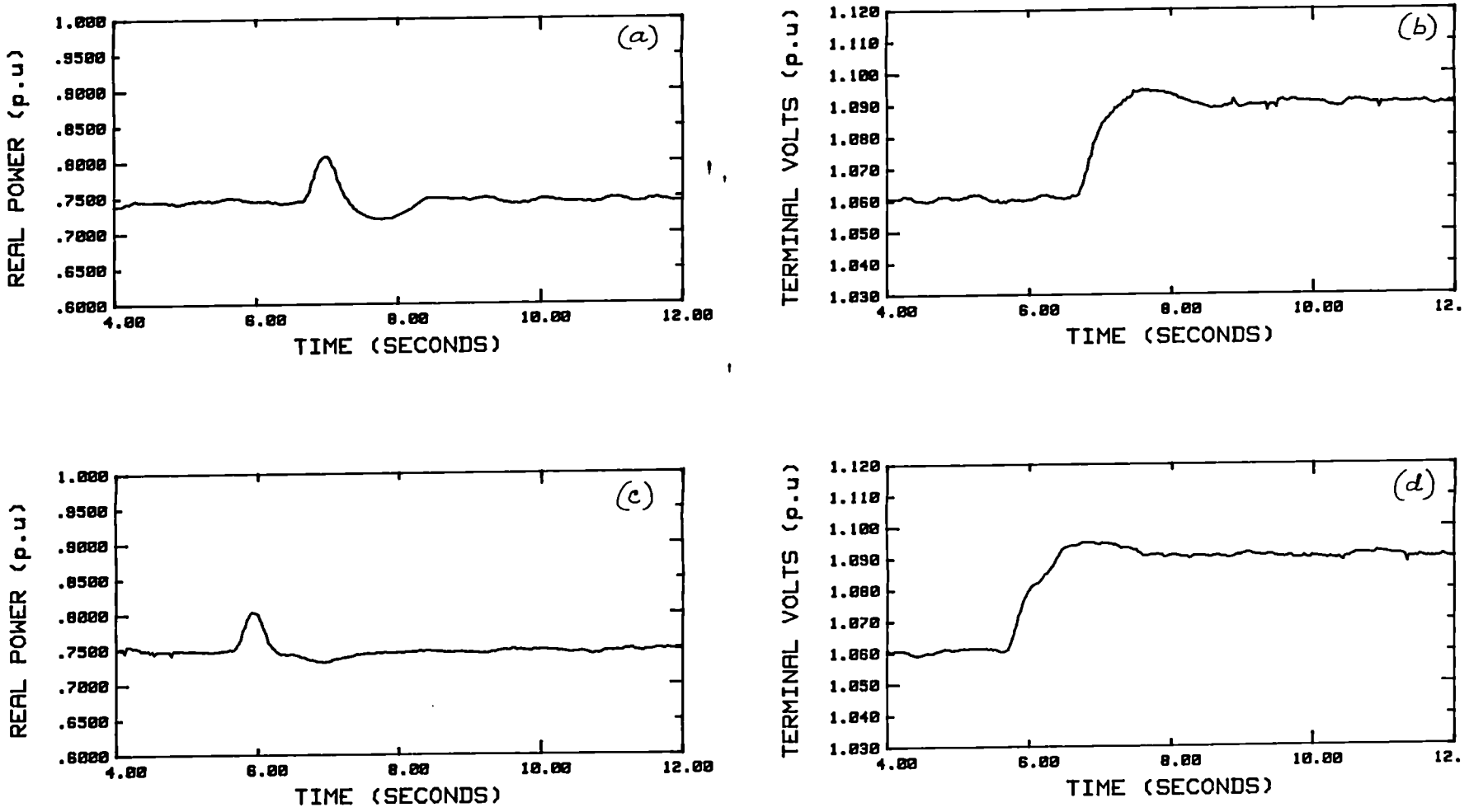

Fig.5.21 Step response of the self-tuning AVR type STAVR-SO using the micro-alternator with and without the power signal. (a), (b) - without power signal; (c), (d) - with power signal.

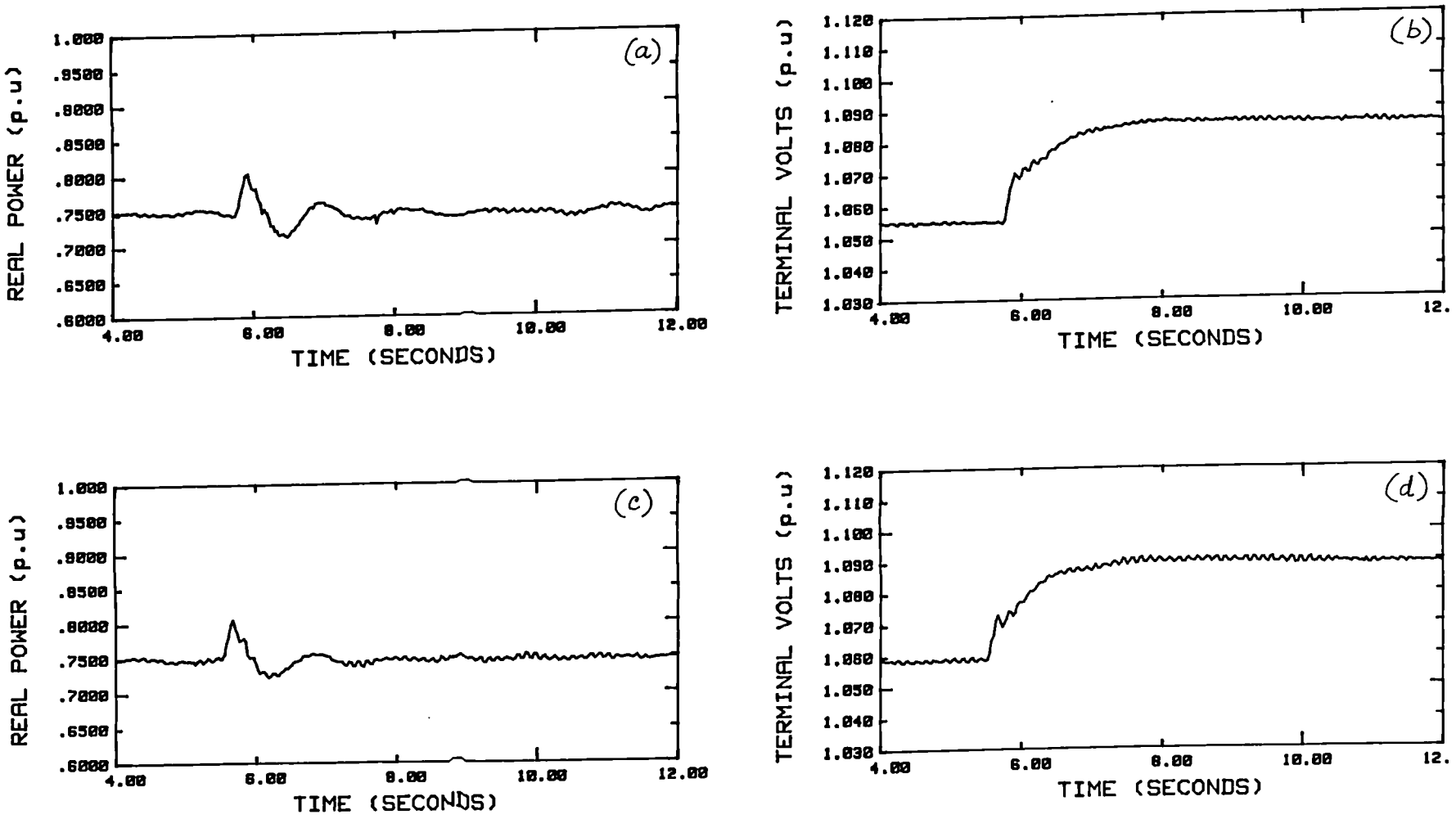

Fig. 5.22 Step response of a conventional digital AVR type DGAVR-SO using the micro-alternator with and without the PSS. (a), (b) - without the PSS; (c), (d) - with the PSS.

5.3.2.2 Three Phase Short Circuit Test

A 3-phase short-circuit lasting for 100 msec. has been applied at the sending end of the transmission line simulator with the micro-alternator operating at P = 2.4 kW and Q = 0 kW during this test. The settings of the micro-alternator system were same as those during the step response test. As before, the self-tuning AVR has been allowed to operate for a short period of time before the tests have been conducted to ensure that the parameter estimates are reasonably steady.

Fig. 5.23 shows the performance of the 'fast' self-tuning AVR (STAVR-F) with and without the power signal during this severe disturbance, while Fig. 5.25 and 5.26 give the corresponding response for the 'slow' designs, viz. STAVR-S and STAVR-SO respectively. Fig. 5.24 and 5.27 illustrate for comparison purposes how a PSS copes with transient instability when used with the corresponding 'fast' and 'slow' designs of a fixed parameter digital AVR. The values of EDR and the settling times of electrical power and load angle as well as the rise and settling times of terminal voltage are tabulated in Table 5.5.

It can be observed from the figures and the table that a significant improvement in the EDR of the load angle is obtained when using the power system stabilised self-tuning AVR. It is also seen that the terminal voltage recovery following the fault is hardly affected by the use of the power signal as a stabilising feedback. However, the improvement in the EDR of the power signal is found to be rather small when compared with that obtained during tests on the TG simulator especially for the 'slow' self-tuning AVR designs. This is mainly due to the fact that the EDR value of the electrical power even without the power feedback is generally low on the micro-alternator system when compared with the TG simulator.

The rather marginal improvement in the damping of the electrical power is not a serious problem since it is the load angle oscillations that are more critical during transient instability and these are found to be satisfactorily damped by the

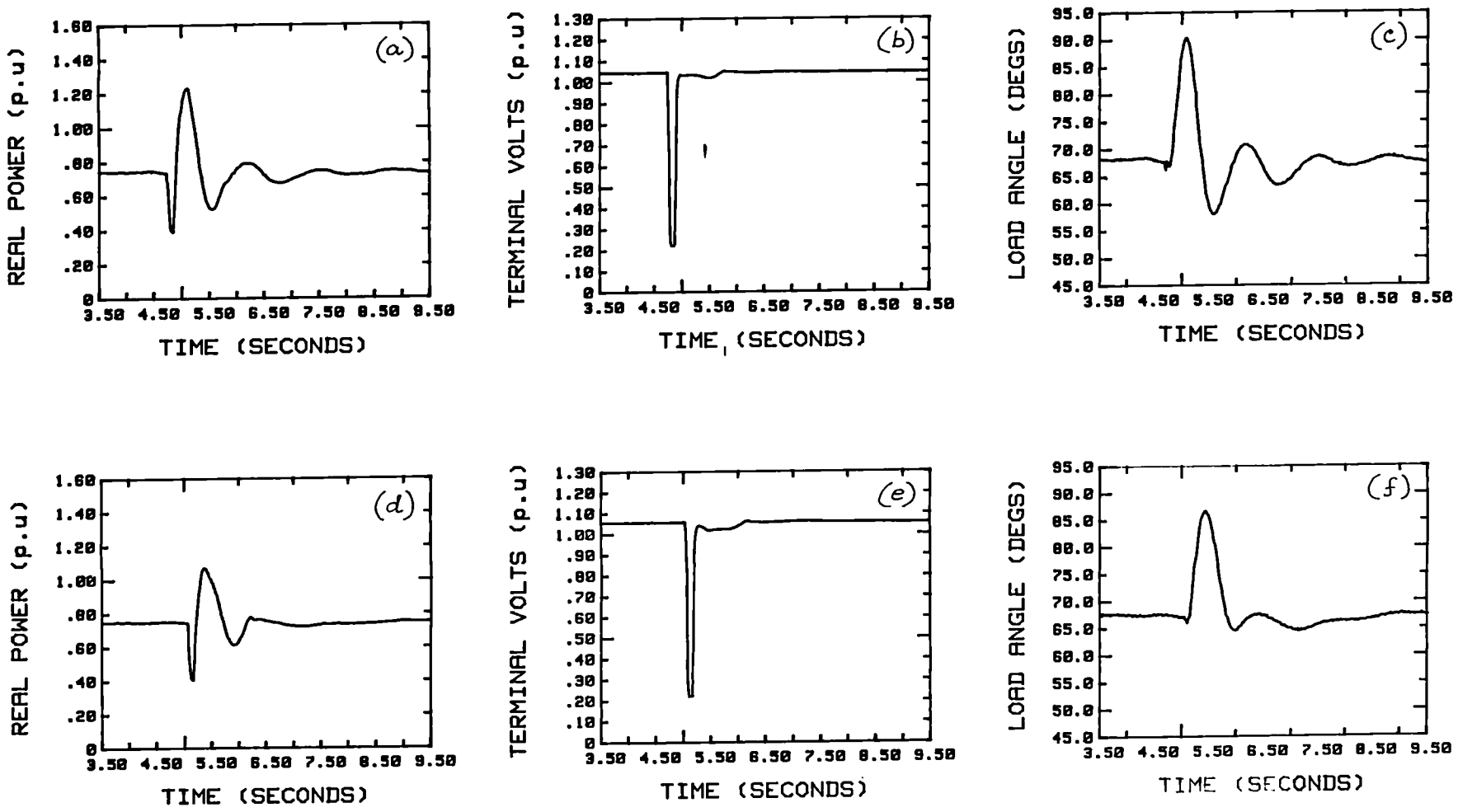

Fig. 5.23 Response of the self-tuning AVR type STAVR-F during short circuit using the micro-alternator with and without the power signal. (a), (b), (c) - without power signal; (d), (e), (f) - with power signal.

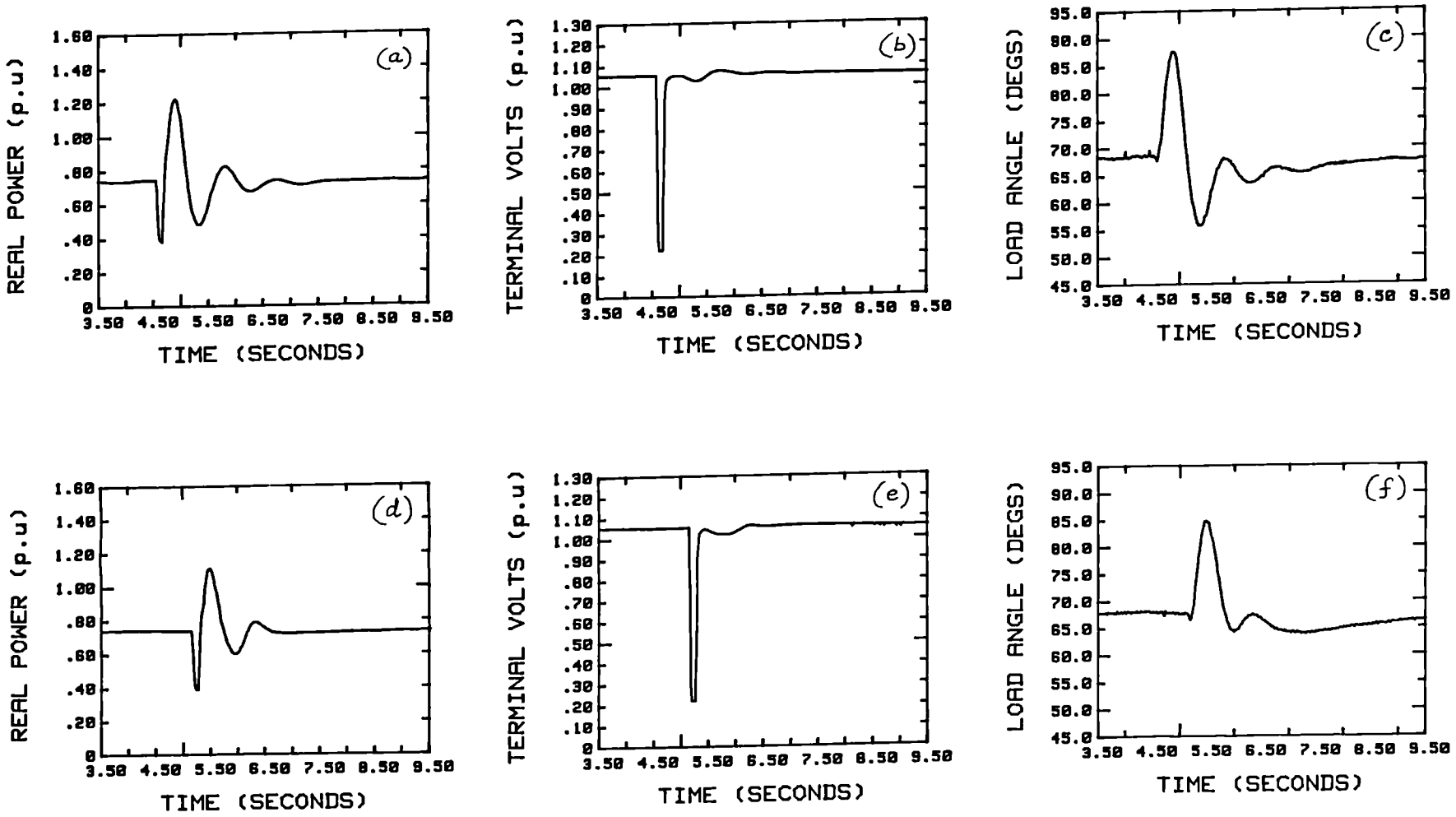

Fig. 5.24 Response of a conventional digital AVR type DGAVR-F during short circuit using the micro-alternator with and without the PSS. (a), (b), (c) - without the PSS; (d), (e), (f) - with PSS.

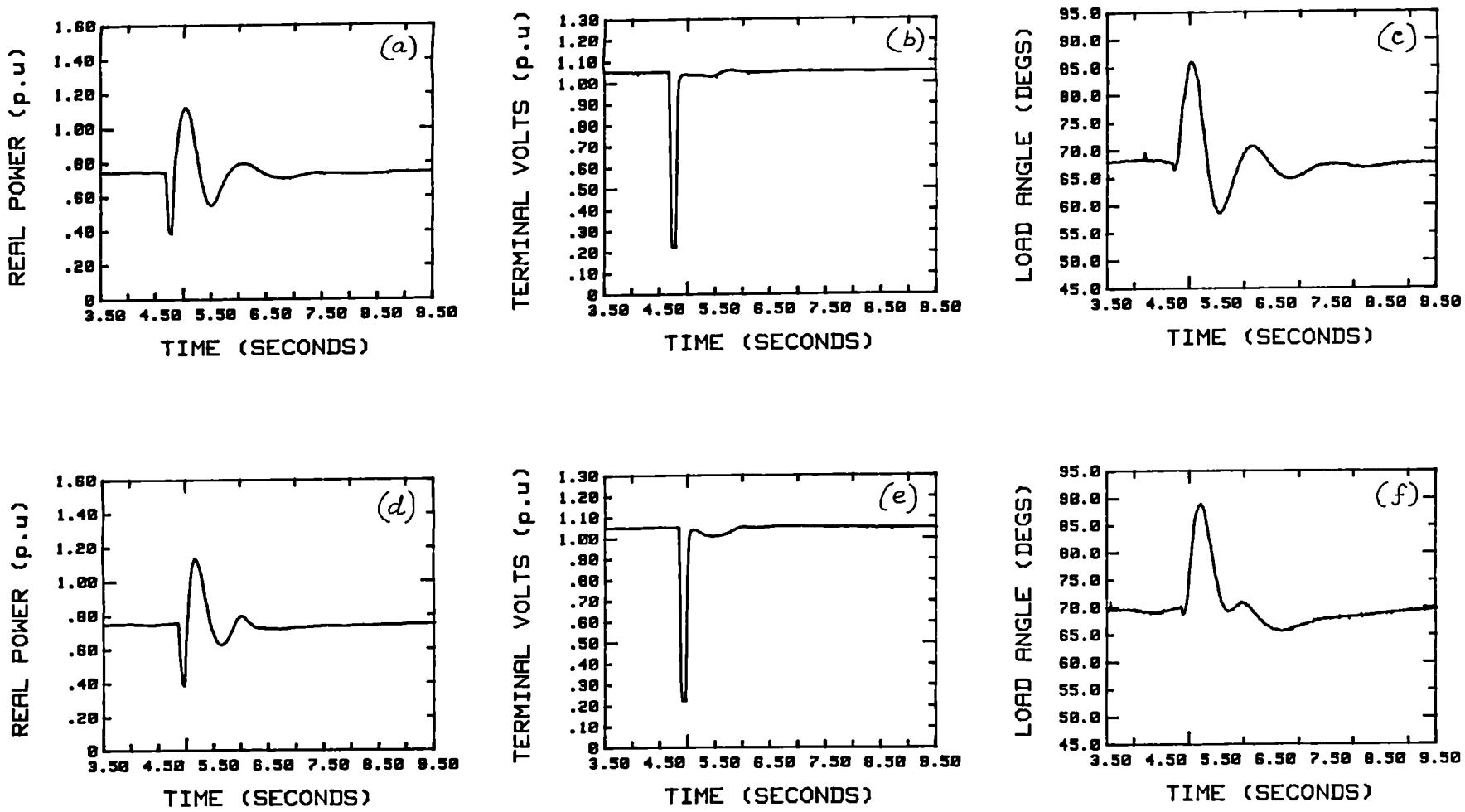

Fig. 5.25 Response of the self-tuning AVR type STAVR-S during short circuit using the micro-alternator with and without the power signal. (a), (b), (c) - without power signal; (d), (e), (f) - with power signal.

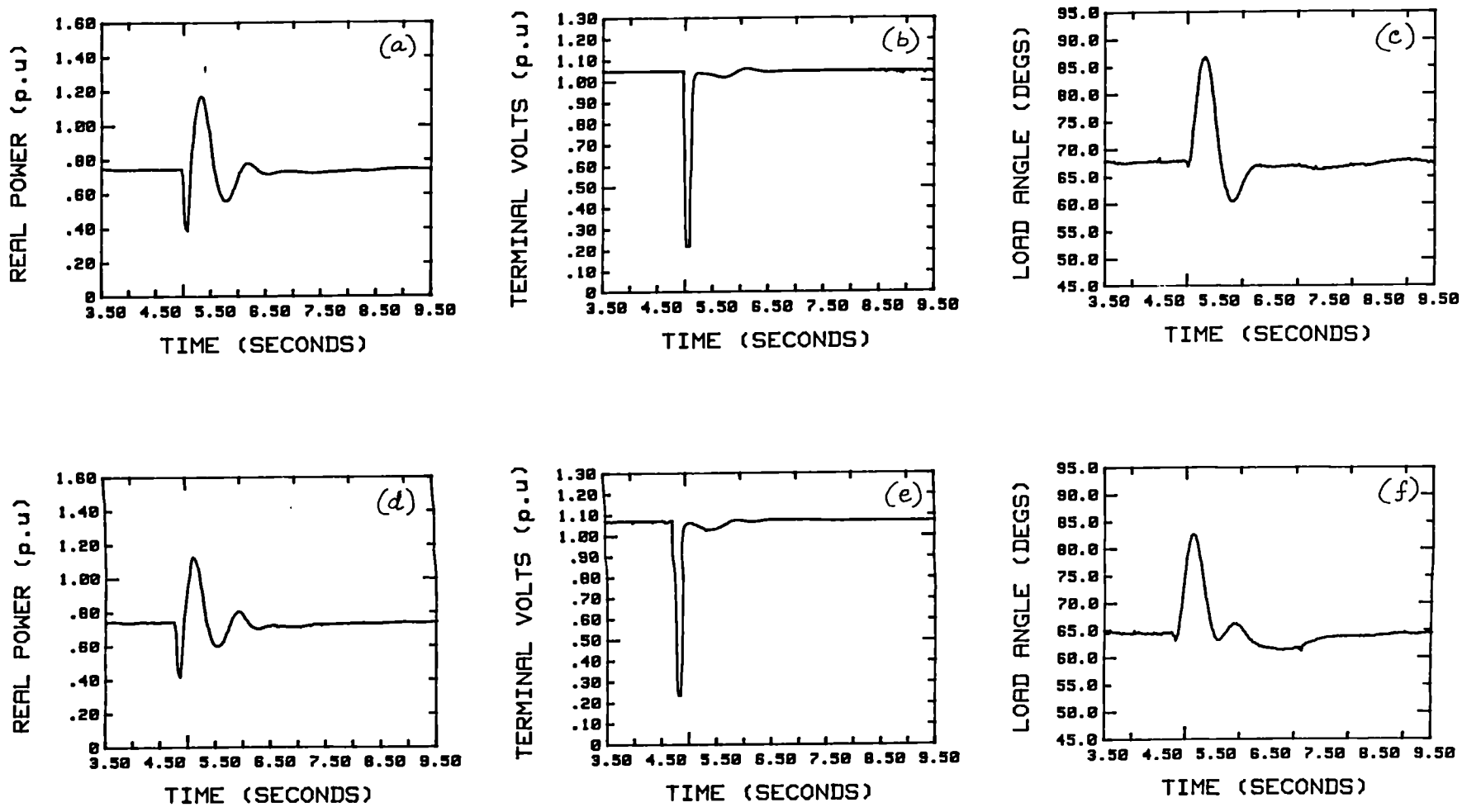

Fig. 5.26 Response of the self-tuning AVR type STAVR-SO during short circuit using the micro-alternator with and without the power signal. (a), (b), (c) - without power signal; (d), (e), (f) - with power signal.

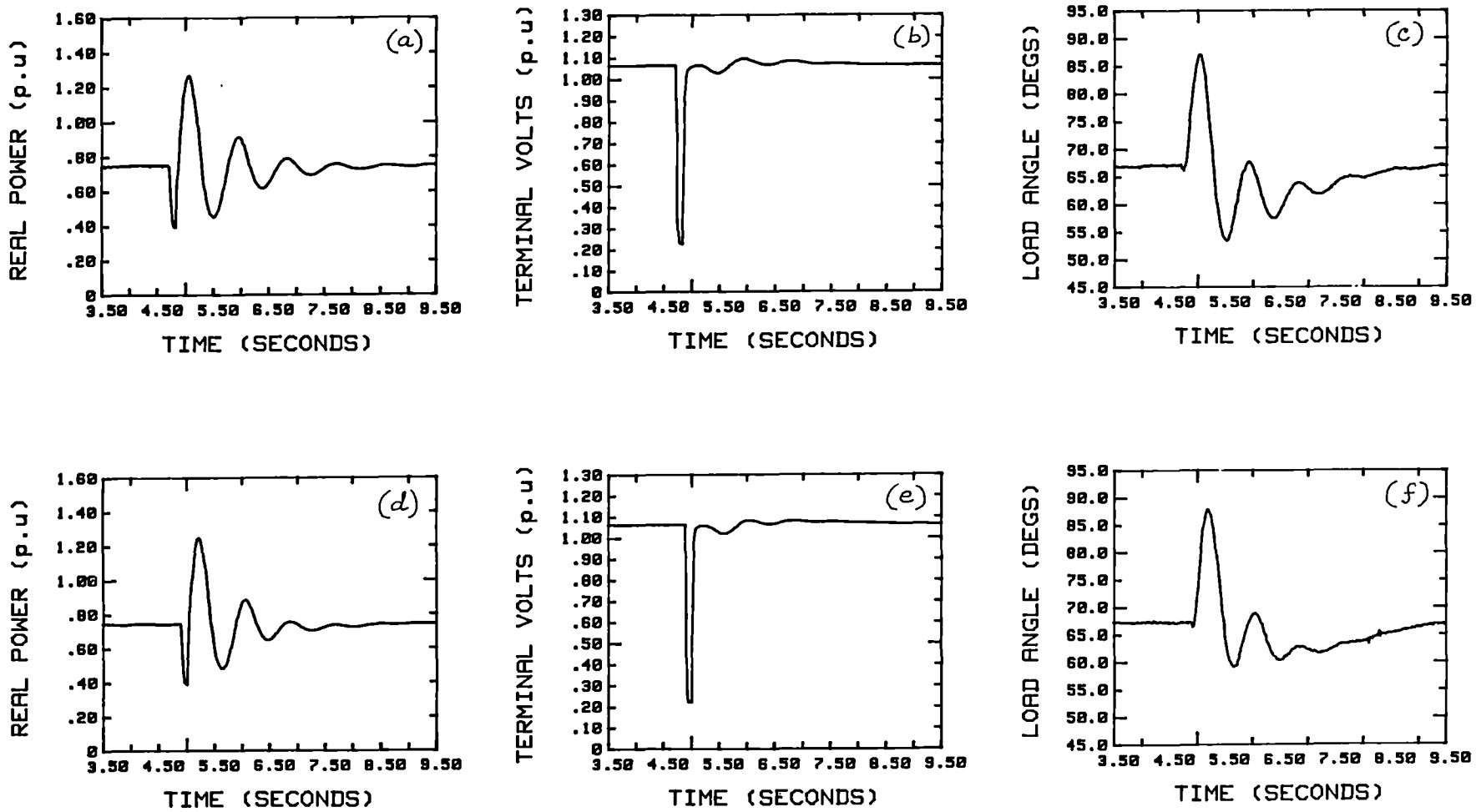

Fig. 5.27 Response of a conventional digital AVR type DGAVR-SO during short circuit using the micro-alternator with and without the PSS. (a), (b), (c) - without the PSS; (d), (e), (f) - with the PSS.

AVR Type	EDR of Elec. Power P	Settling Time (P) (sec.)	Rise time (Vt) (sec.)	Settling time (Vt) (sec.)	EDR of Load Angle δ	Settling time (δ) (sec.)
STAVR-F STAVR-F(P)	0.40 0.37	4.01 2.48	1.01 1.09	1.01 1.09	0.38 0.12	3.58 2.44
DGAVR-F DGAVR-F(P)	0.47 0.37	3.23 3.53	1.01 1.05	1.58 1.05	0.37 0.17	4.16 4.30
STAVR-S STAVR-S(P)	0.44 0.33	3.42 3.26	1.01 1.16	1.01 1.16	0.42 0.10	2.66 3.64
STAVR-SO STAVR-S(P)	0.37 0.37	3.15 3.02	0.94 1.03	1.35 1.35	0.23 0.17	1.24 2.58
DGAVR-SO DGAVR-SO(P)	0.56 0.51	3.75 3.32	1.01 0.94	3.23 3.53	0.43 0.32	4.50 4.02

Table 5.5. Response of various types of AVRs with and without stabilising feedback on the micro-alternator for a 3-phase short circuit.

self-tuning AVR using the power feedback. Once again, the use of the stabilising power input in the self-tuning AVR is found to compare favourably in performance with a PSS acting through a fixed-parameter digital AVR. These results show that transient stability is not adversely affected by the use of the power signal in the self-tuning AVR. On the contrary, the improvement in the EDR of the load angle achieved by the power system stabilised self-tuning AVR is a useful contribution towards transient system stability.

CHAPTER 6

MULTI-INPUT MULTI-OUTPUT SELF-TUNING CONTROL OF A TURBINE GENERATOR

Power system stability is one of the most important considerations in turbine generator control. Traditionally, efforts to improve transient performance of a turbine generator have been concentrated only on excitation control [52]. Although a significant enhancement in the system damping can be obtained through excitation control, there is a limit to which improvement in the stability limit can be achieved by this means. This limit is dictated mainly by the ceiling voltage capability of the exciter.

It has been known for quite some time through simulation studies and tests on micro-alternator systems that improvement in the stability limit can be achieved by the turbine governing system [52,60]. It is therefore prudent to consider the use of a high performance turbine controller for further improvement in the transient performance of the system. This is made possible by the availability of fast-acting steam valves and the associated high performance hydraulic systems in modern generating plant [9]. However, the control of turbine generators using separate governor and excitation control loops does not necessarily give the best performance if there are significant loop interactions [8].

Since the excitation and governing loops can make positive contributions to the improvement of power system stability, it is logical that an integrated control strategy for turbine generators is developed which combines the functions of the AVR and the turbine Governor. Two approaches can be considered for an integrated TG controller, viz. state space and multivariable control [52,60,3]. Since multivariable control is a more closely related approach to the existing single-input single-output philosophy, less problems with familiarisation and customer acceptance can be anticipated with multivariable control than with state space. Hence the multivariable control strategy has been adopted here to integrate the AVR and turbine governing functions. Thus the two control loops can be co-ordinated effectively to optimise the improvement in the stability of the system.

A significant reduction in the hardware and software used for the control of the turbine generator can be achieved with a multivariable approach. This is due to the highly similar nature of the AVR and the Electro-Hydraulic Governor (EHG) in terms of their structure, ie. Triplex Modular Redundant (TMR) architecture, video monitor based Man-Machine Interface, information transfer through serial links etc. [19]. The reduction in the hardware and software will lead to improved reliability and availability due to a lesser number of hardware components and software modules. This will also lead to a decrease in the overall cost of the control system.

This chapter describes the design and testing of a multivariable self-tuning controller for the turbine generator based on the GPC strategy. The extension of the single-input single-output (SISO) GPC theory to a multi-input multi-output (MIMO) control algorithm is explained in section 6.1. Section 6.2 gives the implementation details of the self-tuning TG controller and outlines how the SISO algorithm has been upgraded to a multivariable strategy. The standard MIMO GPC equations need modifying when practical requirements such as constraints on control input are to be incorporated. This is described in section 6.3. Finally, the evaluation of the MIMO self-tuning TG controller using the software simulator and the micro-alternator system is presented in section 6.4.

6.1 Formulation of Multivariable Generalised Predictive Control

The design of a multivariable controller depends on the structure of the plant model used. Irrespective of the real interaction structure that a plant has, it can always be transformed into 'canonical' models [124,127]. The two commonly encountered canonical representations are the P and V structures. The P-canonical structure is one in which each input also affects all other outputs. This treats interactions as feedforward couplings from the inputs to the outputs. The V-canonical structure on the other hand represents interactions within the system as feedback couplings from the outputs back to the inputs thus causing each output to act on all other inputs. Both canonical structures can be converted from one form to the other [124].

The P-canonical structure has been chosen to model the TG plant as a multivariable system. Fig. 6.1 shows the P-canonical representation for a two-input two-output (2 x 2) system. It can be seen that the structure enables the MIMO system to be broken down into a number of multi-input single-output sub-systems. This leads naturally to simpler mathematical treatment by retaining the simplicity of the SISO model and relates more closely to the existing AVR and EHG systems in terms of the structure. The P-canonical representation thus has a form which is more suited for the upgrading of the SISO self-tuning algorithm for use in the MIMO controller.

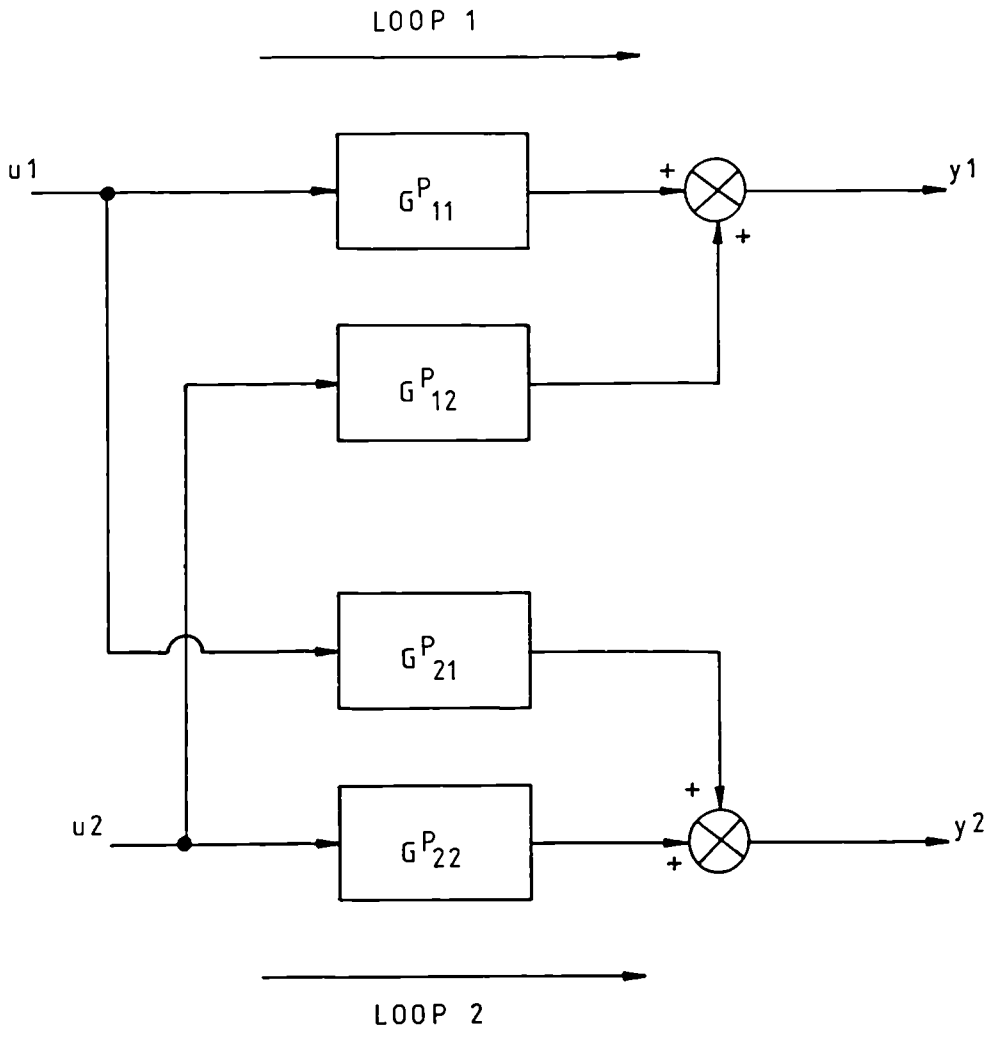

Fig. 6.1 P-canonical structure of a 2 x 2 system.

The derivation of the MIMO GPC for a plant whose interactions are represented by the P-canonical structure is summarised as follows:

A 'r' input, 's' output ($r \geq s$) linear deterministic plant can be modelled as:

$$\boldsymbol{A}\ \boldsymbol{y}(t) = \boldsymbol{B}\ \boldsymbol{u}(t-1) + \frac{\boldsymbol{e}(t)}{\Delta} \tag{6.1}$$

where $\boldsymbol{y}$, $\boldsymbol{u}$ and $\boldsymbol{e}$ are the output, input and noise vectors respectively and are given by:

$$\begin{aligned}
\boldsymbol{y}(t) &= [y_1(t) \quad y_2(t) \quad \text{-----} \quad y_s(t)]^T \\
\boldsymbol{u}(t-1) &= [u_1(t-1) \quad u_2(t-1) \quad \text{-----} \quad u_r(t-1)]^T \\
\boldsymbol{e}(t) &= [e_1(t) \quad e_2(t) \quad \text{-----} \quad e_s(t)]^T
\end{aligned}$$

$\boldsymbol{A}$ and $\boldsymbol{B}$ are polynomial matrices in z^{-1} and are defined as:

$$\boldsymbol{A} = diag\ [\boldsymbol{A}_1(z^{-1}) \quad \boldsymbol{A}_2(z^{-1}) \quad \text{-----} \quad \boldsymbol{A}_s(z^{-1})]$$

$$\boldsymbol{B} = \begin{bmatrix}
B_{11}(z^{-1}) & B_{12}(z^{-1}) & - & - & - & B_{1r}(z^{-1}) \\
B_{21}(z^{-1}) & - & - & - & - & \\
- & & & & & \\
- & & & & & \\
B_{s1}(z^{-1}) & - & - & - & - & B_{sr}(z^{-1})
\end{bmatrix}$$

As in the SISO case, Δ is the differencing function $(1-z^{-1})$.

To obtain the model following feature in MIMO GPC, an auxiliary function vector $\boldsymbol{\phi}$ can be defined as:

$$\boldsymbol{\phi}(t+j) = \boldsymbol{P}\ \boldsymbol{y}(t+j) \tag{6.2}$$

where

$$\begin{aligned}
\boldsymbol{\phi}(t+j) &= [\phi_1(t+j) \quad \phi_2(t+j) \quad \text{-----} \quad \phi_s(t+j)]^T \\
\boldsymbol{P} &= diag\ [P_1(z^{-1}) \quad P_2(z^{-1}) \quad \text{-----} \quad P_s(z^{-1})]
\end{aligned}$$

As with the SISO case, the diagonal elements of $\boldsymbol{P}$ can be chosen as transfer functions.

Disturbance tailoring as in the SISO case can be achieved by incorporating a tailoring polynomial $T_i(z^{-1})$ for loop 'i' which leads to:

$$\boldsymbol{\phi}(t+j) = \frac{\boldsymbol{P}\,\boldsymbol{B}}{\boldsymbol{A}}\,\boldsymbol{u}(t+j-1) + \frac{\boldsymbol{P}\,\boldsymbol{T}}{\boldsymbol{\Delta}\,\boldsymbol{A}}\,\boldsymbol{e}(t+j) \tag{6.3}$$

This leads to the Diophantine identity,

$$\boldsymbol{P}\,\boldsymbol{T} = \boldsymbol{E}_j^f\,\boldsymbol{\Delta}\,\boldsymbol{A} + z^{-j}\,\boldsymbol{F}_j^f \tag{6.4}$$

in which $\boldsymbol{E}_j^f$ and $\boldsymbol{F}_j^f$ are polynomial matrices whose elements can be solved recursively [30] and are given by:

$$\boldsymbol{E}_j^f = diag\ [(E_j^f)_1 \quad (E_j^f)_2 \quad ----- \quad (E_j^f)_s]$$

$$\boldsymbol{F}_j^f = diag\ [(F_j^f)_1 \quad (F_j^f)_2 \quad ----- \quad (F_j^f)_s]$$

As with the SISO case, the degree of $(E_j^f)_i$ is $(j-1)$.

Manipulation of (6.3) and (6.4) yields the prediction equation as:

$$\boldsymbol{\phi}^*(t+j) = \boldsymbol{E}_j^f\,\boldsymbol{B}\,\boldsymbol{\Delta u}^f(t+j-1) + \boldsymbol{F}_j^f\,\boldsymbol{y}^f(t) \tag{6.5}$$

where $\boldsymbol{\Delta u}^f$ and $\boldsymbol{y}^f$ are vectors whose elements are filtered by the tailoring polynomial $T_i(z^{-1})$ for loop 'i'. As with the SISO case, a second identity is required to separate input increment sequences into past filtered and future unfiltered components. This identity is given by:

$$\boldsymbol{E}_j^f\,\boldsymbol{B} = \boldsymbol{T}\,\tilde{\boldsymbol{G}}_j + z^{-j}\,\boldsymbol{G}_j^f \tag{6.6}$$

where $\tilde{\boldsymbol{G}}_j$ and $\boldsymbol{G}_j^f$ are diagonal matrices whose elements are polynomials in z^{-1} and can be calculated recursively [30]. $(\tilde{G}_j)_i$ for loop 'i' is of order $(j-1)$.

Substituting (6.6) into (6.5) leads to:

$$\boldsymbol{\phi}^*(t+j) = \tilde{G}_j\, \Delta\boldsymbol{u}(t+j-1) + G_j^f\, \Delta\boldsymbol{u}^f(t-1) + F_j^f\, \boldsymbol{y}^f(t) \qquad (6.7)$$

The control input increments are thus separated into past filtered and future unfiltered values.

Prediction horizon N_y and control horizon N_u can be incorporated into (6.7) which results in [126]:

$$\boldsymbol{\phi}_m^* = \tilde{G}_m\, \boldsymbol{u}_m + \boldsymbol{S}_m \qquad (6.8)$$

where 'm' stands for the multivariable case. $\boldsymbol{\phi}_m^*$ is a column vector with $(s\ N_y)$ elements as:

$$\boldsymbol{\phi}_m^* = [\phi_1^*(t+1),\ \phi_1^*(t+2),\ ---,\ \phi_1^*(t+N_y),\ \phi_2^*(t+1),$$
$$---,\ \phi_2^*(t+N_y),\ ---,\ \phi_s^*(t+1),\ ---,\ \phi_s^*(t+N_y)]^T$$

$\tilde{G}_m$ is a matrix of dimension $((s\ N_y) \times (r\ N_u))$ and is given as:

$$\tilde{G}_m = \begin{bmatrix} \tilde{G}_{11} & \tilde{G}_{12} & - & - & - & \tilde{G}_{1r} \\ \tilde{G}_{21} & - & - & - & - & \\ - & & & & & \\ - & & & & & \\ \tilde{G}_{s1} & - & - & - & - & \tilde{G}_{sr} \end{bmatrix}$$

where the sub-matrices $\tilde{G}_{11}$, $\tilde{G}_{12}$, $\tilde{G}_{21}$ etc. of the $\tilde{G}_m$ matrix are of dimension $(N_y \times N_u)$ and are of the same form as for the SISO case. $\boldsymbol{u}_m$ is a column vector with $(r\ N_u)$ elements and is given by :

$$\boldsymbol{u}_m = [\Delta u_1(t),\ \Delta u_1(t+1),\ ---,\ \Delta u_1(t+N_u-1),$$
$$\Delta u_2(t),\ ----------,\ \Delta u_2(t+N_u-1),$$
$$---------,\ \Delta u_r(t),\ -----,\ \Delta u_r(t+N_u-1)]^T$$

$\boldsymbol{S}_m$ is a column vector with $(s\ N_y)$ elements and is defined as:

$$\begin{aligned}\boldsymbol{S}_m = [&s_1(t+1),\ s_1(t+2),\ ---,\ s_1(t+N_y),\\ &s_2(t+1),\ ----------,\ s_2(t+N_y),\\ &------,\ s_s(t+1),\ -----,\ s_s(t+N_y)]^T\end{aligned}$$

where the element $s_i(t+j)$ for loop 'i' and the j-step ahead prediction at time t are calculated from (6.7).

The multivariable GPC cost function can be defined as:

$$J_m = E\{(\boldsymbol{\Phi}_m - \boldsymbol{w}_m)^T (\boldsymbol{\Phi}_m - \boldsymbol{w}_m) + \boldsymbol{u}_m^T \boldsymbol{\lambda}\ \boldsymbol{u}_m\} \qquad (6.9)$$

where

$$\boldsymbol{\Phi}_m = \boldsymbol{\Phi}_m^{\bullet} + \boldsymbol{e}_m$$

$\boldsymbol{e}_m$ represents the uncorrelated zero-mean random future noise acting on the MIMO system. $\boldsymbol{w}_m$ is a column vector with $(s\ N_y)$ elements containing future set-points and is defined as:

$$\begin{aligned}\boldsymbol{w}_m = [&w_1(t+1),\ w_1(t+2),\ -----,\ w_1(t+N_y),\ w_2(t+1),\\ &-----,\ w_2(t+N_y),\ -----,\ w_s(t+1),\ ---,\ w_s(t+N_y)]^T\end{aligned}$$

$\boldsymbol{\lambda}$ is a control weighting matrix of the form:

$$\boldsymbol{\lambda} = diag\ [\lambda_1\ ,\ \lambda_2\ ,\ -----\ ,\ \lambda_s]$$

Minimising the GPC cost function of (6.9) yields the MIMO control law as [125]:

$$\boldsymbol{u}_m = (\tilde{\boldsymbol{G}}_m^T\ \tilde{\boldsymbol{G}}_m + \boldsymbol{\lambda})^{-1}\ \tilde{\boldsymbol{G}}_m^T\ (\boldsymbol{w}_m - \boldsymbol{S}_m) \qquad (6.10)$$

6.2 Implementation of the Self-tuning TG Controller

The turbine generator can be considered as a 2-input 2-output system in terms of its primary controls. The two inputs to the system are the excitation demand and power demand, while the two outputs are the terminal voltage and power. In the case of a system with static excitation, the excitation demand signal determines the generator field current by adjusting the firing angle of a thyristor convertor which is fed from the stator terminals through an excitation transformer.

For a rotating exciter system, the field of the exciter is adjusted by the demand signal using a thyristor convertor which is fed from a pilot exciter.

The power demand signal is used to drive the governor and intercept valves. The governor valve controls the steam input to the High Pressure (HP) turbine, while the intercept valve which is located at the inlet of the Intermediate Pressure (IP) turbine regulates the steam flow into the IP and Low Pressure (LP) stages. The power demand signal is used as the governor valve demand directly without any gain or offset adjustment. The intercept valve demand however requires gain and offset adjustment such that the valve is kept fully open above 25% of power demand and is progressively closed from 25% to -25% of power demand in a linear fashion with the valve completely closed at -25%.

There are several quantities that can be considered as outputs of the multivariable TG plant. Electrical power, terminal voltage, reactive volt-ampere, rotor angle, mechanical power, rotor speed and valve position are some of them. The approach taken here is to follow as much as possible the philosophy employed in the existing single-variable controllers currently being used in the TG plant. The AVR uses terminal voltage as its primary feedback signal, hence it is chosen as one of the outputs of the multivariable plant. The EHG has the rotor speed as its main feedback signal, but from practical experience it is found that this signal remains almost constant except during significant disturbances which can cause problems to the parameter estimator of a self-tuning controller. Since the turbine is a sub-system of the TG plant, its output ie. mechanical power can be considered as one of the outputs of the multivariable system. Unfortunately mechanical power is not a directly measurable plant quantity although it can be derived from such signals as the mean power demand or the steam pressure at the inlet of the HP turbine [11,13]. Hence the governor valve position which is a closely related plant quantity to mechanical power is chosen as the second output of the multivariable system. Valve position is also a feedback signal to the standard EHG system, hence its availability is not a problem.

The choice of the governor valve demand for use in the self-tuning TG controller requires an additional quantity such as the rotor angle or speed to be

used to improve transient stability. Since rotor speed is currently being used in the EHG, it has been chosen as the supplementary signal to the valve position in the TG controller. The valve position feedback signal (A_p) is then modified as $(A_p + G_s \omega')$ where ω' is the speed deviation, ie. (actual speed - nominal speed) and G_s is a weighting factor. Since the supplementary feedback is required only during transient conditions, the weighting factor G_s is taken as zero for speed deviations of less than 0.002 pu and is typically 100 for larger speed deviations. As with the self-tuning AVR, electrical power is used as the supplementary feedback to the terminal voltage signal.

The multivariable TG controller is designed to have a 2 x 2 configuration to suit the plant model chosen. The hardware used is the same as that for the self-tuning AVR. The software has been designed in such a way that configurations other than MIMO, such as self-tuning AVR with self-tuning EHG, self-tuning AVR with fixed EHG etc. can be specified through the operator interface. As far as possible, the same software modules are executed twice, one for each sub-system of the MIMO controller during each sampling period with data corresponding to each loop. The control signals of the multivariable TG controller are then calculated using a software module which combines the intermediate results obtained, into a form suitable for the MIMO control law given by (6.10). Thus the main difference between the Data Flow Diagram for the self-tuning AVR (Fig. 3.10) and that for the multivariable TG controller is the inclusion of this software module.

The choice of the prediction and control horizons are most important from a computational point of view in MIMO GPC since the size of the matrices to be manipulated increase proportionately. For the TG controller, a prediction horizon of 10 and control horizon of up to 2 samples are permitted in the software. A sampling period of 20 msec has been chosen for the self-tuning TG controller which is found to be sufficient for the existing hardware to execute the algorithm without any timing problems.

6.3 Incorporation of Constraints in the Multivariable TG Controller

The multivariable control law derived in section 6.1 assumes complete freedom of movement for its control inputs. But in practice, this is seldom the case and restrictions on control inputs are usually imposed. These can be in the form of amplitude limiting and / or rate limiting. If these constraints are not taken into account during the derivation of the control law, the solution obtained may not be optimum [91]. In the case of a multivariable controller, another undesirable effect of these restrictions is that a complete decoupling of the control loops, ie. total elimination of loop interactions, may not be possible with the standard control law. Another situation where only a partial decoupling of the loops is obtained is when the control weighting matrix λ is used to restrict the liveliness of the self-tuning controller.

Techniques to incorporate practical constraints in the self-tuning controller based on GPC are available [126,90,91]. The approach taken is to minimise the GPC cost function subject to the required constraints thus deriving a 'constrained' generalised predictive control law. However, the procedure of minimising a quadratic cost function subject to constraints is computationally intense and is unsuitable for high speed applications such as electromechanical systems [91]. Hence simple techniques which are suitable for incorporation in the TG controller have to be formulated.

The main problems encountered when applying constraints with an unconstrained control law are the resulting non-optimum solution and the partial decoupling of loops. But if the control horizon N_u is chosen to be unity, the constrained minimum of the cost function is provided merely by the unconstrained control clipped by the limits [91]. Hence, the possibility of a non-optimum solution does not arise in the multivariable TG controller as long as N_u is set to 1. If N_u has to be set to its present maximum value of 2, a non-optimum solution can result. This can still be prevented to a great extent by suitably choosing the control weighting matrix such that a higher weight is given to $\Delta u(t+1)$ than to $\Delta u(t)$. This approach will reduce the chance of $\Delta u(t+1)$ exceeding the limits when $\Delta u(t)$ is still within limits. If $\Delta u(t)$ exceeds the limits for $N_u = 2$, the constrained minimum of the

cost function is still obtained by applying the clipped control signal, whether $\Delta u(t+1)$ is within limits or not. Thus it can be seen that the problem of a non-optimum solution when using an unconstrained control law in the TG controller can be satisfactorily tackled. It should however be emphasised that the arguments given above may not be strictly valid for plants which have unstable or poorly damped poles and for controllers with prediction horizons close to their control horizons. Since the TG system does not fall in these categories, the arguments hold good.

The other problem, viz. the partial decoupling of control loops in the multivariable TG controller when using an unconstrained control law can be successfully tackled by compensating for the constraints external to the control law. A simple method of compensation which does not depend upon the choice of N_u is proposed here for the multivariable TG controller and is explained below.

For a multivariable control system, each control input to the plant can be considered to have 2 components, one to control the plant output which it is directly responsible for, and the other to minimise the effect of interactions from other control loops. Thus for a 2 x 2 system,

$$\Delta u_1 = \Delta u_{11} + \Delta u_{12} \tag{6.11}$$

$$\Delta u_2 = \Delta u_{22} + \Delta u_{21} \tag{6.12}$$

where

Δu_1 is the total change in control input 1,

Δu_2 is the total change in control input 2,

Δu_{11} is the change in component responsible for regulating y_1 to its set point w_1,

Δu_{12} is the change in component which nullifies the effect of change in u_2 on y_1,

Δu_{22} is the change in component responsible for regulating y_2 to its set point w_2,

and

Δu_{21} is the change in component which nullifies the effect of change in u_1 on y_2.

In the multivariable GPC, the following identities can then be given to nullify the loop interactions:

$$\Sigma G_{21}\ \Delta u_1 + \Sigma G_{22}\ \Delta u_{21} = 0 \tag{6.13}$$

$$\Sigma G_{12}\ \Delta u_2 + \Sigma G_{11}\ \Delta u_{12} = 0 \tag{6.14}$$

where ΣG_{11}, ΣG_{12}, ΣG_{21} and ΣG_{22} are obtained by summing the first column of the respective sub-matrices which form part of the $\tilde{G}_m$ matrix defined in section 6.1. It may be noted that, in GPC, the N_y elements of the $\tilde{G}$ matrix correspond to the first N_y points on the plant's unit step response curve [30]. Thus, in (6.13), $\Sigma G_{21}\ \Delta u_1$ represents the effect of Δu_1 on y_2, while $\Sigma G_{22}\ \Delta u_{21}$ cancels this interaction. Similarly, in (6.14), $\Sigma G_{12}\ \Delta u_2$ gives the effect of interaction of Δu_2 on y_1 and $\Sigma G_{11}\ \Delta u_{12}$ nullifies it. Indeed, instead of summing the first column of the $\tilde{G}$ matrix a particular element of it can also be used, but the summing approach can help to reduce the effect of estimation errors in the adaptive case.

6.3.1 Compensation for Amplitude Limiting in the TG Controller

Compensation for amplitude limiting in the multivariable TG controller can be achieved by using (6.13) and (6.14) as follows:
For a 2 x 2 control system, if u_1 is outside its limits, the 'overshoot' (OS_1) of the signal is given by:

$$OS_1 = u_1^r - u_1^l \tag{6.15}$$

where u_1^r , and u_1^l are the raw and limited control signals respectively. The effect of changing Δu_1^r from its original value by an amount equal to OS_1 on Δu_{21} can then be calculated using (6.13). This can be used to compute the compensated u_2 (u_2^c) as:

$$u_2^c = u_2^r + OS_1\ \frac{\Sigma G_{21}}{\Sigma G_{22}} \tag{6.16}$$

If u_2 is outside its limits, u_1 can be compensated in a similar manner using (6.14) as:

$$u_1^c = u_1^r + OS_2 \frac{\Sigma G_{12}}{\Sigma G_{11}} \tag{6.17}$$

If both u_1 and u_2 are outside their limits, the deviation of the predicted outputs from their respective future set points can be checked to decide whether compensation should be applied or not. The deviation can be obtained from the $\boldsymbol{S}_m$ vector defined in section 6.1 in a 'sum of squares' form as:

$$(\Sigma e^2)_1 = (\boldsymbol{S}_m[1])^2 + (\boldsymbol{S}_m[2])^2 + --- + (\boldsymbol{S}_m[N_y])^2 \tag{6.18}$$

$$(\Sigma e^2)_2 = (\boldsymbol{S}_m[N_y+1])^2 + (\boldsymbol{S}_m[N_y+2])^2 + --- + (\boldsymbol{S}_m[N_y+N_y])^2 \tag{6.19}$$

where $(\Sigma e^2)_1$ and $(\Sigma e^2)_2$ are the sum of square of the deviations for loops 1 and 2 respectively. The strategy adopted in the TG controller is to discard the compensation scheme if both the sums are greater than a pre-defined threshold. Otherwise, the control signal corresponding to the loop with the greater 'sum' is clipped and the other control input is compensated.

In theory, the scheme proposed here to compensate for amplitude limiting can also be extended to multivariable systems which are larger than 2 x 2. A significant number of simultaneous equations may then have to be solved to obtain the solution. For example, in a 3 x 3 system, if one of the control signals is amplitude limited, 4 simultaneous equations will have to be solved to achieve complete compensation. Moreover, conflicting constraint violations can also occur which can lead to further complications in arriving at the solution. For a 2 x 2 multivariable system such as the TG controller, these problems do not arise.

The proposed compensation scheme has been verified using a simulated multivariable plant. Following are the coefficients of the A and B polynomials of the 2 x 2 plant used for simulation.

$$A_1 = 1 - 0.59z^{-1} - 0.38z^{-2} \; ; \; A_2 = 1 - 0.58z^{-1} - 0.38z^{-2}$$

$$B_{11} = 0.004z^{-1} + 0.002z^{-2} \; ; \; B_{12} = 0.001z^{-1} + 0.0005z^{-2}$$

$$B_{22} = 0.0025z^{-1} + 0.0015z^{-2} \; ; \; B_{21} = 0.0008z^{-1} + 0.0004z^{-2}$$

A multivariable controller based on GPC with $N_y = 10$, $N_u = 1$, and $\lambda = 0$ was used. Figure 6.2 shows the response of the closed-loop system to a square wave set-point when the amplitude limiting of control inputs was not used. It can be observed that set point changes in one loop does not affect the other loop at all, indicating complete decoupling. The simulation was repeated with amplitude limiting of control inputs. The limits of u_1 and u_2 were set to +/- 2.5 pu and +/- 2.0 pu respectively. The resulting performance as shown in Fig. 6.3 indicates that a complete removal of loop interactions is not achieved in this case which confirms the need for compensation. The response of the multivariable controller with compensation for amplitude limiting as proposed above is given in Fig. 6.4 which indicates that a successful decoupling of the loops is achieved.

6.3.2 Compensation for Rate Limiting in the TG Controller

Rate limiting of the control input prevents the signal from varying freely by imposing a limit on its rate of change, ie. magnitude of increment. Compensation is required in this case also, since rate limiting is equivalent to amplitude limiting with varying amplitude limits. The approach taken is to convert the rate limiting problem to an equivalent amplitude limiting requirement and proceed to calculate the compensation required. Thus for a 2 x 2 system, if Δu_1 has exceeded the maximum rate *(RL) specified*, OS_1 *is calculated* either as $(\Delta u_1' - RL)$ if $\Delta u_1'$ is positive, or as $(\Delta u_1' + RL)$ if $\Delta u_1'$ is negative. The compensated value of u_2 is then calculated by (6.16).

The operation of the compensation scheme for rate limiting also has been verified by simulation studies. Fig. 6.5 gives the response of the closed-loop system when the rate limits for u_1 and u_2 were set to 0.05 and 0.03 pu respectively. It can be seen that the loop interactions are only partially decoupled in this case. Fig. 6.6 which shows the performance of the MIMO controller with rate limit compensation incorporated confirms that loop interactions are nullified with the proposed scheme.

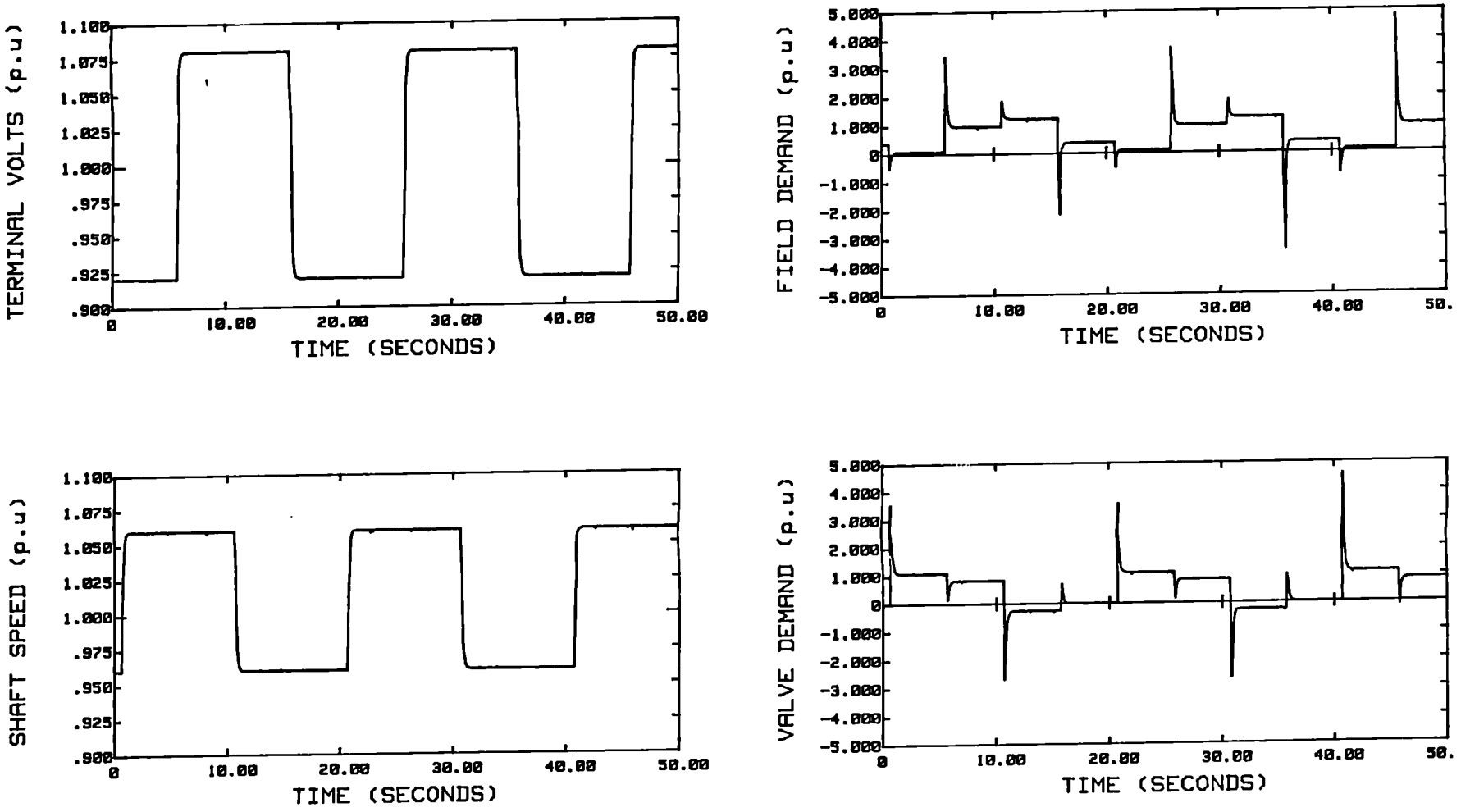

Fig. 6.2 Response to square wave set-points of a 2 x 2 MIMO plant without control input amplitude limiting when using a multivariable GP controller.

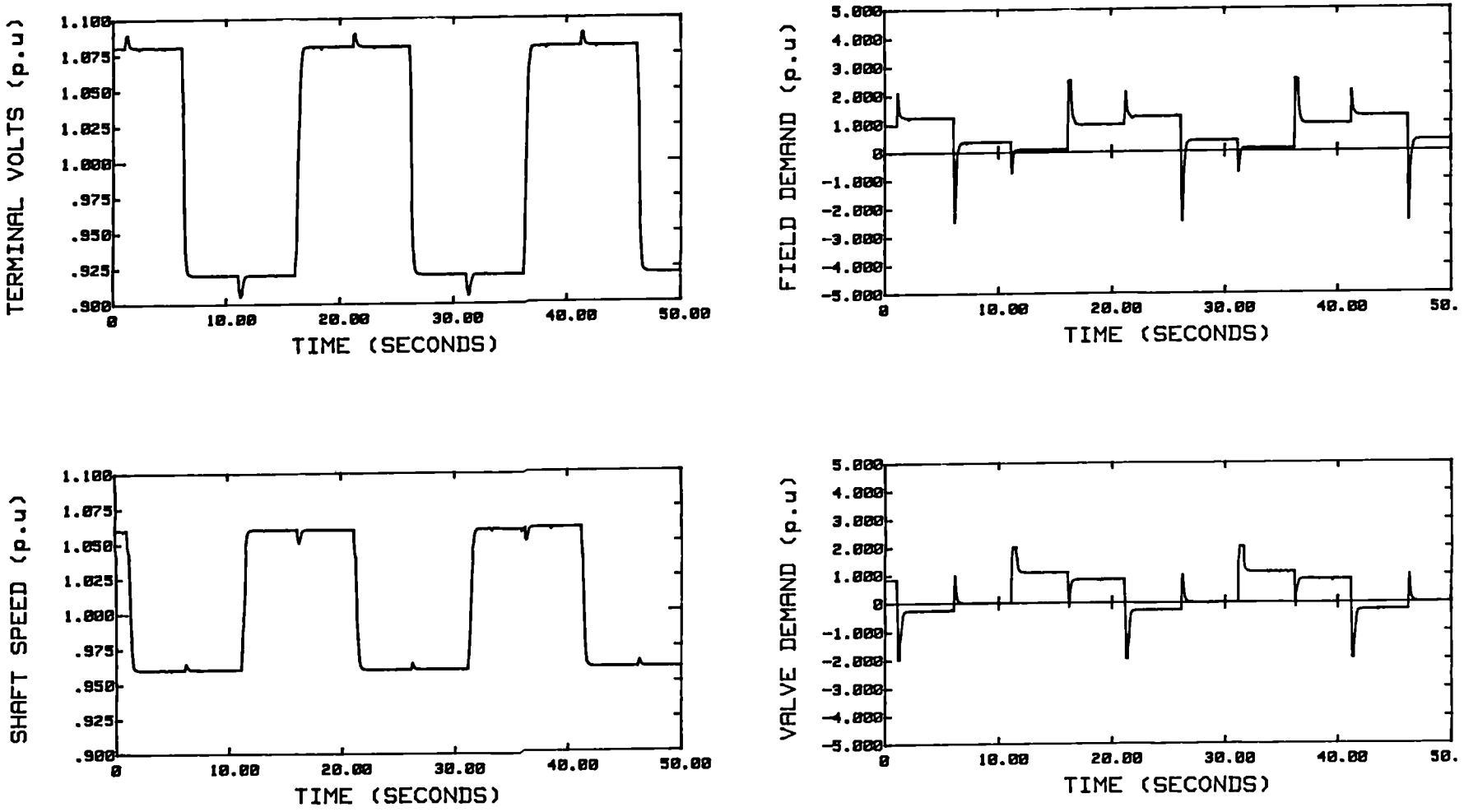

Fig. 6.3 Response to square wave set-points of a 2 x 2 MIMO plant with control input amplitude limiting when using a multivariable GP controller without limit compensation.

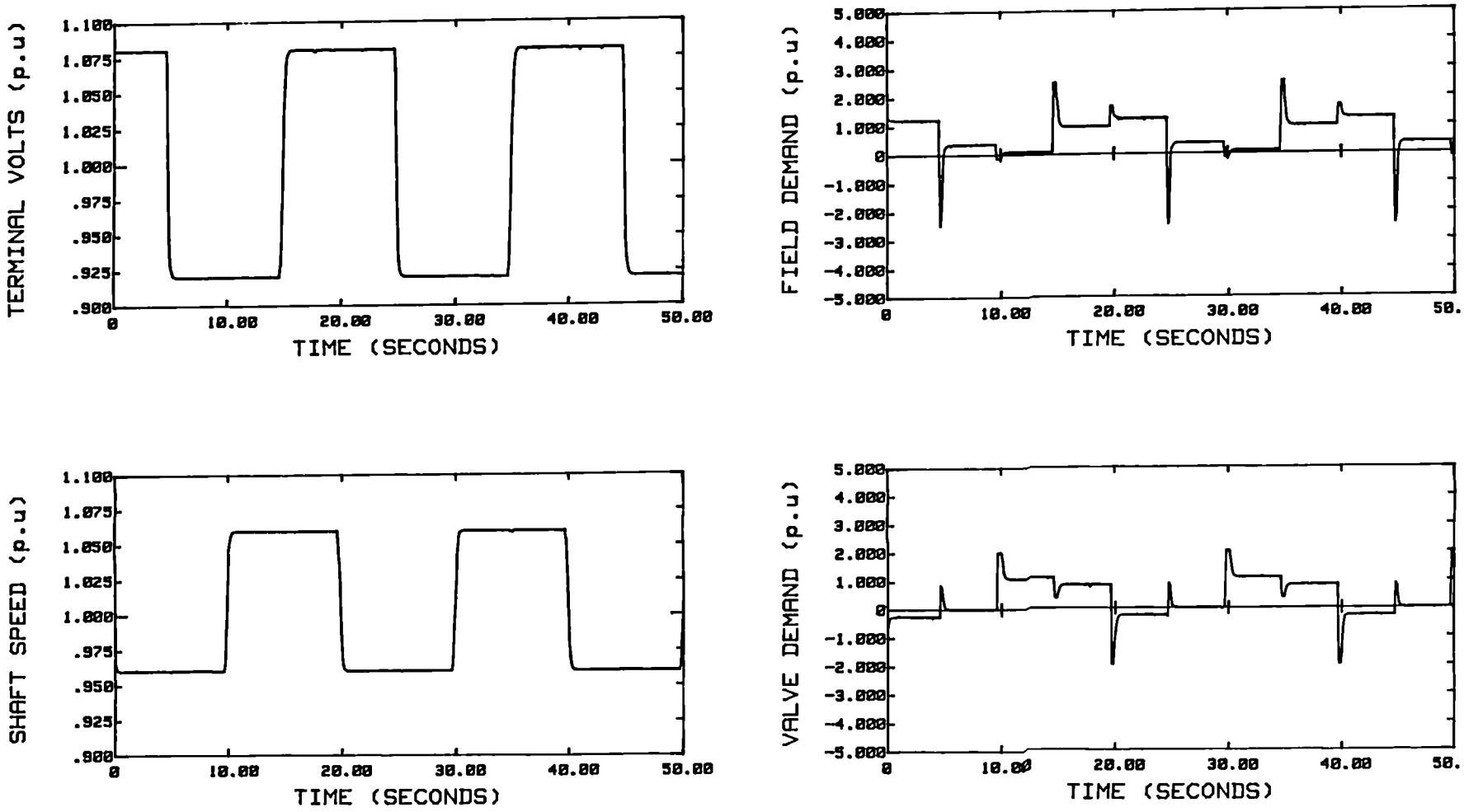

Fig. 6.4 Response to square wave set-points of a 2 x 2 MIMO plant with control input amplitude limiting when using a multivariable GP controller with limit compensation.

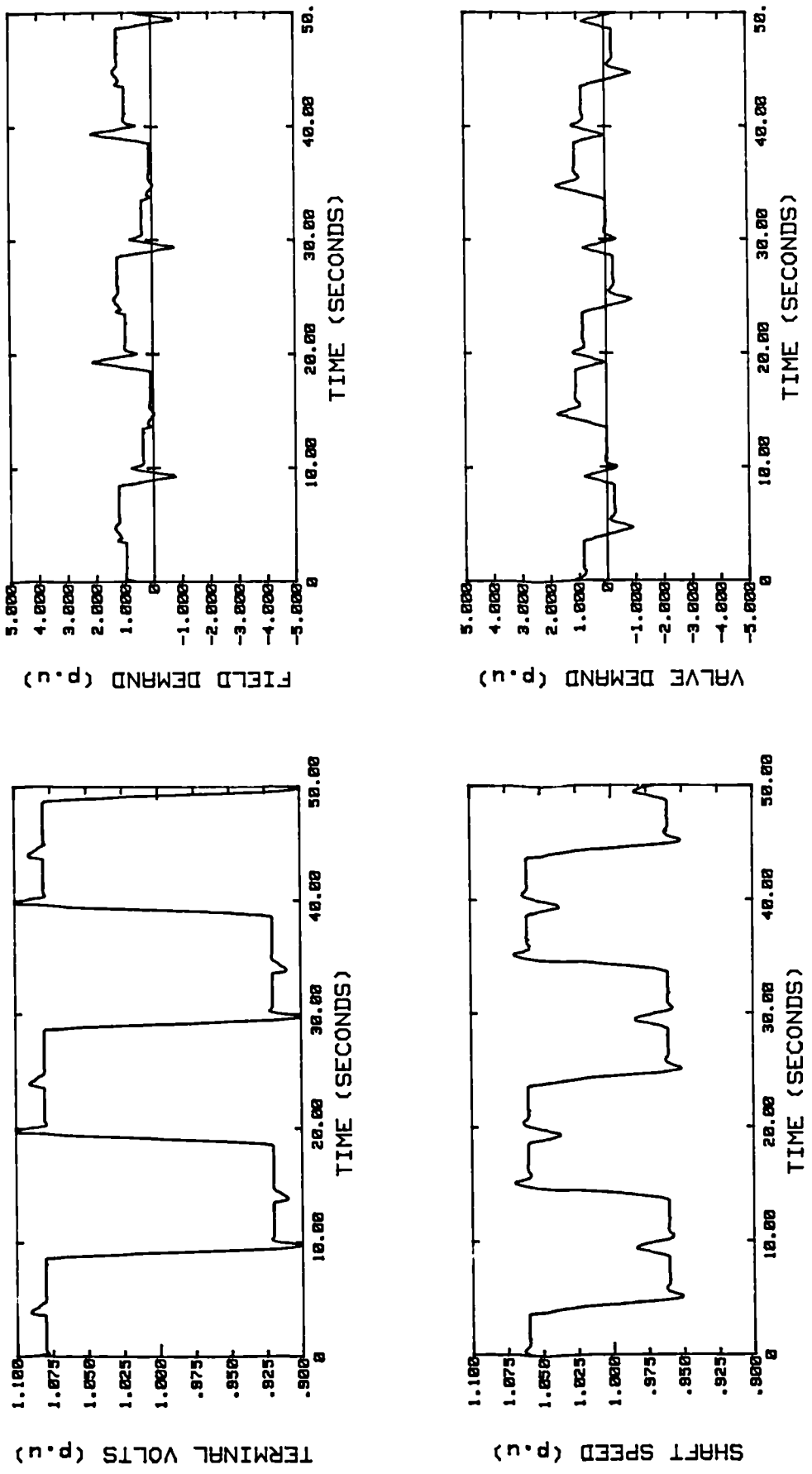

Fig. 6.5 Response of a 2 x 2 MIMO plant with control input rate limiting when using a multivariable GP controller.

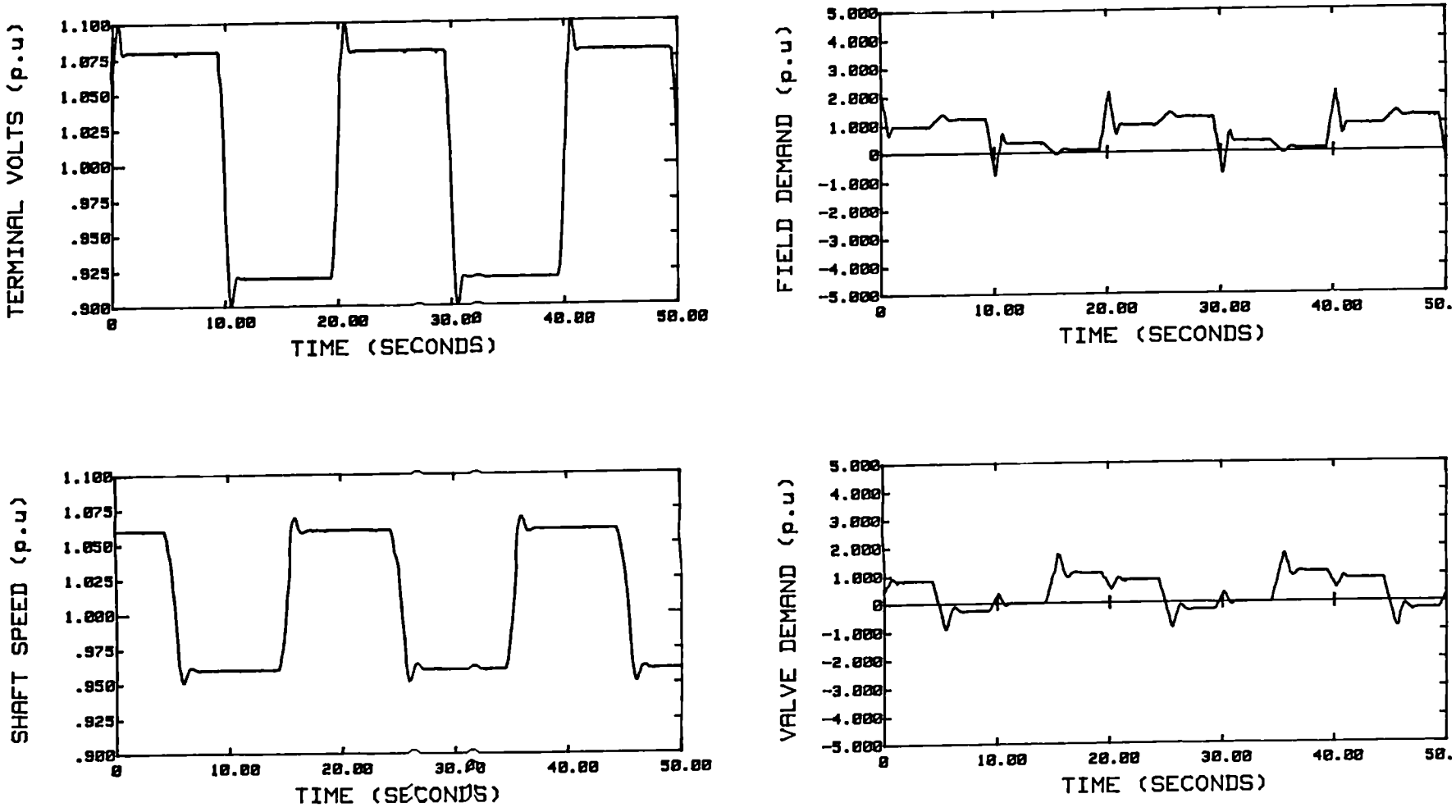

Fig. 6.6 Response of a 2 x 2 MIMO plant with control input rate limiting when using a multivariable GP controller with compensation for rate limiting.

6.3.3 Compensation for 'Control Weighting' λ in the TG Controller

Control weighting in GPC is effectively a constraint to the control input. In multivariable controllers based on GPC, the use of control weighting also can lead to a partial decoupling of the loop interactions. This phenomenon is due to the fact that the application of control weighting affects both components of each of the control inputs as defined by (6.11) and (6.12), ie. Δu_{11} and Δu_{12} for loop 1, and Δu_{22} and Δu_{21} for loop 2. Since Δu_{12} and Δu_{21} are responsible for decoupling, any restriction to their movement can cause the loop interactions to be only partially rejected. This undesirable effect of control weighting can be minimised by applying λ only to the components that are responsible for regulating the plant outputs.

The scheme proposed for use in the TG controller to compensate for control weighting is as follows:

For a 2 x 2 system such as the TG controller, Δu_{11} and Δu_{22} are calculated independently using their corresponding control weighting factors as:

$$\Delta u_{11} = (\tilde{G}_{11}^T \tilde{G}_{11} + \lambda_{11} I)^{-1} \tilde{G}_{11}^T (w_1 - s_1) \tag{6.20}$$

$$\Delta u_{22} = (\tilde{G}_{22}^T \tilde{G}_{22} + \lambda_{22} I)^{-1} \tilde{G}_{22}^T (w_2 - s_2) \tag{6.21}$$

Eqns. (6.20) and (6.21) are very similar to the SISO GPC law except that the prediction vector s_i uses control increments of other loops also, ie. MIMO prediction. Having calculated Δu_{11} and Δu_{22}, the decoupling components viz. Δu_{12} and Δu_{21} are computed by solving the following simultaneous equations which are obtained by combining (6.11) and (6.12) with (6.13) and (6.14) respectively, and rearranging:

$$\Sigma G_{21} \Delta u_{12} + \Sigma G_{22} \Delta u_{21} = -\Sigma G_{21} \Delta u_{11} \tag{6.22}$$

$$\Sigma G_{11} \Delta u_{12} + \Sigma G_{12} \Delta u_{21} = -\Sigma G_{12} \Delta u_{22} \tag{6.23}$$

The control inputs Δu_1 and Δu_2 which are compensated for control weighting are then calculated using (6.11) and (6.12).

The main advantage of the proposed scheme is that it is computationally simple. For example, a 2 x 2 system with $N_u = 2$ would require a 4 x 4 matrix to be inverted using the original MIMO method, while the proposed scheme would need only two 2 x 2 matrices to be inverted which is simpler. However, the

number of simultaneous equations to be solved for *a (n x n)* system is *n(n-1)* which can give a significant computational load when 'n' is large. Also, the proposed technique in its present form cannot be applied to cases where the number of inputs of the MIMO plant is greater than the number of outputs. Since the TG plant is only a 2 x 2 system, these disadvantages do not apply and hence the proposed technique is well suited for this application.

The operation of the compensation scheme for control weighting has been successfully verified using the 2 x 2 simulated plant given in section 6.3.1. Fig. 6.7 shows the response of the closed-loop system when control weighting is used. Here, $\lambda_{11} = 0.025$ and $\lambda_{22} = 0.04$ with $N_u = 1$. It may be noted that no limit constraints are imposed on the control inputs in this example. Fig. 6.7 clearly illustrates the need for control weight compensation through the partial decoupling achieved. The simulation was repeated with the proposed compensation scheme incorporated in the algorithm and the performance obtained is given in Fig. 6.8. It can be observed that a complete decoupling of the loops is achieved with the proposed compensation method. The simulation was then repeated after incorporating the amplitude limit constraints also, but with no compensation for this limit. The resulting response shown in Fig. 6.9 indicates that interactions are not completely eliminated. This is because compensation for every constraint imposed should be applied for a total removal of loop interactions. Fig. 6.10 gives the performance of the closed-loop system when compensation for amplitude limiting was also incorporated in the multivariable control algorithm. It can be observed that the loops are now completely decoupled which prove that the compensation schemes work together without any conflict. The simulation was then repeated with $N_u = 2$ and the result is shown in Fig. 6.11 which confirms that the compensation schemes used in the TG controller are satisfactory for $N_u = 2$ also.

6.4 Evaluation of the Self-tuning TG Controller

The multivariable self-tuning TG controller has been evaluated using the state space TG simulator as well as the micro-alternator system. The primary aim of this evaluation was to prove that a MIMO self-tuning TG controller can provide

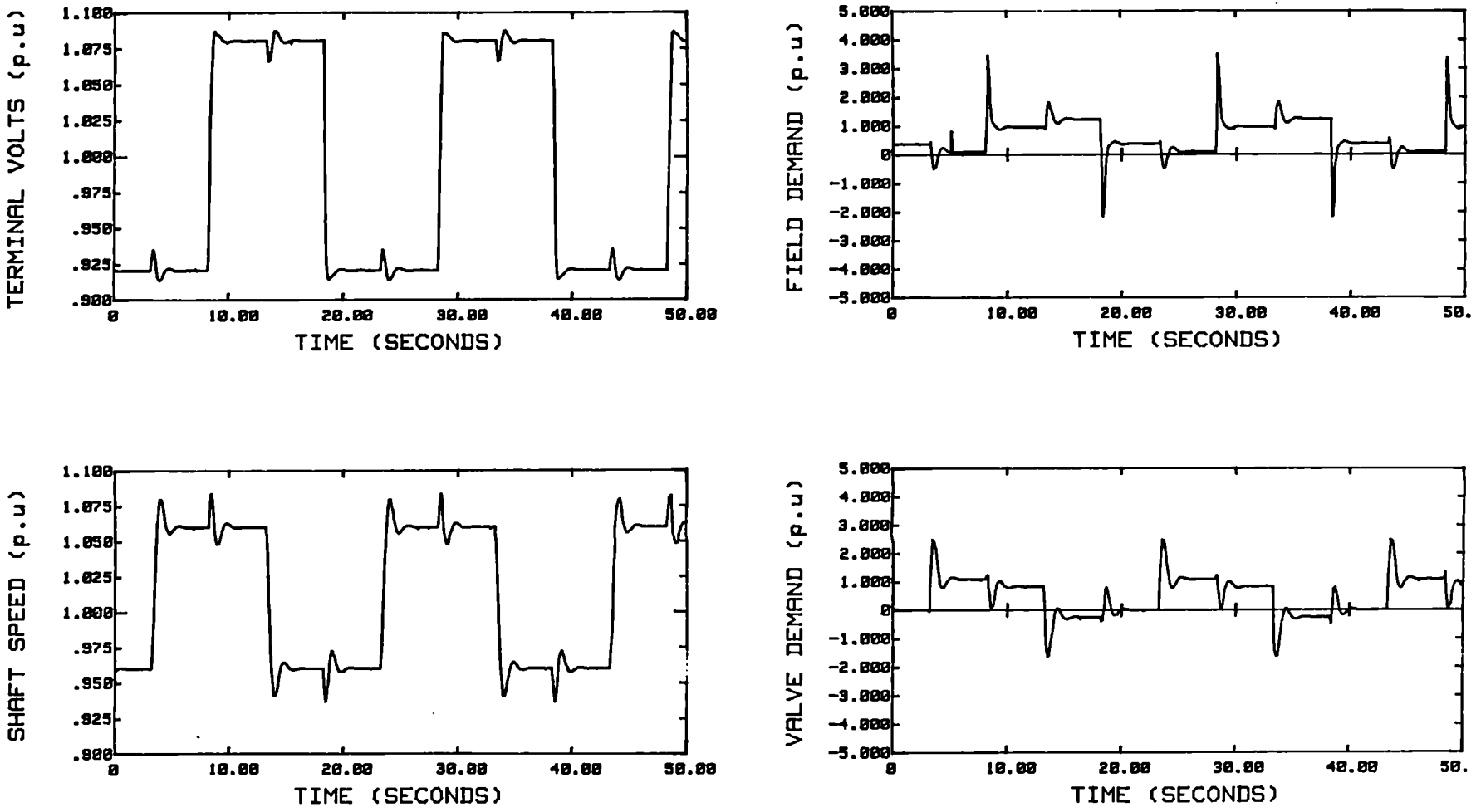

Fig. 6.7 Response to square wave set-points of a 2 x 2 MIMO plant without control input amplitude limiting when using a multivariable GP controller with control weighting factor.

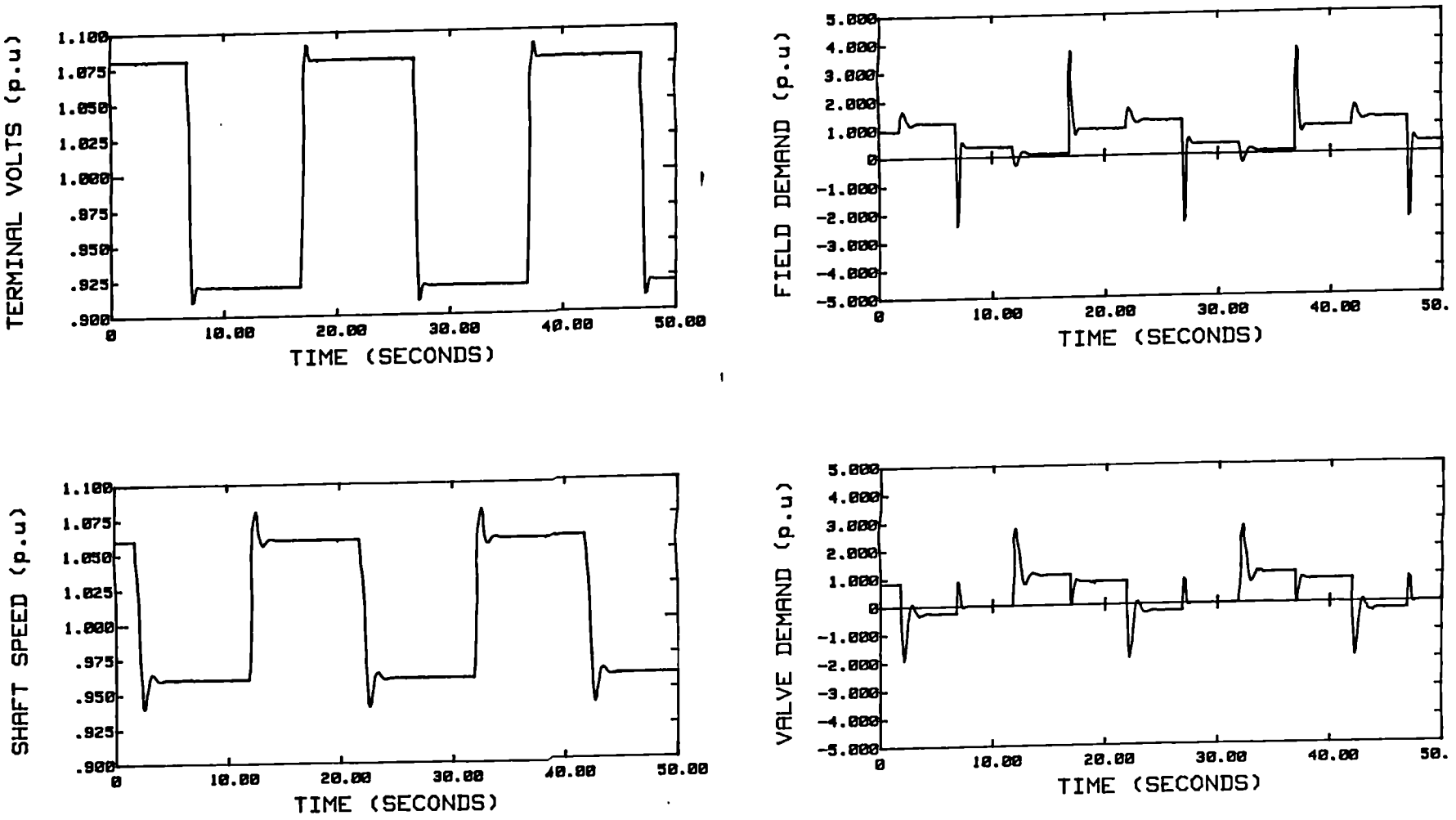

Fig. 6.8 Response to square wave set-points of a 2 x 2 MIMO plant without control input amplitude limiting when using a multivariable GP controller with compensation for control weighting.

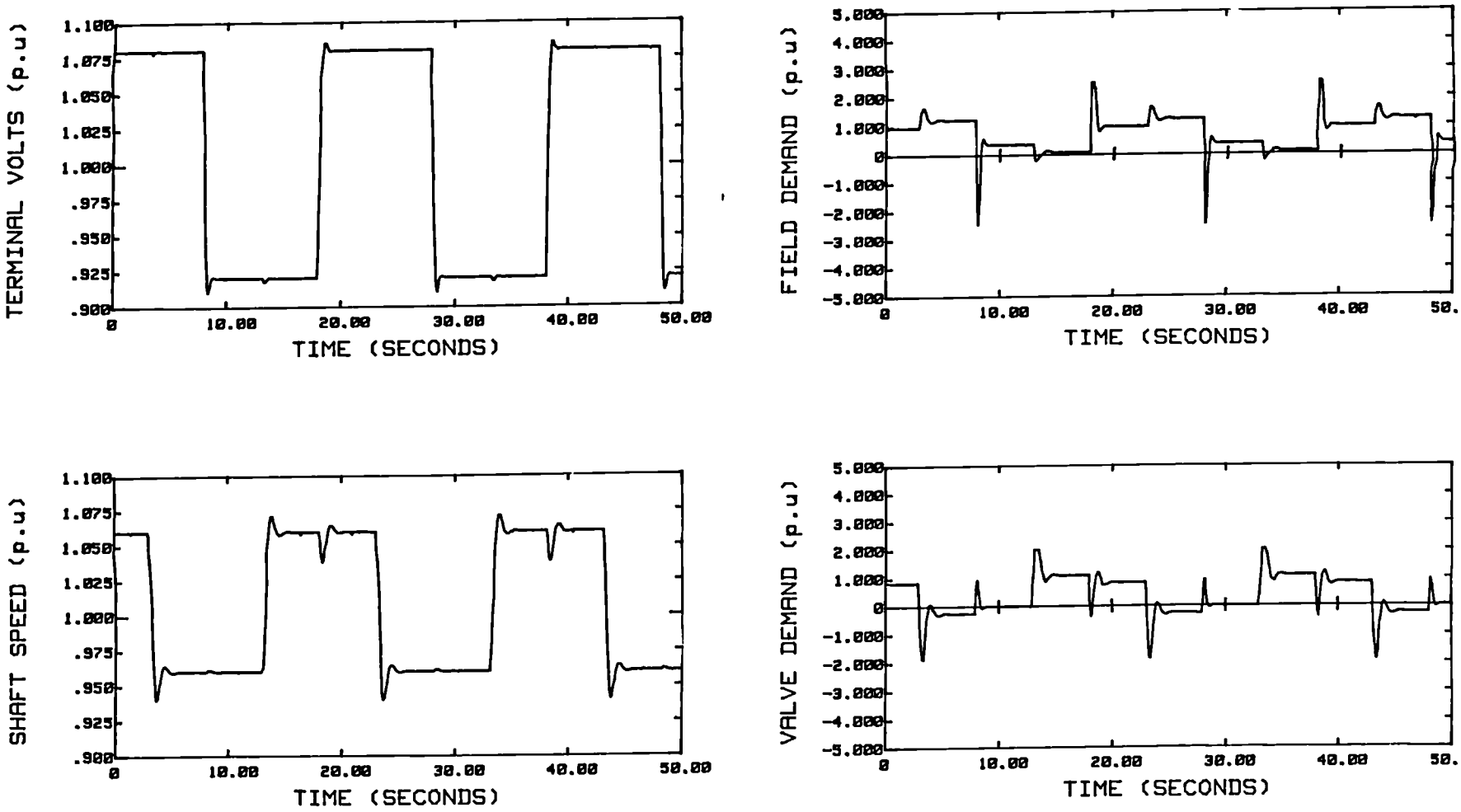

Fig. 6.9 Response to square wave set-points of a 2 x 2 MIMO plant with control input amplitude limiting when using a multivariable GP controller with compensation for control weighting.

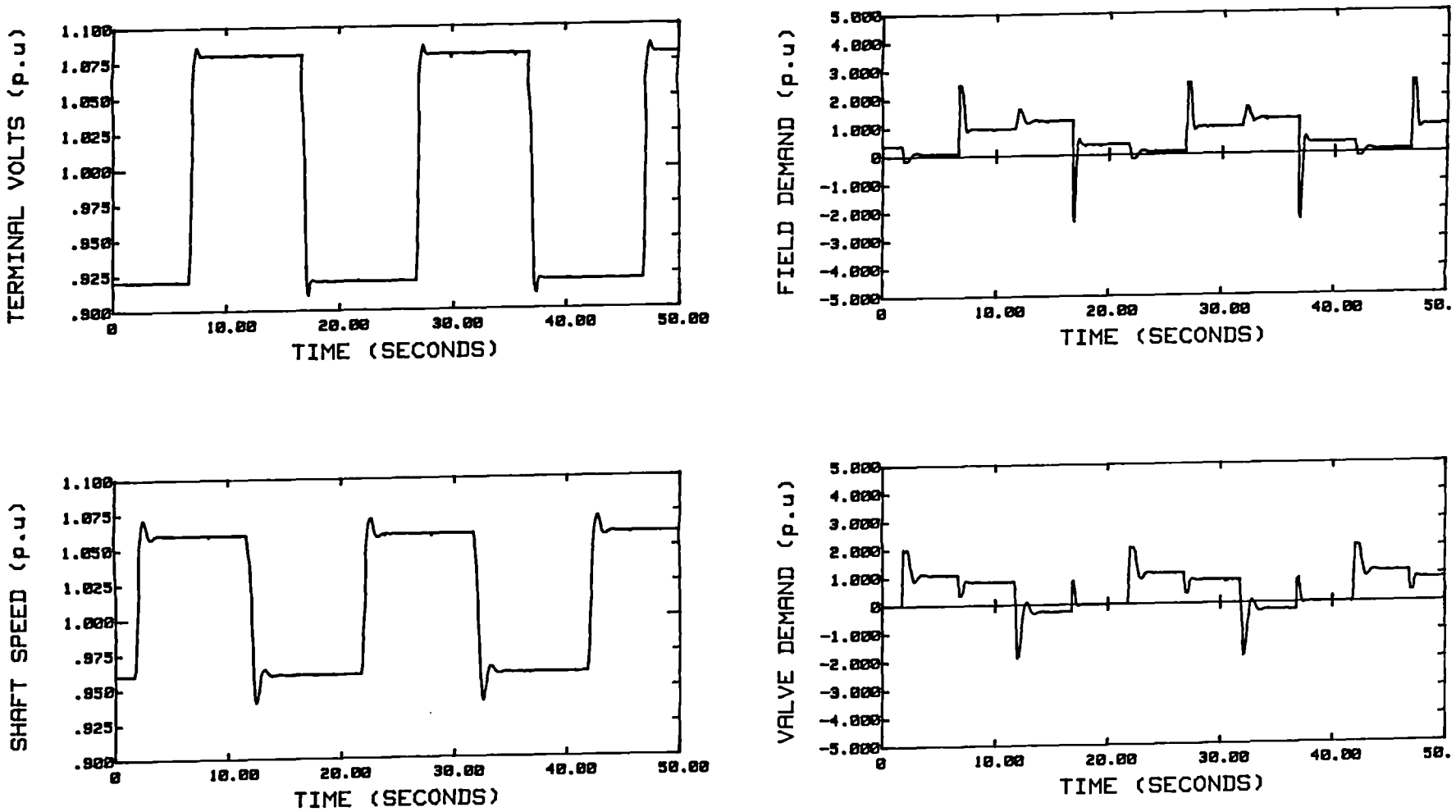

Fig. 6.10 Response to square wave set-points of a 2 x 2 MIMO plant with control input amplitude limiting when using a multivariable GP controller with compensation for amplitude limit and control weighting. (N_u = 1).

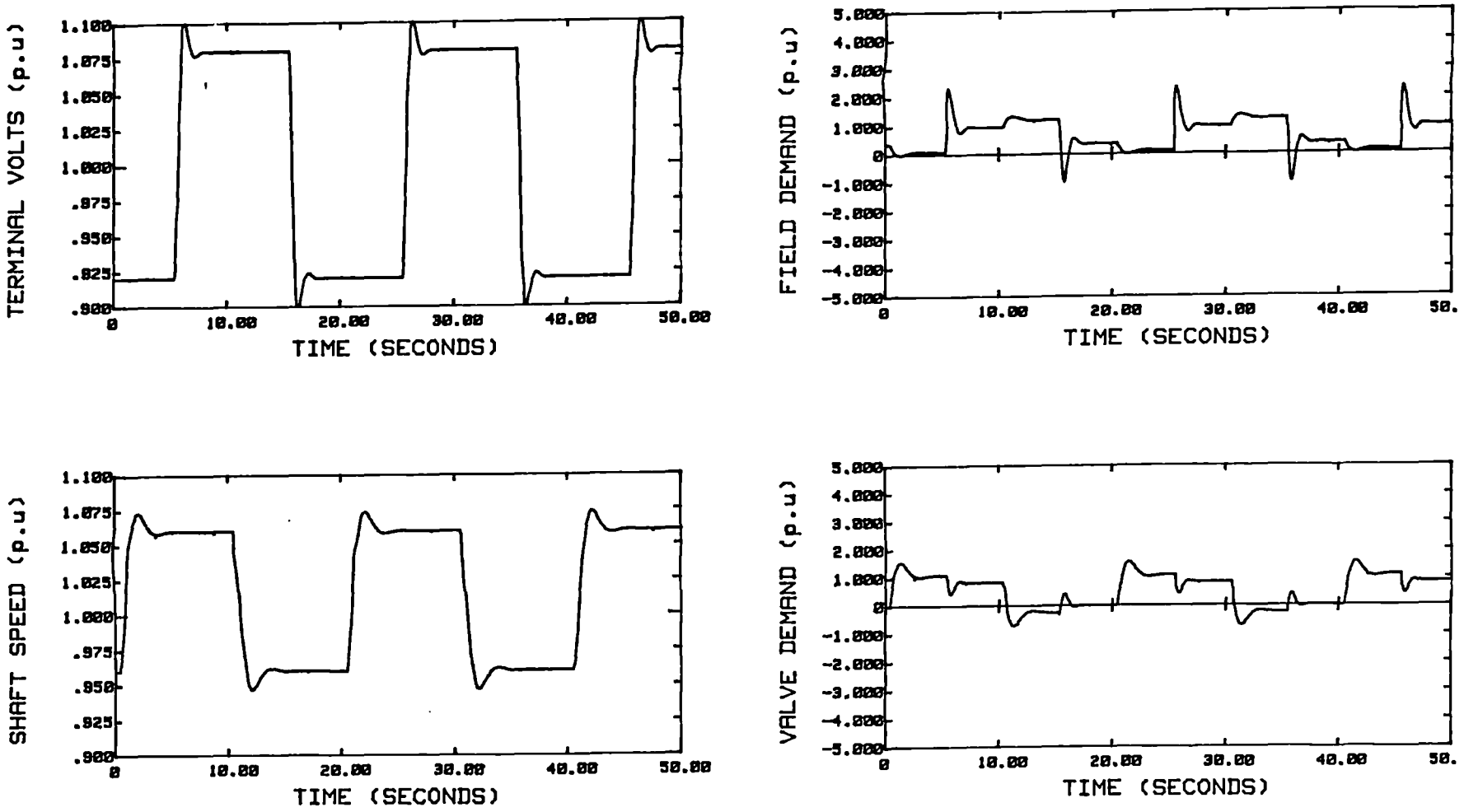

Fig. 6.11 Response of a 2 x 2 MIMO plant when using a multivariable GP controller with compensation for amplitude limiting and control weighting ($N_u = 2$).

a further improvement in performance to a self-tuning AVR. Since the objective was to show that the MIMO TG controller is a potential candidate for further enhancement in the overall control performance, the full range of tests which were done using the self-tuning AVR were not repeated with the TG controller. Instead, only the 3-phase short-circuit test which illustrates the transient performance of the turbine generator was used for comparison purposes. This is justified by the fact that stability improvement is one of the most important requirements of TG control during on-load operation, hence a system which can give a significant improvement in transient stability is worth investigating further. The following sub-sections briefly describe the observations made during the short-circuit test on the TG simulator and the micro-alternator system.

6.4.1 Short-circuit Test using the TG Simulator

A sudden 3-phase short-circuit was applied to the stator terminals of the generator of the TG simulator and was cleared after 100 msec. The operating point of the generator was chosen as $P = 0.8\,pu;\ Q = 0.1\,pu$ lead. Various controllers were used for the test and the results obtained are shown in Fig. 6.12 to 6.16. The Effective Damping Ratio (EDR) as defined in Chapter 4 has been used to compare the performance improvement achieved with the various controllers. The EDR of the load angle as well as the settling times of terminal voltage and load angle are tabulated in Table 6.1 for comparison purposes. It should be noted that the simulation was run 10 times slower than 'real' time, hence the X-axis of the graphs need correction by a factor of 10 to arrive at the real time.

To illustrate a progressive improvement pattern, the short-circuit test was first of all performed with the AVR and EHG in the 'manual' mode of operation, ie. constant excitation and steam valve demands. The response obtained is given by Fig. 6.12. It can be seen that a reasonable response can be obtained even without any control action as long as the disturbance is not too severe and the operating point is such that there is sufficient stability margin. Fig. 6.13 gives the response of the closed loop system during the short-circuit test when 'fixed parameter' AVR and EHG were used. The 'fixed' digital AVR is of type DGAVR-SO

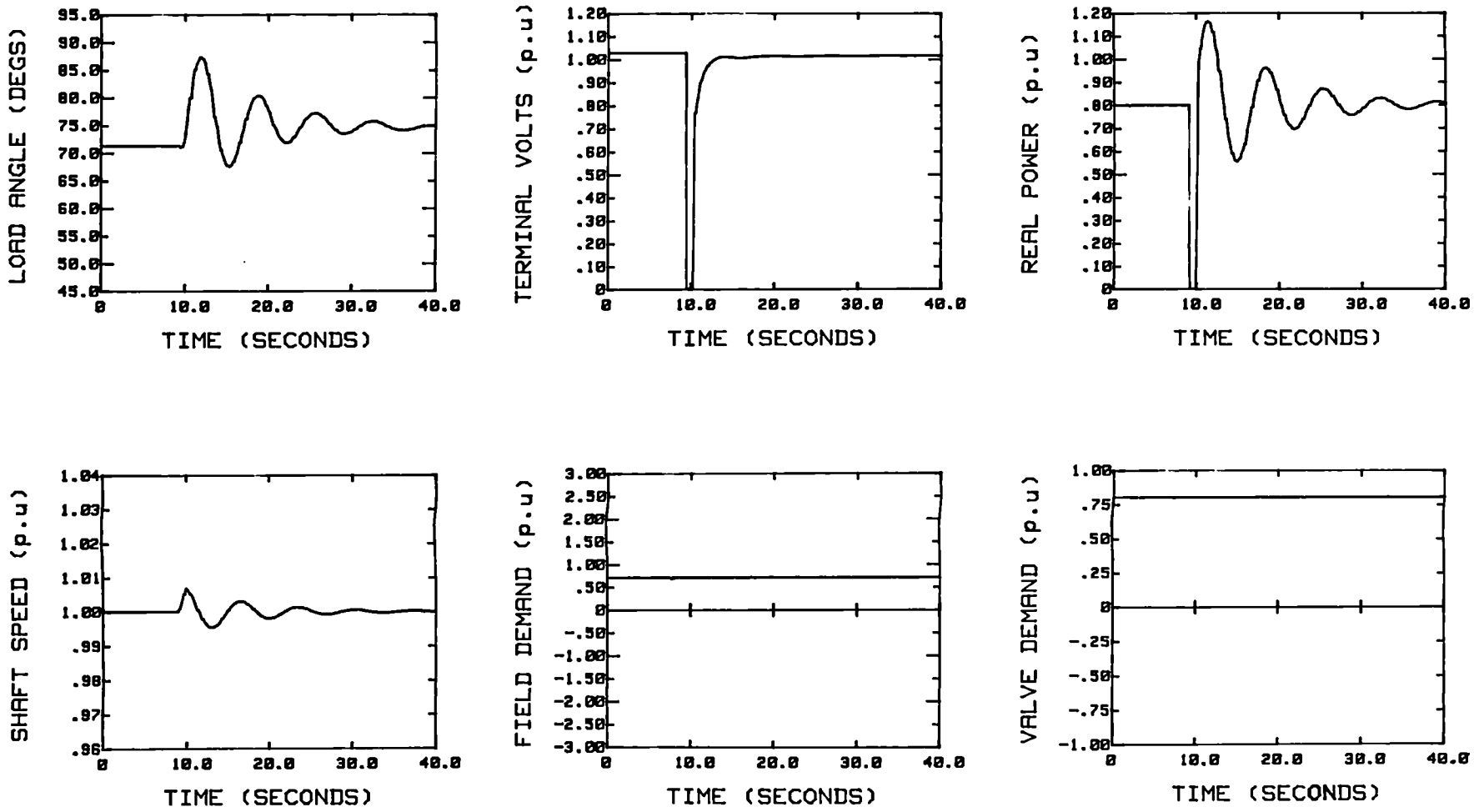

Fig. 6.12 Response of the TG simulator to a 3-phase short circuit when the AVR and EHG loops are in the manual mode.

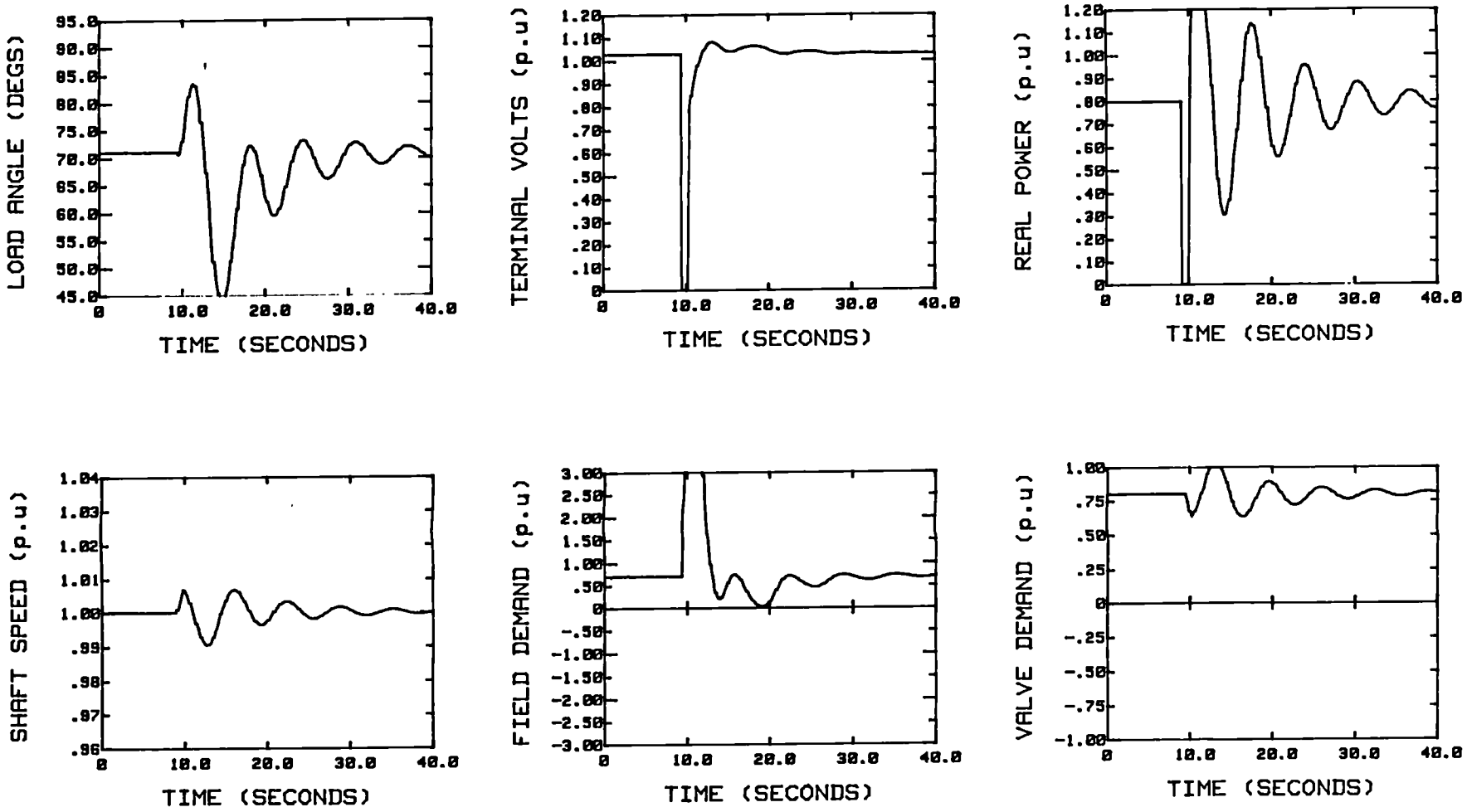

Fig. 6.13 Response of the TG simulator to a 3-phase short circuit when the AVR and EHG are in the fixed parameter mode.

Type of Controller	EDR δ	Settling time δ (sec)	Settling time V_t (sec)
Manual control	0.67	3.0	0.38
Fixed AVR & Fixed EHG	0.68	3.0	1.13
STAVR & Fixed EHG	0.30	1.92	0.60
STAVR & STEHG	0.10	1.20	0.68
ST-TG (MIMO)	Negligible	1.26	0.78

Table 6.1 Comparison of performance of various controllers during a 3-phase short-circuit using the TG simulator.

and the 'fixed' EHG has a droop setting of 4%. It can be observed that the performance has not improved as far as the load angle is concerned, but the rise time of the terminal voltage has improved considerably. This is due to the design criterion used for the digital AVR which concentrates on the step response characteristic of the terminal voltage and ignores other quantities such as the load angle. It should also be noted that the 'fixed' digital AVR parameters were arrived at by tuning the controller with the micro-alternator system, hence they can be different to some extent for the TG simulator. Hence a re-tuning of the AVR with the TG simulator can give a better performance than that shown in Fig. 6.13.

The response of the closed-loop system when a self-tuning AVR and a 'fixed' EHG were used is given in Fig. 6.14. The self-tuning AVR is of type STAVR-SO and the EHG has a droop setting of 4%. It is seen that the response of the load angle both in terms of its EDR and settling time has improved significantly from 0.68 to 0.30 and 3.0 sec. to 1.92 sec. respectively. The response of terminal voltage is also found to be well-behaved. The improvement achieved when using a self-tuning EHG together with a self-tuning AVR is illustrated in Fig. 6.15. A simple self-tuning EHG (STEHG) with $P_n = 1 - 0.9\,z^{-1}$, $N_y = 10$, $N_u = 1$, and $\lambda = 0$ has been used in this case. It can be observed that

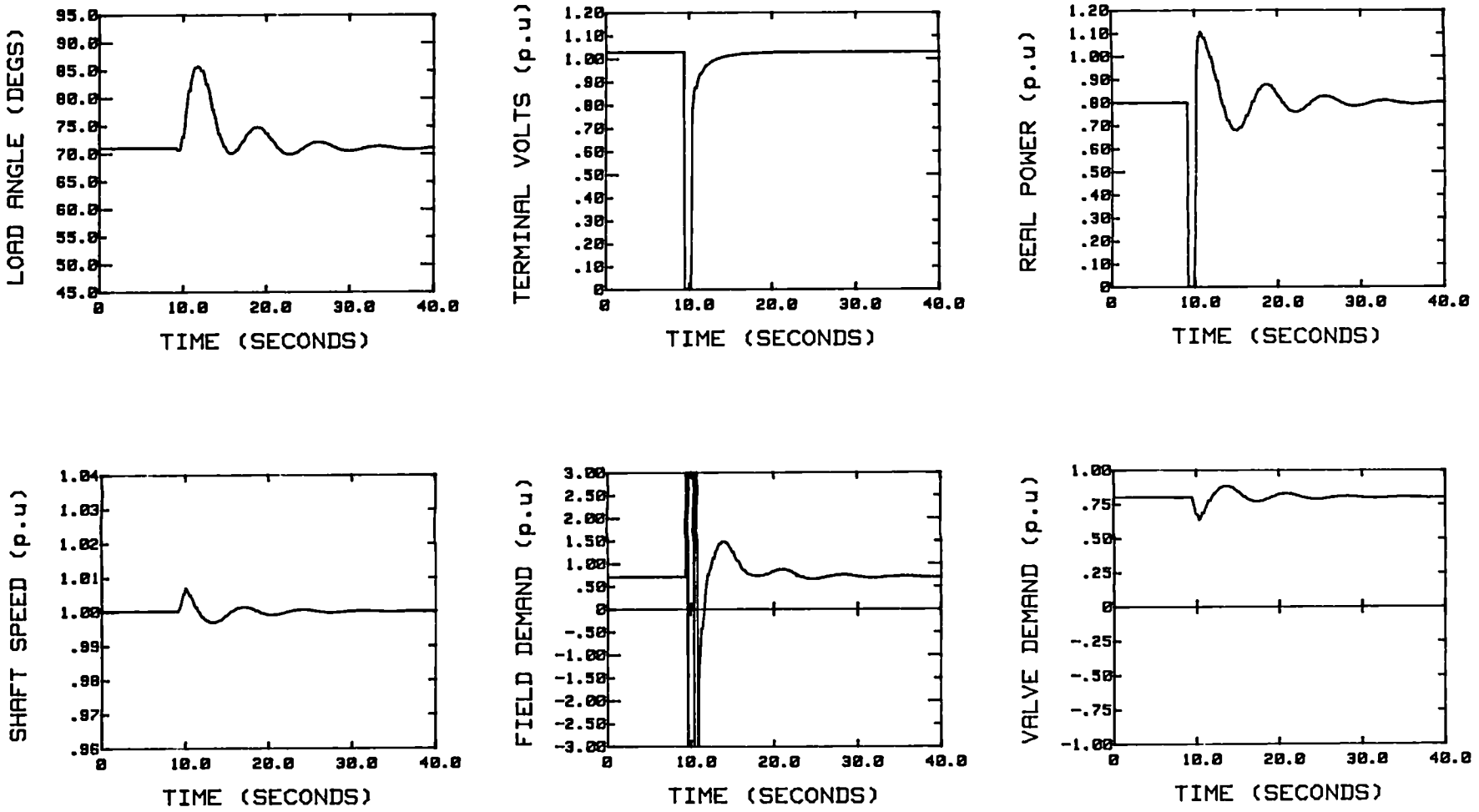

Fig. 6.14 Response of the TG simulator to a 3-phase short circuit when the AVR is in the self-tuning mode and the EHG in the fixed-parameter mode.

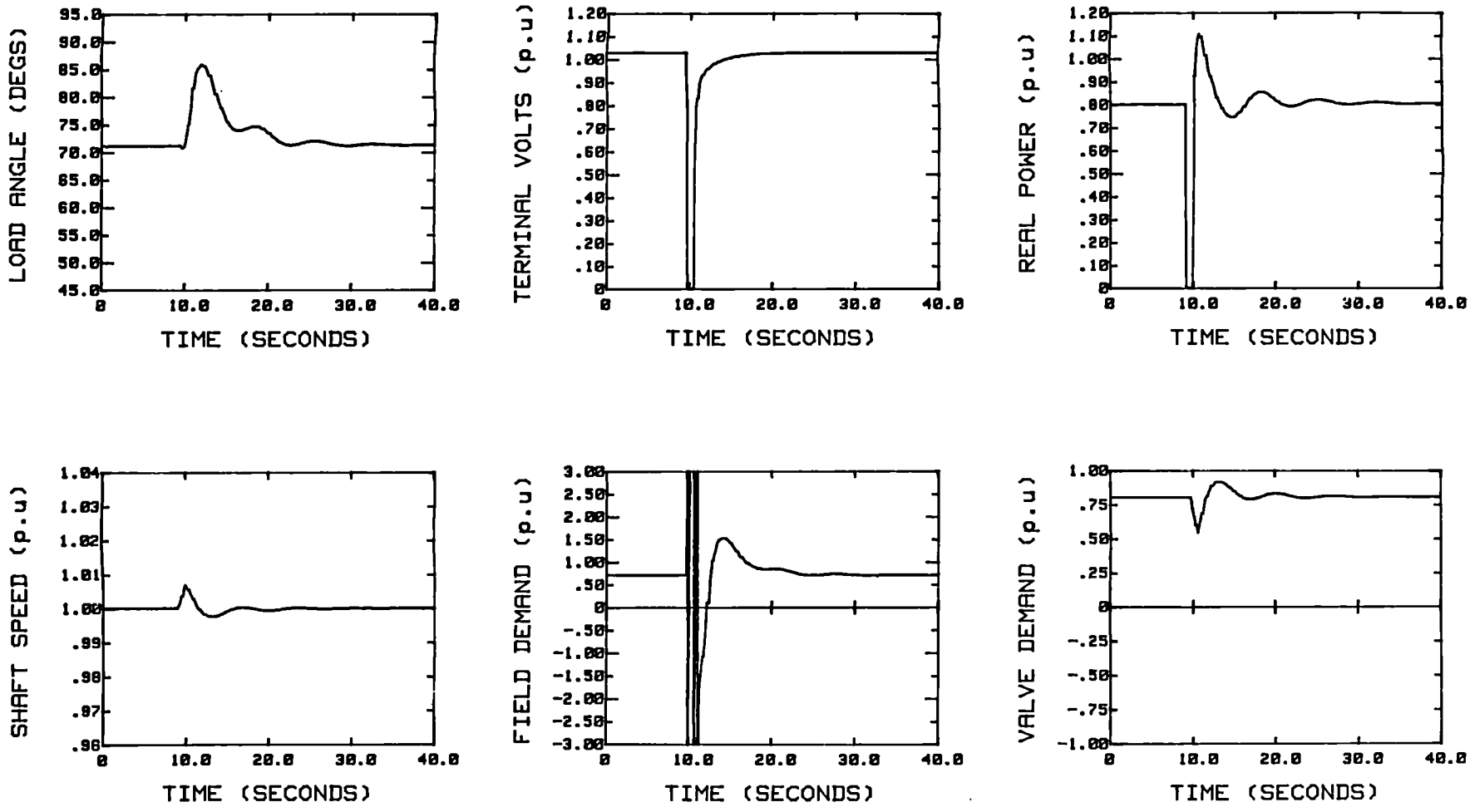

Fig. 6.15 Response of the TG simulator to a 3-phase short circuit when the AVR and EHG are in the SISO self-tuning mode.

the EDR and settling time of the load angle have been reduced to 0.1 and 1.2 sec. respectively. Once again, the terminal voltage is found to recover after the fault satisfactorily.

Fig. 6.16 shows the performance of the MIMO self-tuning TG controller during the short-circuit test using the TG simulator. Controller settings similar to the ones used for the STAVR and STEHG combination were used in this case also for comparison purposes. Third order plant models were estimated for both the loops of the MIMO controller with the B polynomials having three coefficients each to estimate. Thus 18 parameters were estimated in the TG controller. The compensation schemes for input constraints described in section 6.3 were incorporated in the software and a sampling period of 20 msec. was used. The weighting factor G_s for the rotor speed deviation has been set to 25. It can be observed from the figure that the response of the load angle has improved slightly in terms of its EDR when compared with the multi-loop self-tuning control scheme of the earlier run. This proves that a considerable improvement in performance can be achieved by upgrading a self-tuning AVR to a multivariable self-tuning TG controller. The results also indicate that the improvement is mainly due to making the speed governing part of TG control self-tuning.

6.4.2 Short-circuit Test using the Micro-alternator System

The 3-phase short-circuit test with the various controllers was conducted on the micro-alternator system. The short-circuit was applied at the sending end of the transmission line simulator and was cleared after 100 msec. The operating point of the machine was set to $P = 0.7\ pu$ and $Q = 0.1\ pu$ lead. The Time Constant Regulator (TCR) of the machine was set to 6.0 sec. which is representative of a full-size machine. The results obtained with the various controllers are shown in Fig. 6.17 to 6.21. The performance of the various controllers are evaluated by measuring the EDR and settling time of signals such as the load angle, terminal power and voltage during the test. These are tabulated for comparison purposes in Table 6.2.

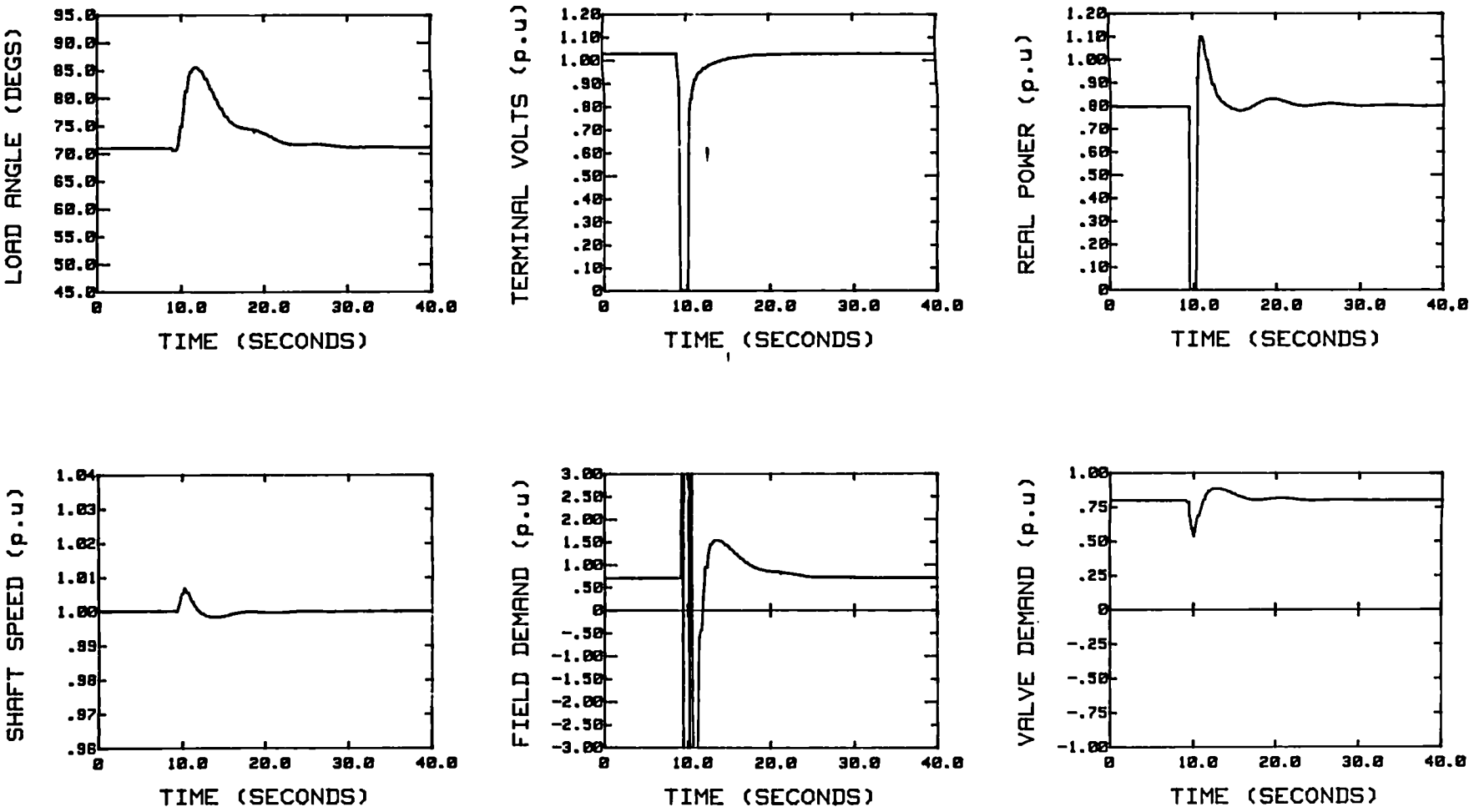

Fig. 6.16 Response of the TG simulator to a 3-phase short circuit when the AVR and EHG loops are combined into a MIMO self-tuning TG controller.

Type of Controller	EDR δ	Settling time δ (sec)	EDR P	Settling time P (sec)	Settling time V_t (sec)
Manual Control	0.75	5.00	0.80	> 5.0	4.20
Fixed AVR & Fixed EHG	0.48	2.95	0.65	5.0	2.55
STAVR & Fixed EHG	0.40	1.90	0.58	2.8	1.75
STAVR & STEHG	0.35	1.32	0.42	2.0	1.25
ST - TG (MIMO)	0.16	1.38	0.34	1.9	1.20

Table 6.2 Comparison of performance of various controllers during a 3-phase short-circuit using the micro-alternator system.

As with the TG simulator, the short-circuit test on the micro-alternator was repeated for a collection of controllers ranging from 'manual' to multivariable self-tuning control to confirm a progressive pattern of improvement that can be achieved. Fig. 6.17 illustrates the response of load angle, power and terminal voltage to the short-circuit when the AVR and EHG are in the 'manual' mode of operation. This test helps to establish a 'datum' level of controller performance and is useful to evaluate the extent of improvement that is possible with the various control strategies. It can be observed that the load angle and power are poorly damped in this case as indicated by the rather high EDR's of 0.75 and 0.80 respectively. The settling times of the various signals as given in Table 6.2 are also found to be large.

The response of the closed-loop system when the 'fixed parameter' digital AVR and EHG are used is shown in Fig. 6.18. The AVR is of type DGAVR-SO and the EHG is a proportional controller with a droop setting of 4%. It can be seen that the EDR of the load angle has reduced to 0.48 and that for the power to 0.65

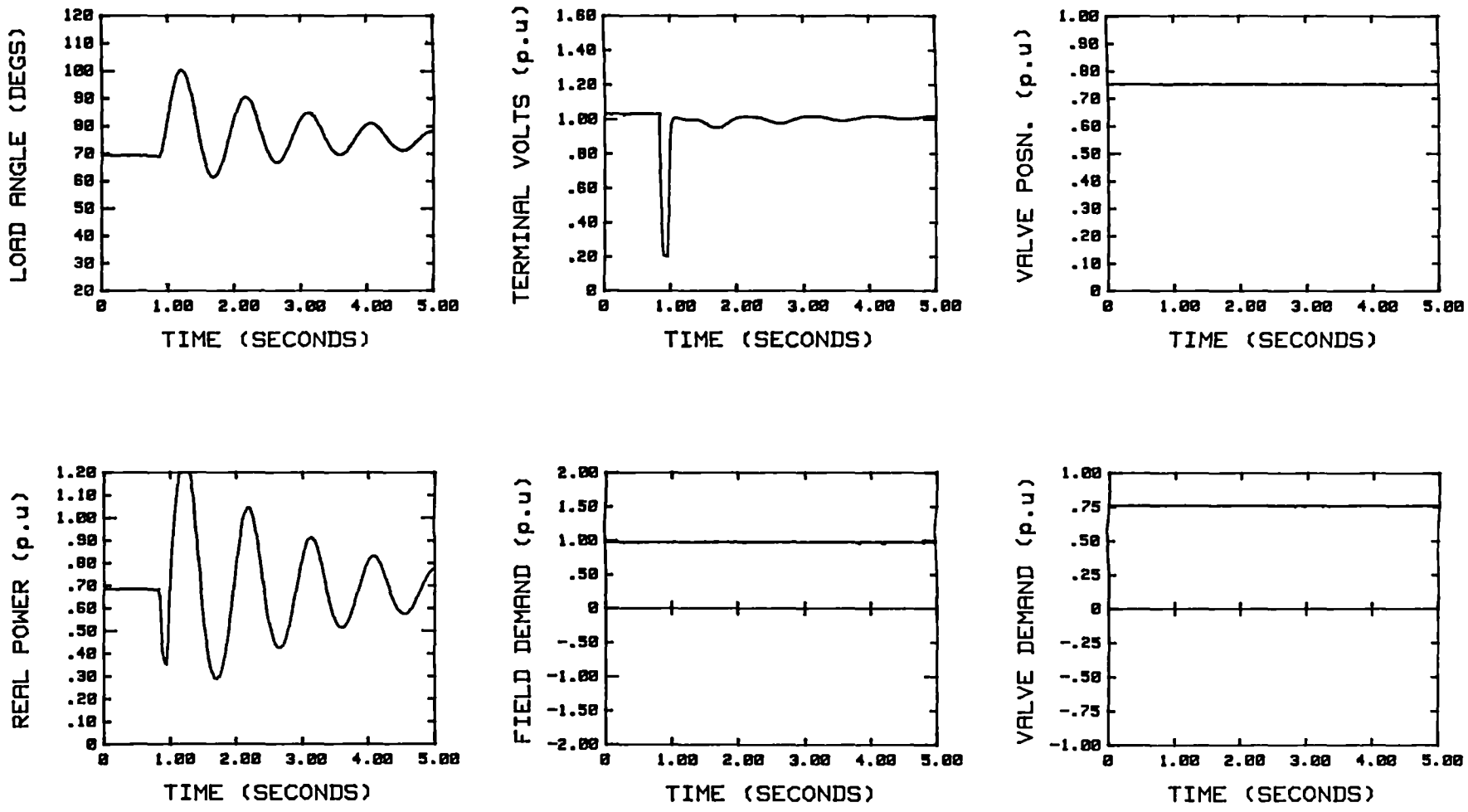

Fig. 6.17 Response of the micro-alternator to a 3-phase short circuit when the AVR and EHG loops are in the manual mode.

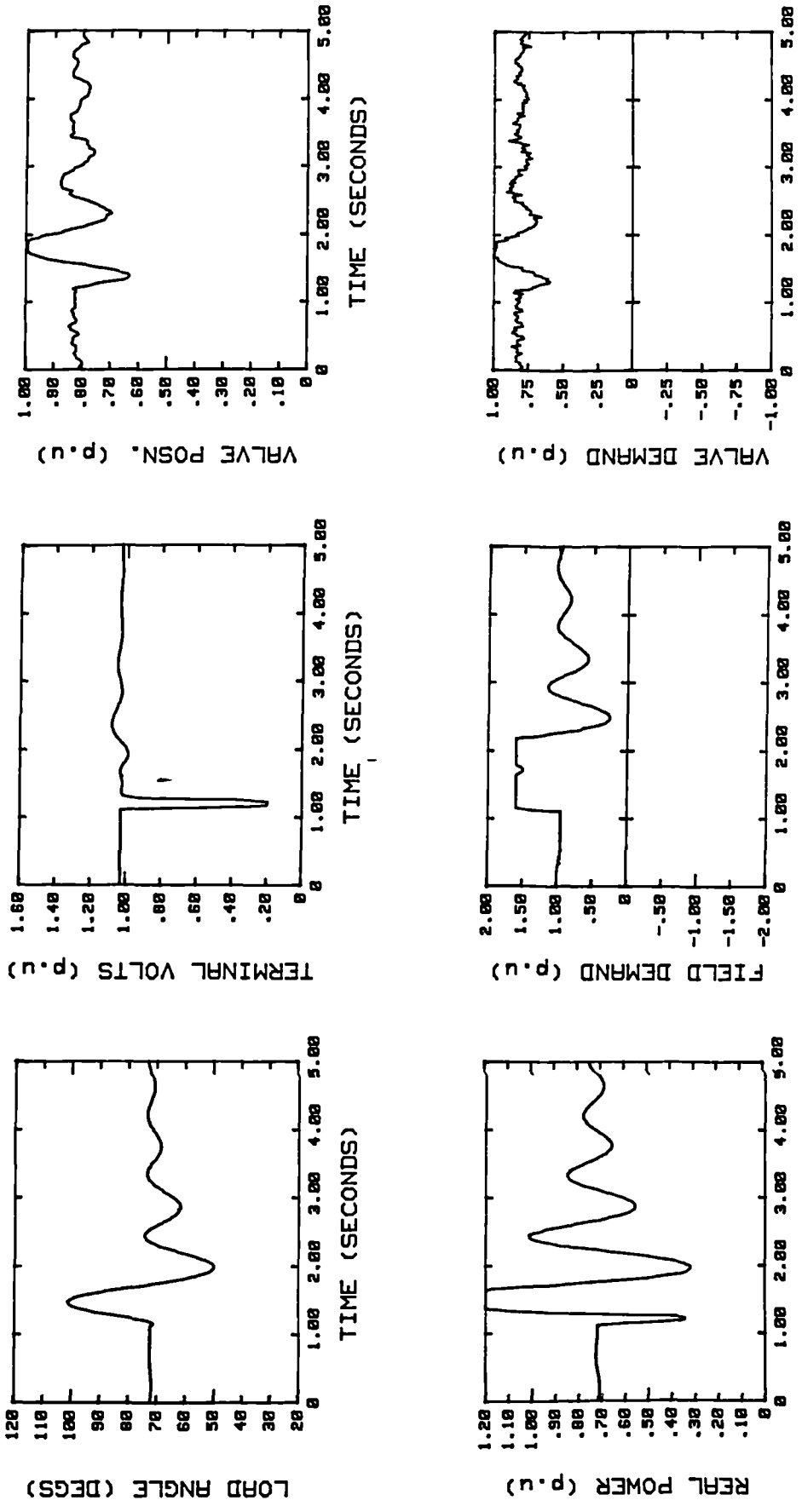

Fig. 6.18 Response of the micro-alternator to a 3-phase short circuit when the AVR and EHG are in the fixed parameter mode.

indicating better damping. The settling times of the various signals have also reduced as indicated in Table 6.2. The response when the 'fixed parameter' digital AVR has been upgraded to a self-tuning AVR of type STAVR-SO is shown in Fig. 6.19. The EDR of the load angle has been further reduced by the self-tuning AVR to 0.40 and its settling time to 1.9 sec. Similar improvement in the terminal power and voltage is also obtained as indicated in Table 6.2.

Fig. 6.20 illustrates the performance of the system when a multi-loop self-tuning control strategy is employed. The self-tuning AVR is of type STAVR-SO and the self-tuning EHG has $P_n = 1 - 0.9\,z^{-1}$, $N_y = 10$, $N_u = 1$, and $\lambda = 0$. The weighting factor G_s for speed deviation has been set to 100 in this case. It can be observed that further improvement in the damping of the load angle and terminal power are obtained which is indicated by EDR's of 0.35 and 0.42 and settling times of 1.32 sec. and 2.0 sec. respectively. The settling time of the terminal voltage is also found to reduce to 1.25 sec.

Finally, the performance of the MIMO self-tuning TG controller was evaluated on the micro-alternator system using the short-circuit test. The controller settings were similar to those used in the multi-loop self-tuning control strategy employed in the previous test. Second order sub-systems with two coefficients for each of the B polynomials were estimated for the MIMO controller. Thus 12 parameters were estimated in total. A sampling period of 20 msec. was achieved without any timing problems. Amplitude limiting of control inputs were used for which compensation was provided by the technique proposed earlier. The response of the closed-loop system is given in Fig. 6.21. It can be seen that a further improvement in the damping of the load angle and power are achieved with the MIMO self-tuning controller. The EDR's of the load angle and terminal power are found to be 0.16 and 0.34 respectively. The settling times of the various signals remain more or less unchanged when compared with those achieved with the multi-loop self-tuning approach as can be observed from Table 6.2.

It can be concluded that as the control strategy becomes more and more advanced, a progressive improvement in the performance on the micro-alternator

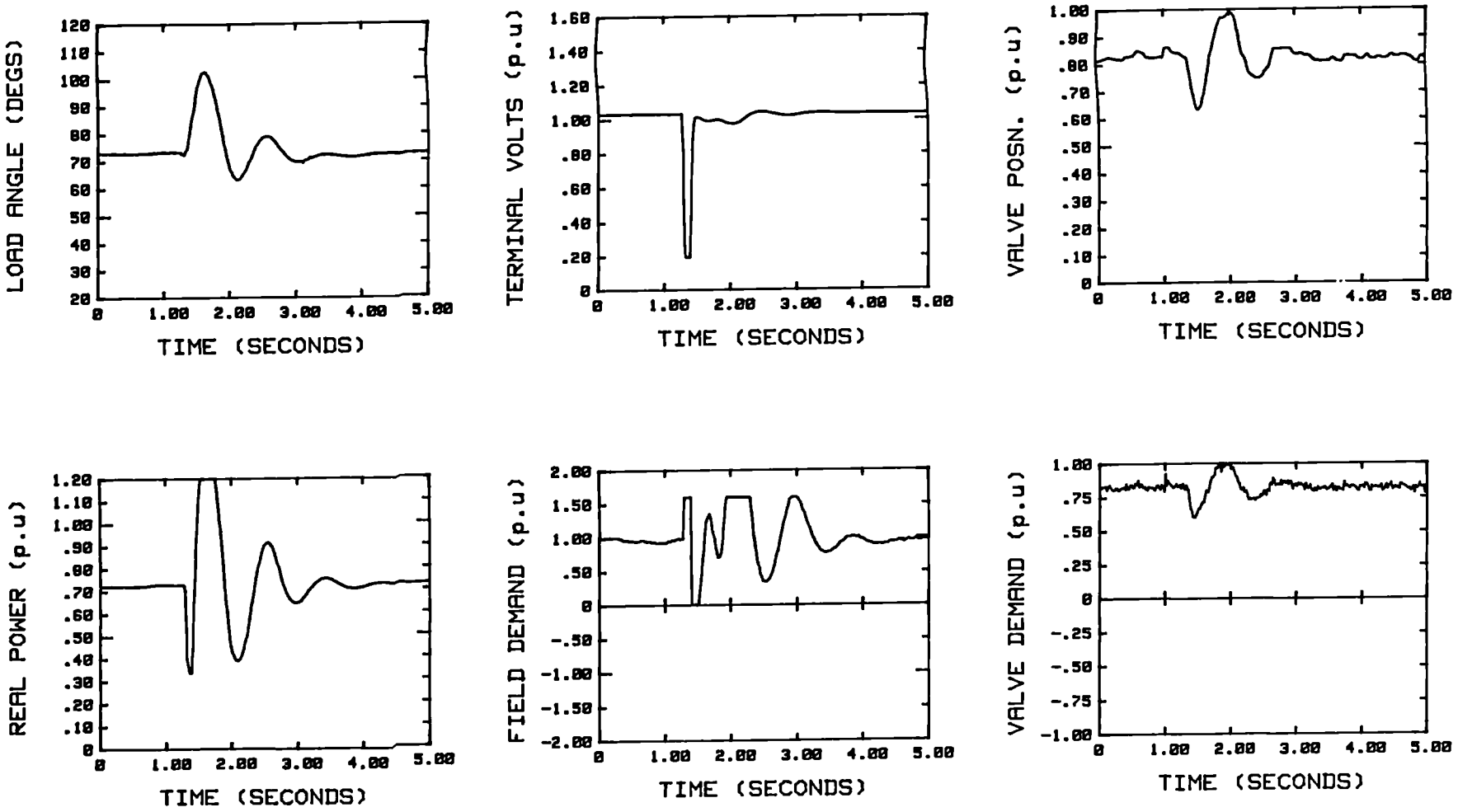

Fig. 6.19 Response of the micro-alternator to a 3-phase short circuit when the AVR is in the self-tuning mode and the EHG in the fixed parameter mode.

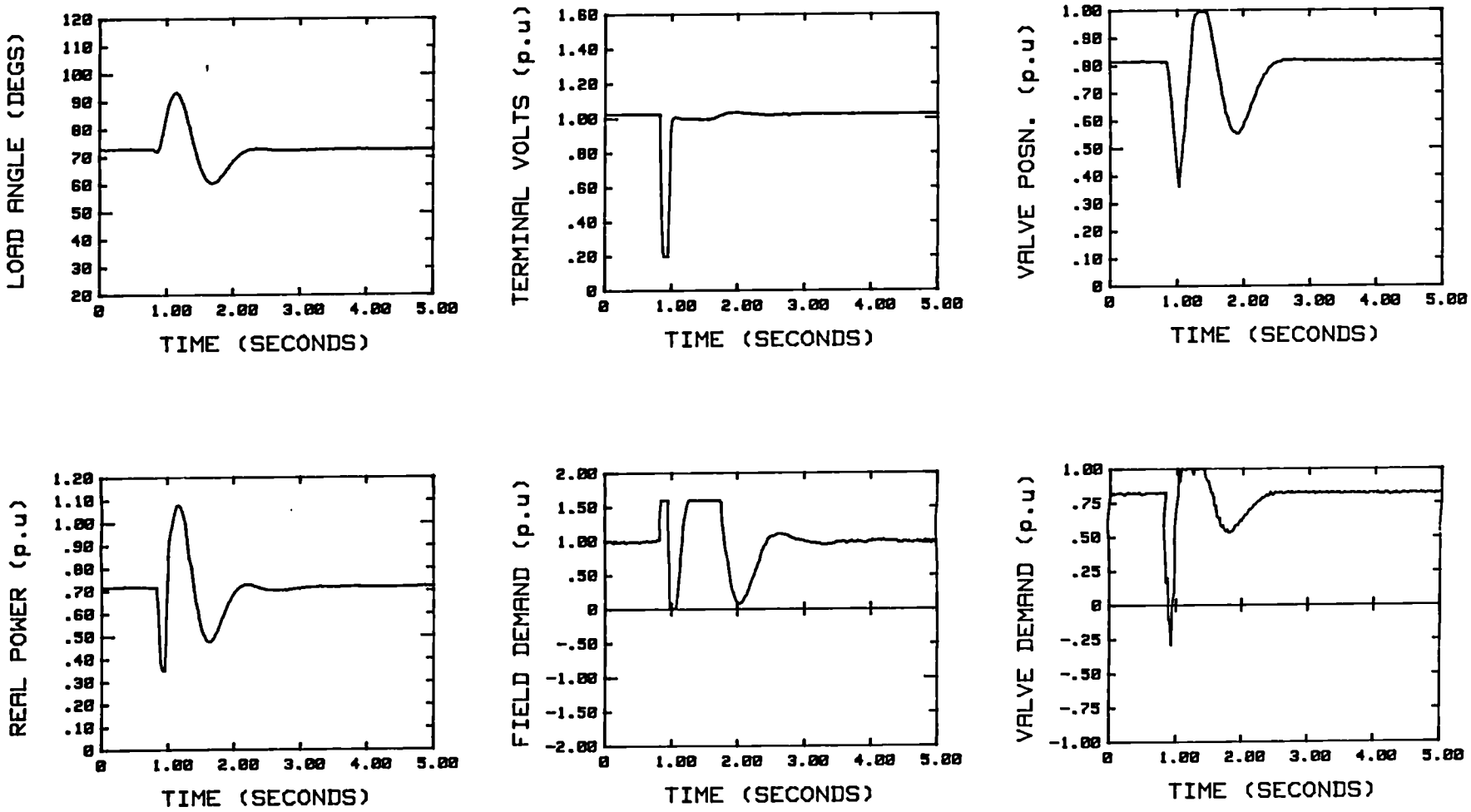

Fig. 6.20 Response of the micro-alternator to a 3-phase short circuit when the AVR and EHG are in the SISO self-tuning mode.

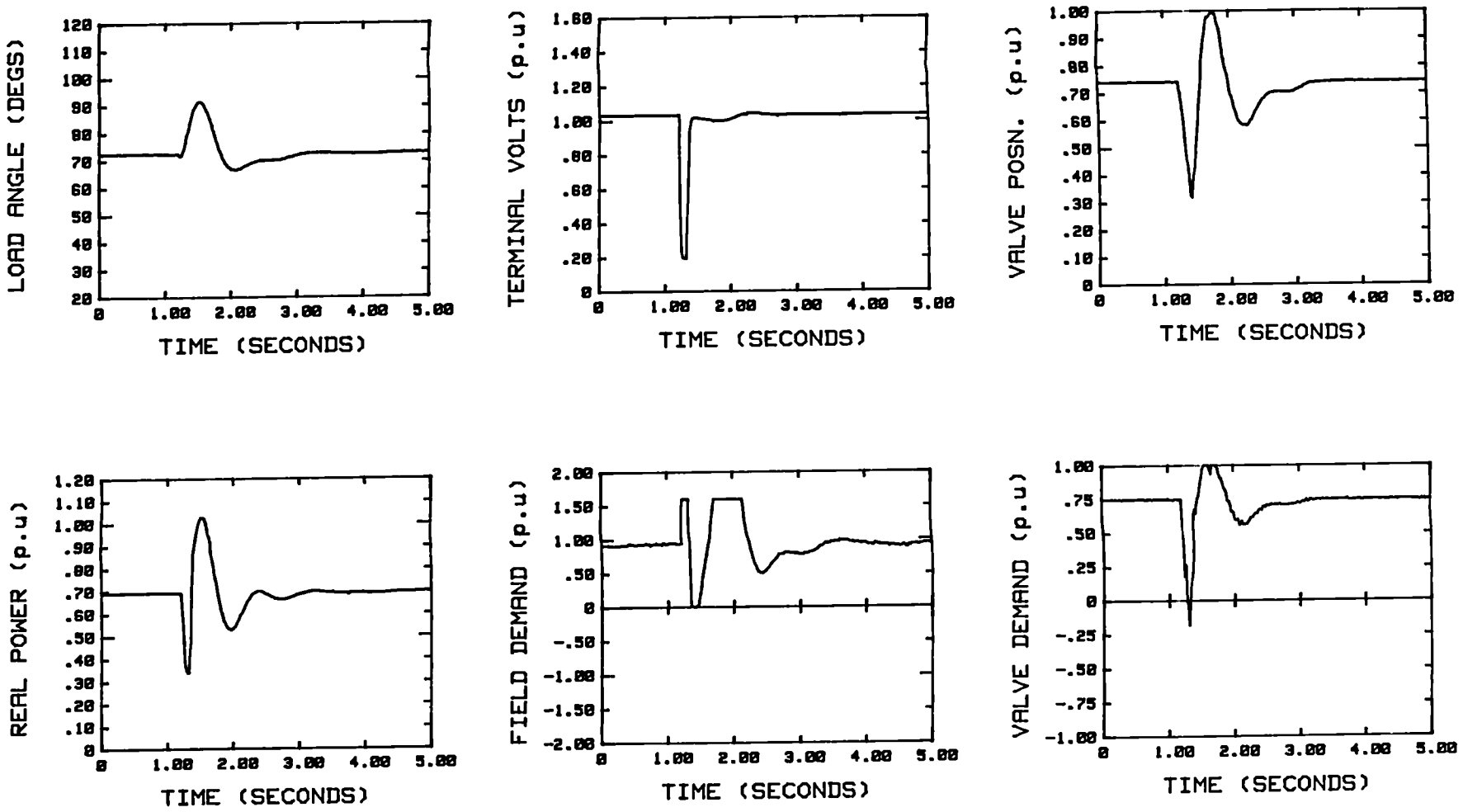

Fig. 6.21 Response of the micro-alternator to a 3-phase short circuit when the AVR and EHG loops are combined into a MIMO self-tuning TG controller.

as indicated by Fig. 6.17 to 6.21 is possible. The results obtained using the MIMO self-tuning TG controller illustrate the significant improvement that can be achieved, compared with the corresponding performance when the turbine generator has a self-tuning excitation control system only. The improvement in performance with the multivariable self-tuning controller when compared with the multi-loop self-tuning control approach is more pronounced in the micro-alternator system than with the TG simulator. A possible explanation for this could be the inability to repeat tests on the micro-alternator system under exactly identical system conditions for comparison purposes.

CHAPTER 7

CONCLUSIONS

7.1 General Conclusions

Self-tuning control may be implemented in such a way that commercial turbine generator controllers based on this advanced strategy can be readily evolved. This work has adequately demonstrated that the development of a self-tuning controller based on the GPC strategy using standard off-the-shelf microprocessor hardware and structured software design techniques is a feasible approach to turbine generator control. The proposed design is flexible, cost-effective and readily applicable to 'real' generating plant. The primary objective of developing a 'practical' self-tuning controller for the turbine generator plant has thus been satisfactorily achieved.

It has been shown practically that a significant enhancement in the overall performance can be achieved by improving the primary controls of a turbine generator using self-tuning control. Several practical issues have been tackled during the design of the self-tuning controller and techniques to improve the robustness of the measurement system, controller and parameter estimator have been proposed. It has been shown that the self-tuning AVR based on the GPC strategy is robust, flexible, and expandable, and that it performs better than a conventional fixed-parameter digital AVR. It has also been shown that a sampling period of 20 msec or less can be achieved for a computationally demanding self-tuning algorithm such as GPC with standard off-the-shelf microprocessor hardware of moderate cost.

Practical aspects such as simplicity, long-term reliability and minimum use of specialised hardware have been considered during the design of the software-based measurement system for terminal quantities. The bandwidth and signal-to-noise ratio achieved with the proposed software measurement system when working with the micro-alternator were found to be adequate even for a high performance system such as the self-tuning controller. The measurement system

was shown to tolerate unwanted characteristics such as signal noise, harmonics, and unbalance which are normally present in the turbine generator plant, without a significant degradation in its performance. It was seen that the measurement algorithms chosen were numerically robust and that the computational burden imposed was so modest that an extension of the sampling period was not required. It can therefore be concluded that the software-based terminal quantity measurement system developed for the self-tuning controller is robust and adequate for feedback purposes in the turbine generator.

Several techniques have been proposed for use in the parameter estimator of the self-tuning controller to improve its robustness. The use of a 'washout' data pre-filter is an excellent way of including the low frequency dynamics of the plant in the estimated model without causing biased estimates. The undesirable effect of amplifying high frequency noise when using differential data can thus be avoided. The variable forgetting factor and automatic adjustment of the memory length of the estimator improve the robustness of the estimator particularly during long-term operation of the self-tuning controller.

The 'freezing' of the parameter estimator based on the dynamic information content in the incoming plant data improves the estimator robustness during large disturbances and steady-state operating periods of the plant. The scheme to automatically adjust the sensitivity of the estimator by monitoring the trace of the covariance matrix helps the estimator to 'adapt' quickly to changes in the dynamics of the plant. The artificial 'boosting' of the dc gain of the plant assists the convergence of the coefficients of the $B(z^{-1})$ polynomial in the plant model thus improving the performance of the estimator.

The convergence, adaptation and robustness aspects of the parameter estimator used in this work have been adequately evaluated using the micro-alternator system. The convergence of the estimator has been assessed by comparing the frequency response of the estimated plant model with that of the plant itself. This has been done with second and third order plant models, with the micro-alternator on open-circuit as well as on load, and with 'lively' and 'sluggish' control.

It has been shown that the estimator is able to capture the low frequency dynamics of the micro-alternator system satisfactorily under all conditions thus confirming its ability to converge. This illustrates the effectiveness of the 'washout' pre-filter to enable low frequency dynamic models of systems to be obtained and to reject dc offsets as well as high frequency noise. It was also shown that the estimator is able to produce a reasonable plant model even when it is in the process of convergence. As expected, the use of a 'lively' controller is seen to improve the speed of parameter convergence in comparison with that of a 'sluggish' controller. The tests have indicated that the use of a second order plant model for the self-tuning AVR is sufficient and is not significantly different in model accuracy when compared with a third order estimated model. This helps to reduce the computational burden imposed by the self-tuning algorithm during real-time implementation.

It has been shown that substantial changes in the steady state gain and dominant time constant of the generator occur when it is switched from unsynchronised to synchronised mode of operation. The recursive parameter estimator was shown to 'adapt' quickly to these drastic system changes thereby facilitating a more consistent response characteristic under various operating conditions of the system.

The robustness of the estimator has been enhanced by the parameter 'freeze' and covariance 'trace' monitoring facilities which are incorporated in the software. The parameter 'freeze' facility was shown to work in conjunction with the variable forgetting factor scheme to prevent the estimator from loosing its information content during steady state operation of the plant. The scheme to protect the estimator from model corruption during transient disturbances was found to work satisfactorily. The covariance 'trace' monitoring feature which adjusts the sensitivity of the estimator thereby improving its adaptability also performs correctly. The various techniques employed in the parameter estimator are thus very effective in improving the robustness of the self-tuning controller.

The flexibility provided by GPC to the self-tuning AVR has been adequately demonstrated. The use of the pole polynomial to specify the desired response of

the closed-loop system was shown to be a simple and convenient approach. It was demonstrated that the response of the closed-loop system can be moved closer to that of the design in terms of overshoot, rise and settling times, and bandwidth by increasing the control horizon. The same effect can also be achieved by reducing the prediction horizon. The controller 'liveliness' is varied by the control horizon and control weighting factor. The disturbance tailoring polynomial pre-filters the data before its use in the control law thus improving the robustness of the controller. Thus the self-tuning AVR using GPC has been shown to be a flexible control system which is a very useful feature in practical applications.

The wide variation in the gain and dominant time constant of the plant between its synchronised and unsynchronised operating modes can lead to a large difference in the closed-loop response between the two modes. This has been demonstrated by step response tests on the micro-alternator system using the various self-tuning and fixed-parameter AVR designs. It was observed that the closed-loop response of the non-adaptive AVR is significantly different, while that of the self-tuning AVR is only marginally different. This helps to confirm the adaptive capability of the algorithm and illustrate the usefulness of the self-tuning facility for excitation control.

The response of the excitation control system when the turbine generator is on load is of critical importance since the system operates in this mode most of its life. A significant variation in the dynamic response of the closed-loop system at various operating points is generally observed when using a conventional fixed-parameter AVR. The change in response characteristic of the closed-loop system with the generator on load therefore has been investigated with the various self-tuning and conventional lag-lead type fixed-parameter AVR designs. A number of operating points were chosen for the micro-alternator system for this investigation. It was shown that the variation in response when using the self-tuning AVR is significantly less than that for the fixed-parameter AVR. The responses obtained were much more closer to the design values for the self-tuning AVR than for the standard AVR. Thus the self-tuning AVR was found to be better than the fixed-parameter AVR in terms of its consistency of performance over the whole operating range of the turbine generator. Step response tests using the

software TG simulator were also seen to give similar results thus reconfirming the above conclusion.

The performance of the system with the self-tuning AVR has been evaluated during abnormal operating conditions of the generator such as short circuits, faults followed by transmission line switching, and full load rejection. These tests have been conducted on the micro-alternator system as well as the software TG simulator and compared with the performance obtained for a conventional AVR under similar conditions. It may be noted that no stabilising signals such as speed, or power were used in the excitation controller for these tests. The tests have indicated that although the self-tuning AVR is generally a more active controller than the corresponding conventional type, the damping torque of the system has not been adversely affected. On the contrary, the self-tuning AVR has been shown to give better synchronising and damping torque components than the conventional controller in most cases due to its fast-acting nature. The damping of rotor oscillations and settling of the rotor and terminal voltage were shown to be better for the self-tuning AVR when compared with the conventional type. The self-tuning AVR was also found to perform considerably better in terms of the regulation of terminal voltage than the corresponding fixed-parameter AVR during a full-load rejection test. Although the responses obtained on the micro-alternator system and the software simulator were not exactly similar, the trend observed in the damping and settling of the system was however the same.

The tests performed with the self-tuning AVR under normal operating conditions of the turbine generator have indicated that it 'adapts' well to the changing conditions thereby giving a consistent performance. It has also been shown that the self-tuning AVR is able to cope with abnormal operating conditions of the plant better than the fixed-parameter type. Thus it can be concluded that the various self-tuning AVR designs are superior in performance when compared with the corresponding conventional lag-lead type of fixed-parameter AVR's.

The excitation control system of a turbine generator can greatly influence the stability during synchronised operation with the power system. A supplementary feedback signal is normally employed in conventional systems to

enhance power system stability. In the self-tuning AVR, the use of electrical power as a stabilising feedback signal for dynamic stability improvement has been shown to be possible and effective. It has been shown that the GPC cost function can be modified to include the stabilising signal and its minimisation can lead to a power system stabilised control law. Thus the damping of oscillations in the electrical power and rotor angle can be further improved by the use of the power system stabilised self-tuning AVR.

The incorporation of the supplementary feedback signal in the self-tuning AVR has been shown to be simple as well as straight forward, and does not cause a significant computational burden. The 'washout' pre-filtering of the electrical power signal was found to be effective in preventing any dc bias in the excitation system due to supplementary feedback. It may be noted that the washout filter together with the low-pass filter for the electrical power signal in the measurement system gives a band-pass characteristic. The pass-band can be adjusted to match the range of frequencies of interest thereby achieving maximum effectiveness. The use of a simple scalar weighting factor for the 'washed-out' electrical power signal was shown to be sufficient to achieve an acceptable improvement in the damping torque of the system during disturbances. Limiting of the stabilising signal to conserve the benefit derived from voltage regulator action in the early part of a transient was also found to be effective.

The self-tuning AVR with supplementary feedback has been evaluated on the micro-alternator system and the software TG simulator by injecting moderate system disturbances such as step inputs and transmission line switching. It was observed that a significant improvement in the damping of dynamic oscillations can be achieved with the various fast and slow self-tuning AVR designs. The tests have shown that the improvement obtained with the power system stabilised self-tuning AVR is at least as good as that obtained with a conventional fixed-parameter AVR employing a well-tuned PSS. As expected, the improvement in dynamic stability has been achieved at the expense of the terminal voltage response. Since this degradation in the response of the terminal voltage is only marginal, it can be tolerated especially when considering the stability improvement obtained.

The performance of the power system stabilised self-tuning AVR has been investigated during transient disturbances also. This was carried out on the micro-alternator system and the software simulator using the three-phase short-circuit test. It was observed that the 'first swing' of the rotor after the fault is unchanged which proves that the stabilising signal does not pull the generator field out of ceiling too early. The oscillations which follow after the first swing exhibit better damping when the stabilising signal is used in the self-tuning AVR. Once again, it was observed that the performance obtained is comparable with that of a fixed-parameter AVR with a well-tuned PSS.

The tests performed on the micro-alternator system and the software TG simulator using the power system stabilised self-tuning AVR have demonstrated the significant improvement that can be obtained in the dynamic stability margin of the system. It was shown that the use of the power signal in the controller does not have an adverse effect on the transient stability improvement achieved with a standard self-tuning AVR. It was also demonstrated that the scheme proposed for stability improvement does not significantly affect the voltage regulation characteristic of the excitation control system.

The possibility of a further improvement in stability through the turbine governing system has also been investigated. It has been shown that an appreciable improvement can be obtained by employing self-tuning control for the governor. Thus, there are significant advantages in using self-tuning control for excitation as well as governing systems in the turbine generator. The use of a self-tuning integrated control system which combines the AVR and EHG functions is therefore proposed and evaluated.

A multivariable approach which extends the Single-Input Single-Output (SISO) GPC strategy used in the self-tuning AVR has been implemented for the integrated controller. This is advantageous from the point of view of familiarity and customer acceptance because of the ease with which upgrading can be performed. The reduction that can be achieved in the hardware and software of the control system by the integrated approach can lead to improved reliability and availability.

The use of the P-canonical structure to model the interactions between the AVR and EHG loops was shown to be advantageous from the point of view of extending the SISO control software to the MIMO application. This approach enables a multivariable system to be viewed as a number of multi-input single-output sub-systems thereby simplifying the mathematical analysis. Thus the majority of the SISO self-tuning control software used in the AVR can be re-used for the integrated controller which is a great advantage during implementation and subsequent field trials. The derivation of the MIMO GPC control law which incorporates such useful extensions as the model following, and disturbance tailoring features has been presented to demonstrate the ease with which the GPC algorithm can be expanded and to show the closeness between the SISO and MIMO controllers.

The integrated self-tuning controller has been implemented as a 2 x 2 system. The feedback signals chosen for the multivariable controller are readily available and are currently used in the SISO controllers thus leading to a close similarity. The terminal voltage and steam valve position have been used as the primary feedback signals while the electrical power and rotor speed have been employed as supplementary feedback signals for improving the power system stability. A sampling period of 20 msec can be achieved for the integrated controller when using the self-tuning AVR hardware. Since this is an acceptable sampling rate, no changes in the hardware are needed for the integrated controller, thus leading to further standardisation.

It has been demonstrated through simulation studies that a total elimination of loop interactions may not be achieved when applying constraints in the multivariable controller. This problem has been investigated and simple techniques to incorporate practical constraints on control inputs of the integrated controller have been proposed. The emphasis has been to produce computationally simple methods which are particularly suited for less complex configurations such as the 2 x 2 integrated controller.

Three popular cases of constraint on control input have been addressed. They are amplitude limiting, rate limiting, and weighting of control inputs. The

cause of incomplete elimination of loop interactions during constrained control has been investigated and schemes to tackle the problem for each case have been derived. The successful operation of the proposed schemes have been verified by simulation studies. It has been shown that the techniques proposed work together without any conflict and are effective in minimising the loop interactions during constrained control of multivariable systems.

The multivariable self-tuning integrated controller has been evaluated using the software TG simulator and the micro-alternator system. The tests were aimed at demonstrating the use of such a controller in turbine generating plant for further improvement in performance. The three-phase short-circuit test has been chosen for this purpose due to its severity and its ability to demonstrate the transient response of the control system. Various controller configurations from manual excitation and governing loops to multivariable self-tuning control have been used for comparison purposes. It has been shown that a progressive improvement in the system response can be achieved when upgrading the controllers from manual mode to fixed-parameter automatic control and to self-tuning control.

The results obtained with the micro-alternator system and the software simulator have shown a similar trend as far as performance improvement is concerned. A significant improvement has been achieved with the multivariable self-tuning controller in comparison with a self-tuning AVR and fixed-parameter EHG. This further enhancement has been mainly obtained by self-tuning the speed governor of the turbine generator. Hence, the performance improvement of the multivariable self-tuning controller when compared with the self-tuning multi-loop configuration was not found to be substantial.

This work has demonstrated that the use of a self-tuning AVR can greatly improve the overall performance of the turbine generator plant in terms of its control and stability. The self-tuning AVR design using the GPC strategy has been shown to be robust and the implementation has been done to facilitate its easy integration with the standard digital AVR for field trials. It was also shown that a further improvement in performance can be achieved by upgrading the self-tuning

AVR to a multivariable self-tuning integrated controller which combines the AVR and EHG functions.

7.2 Recommendations for future work

a) It is desirable to conduct multi-machine simulation studies to assess the performance of the GPC-based self-tuning controller. This would help to gain further confidence in the proposed design for field trials. This study could usefully investigate the case when all the machines in the system are equipped with self-tuning controllers, as well as the case when only one or a limited number of machines has self-tuning control with the remaining machines controlled by conventional systems.

b) An evaluation of the performance of the self-tuning AVR with detailed models of exciters and prime movers is desirable. The study may be conducted for the various types of exciters currently in use. This will help possible field trials of the self-tuning AVR on existing or older plant.

c) The facility to modify the sub-transient reactance of the micro-alternator to match that of a full-size machine can be beneficial for a more accurate representation of the 'real' plant.

d) Since the customers are familiar with time constants and gains in conventional control systems for the generating plant, it would help with their understanding if the self-tuning controller is able to present its current operating coefficients in that form. This would also help with any simulation studies that they would like to conduct and can improve customer confidence.

e) The self-tuning AVR design may be modified in such a way that it can be initially made available as an add-on feature to a standard digital AVR. This will enable its supply to customers for long term field trials as part of the standard AVR. The client would then have the option of

switching out the self-tuning feature on-line at any time if wanting to go back to the fixed-parameter AVR. It is felt that this approach would help to gain customer confidence and facilitate the easy introduction of self-tuning control for generator excitation.

APPENDIX A

GPC COST FUNCTION MINIMISATION

The cost function for GPC is given in (1.2) as:

$$J' = \sum_{j=1}^{N_y} [\phi(t+j) - w(t+j)]^2 + \sum_{j=1}^{N_u} \lambda[\Delta u(t+j-1)]^2 \qquad (A.1)$$

The auxiliary plant output ϕ can be written as:

$$\phi(t+j) = \tilde{G}_j \, \Delta u(t+j-1) + G_j^f \, \Delta u^f(t-1) + F_j^f \, \frac{y^f(t)}{P_d} + E_j^f \, e(t+j) \qquad (A.2)$$

and the prediction of $\phi(t+j)$ denoted as $\phi^*(t+j)$ is:

$$\phi^*(t+j) = \tilde{G}_j \, \Delta u(t+j-1) + G_j^f \, \Delta u^f(t-1) + F_j^f \, \frac{y^f(t)}{P_d} \qquad (A.3)$$

The derivation of (A.2) and (A.3) is given in Appendix B.

Let $s(t+j)$ be that part of $\phi(t+j)$ which is known at the beginning of time t. Then,

$$s(t+j) = G_j^f \, \Delta u^f(t-1) + F_j^f \, \frac{y^f(t)}{P_d} \qquad (A.4)$$

The set of equations given by (A.2) for $j = 1$ to N_y can be written in vector form as:

$$\boldsymbol{\phi} = \tilde{\boldsymbol{G}} \, \bar{\boldsymbol{u}} + \boldsymbol{s} + \boldsymbol{e} \qquad (A.5)$$

where

$$\boldsymbol{\phi} = [\phi(t+1), \ \phi(t+2), \ \text{-------}, \ \phi(t+N_y)]^T$$

$$\bar{\boldsymbol{u}} = [\Delta u(t), \ \Delta u(t+1), \ \text{-----}, \ \Delta u(t+N_u-1)]^T$$

$$\boldsymbol{s} = [s(t+1), \ s(t+2), \ \text{-----}, \ s(t+N_y)]^T$$

$$\boldsymbol{e} = [E_1^f e(t+1), \ E_2^f e(t+2), \ \text{-----}, \ E_{N_y}^f e(t+N_y)]^T$$

and $\tilde{G}$ is a $(N_y \times N_u)$ matrix given by:

$$\tilde{G} = \begin{bmatrix} \tilde{g}_0 & 0 & 0 & - & - & - & 0 \\ \tilde{g}_1 & \tilde{g}_0 & 0 & - & - & - & 0 \\ \tilde{g}_2 & \tilde{g}_1 & \tilde{g}_0 & - & - & - & 0 \\ | & | & & & & & \\ | & | & & & & & \\ \tilde{g}_{N_y-1} & \tilde{g}_{N_y-2} & - & - & - & - & \tilde{g}_{N_y-N_u} \end{bmatrix}$$

The expectation of the cost function (A.1) for $j = 1$ to N_y can then be written as:

$$J_1 = E \{ (\tilde{G}\,\bar{u} + s + e - w)^T (\tilde{G}\,\bar{u} + s + e - w) + \lambda\,\bar{u}^T\,\bar{u} \} \qquad (A.6)$$

where J_1 is the expectation, $E\{.\}$ is the expectation operator and w is a vector of future set points such that

$$w = [w(t+1),\ w(t+2),\ -----,\ w(t+N_y)]^T$$

Equation (A.6) must be minimised assuming no constraints on future controls to obtain the control law. Therefore, $\frac{\partial J_1}{\partial \bar{u}} = 0$ for an optimal cost.

Since the future noise vector e is uncorrelated with the future control increments at time t,

$$\frac{\partial J_1}{\partial \bar{u}} = E \{ 2\,\tilde{G}^T (\tilde{G}\,\bar{u} + s + e - w) + 2\,\lambda\,\bar{u} \}$$

which can be simplified as:

$$\frac{\partial J_1}{\partial \bar{u}} = 2\,[(\tilde{G}^T\,\tilde{G} + \lambda\,I)\,\bar{u} + \tilde{G}^T (s - w)] \qquad (A.7)$$

For an optimal cost, (A.7) should be equated to zero. This gives

$$(\tilde{G}^T\,\tilde{G} + \lambda\,I)\,\bar{u} + \tilde{G}^T (s - w) = 0 \qquad (A.8)$$

Thus the control increment vector $\bar{u}$ is given by:

$$\bar{u} = (\tilde{G}^T\,\tilde{G} + \lambda\,I)^{-1}\,\tilde{G}^T (w - s) \qquad (A.9)$$

APPENDIX B

PREDICTION OF AUXILIARY OUTPUT ϕ IN GPC

Using (1.1), (1.3), (1.4) and the observer polynomial $T(z^{-1})$, the auxiliary output ϕ can be written as:

$$\phi(t+j) = \frac{p\ P_n\ B}{P_d\ A}\ u(t+j-1) + \frac{p\ P_n\ T}{A\ \Delta\ P_d}\ e(t+j) \qquad \text{(B.1)}$$

Using the Diophantine identity (1.10), (B.1) can be rewritten as:

$$\phi(t+j) = \frac{p\ P_n\ B}{P_d\ A}\ u(t+j-1) + \frac{F_j^f}{A\ \Delta\ P_d}\ e(t) + E_j^f\ e(t+j) \qquad \text{(B.2)}$$

where E_j^f is of order $(j-1)$. Substituting for $e(t)$ gives:

$$\phi(t+j) = \frac{p\ P_n\ B}{P_d\ A}\ u(t+j-1) + \frac{F_j^f}{P_d}\left[\frac{y(t)}{T} - \frac{B}{A\ T}\ u(t-1)\right] + E_j^f\ e(t+j)$$

which on simplification gives:

$$\phi(t+j) = \frac{B}{A}\ u(t+j-1)\left[\frac{p\ P_n}{P_d} - \frac{z^{-j}\ F_j^f}{T\ P_d}\right] + \frac{F_j^f}{T\ P_d}\ y(t) + E_j^f\ e(t+j)$$

Using the Diophantine identity of (1.10) leads to:

$$\phi(t+j) = \frac{B}{A}\ u(t+j-1)\ \frac{E_j^f\ A\ \Delta}{T} + \frac{F_j^f}{T\ P_d}\ y(t) + E_j^f\ e(t+j)$$

which can be rewritten using (1.9) as:

$$\phi(t+j) = \frac{E_j^f\ B}{T}\ \Delta u(t+j-1) + F_j^f\ \frac{y^f(t)}{P_d} + E_j^f\ e(t+j) \qquad \text{(B.3)}$$

Using the Diophantine identity of (1.11) in (B.3) gives:

$$\phi(t+j) = \tilde{G}_j\ \Delta u(t+j-1) + G_j^f\ \Delta u^f(t-1) + F_j^f\ \frac{y^f(t)}{P_d} + E_j^f\ e(t+j) \qquad \text{(B.4)}$$

where $\tilde{G}_j$ is of order $(j-1)$. Thus the present and future control increments are unfiltered in (B.4) while the past values of control increment and the present and past values of output are filtered by $T(z^{-1})$.

Since E_j^f is of order $(j-1)$, the prediction of $\phi(t+j)$, denoted as $\phi^*(t+j)$, can be written as:

$$\phi^*(t+j) = \tilde{G}_j \, \Delta u(t+j-1) + G_j^f \, \Delta u^f(t-1) + F_j^f \, \frac{y^f(t)}{P_d} \qquad \text{(B.5)}$$

It may be noted that since $T(z^{-1})$ is a user-defined design polynomial, the prediction $\phi^*(t+j)$ will not be 'optimal'. A special case is when $T(z^{-1})$ is chosen to be the same as the noise colouring polynomial $C(z^{-1})$ which produces 'optimal' predictions [30,88].

APPENDIX C

RECURSION OF THE GPC DIOPHANTINE EQUATION

The general Diophantine equation for GPC (1.10) is given as:

$$p\ P_n\ T = E_j^f\ \bar{A} + z^{-j}\ F_j^f \tag{C.1}$$

where $\bar{A} = A\ \Delta\ P_d$.

The equation for $(j+1)$ can be written using (C.1) as:

$$p\ P_n\ T = E_{j+1}^f\ \bar{A} + z^{-(j+1)}\ F_{j+1}^f \tag{C.2}$$

Subtracting (C.1) from (C.2) gives:

$$0 = \bar{A}\ (E_{j+1}^f - E_j^f) + z^{-j}\ (z^{-1}\ F_{j+1}^f - F_j^f) \tag{C.3}$$

The polynomial $(E_{j+1}^f - E_j^f)$ is of degree j by definition and can be split into two parts as:

$$(E_{j+1}^f - E_j^f) = \tilde{E} + e_j\ z^{-j} \tag{C.4}$$

Combining (C.4) with (C.3) gives:

$$\bar{A}\ \tilde{E} + z^{-j}\left[z^{-1}\ F_{j+1}^f - F_j^f + \bar{A}\ e_j\right] = 0 \tag{C.5}$$

Since $\tilde{E}$ is of degree $(j-1)$, it is evident from (C.5) that:

$$\begin{aligned} \tilde{E} &= 0 \\ F_{j+1}^f &= z^{+1}\ [F_j^f - \bar{A}\ e_j] \end{aligned} \tag{C.6}$$

Since the leading element of $\bar{A}$ is unity, it is seen from (C.6) that:

$$e_j = (f_0)_j \tag{C.7}$$

Also,

$$(f_i)_{j+1} = (f_{i+1})_j - (f_0)_j\ \bar{a}_{i+1} \tag{C.8}$$

The index i in (C.8) is valid from 0 to the degree of F^f_{j+1} and $\bar{a}_{i+1}$ is the $(i+1)$th coefficient of the $\bar{A}$ polynomial.

Combining (C.7) with (C.4) gives:

$$E_{j+1}^f = E_j^f + (f_0)_j\ z^{-j} \tag{C.9}$$

(C.8) and (C.9) are the recursive formulae for solving the Diophantine equation of (1.10) for $j=1$ to N_y .

To commence the recursion, the starting value of F_j^f and E_j^f , viz. F_1^f and E_1^f are needed. For $j=1$, (C.1) can be written as:

$$p\ P_n\ T = E_1^f\ \bar{A} + z^{-1}\ F_1^f \tag{C.10}$$

Since the leading element of $\bar{A}$, P_n and T are unity,

$$E_1^f = p$$

and (C.11)

$$F_1^f = p\ (P_n\ T - \bar{A})\ z^{+1}$$

APPENDIX D

RECURSIVE FORMULAE TO INCORPORATE THE OBSERVER POLYNOMIAL $T(z^{-1})$ IN GPC

Consider the Diophantine identities:

$$E_j^f\ B = \tilde{G}_j\ T + z^{-j}\ G_j^f \tag{D.1}$$

$$E_{j-1}^f\ B = \tilde{G}_{j-1}\ T + z^{-(j-1)}\ G_{j-1}^f \tag{D.2}$$

where $\tilde{G}_j$ is of order $(j-1)$ and is given by:

$$\tilde{G}_j = \tilde{g}_0 + \tilde{g}_1\ z^{-1} + \text{-----} + \tilde{g}_{j-1}\ z^{-(j-1)}$$

and G_j^f is of order n where $n = [\,MAX\,(EnB,\ nT)] - 1$ and is given by:

$$G_j^f = (g_0^f)_j + (g_1^f)_j\ z^{-1} + \text{---} + (g_n^f)_j\ z^{-n}$$

EnB and nT are the order of the estimated B polynomial and the T polynomial respectively.

Subtracting (D.2) from (D.1) gives:

$$e_{j-1}^f\ z^{-(j-1)}\ B = \tilde{g}_{j-1}\ z^{-(j-1)}\ T + z^{-(j-1)}\left[z^{-1}\ G_j^f - G_{j-1}^f\right]$$

which can be simplified to:

$$e_{j-1}^f\ B = \tilde{g}_{j-1}\ T + z^{-1}\ G_j^f - G_{j-1}^f \tag{D.3}$$

Assume $T(z^{-1})$ to be a monic polynomial. Equating like coefficients gives:

$$\begin{aligned}
e_{j-1}^f\ b_0 &= \tilde{g}_{j-1} \quad + 0 \quad - (g_0^f)_{j-1} \\
e_{j-1}^f\ b_1 &= \tilde{g}_{j-1}\ t_1 + (g_0^f)_j - (g_1^f)_{j-1} \\
e_{j-1}^f\ b_2 &= \tilde{g}_{j-1}\ t_2 + (g_1^f)_j - (g_2^f)_{j-1} \\
&\textit{etc.}
\end{aligned}$$

Generalising the above leads to the following algorithm:

$$
\begin{aligned}
&\textit{For } j = 1 \textit{ to } Ny \\
&\quad \tilde{g}_{j-1} = e^{f}_{j-1}\, b_0 + (g^{f}_{0})_{j-1} \\
&\quad \textit{For } k = 1 \textit{ to } [\, MAX\ (EnB, nT)] \\
&\qquad (g^{f}_{k-1})_j = e^{f}_{j-1}\, b_k + (g^{f}_{k})_{j-1} - \tilde{g}_{j-1}\, t_k
\end{aligned}
\qquad \text{(D.4)}
$$

It may be noted that (D.4) assumes the following:

a) G^{f}_{o} does not exist, hence zero, and

b) Coefficients of $B(z^{-1})$ and $T(z^{-1})$ with indices greater than their respective degrees are zero.

APPENDIX E

UPPER-DIAGONAL FACTORISATION ALGORITHM

The covariance matrix $P(t)$ is factored as [78]:

$$P(t) = U(t)\ D(t)\ U^T(t) \qquad \text{(E.1)}$$

where $U(t)$ is an upper triangular matrix with all its diagonal elements equal to unity and $D(t)$ is a diagonal matrix.

The algorithm to update the factors $D(t)$ and $U(t)$ of the factorised covariance matrix and to calculate the gain vector $K(t)$ is as follows [95]:

Initialise $U(0)$ and $D(0)$ during start-up $(t=0)$ such that
$U(0)\ D(0)\ U^T(0) = P(0)$.
If $P(0)$ is set to αI , $U(0)$ will have all its off-diagonal elements set to zero and $D(0)$ will have its diagonal elements equal to α .

1. Calculate vector $f = u^T(t-1)\ d(t)$, where $d(t)$ is the data vector at time t .
   Calculate vector $g = D(t-1)\ f$.
   Set $k_0 = \beta(t)$, where $\beta(t)$ is the exponential forgetting factor.

2. For $j=1$ to n, go through steps 3 to 5 below, where 'n' is the number of parameters in the estimated parameter vector $\hat{\theta}(t)$.

3. Calculate the following:
   $k_j = k_{j-1} + f_j g_j$, where f_j and g_j are the j-th element of vectors f and g respectively.
   $D(t)_{jj} = k_{j-1}\ D(t-1)_{jj} \ /\ (k_j\ \beta(t))$
   $v_j = g_j$
   $r_j = -f_j \ /\ k_{j-1}$

4. For $i=1$ to $(j-1)$, go through step 5 below. (If $j = 1$, skip step 5).

5. Compute the following:

$$U(t)_{ij} = U(t\text{-}1)_{ij} + v_i\, r_j$$

$$v_i = v_i + U(t\text{-}1)_{ij}\, v_j$$

6. Calculate the gain vector $K(t)$ as:

$$\mathbf{v} = [v_1, v_2, \text{----}, v_n]^T \; ; \; K(t) = \mathbf{v} / k_n$$

APPENDIX F

NON-LINEAR POWER SYSTEM MODEL

The non-zero elements of the state matrix A_{ps} are given by:

$$A_{ps}(1,2) = 1 ;$$

$$A_{ps}(2,2) = -\frac{D}{J} ; \qquad A_{ps}(2,10) = -\frac{1}{J} ;$$

$$A_{ps}(3,3) = -\omega_0 (R_a+R_t+R_e) B_{d11} ; \qquad A_{ps}(3,4) = -\omega_0 (R_a+R_t+R_e) B_{d12} ;$$

$$A_{ps}(3,5) = -\omega_0 (R_a+R_t+R_e) B_{d13} ; \qquad A_{ps}(3,6) = -\omega_0 ;$$

$$A_{ps}(4,3) = -\omega_0 R_f B_{d21} ; \qquad A_{ps}(4,4) = -\omega_0 R_f B_{d22} ;$$

$$A_{ps}(4,5) = -\omega_0 R_f B_{d23} ; \qquad A_{ps}(4,8) = -\omega_0;$$

$$A_{ps}(5,3) = -\omega_0 R_{kd} B_{d31} ; \qquad A_{ps}(5,4) = -\omega_0 R_{kd} B_{d32} ;$$

$$A_{ps}(5,5) = -\omega_0 R_{kd} B_{d33} ;$$

$$A_{ps}(6,3) = \omega_0 ;$$

$$A_{ps}(6,6) = -\omega_0 (R_a+R_t+R_e) B_{q11} ; \qquad A_{ps}(6,7) = -\omega_0 (R_a+R_t+R_e) B_{q12} ;$$

$$A_{ps}(7,6) = -\omega_0 R_{kq} B_{q21} ; \qquad A_{ps}(7,7) = -\omega_0 R_{kq} B_{q22} ;$$

$$A_{ps}(8,8) = -\frac{1}{T_e} ;$$

$$A_{ps}(9,2) = \frac{G_g}{T_v} ; \qquad A_{ps}(9,9) = -\frac{1}{T_v} ;$$

$$A_{ps}(10,9) = \frac{1}{T_s} ; \qquad A_{ps}(10,10) = -\frac{1}{T_s} ;$$

where

$$X_{gd}^{-1} = B_d = \begin{bmatrix} B_{d11} & B_{d12} & B_{d13} \\ B_{d21} & B_{d22} & B_{d23} \\ B_{d31} & B_{d32} & B_{d33} \end{bmatrix} ; \qquad X_{gq}^{-1} = B_q = \begin{bmatrix} B_{q11} & B_{q12} \\ B_{q21} & B_{q22} \end{bmatrix}$$

The non-zero elements of the control matrix B_{ps} are:

$$B_{ps}(8,1) = \frac{-G_e}{T_e} \; ; \qquad B_{ps}(9,2) = \frac{1}{T_v}$$

The non-zero elements of the $N_{ps}(x)$ vector which contains the non-linearities are:

$$N_{ps}(2) = \frac{M_e}{J} \; ; \qquad N_{ps}(3) = \omega_0 \, (V_{bd} + \psi_q \, \dot{\delta}) \; ; \qquad N_{ps}(6) = \omega_0 \, (V_{bq} - \psi_d \, \dot{\delta})$$

APPENDIX G

NUMERICAL INTEGRATION METHOD

The Runge-Kutta integration method calculates the vector $x_f = x(t_0+h)$ at the end of the integration step of length h for the set of differential equations:

$$\frac{dx}{dt} = f(t,x) \tag{G.1}$$

Assuming $x_0 = x(t_0)$, the intermediate steps involved are given by:

$$\begin{aligned} x_1 &= h\ f(t_0\ ,\ x_0) \\ x_2 &= h\ f(t_0+\frac{h}{2}\ ,\ x_0+\frac{x_1}{2}) \\ x_3 &= h\ f(t_0+\frac{h}{2}\ ,\ x_0+\frac{x_2}{2}) \\ x_4 &= h\ f(t_0+h\ ,\ x_0+x_3) \end{aligned} \tag{G.2}$$

The vector x_f at the end of the integration step is the given by:

$$x_f = x_0 + \frac{1}{6}\ (x_1 + 2x_2 + 2x_3 + x_4) \tag{G.3}$$

APPENDIX H

CALCULATION OF INITIAL CONDITIONS OF THE POWER SYSTEM SOFTWARE SIMULATOR

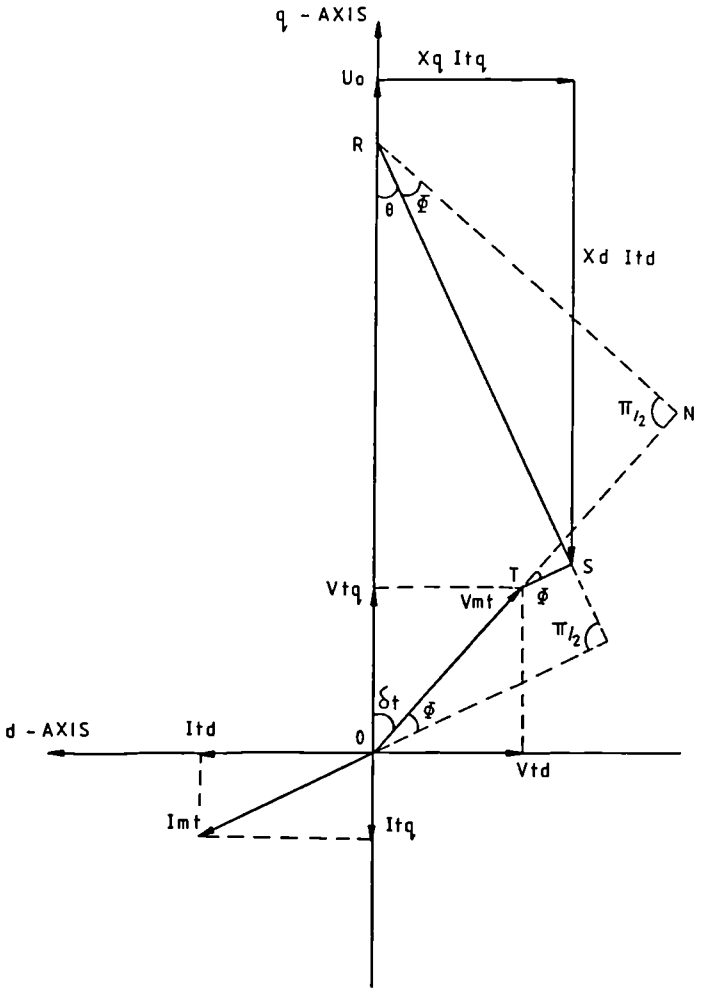

Figure H.1 Synchronous machine steady state phasor diagram

The calculation of the initial conditions of the power system requires that the parameters of the generator and transmission line are known and that the operating point in terms of the real and reactive power as well as the terminal voltage have been specified. A phasor diagram as given in Figure H.1 can then be used to derive the various quantities required.

The angle Φ and the peak value of the current I_{mt} can be calculated as:

$$\Phi = \tan^{-1}\left(\frac{Q}{P}\right)$$
$$I_{mt} = \frac{2\sqrt{(P^2 + Q^2)}}{V_{mt}} \qquad \text{(H.1)}$$

The rotor angle δ_t with respect to the machine terminals can be calculated as follows:

$$\tan \delta_t = \frac{RN}{ON} \qquad \text{(H.2)}$$

In Figure H.1, TS is the resistive drop ($= R_a I_{mt}$), SR is perpendicular to the current phasor and RN is the perpendicular to OT produced. SR is then given by:

$$SR = \frac{X_q I_{tq}}{\sin \theta} = X_q I_{mt} \qquad \text{(H.3)}$$

Therefore,

$$\tan \delta_t = \frac{-(X_q I_{mt} \cos \Phi - R_a I_{mt} \sin \Phi)}{V_{mt} + R_a I_{mt} \cos \Phi + X_q I_{mt} \sin \Phi} \qquad \text{(H.4)}$$

This gives δ_t as a negative angle for generation as per the motoring sign convention.

The d and q-axis components of the terminal voltage and current can then be calculated from:

$$V_{td} = V_{mt} \sin \delta_t$$
$$V_{tq} = V_{mt} \cos \delta_t$$
$$I_{td} = -I_{mt} \sin (\delta_t - \Phi)$$
$$I_{tq} = -I_{mt} \cos (\delta_t - \Phi) \qquad \text{(H.5)}$$

From the transmission line equations (2.9); the steady state busbar voltage components and the load angle δ_b with respect to the infinite bus can be calculated as:

$$V_{bd} = V_{td} + R_{ex} I_{td} + X_{ex} I_{tq}$$
$$V_{bq} = V_{tq} + R_{ex} I_{tq} - X_{ex} I_{td}$$
$$\delta_b = \tan^{-1}\left[\frac{V_{bd}}{V_{bq}}\right] \qquad \text{(H.6)}$$

The steady state values of flux-related state variables are calculated using (2.1) and (2.2) as:

$$\begin{aligned}
\omega_0 \psi_d &= (R_a + R_{ex})\, I_{tq} - V_{bq} \\
I_f &= \frac{\omega_0 \psi_d - (X_{md} + X_a + X_{ex})\, I_{td}}{X_{md}} \\
\omega_0 \psi_f &= X_{md}\, I_{td} + (X_{md} + X_f)\, I_f \\
\omega_0 \psi_{kd} &= X_{md}\, (I_{td} + I_f) \\
\omega_0 \psi_q &= (X_{mq} + X_a + X_{ex})\, I_{tq} \\
\omega_0 \psi_{kq} &= X_{mq}\, I_{tq}
\end{aligned} \tag{H.7}$$

The field and exciter voltages are given by:

$$\begin{aligned}
V_f &= R_f\, I_f \\
V_e &= \frac{V_f}{G_e}
\end{aligned} \tag{H.8}$$

The electrical torque is given by (2.4) as:

$$M_e = \frac{1}{2}\, (\omega_0 \psi_d\, I_{tq} - \omega_0 \psi_q\, I_{td}) \tag{H.9}$$

Under steady state conditions, the mechanical torque M_t, steam valve position A_p, the valve demand A_d, and the load set-point P_{ref} are all equal to the electrical torque M_e if the constant mechanical losses are neglected.

APPENDIX I

PARAMETERS OF THE MICRO-ALTERNATOR SYSTEM

The parameter values of the micro-alternator system with Time Constant Regulator which models a typical turbine generator system are the following:

D-axis mutual reactance	X_{md}	= 2.279 pu
Q-axis mutual reactance	X_{mq}	= 2.145 pu
Armature resistance	R_a	= 0.00528 pu
Armature leakage reactance	X_a	= 0.149 pu
Field resistance	R_f	= 0.00116 pu
Field leakage reactance	X_f	= 0.16 pu
D-axis damper resistance	R_{kd}	= 0.0179 pu
D-axis damper reactance	X_{kd}	= 0.09 pu
Q-axis damper resistance	R_{kq}	= 0.0179 pu
Q-axis damper reactance	X_{kq}	= 0.146 pu
Generator transformer resistance	R_t	= 0.0 pu
Generator transformer reactance	X_t	= 0.0 pu
Transmission line resistance	R_e	= 0.06 pu
Transmission line reactance	X_e	= 0.25 pu
Inertia constant	H	= 3.875 sec
Damping coefficient	D	= 0.025 pu
Open-circuit field time constant	T_{do}'	= 6.0 sec
Exciter time constant	T_e	= 0.01 sec
Steam time constant	T_s	= 0.3 sec
Valve time constant	T_v	= 0.1 sec
Exciter gain	G_e	= 5.56
Governor gain	G_g	= 0.0796 (4% droop)

APPENDIX J

REAL POWER MEASUREMENT IN 3-PHASE SYSTEMS

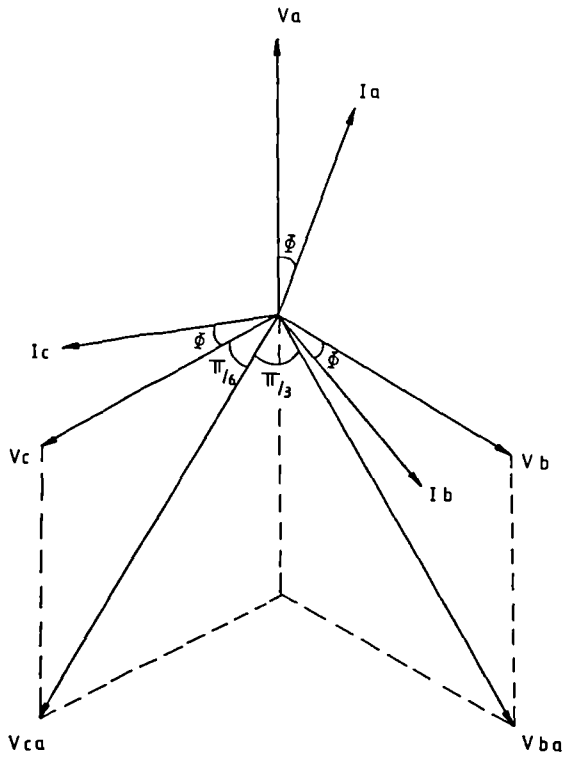

Fig. J.1 Voltages and currents in a 3-phase system

Instantaneous power p' by the 2-wattmeter method is given by:

$$p' = v_{ba}\, i_b + v_{ca}\, i_c$$

Under balanced conditions,

$$\begin{aligned} p' = {} & [\sqrt{2}\ V_L \sin(\omega t)]\ [\sqrt{2}\ I_L \sin(\omega t + \tfrac{\pi}{6} \pm \Phi)] \\ & + [\sqrt{2}\ V_L \sin(\omega t - \tfrac{\pi}{3})]\ [\sqrt{2}\ I_L \sin(\omega t - (\tfrac{\pi}{2} \mp \Phi))] \end{aligned} \qquad \text{(J.1)}$$

where V_L and I_L are the rms value of line voltage and current respectively and $\pm\Phi$ denotes lead / lag power factor.

Simplifying (J.1) gives:

$$p' = 2\,V_L\,I_L \sin \omega t \,[\sin \omega t \cos (\tfrac{\pi}{6} \pm \Phi) + \cos \omega t \sin (\tfrac{\pi}{6} \pm \Phi)]$$

$$+ 2\,V_L\,I_L\,[(\tfrac{1}{2} \sin \omega t - \tfrac{\sqrt{3}}{2} \cos \omega t)\,(\pm \sin \omega t \sin \Phi - \cos \omega t \cos \Phi)]$$

$$= 2\,V_L\,I_L \sin \omega t \,[\sin \omega t\,(\tfrac{\sqrt{3}}{2}\cos \Phi \mp \tfrac{1}{2}\sin \Phi) + \cos \omega t\,(\tfrac{1}{2}\cos \Phi \pm \tfrac{\sqrt{3}}{2}\sin \Phi)]$$

$$+ 2\,V_L\,I_L\,[(\tfrac{1}{2} \sin \omega t - \tfrac{\sqrt{3}}{2} \cos \omega t)\,(\pm \sin \omega t \sin \Phi - \cos \omega t \cos \Phi)]$$

$$= 2\,V_L\,I_L\,[\tfrac{\sqrt{3}}{2} \sin^2 \omega t \cos \Phi \mp \tfrac{1}{2} \sin^2 \omega t \sin \Phi$$

$$+ \tfrac{1}{2} \sin \omega t \cos \omega t \cos \Phi \pm \tfrac{\sqrt{3}}{2} \sin \omega t \cos \omega t \sin \Phi$$

$$\pm \tfrac{1}{2} \sin^2 \omega t \sin \Phi - \tfrac{1}{2} \sin \omega t \cos \omega t \cos \Phi$$

$$\mp \tfrac{\sqrt{3}}{2} \sin \omega t \cos \omega t \sin \Phi + \tfrac{\sqrt{3}}{2} \cos^2 \omega t \cos \Phi]$$

Therefore,

$$p' = 2\,V_L\,I_L\,\tfrac{\sqrt{3}}{2} \cos \Phi\,[\sin^2 \omega t + \cos^2 \omega t] \qquad \text{(J.2)}$$

i.e.

$$p' = \sqrt{3}\,V_L\,I_L \cos \Phi$$

It is seen that (J.2) does not have any ac components under balanced conditions.

APPENDIX K

REACTIVE POWER MEASUREMENT IN 3-PHASE SYSTEMS

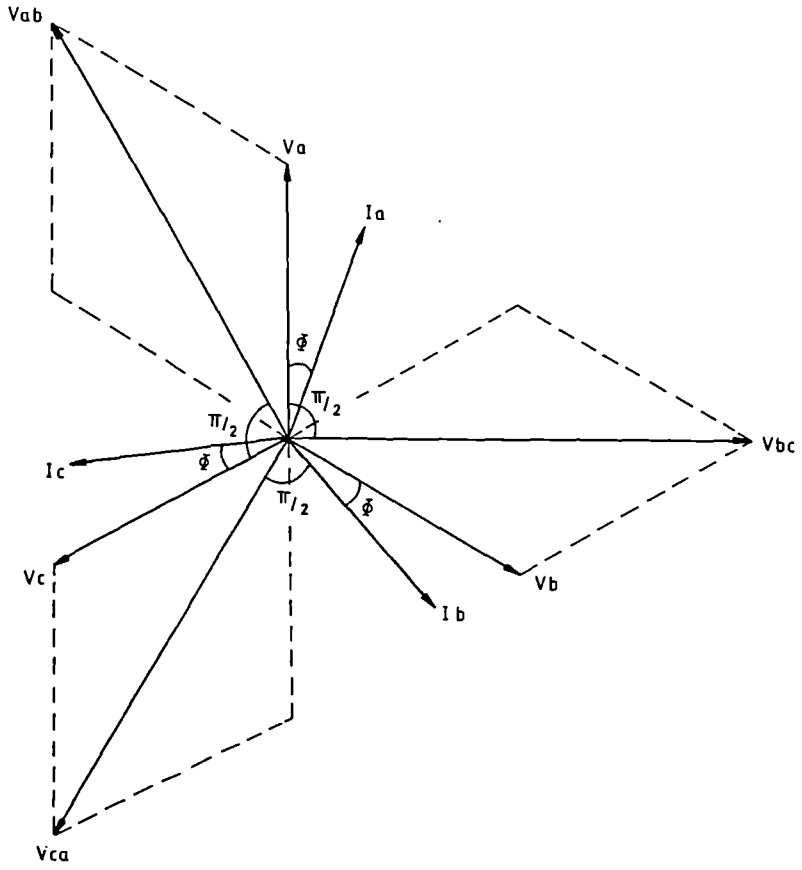

Fig. K.1 Voltages and currents in a 3-phase system

The total instantaneous reactive power q in a 3-phase system is given by:

$$q = v_a\, i'_a + v_b\, i'_b + v_c\, i'_c \qquad \text{(K.1)}$$

where v_a, v_b, and v_c are the instantaneous values of phase voltages. i'_a, i'_b, and i'_c are the instantaneous values of line currents $\pi/2$ radians before the sampling instant.

Let V_L and I_L be the rms line voltage and current and let v_a coincide with the reference vector. Under balanced conditions,

$$q = \frac{\sqrt{2}}{\sqrt{3}} V_L \sin(\omega t) \sqrt{2} I_L \sin(\omega t \pm \Phi - \frac{\pi}{2})$$
$$+ \frac{\sqrt{2}}{\sqrt{3}} V_L \sin(\omega t - \frac{2\pi}{3}) \sqrt{2} I_L \sin(\omega t - \frac{2\pi}{3} \pm \Phi - \frac{\pi}{2})$$
$$+ \frac{\sqrt{2}}{\sqrt{3}} V_L \sin(\omega t + \frac{2\pi}{3}) \sqrt{2} I_L \sin(\omega t + \frac{2\pi}{3} \pm \Phi - \frac{\pi}{2})$$

Simplification of the above gives:

$$q = \frac{2}{\sqrt{3}} V_L I_L [-\sin \omega t \cos(\omega t \pm \Phi) + \cos(\omega t - \frac{\pi}{6}) \sin(\omega t \pm \Phi - \frac{\pi}{6}) \quad (2)$$
$$+ \cos(\omega t + \frac{\pi}{6}) \sin(\omega t \pm \Phi + \frac{\pi}{6})]$$

Further simplification yields:

$$q = \frac{2}{\sqrt{3}} V_L I_L [-\sin \omega t \cos(\omega t \pm \Phi)$$
$$+ (\frac{\sqrt{3}}{2} \cos \omega t + \frac{1}{2} \sin \omega t)(\frac{\sqrt{3}}{2} \sin(\omega t \pm \Phi) - \frac{1}{2} \cos(\omega t \pm \Phi))$$
$$+ (\frac{\sqrt{3}}{2} \cos \omega t - \frac{1}{2} \sin \omega t)(\frac{\sqrt{3}}{2} \sin(\omega t \pm \Phi) + \frac{1}{2} \cos(\omega t \pm \Phi))]$$

$$= \frac{2}{\sqrt{3}} V_L I_L [-\sin \omega t \cos(\omega t \pm \Phi)$$
$$+ \frac{3}{2} \cos \omega t \sin(\omega t \pm \Phi) - \frac{1}{2} \sin \omega t \cos(\omega t \pm \Phi)]$$

$$= \frac{2}{\sqrt{3}} V_L I_L \frac{3}{2} [\sin(\omega t \pm \Phi) \cos \omega t - \cos(\omega t \pm \Phi) \sin \omega t]$$

$$= \sqrt{3} V_L I_L \sin(\omega t \pm \Phi - \omega t)$$

Therefore,

$$q = \sqrt{3} V_L I_L \sin(\pm \Phi) \quad (K.3)$$

This shows that the reactive power calculated by this method does not have any ac components under balanced load conditions. Hence the instantaneous reactive power is equal to the average value if the load is balanced and the

averaging period T is small when compared with the rate at which the reactive power can change.

Equation (K.1) is not very easy to implement since the value of instantaneous currents $\pi/2$ radians before the sampling instant has to be known accurately. To avoid this difficulty, another equation to calculate the reactive power may be used which is derived as follows:

If the reference vector is rotated by $\pi/2$ radians in the clockwise direction,

$$\begin{aligned} v_{bc} &= \sqrt{2}\ V_L \sin \omega t \\ i_a &= \sqrt{2}\ I_L \cos (\omega t \pm \Phi) \\ v_{ca} &= -\sqrt{2}\ V_L \cos (\omega t - \frac{\pi}{6}) \\ i_b &= \sqrt{2}\ I_L \sin (\omega t \pm \Phi - \frac{\pi}{6}) \\ v_{ab} &= \sqrt{2}\ V_L \cos (\omega t + \frac{\pi}{6}) \\ i_c &= -\sqrt{2}\ I_L \sin (\omega t \pm \Phi + \frac{\pi}{6}) \end{aligned} \qquad \text{(K.4)}$$

Substituting these values in (K.2) gives:

$$q = \frac{-1}{\sqrt{3}} \left[v_{bc}\ i_a + v_{ca}\ i_b + v_{ab}\ i_c\right] \qquad \text{(K.5)}$$

Since $i_a + i_b + i_c = 0$ in a 3-wire system,

$$q = \frac{-1}{\sqrt{3}} \left[i_b\ (v_{ca} - v_{bc}) + i_c\ (v_{ab} - v_{bc})\right]$$

which can be re-written as:

$$q = \frac{-1}{\sqrt{3}} \left[i_b\ (v_{ca} + v_{cb}) + i_c\ (v_{cb} - v_{ba})\right] \qquad \text{(K.6)}$$

It may be noted that when using (K.1) and (K.6), the polarity of the reactive power is +ve for leading power factors.

APPENDIX L

TERMINAL VOLTAGE MEASUREMENT IN 3-PHASE SYSTEMS

Let V_r be the rms value of the phase voltages v_a, v_b, and v_c of the 3-phase system. Then,

$$\begin{aligned} v_a &= \sqrt{2}\ V_r \sin \omega t \\ v_b &= \sqrt{2}\ V_r \sin (\omega t - \frac{2\pi}{3}) \\ v_c &= \sqrt{2}\ V_r \sin (\omega t + \frac{2\pi}{3}) \end{aligned} \qquad \text{(L.1)}$$

Let Σv^2 be the sum of square of instantaneous values of v_a, v_b, and v_c.

$$\begin{aligned} \Sigma v^2 &= v_a^2 + v_b^2 + v_c^2 \\ &= 2V_r^2 [\sin^2 \omega t + \sin^2 (\omega t - \frac{2\pi}{3}) + \sin^2 (\omega t + \frac{2\pi}{3})] \\ &= 2V_r^2 [\sin^2 \omega t + (\sin \omega t \cos \frac{2\pi}{3} + \cos \omega t \sin \frac{2\pi}{3})^2 \\ &\qquad + (\sin \omega t \cos\frac{2\pi}{3} - \cos \omega t \sin\frac{2\pi}{3})^2] \\ &= 2V_r^2 [\sin^2 \omega t + 2(\sin^2 \omega t \cos^2 \frac{2\pi}{3} + \cos^2 \omega t \sin^2 \frac{2\pi}{3})] \\ &= 2V_r^2 [\sin^2 \omega t + 2(\frac{1}{4} \sin^2 \omega t + \frac{3}{4} \cos^2 \omega t)] \\ &= 2V_r^2 [\frac{3}{2}(\sin^2 \omega t + \cos^2 \omega t)] \\ &= 3V_r^2 \end{aligned}$$

Therefore,

$$V_r = \frac{\sqrt{\Sigma\ \bar{v}^2}}{\sqrt{3}} \qquad \text{(L.2)}$$

APPENDIX M

FREQUENCY MEASUREMENT IN 3-PHASE SYSTEMS

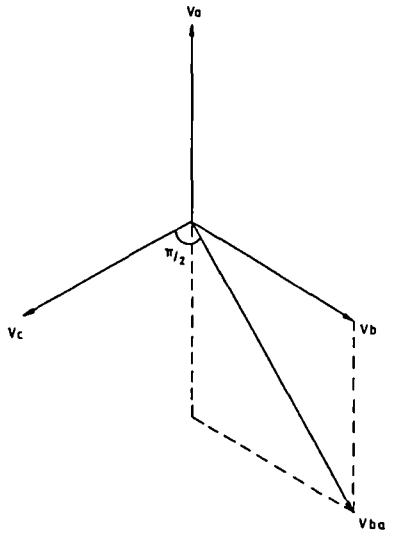

Fig. M.1 Voltages in a 3-phase system

The trigonometric functions used for the measurement of frequency are:

$$\begin{aligned} \sin(a-b) &= \sin(a)\cos(b) - \cos(a)\sin(b) \\ \cos(a-b) &= \cos(a)\cos(b) + \sin(a)\sin(b) \\ \tan(a-b) &= \frac{\sin(a-b)}{\cos(a-b)} \end{aligned} \qquad \text{(M.1)}$$

For a balanced 3-phase system, the line voltage v_{ba} leads the phase voltage v_c by $\pi/2$ radians, as can be seen from Fig. M.1. Then, the voltages can be written as:

$$\begin{aligned} v_c &= \frac{\sqrt{2}}{\sqrt{3}} V_L \sin \omega t \\ v_{ba} &= \sqrt{2}\, V_L \cos \omega t \end{aligned} \qquad \text{(M.2)}$$

where V_L is the rms line voltage.

Let *'a'* be the phase angle of the sine wave at the present sampling instant t_a and *'b'* be the phase angle at the previous instant t_b .

Then (M.1) can be written as:

$$\sin(a-b) = \frac{\sqrt{3}}{\sqrt{2}V_L} v_c(t_a) \frac{1}{\sqrt{2}V_L} v_{ba}(t_b) - \frac{1}{\sqrt{2}V_L} v_{ba}(t_a) \frac{\sqrt{3}}{\sqrt{2}V_L} v_c(t_b)$$

$$\cos(a-b) = \frac{1}{\sqrt{2}V_L} v_{ba}(t_a) \frac{1}{\sqrt{2}V_L} v_{ba}(t_b) + \frac{\sqrt{3}}{\sqrt{2}V_L} v_c(t_a) \frac{\sqrt{3}}{\sqrt{2}V_L} v_c(t_b)$$

which can be simplified to:

$$\sin(a-b) = \frac{\sqrt{3}}{2V_L^2} \left[v_c(t_a)\, v_{ba}(t_b) - v_{ba}(t_a)\, v_c(t_b) \right]$$

$$\cos(a-b) = \frac{3}{2V_L^2} \left[\frac{v_{ba}(t_a)\, v_{ba}(t_b)}{3} + v_c(t_a)\, v_c(t_b) \right]$$

Then, tan *(a-b)* can be written as:

$$\tan(a-b) = \frac{\left[v_c(t_a)\, v_{ba}(t_b) - v_{ba}(t_a)\, v_c(t_b) \right]}{\sqrt{3} \left[\frac{v_{ba}(t_a)\, v_{ba}(t_b)}{3} + v_c(t_a)\, v_c(t_b) \right]} \qquad \text{(M.3)}$$

The inverse tangent function using (M.3) gives the angle difference *(a-b)* in radians which leads to:

$$\omega = \frac{(a-b)}{(t_a - t_b)} \qquad \text{(M.4)}$$

where ω is the angular frequency in radians/second.

APPENDIX N

EFFECT OF PLANT GAIN *'BOOST'* ON THE CONTROL WEIGHTING FACTOR λ

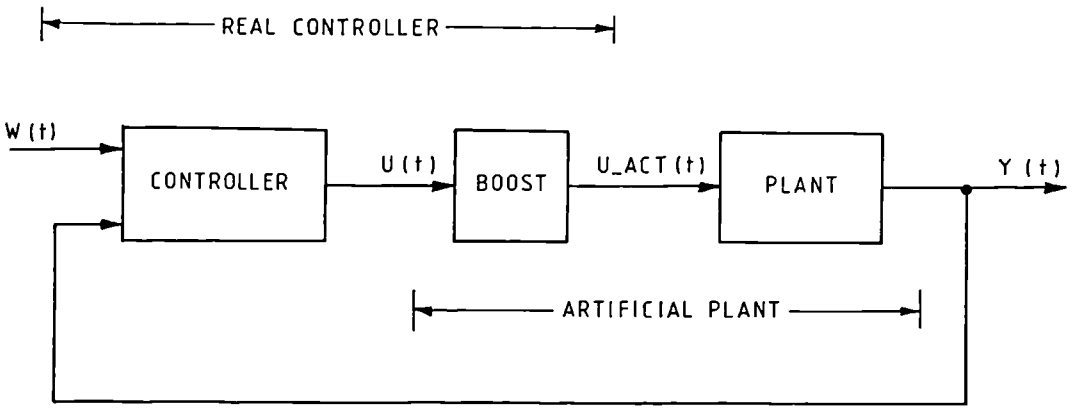

Fig. N.1 Closed-loop system

Let *u_act (t)* be the actual control input applied to the plant and *u(t)* be the input signal used by the identification and control algorithms.

GPC law without the *'Boost'* gain block is given by:

$$u\_act\ (t) = u\_act\ (t-1) + (\tilde{G}^T\ \tilde{G} + \lambda\ I)^{-1}\ \tilde{G}^T\ (w - s) \qquad (N.1)$$

Dividing throughout by *'Boost'* gives:

$$u\ (t) = u\ (t-1) + \frac{(\tilde{G}^T\ \tilde{G} + \lambda\ I)^{-1}\ \tilde{G}^T\ (w - s)}{Boost} \qquad (N.2)$$

The $B(z^{-1})$ polynomial of the artificial plant is given by:

$$B' = B\ Boost \qquad (N.3)$$

Since the $\tilde{G}$ matrix in (N.2) is formed from the coefficients of the product $(E_j\ B)$,

$$G' = \tilde{G}\ Boost \qquad (N.4)$$

where G' is for the control law which calculates *u(t)*.

Then (N.2) can be rewritten as:

$$u(t) = u(t-1) + \frac{\left[\frac{G'^T G'}{Boost^2} + \lambda I\right]^{-1} \frac{G'^T}{Boost} (w - s)}{Boost} \qquad \text{(N.5)}$$

Let

$$\lambda' = \lambda \, Boost^2 \qquad \text{(N.6)}$$

Then (N.5) can be written as:

$$u(t) = u(t-1) + \frac{\left[\frac{G'^T G'}{Boost^2} + \frac{\lambda' I}{Boost^2}\right]^{-1} G'^T (w - s)}{Boost^2}$$

which can be simplified to:

$$u(t) = u(t-1) + (G'^T G' + \lambda' I)^{-1} G'^T (w - s) \qquad \text{(N.7)}$$

Hence λ in the cost function without '*Boost*' is equivalent to λ' in the cost function with the '*Boost*' block as far as weighting of control increment is concerned. Therefore λ has to be modified using (N.6) when the '*Boost*' gain block is used.

REFERENCES

1. British Electricity International : 'Modern Power Station Practice - Vol: G - Station Operation and Maintenance', Pergamon Press (1991).

2. Demello, F.P. and Concordia, C. : 'Concepts of synchronous machine stability as affected by excitation control', IEEE Trans. PAS-88, No: 4, 316-329 (1969).

3. Wu, Q.H. and Hogg, B.W. : 'Adaptive controller for a turbogenerator system', Proc. IEE, Pt. D, Vol: 135, No. 1, 35-42 (1988).

4. Arnold, J.J., Rhodes, J.R. and Capener, J.R. : 'Specification choices for the larger turbine-driven generators', IEE Third International Conference on Electrical Machines and Drives, IEE publication No: 282, 17-21,London, UK (1987).

5. Lim, C.M. and Hiyama, T. : 'Self-tuning control scheme for stability enhancement of multimachine power systems', Proc. IEE, Pt. C, Vol: 137, No: 4, 269-275 (1990).

6. IEEE Standard 421.2-1990 : 'IEEE guide for identification, testing and evaluation of the dynamic performance of excitation control systems' (1990).

7. Yu, Y. : 'Electric power system dynamics', Academic Press (1983).

8. Pahalawathatha, N.C., Hope, G.S. and Malik, O.P. : 'MIMO self-tuning power system stabiliser', IJC, Vol: 54, No: 4, 815-829 (1991).

9. Ham, P.A.L. and Green, N.J. : 'Developments and experience in digital turbine control', IEEE Trans. on EC, Vol: EC 3, No. 3, 568-574 (1988).

10. Larsen, E.V. and Swann, D.A. : 'Applying power system stabilizers - Parts 1 to 3, IEEE Trans. on PAS, Vol: PAS-100, No: 6, 3017-3046 (1981).

11. White, B.J., Zachariah, K.J. and Hingston, R.S.: 'Commissioning of a power system stabiliser using a Dynamic Signal Analyser' to be presented at the IEE 'Control 94' Conference, UK (1994).

12. Czuba, J.S., Hannett, L.N. and Parkinson, D.W. : 'Generic power system stabilizer design', Proc. Waterpower '85 Conference, American Society of Civil Engineers, Las Vegas, USA (1985).

13. White, B.J. and Zachariah, K.J. : 'Development of a digital power system stabiliser', 24th Universities Power Engineering Conference 'UPEC 89', 225-228, Belfast, UK (1989).

14. White, B.J., Zachariah, K.J. and Hingston, R.S. : 'Commissioning of an analogue power system stabiliser', 25th Universities Power Engineering Conference 'UPEC 90', 17-20, Aberdeen, UK (1990).

15. Fenwick, D.R. and Wright, W.F. : 'Review of trends in excitation systems and possible future developments', Proc. IEE (Power), Vol: 123, No: 5, 413-420 (1976).

16. IEEE Tutorial Course Text : 'Power System Stabilization via excitation control', 81 EHO 175-0 PWR (1980).

17. Swidenbank, E. and Hogg, B.W. : 'Application of system identification techniques to modelling a turbogenerator', Proc. IEE, Part D, Vol: 136, No: 3, 113-121 (1989).

18. Rush, P.W. and White, B.J. : 'Digital Excitation System Control for large steam turbine generators', UPEC-21, Imperial College, London, UK (1986).

19. Hingston, R.S., Ham, P.A.L. and Green, N.J. : 'Development of a digital automatic voltage regulator', UPEC 89, 237-240, Belfast, UK (1989).

20. Finch, J.W., Zachariah, K.J., Farsi, M. and Ham, P.A.L. : 'Advanced Digital Techniques Applied to Turbine Generator Excitation Control', IEE International Conference 'CONTROL 91', 1089-1094, Heriot-Watt University, Edinburgh, UK (1991).

21. Brown, M.D. and Swidenbank, E. : 'Supervisory control of a self-tuning Automatic Voltage Regulators', Proc. IEE 'Control 91' Conference, Heriot-Watt University, Edinburgh, UK (1991).

22. Hogg, B.W., Capener, J.R. and Swidenbank, E. : 'The design and development of a self-tuning voltage regulator for a turbine generator', IEE Third International Conference on Electrical Machines and Drives, IEE Publication No: 282, London, UK (1987).

23. Zachariah, K.J., Ham, P.A.L., Finch, J.W. and Farsi, M. : 'A self-tuning voltage regulator for turbogenerators', IEE International Conference 'CONTROL 88', Conference Publication No. 285, 366-370, Oxford, UK (1988).

24. Flynn, D., Swidenbank, E. and Hogg, B.W. : 'Expert adaptive control for turbogenerator systems', UPEC 93, 182-185, Stafford, UK (1993).

25. Harris, C.J. and Billings, S.A. (Editors) : 'Self-tuning and adaptive control : theory and applications', Peter Peregrinus (1985).

26. Zachariah, K.J. : 'Some practical extensions of self-tuning control', MSc Thesis, University of Newcastle upon Tyne, UK (1986).

27. Astrom, K.J. and Wittenmark, B. : 'On self-tuning regulators', Automatica, 9, 185-199 (1973).

28. Clarke, D.W. and Gawthrop, P.J. : 'Self-tuning controller', Proc. IEE, 122, 929-934 (1975).

29. Wellstead, P.E., Prager, D. and Zanker, P. : 'Pole assignment self-tuning regulators'. Proc. IEE, 126, 781-787 (1979).

30. Clarke, D.W., Mohtadi, C. and Tuffs, P.S. : 'Generalised Predictive Control - Part 1. The Basic Algorithm' and ' - Part 2. Extensions and Interpretations', Automatica, Vol: 23, No: 2, 137-160 (1987).

31. Hogg, B.W. : 'Representation and control of turbogenerators in electric power systems', Chapter 5 in 'Modelling of dynamical systems', Vol: 2 (H. Nicholson, Ed), Peter Peregrinus, 112-149 (1981).

32. Sharaf, M.M. and Hogg, B.W. : 'Identification and control of a laboratory model turbogenerator', IJC, Vol: 31, No:4, 723-739 (1980).

33. Harris, D.J. and Cheetham, R.G. : 'Self-tuning controller for a turbogenerator system with reduced excitation time', UPEC 89, 229-232, Belfast, UK (1989).

34. Kanniah, J., Malik, O.P. and Hope, G.S. : 'Excitation control of synchronous generators using adaptive regulators Part 1 - Theory and simulation results, Part 2 - Implementation and test results', IEEE Trans. on PAS, Vol: 103, No. 5, 897-910 (1984).

35. Ibrahim, A.S., Hogg, B.W. and Sharaf, M.M. : 'Self-tuning automatic voltage regulator for a synchronous generator', Proc. IEE, Pt. D, Vol: 136, No. 5, 252-260 (1989).

36. Fan, J.Y., Ortmeyer, T.H. and Mukundan, R. : 'Stability control of multimachine power systems using STAC technique', IJC, Vol: 50, No. 3, 977-991 (1989).

37. Chandra, A., Wong, K.K., Malik, O.P. and Hope, G.S. : 'Implementation and test results of a generalised self-tuning excitation controller', IEEE Trans. on Energy Conversion, Vol: 6, No: 1, 186-192 (1991).

38. Wu, Q.H. and Hogg, B.W. : 'Self-tuning control for turbogenerators in multimachine power systems', Proc. IEE, Vol: 137, Part C, No: 2, 146-158 (1990).

39. Wu, Q.H. and Hogg, B.W. : 'Robust self-tuning regulator for a synchronous generator', Proc. IEE, Part D, Vol: 135, No: 6, 463-473 (1988).

40. Zachariah, K.J., Farsi, M. and Finch, J.W. : 'A self-tuning controller for turbogenerator excitation systems', Sixth International Conference on Systems Engineering, 311-317, Coventry, UK (1988).

41. Tham, M.T. and Morris, A.J. : 'An introduction to self-tuning control', IEE Fourth Workshop on self-tuning and adaptive control, Oxford, UK (1987).

42. Farsi, M., Zachariah, K.J. and Warwick, K. : 'Adaptive control alogrithms for intelligent robot manipulators', IEE Workshop on 'Robot Control : Theory and Applications', Oxford, UK, IEE Control Engineering Series 36, Chapter 4, 37-44, Edited by K. Warwick and A. Pugh, Peter Peregrinus Ltd. (1988).

43. Finch, J.W., Zachariah, K.J. and Farsi, M. : 'Generalised Predictive Control applied to a turbogenerator voltage regulator', Fourth International Conference on 'Electrical Machines and Drives', Conference Publication No. 310, 130-134, London, UK (1989).

44. Finch, J.W., Zachariah, K.J. and Farsi, M. : 'A turbogenerator voltage regulator using generalised predictive control', 24th Universities Power Engineering Conference 'UPEC 89', 267-270, Belfast, UK (1989).

45. Finch, J.W., Zachariah, K.J. and Farsi, M. : 'Voltage control for a Turbo-generator using digital Self-tuning techniques', International Conference on Electrical Machines 'ICEM 90', 1188-1193, Massachusetts, USA (1990).

46. Zachariah, K.J., Finch, J.W. and Farsi, M. : 'Application of digital self-tuning techniques for turbine generator AVRs', 25th Universities Power Engineering Conference 'UPEC 90', 623-626, Aberdeen, UK (1990).

47. Zachariah, K.J., Ham, P.A.L., Finch, J.W. and Farsi, M. : 'Turbine generator excitation control using advanced digital techniques', IFAC International Symposium on Intelligent Tuning and Adaptive Control 'ITAC 91', Singapore (1991).

48. Farsi, M., Zachariah, K.J., Finch, J.W. and Ham, P.A.L. : 'A self-tuning voltage regulator for Turbogenerators', American Control Conference 1991, 1026-1031, Boston, Massachusetts, USA (1991).

49. Finch, J.W., Zachariah, K.J. and Farsi, M. : 'Self-tuning control applied to the Turbogenerator voltage regulator', International Conference on the Evolution and modern aspects of Synchronous Machines, 1021-1025, Zurich, Switzerland (1991).

50. Brown, M.D. : 'The use of expert systems in real-time turbogenerator control', Institute of Measurement & Control Symposium, University of Nottingham, UK (1990).

51. Newton, M.E. and Hogg, B.W. : 'Optimal control of a turbo-generator', IJC, Vol: 26, No: 5, 783-795 (1977).

52. Pullman, R.T. and Hogg, B.W. : 'Discrete state-space controller for a turbogenerator', Proc. IEE, Vol: 126, No: 1, 87-92 (1979).

53. Yokokawa, S., Ueki, Y., Tanaka, H., Doi, H., Ueda, K. and Taniguchi, N. : 'Multivariable adaptive control for a thermal generator', IEEE Trans. on EC, Vol: 3, No: 3, 479-486 (1988).

54. Walker, P.A.W., Serag, A.M. and Abdalla, O.H. : 'Integrated excitation and turbine control in a multimachine power station', Proc. IEE, Pt. C, Vol: 136, No: 6, 331-340 (1989).

55. Sharaf, S.M., Hogg, B.W. Abdalla, O.H. and El-Sayed. : 'Multivariable adaptive controller for a turbo-generator', Proc. IEE, Pt. D, 133 (2), 83-89 (1986).

56. Sharaf, M.M., Hogg, B.W., 'Evaluation of online identification methods for optimal control of a laboratory model turbogenerator', Proc. IEE, Part D, Vol: 28, No: 2, 65-73 (1981).

57. Sharaf, M.M. and Hogg, B.W., 'Indirect identification and control of a laboratory system', Proc. IEE, Pt. D, 128 (6), 253-262 (1981).

58. Sharaf, S.M., Hogg, B.W., Abdalla, O.H. and El-Sayed. : 'Model reference adaptive control for a turbogenerator', IEE 'Control 85' conference, 48-53, Cambridge, UK (1985).

59. Sharaf, S.M., Hogg, B.W. and Abdalla, O.H. : 'Real time adaptive controllers for a turbine generator', IJC, Vol: 50, No: 2, 603-626 (1989).

60. Hogg, B.W., Ibrahim, A.S. and Sharaf, M.M. : 'Multivariable adaptive control of a turbogenerator', IEE Workshop on Self-tuning and adaptive control, Oxford, UK (1987).

61. Ibrahim, A.S., Hogg, B.W. and Sharaf, M.M. : 'Self-tuning controllers for turbogenerator excitation and governing systems', Proc. IEE, Pt. D, Vol: 136, No: 5, 238-251 (1989).

62. Fan, J.Y., Ortmeyer, T.H. and Mukundan, R. : 'Power system stability improvement with multivariable self-tuning control', IEEE Trans. or Power Systems, Vol: 5, No: 1, 227-233 (1990).

63. Malik, O.P., Hope, G.S., Gorzski, Y.M., Ushakov, V.A. and Rackevich, A.L.: 'Experimental studies on adaptive microprocessor stabilisers for synchronous generators', IFAC Power Systems and Power Plant Control, 125-130, Beijing, China (1986).

64. Seifi, H. and Hughes, F.M. : 'Self-tuning power system stabiliser using an acceleration signal', IJC, Vol: 51, No: 2, 469-485 (1990).

65. Chow, Y.S., Cheng, S., Malik, O.P. and Hope, G.S. : 'An adaptive power system stabiliser', IFAC Power Systems and Power Plant Control, 119-124, Beijing, China (1986).

66. Tham, M.T. : 'Some aspects of multivariable self-tuning control', Ph.D Thesis, Dept. of Chemical Eng., University of Newcastle upon Tyne, UK (1985).

67. Gu, W. and Bollinger, K.E. : 'A self-tuning power system stabiliser for wide range synchronous generator operation', IEEE Winter Power meeting, New York (1989).

68. Hiyama, T. : 'Application of rule-based stabilising controller to electrical power system', Proc. IEE, Pt. C, Vol: 136, No. 3, 175-181 (1989).

69. Hassan, M.A.M. and Malik, O.P. : 'Implementation and laboratory test results for a fuzzy logic based self-tuned power system stabiliser', IEEE Trans. on EC, Vol: 8, No: 2, 221-228 (1993).

70. Noble, A.D. : 'On-line computer control of turbine generators using state estimation and optimal feedback', Ph.D thesis, University of London, UK (1984).

71. Elmetwally, M.M., Rao, N.D. and Malik, O.P. : 'Experimental results on the implementation of an optimal controller for synchronous machines'. IEEE Trans. PAS-94, 1192-1200 (1975).

72. Asgharian, R. : 'Optimal controllers for turbine generators with multiple modes of oscillation', Ph. D Thesis, Imperial College, London (1986).

73. Kasenally, E.M. : 'The four block distance problem in H^{∞} control', Ph. D Thesis, Imperial College, London (1989).

74. Hogg, B.W., Swidenbank, E. and Capener, J.R. : 'The design and development of a self-tuning voltage regulator for a turbine generator', CIGRE Conference, paper No: 11-08, Paris, France (1988).

75. Bhatt, N.B., DeGroff, A.G. and Heyeck, M. : 'Benefits of Excitation Control System testing at AEP's Rockport Plant', IEEE Trans. on EC, Vol: 6, No:1, 21-28 (1991).

76. Franklin, G.F. and Powell, J.D. : 'Digital control of dynamic systems', Addison-Wesley Publishing Co., Mass. (1980).

77. Isermann, R. : 'Parameter adaptive control algorithms - A tutorial', Automatica, 18, 513-528 (1982).

78. Bierman, G.J. : 'Measurement updating using the U-D factorisation', Automatica, 12, 375-382 (1976).

79. Farsi. M., Karam, K.Z., and Warwick, K. : 'Simplified recursive identifier for ARMA processes', Electronic Letters, 20, 913-915 (1984).

80. Dexter, A.L. : 'Self-tuning control algorithm for single chip micro-computer implementation', Proc. IEE, 130, Pt. D, 255-260 (1983).

81. Fostescue, T.R., Kershenbaum, L.S. and Ydstie, B.E. : 'Implementation of self-tuning regulators with variable forgetting factors', Automatica, Vol: 17, No: 6, 831-835 (1981).

82. Astrom, K.J. : 'Introduction to stochastic control theory', Academic Press, London (1970).

83. Clarke, D.W., Tuffs, P.S. and Mohtadi, C. : 'Self-tuning control of a difficult process' IEE Workshop on The theory and application of self-tuning and adaptive control, Oxford, UK (1985).

84. Clarke, D.W., Hodgston, A.J.F. and Tuffs, P.S. : 'Offset Problem and K-incremental predictors in self-tuning control', Proc, IEE, Vol: 130, Pt. D, No: 5, 217-225 (1983).

85. Rossiter, J.A., Kouvaritakis, B. and Dunnett, R.M. : 'Application of generalised predictive control to a boiler turbine unit for electricity generation', Proc. IEE, Part D, 138 (1), 59-67 (1991).

86. Hogg. B.W., El-Rabaie, N.M. : 'Generalised predictive control of steam pressure in a drum boiler', IEEE/PES 1990 Winter Meeting, Paper No: 90 WM 218-8 EC, Atlanta, Georgia, USA (1990).

87. Clarke, D.W. : 'Designing robustness into predictive control', Colloquium on Industrial applications of model based predictive control, IEE Digest No: 1991/174, London (1991).

88. Clarke, D.W. and Mohtadi, C. : 'Properties of Generalised Predictive Control', Automatica, Vol: 25, No: 6, 859-875 (1989).

89. Mohtadi, C. : 'On the role of pre-filtering in parameter estimation and control', Proceedings of a Workshop on Adaptive control strategies for industrial use, 121-144, Canada (1988).

90. Clarke, D.W. and Scattolini, R. : 'Constrained receding-horizon predictive control', Proc. IEE, Vol: 138, Pt. D, No. 4, 347-354 (1991).

91. Tsang, T.T.C., and Clarke, D.W. : 'Generalised Predictive Control with input constraints', Proc. IEE, Pt. D, Vol: 135, No. 6, 451-460 (1988).

92. Clarke, D.W. and Mohtadi, C. : 'Properties of Generalised Predictive Control', Automatica, Vol: 25, No: 6, 859-875 (1989).

93. Robinson, B.D. and Clarke, D.W. : 'Robustness effects of a pre-filter in generalised predictive control', Proc, IEE, Pt. D, Vol: 138, No: 1, 2-8 (1991).

95. Bierman, G.J. : 'Factorisation methods for discrete sequential estimation', Academic Press, New York (1977).

96. Sharaf, M.M. and Hogg, B.W. : 'Self-tuning voltage regulator for a turbogenerator', UPEC-20, 267-270, Huddersfield, UK (1985).

97. Wong, K.Y., Bayoumi, M.M. and Nuyan, S. : 'Comparative study of some estimation algorithms for the self-tuning control of time varying systems', ACI '83, Denmark (1983).

98. Sanoff, S.P. and Wellstead, P.E. : 'Comments on Implementation of self-tuning regulators with variable forgetting factors', Automatica, Vol: 19, No: 3, 345-346 (1983).

99. Adkins, B. and Harley, R.G. : 'The general theory of alternating current machines : Application to practical problems', Chapman and Hall, London (1975).

100. IEEE Committee report: 'Excitation system models for power system stability studies', IEEE Vol: PAS-100, 494-509 (1981).

101. IEEE Working group on prime mover and energy supply models for System Dynamic performance studies: 'Dynamic models for fossil fuelled steam units in power system studies', IEEE/PES 1990 summer meeting, Minnesota, USA (1990).

102. Mawdsley's Limited : 'Operating and maintenance manual for the Mawdsley micro-synchronous generator set', Mawdsley's Ltd., Dursley, Glos., UK (1980).

103. Auckland, D.W. and Shuttleworth, R : 'Compensation systems for a micromachine model', Proc. IEE, Vol: 128, Pt. C, No: 1, 12-17 (1981).

104. Osheba, S.M. and Hogg, B.W. : 'Compensation of rotor backswing in a micro-alternator', Indian Journal of Technical Education, Vol: 6, No. 2, 63-67 (1979).

105. Zachariah, K.J., Finch, J.W., Lawson, P. and Farsi, M. : 'A software approach to the measurement of terminal quantities for digital excitation control of turbine generators', IEE Fifth International Conference on Electrical Machines and Drives 'EMD 91', 198-202, London, UK (1991).

106. Bo, Z., Swidenbank, E. and Hogg, B.W. : 'An advanced microcomputer system for control of a laboratory turbogenerator', Proc. IEE 'Control 88' Conference, 383-386, Oxford, UK (1988).

107. Mann, B.J. and Morrison, I.F. : 'Relaying a three phase transmission line with a digital computer', IEEE trans. on PAS, Vol: PAS 90, No. 2, 742-750 (1971).

108. BICC-VERO Microsystems Ltd. : 'BVME 370/380 MC68030 32-bit processor board user manual' (1989).

109. BICC-VERO Microsystems Ltd. : 'BVME650 Analogue Input/Output Board User's Manual' (1991).

110. Yourdon, E. and Constantine, L.L. : 'Structured Design', Yourdon Press, New York, USA (1978).

111. Kernighan, B.W. and Ritchie, D.M. : 'The C Programming Language', Prentice Hall Software Series, New Jersey, USA (1978).

112. Motorola Inc. : 'System V/68 Technical Documentation' (1985).

113. BICC-VERO Microsystems Ltd. : 'FBUG+ Enhanced Debug Monitor User's Manual' (1990).

114. Motorola Inc. : 'MVME133 32-bit Microcomputer User's Manual' (1986).

115. Motorola Inc. : 'MVME340 Parallel Interface/Timer Module User's Manual' (1984).

116. Burr-Brown Ltd. : 'Operating Manual MPV904' (1985).

117. Tham, M.T. and Mansoori, S.N. : 'Covariance resetting in recursive least squares estimation', IEE International conference 'CONTROL 88', Conference Publication No: 285, 366-370, Oxford, UK (1988).

118. Astrom, K.J. and Wittenmark, B. : 'Computer controlled systems - Theory and Design', Prentice-Hall (1984).

119. Hewlett Packard : 'HP35665A Dynamic Signal Analyser Operator's Guide (1991).

120. Kimbark, E.W. : 'Power System Stability : Synchronous Machines', Dover Publications Inc., New York (1968).

121. Sen Gupta, D.P., Narahari, N.G., Boyd, I. and Hogg, B.W. : 'An adaptive power system stabiliser which cancels the negative damping torque of a synchronous generator', Proc. IEE, Pt. C, Vol: 132, No: 3, 109-117 (1985).

122. Farmer, R.G. and Agrawal, B.L. : 'State-of-the-art technique for power system stabiliser tuning', IEEE trans. on PAS, Vol: PAS-102, No: 3, 699-709 (1983).

123. Byerly, R.T., Skooglund, J.W. and Keay, F.W. : 'Control of generator excitation for improved power system stability', Proceedings of the American Power Conference, 1011-1022 (1967).

124. Isermann, R. : 'Digital Control Systems', Springer-Verlag, Berlin (1981).

125. Shah, S.L., Mohtadi, C, and Clarke, D.W. : 'Multivariable adaptive control without a prior knowledge of the delay matrix', Systems & Control Letters, 9, 295-306 (1987).

126. Wilkinson, D.J., Tham, M.T. and Morris, A.J. : 'Constrained multivariable generalised predictive control', Proc. American Control Conference, San Diego, USA (1990).